



University
of Glasgow

Karvela, Maria (2013) Investigation of autophagy as a survival factor for chronic myeloid leukaemia. PhD thesis

<http://theses.gla.ac.uk/4271/>

Copyright and moral rights for this thesis are retained by the author

A copy can be downloaded for personal non-commercial research or study, without prior permission or charge

This thesis cannot be reproduced or quoted extensively from without first obtaining permission in writing from the Author

The content must not be changed in any way or sold commercially in any format or medium without the formal permission of the Author

When referring to this work, full bibliographic details including the author, title, awarding institution and date of the thesis must be given.

**Investigation of autophagy as a survival factor
for chronic myeloid leukaemia**

by

Maria Karvela

A thesis submitted for the degree of Doctor of Philosophy

March 2013



Section of Experimental Haematology

Institute of Cancer Sciences

College of MVLS

Abstract

Tyrosine kinase inhibitors (TKIs) have revolutionised the treatment of chronic myeloid leukemia (CML), however, fail to cure the disease due to the persistence of a refractory fraction of stem/progenitor cells. Autophagy is a recycling mechanism utilised by the cell as a survival mechanism under stressful conditions, and its induction has been suggested to have a cytoprotective role in cancer cells.

In this study we demonstrate that autophagy is triggered in CML upon TKI-mediated inhibition of BCR-ABL, and protects from cell death. In order to evaluate if specific autophagy inhibition enhances TKI effects, we stably transduced primary CML stem/progenitor cells with a vector carrying a short-hairpin against the key autophagy gene *ATG7*. Knock-down of basal *ATG7*/autophagy levels in CML stem/progenitor cells inhibited by approximately 50% the survival of the cells in a clonogenic assay, and reduced by 75% their erythroid differentiation potential. Furthermore, *ATG7* knock-down enhanced the effects of TKIs imatinib (IM; 1st), dasatinib (DAS; 2nd), nilotinib (NIL; 2nd) and ponatinib (PON; 3rd generation), reducing by 92-98% the survival of these cells in a clonogenic assay. In contrast, *ATG7* knock-down in normal stem cells, with or without TKI treatment, did not have a significant effect on survival and proliferation.

ATG7 was also knocked-down in final disease stage, blast crisis (BC), patient-derived K562 and KCL22 cell lines. Both cell lines appeared to depend significantly on autophagy for survival as indicated by high apoptosis levels (70-100%) after *ATG7* knock-down. Interestingly, *ATG7* knock-down cells appeared to be more differentiated compared to the control (scrambled shRNA).

Our findings suggest a role for basal autophagy in the survival, differentiation decisions and clonogenicity of CML cells, and support the combined use of autophagy inhibition with TKIs for the eradication of CML stem/progenitor cells. This could be partially attributed to a bypass of the differentiation block upon autophagy inhibition, which facilitates TKI-targeting. We underline the necessity for the development of specific autophagy inhibitors that in combination with TKIs could potentially eradicate the fraction of persistent CML stem/progenitor cells and offer a curative option for CML patients.

1 Table of Contents

Abstract	2
List of Tables	6
List of Figures	7
Acknowledgements	11
Author’s Declaration	12
Abbreviations	13
1 Introduction	19
1.1 Haemopoiesis and haemopoietic stem cells	19
1.2 The cancer stem cell hypothesis	24
1.3 CML	25
1.3.1 Historical overview.....	25
1.3.2 Disease incidence, course and progression.....	26
1.3.3 Diagnosis and monitoring.....	28
1.3.4 BCR-ABL structure.....	28
1.3.5 BCR-ABL function.....	30
1.3.6 CML treatment.....	37
1.4 Autophagy	51
1.4.1 Molecular mechanism.....	53
1.4.2 Autophagy in cancer	57
1.4.3 Autophagy in CML.....	62
2 Materials and Methods	66
2.1 Materials	66
2.1.1 Small molecule inhibitors	66
2.1.2 Tissue culture materials	67
2.1.3 Molecular biology materials.....	69
2.1.4 TaqMan® probes	71
2.1.5 Fluorescence microscopy supplies.....	72
2.1.6 PCR primer sequences.....	72
2.1.7 Equipment.....	72
2.1.8 Preparation of medium and solutions	73
2.2 Methods	80
2.2.1 Cell Culture.....	80
2.2.2 Flow cytometry	84
2.2.3 Western blotting.....	87

2.2.4	Immunofluorescence microscopy	92
2.2.5	PCR-based assays	93
2.2.6	Statistics	98
2.2.7	Cellular techniques	99
2.2.8	Gene knock-down	102
2.2.9	Cloning	105
2.2.10	Morphological analysis of CML cells.....	109
3	Results (I): Effects of first, second, and third generation TKIs on proliferation, survival and autophagy in CML cell lines and primary cells	110
3.1	TKIs in the proliferation, survival and autophagy of CML cells expressing native BCR-ABL	111
3.1.1	Optimisation of IM, DAS and PON treatment to maximise targeting of BCR-ABL activity in K562 cells	111
3.1.2	Effects of TKI-mediated BCR-ABL inhibition on autophagy.....	116
3.1.3	Pharmacological inhibition of autophagy enhances TKI-induced effects in CML cells	134
3.2	PON and mTOR inhibitors in the treatment of CML cells expressing BCR-ABL^{T315I}	142
3.2.1	Effect of PON on the proliferation of CML cells carrying BCR-ABL ^{T315I}	142
3.2.2	Effects of mTOR inhibitors' treatment in CML cells.....	145
3.3	TKI treatment in the autophagy and survival of Ph- cells	154
3.3.2	Analysis of the effect of DAS/CQ combination treatment on a co-culture of Ph-/Ph+ cells.....	157
4	Results (II): Investigation of ATG7 knock-down in combination with TKIs for the elimination of CP CML CD34+ primary cells.....	159
4.1	Optimisation of ATG7 knock-down techniques in human CD34+ progenitor cells.....	160
4.1.1	Assessment of the siRNA nucleofection method for the knock-down of ATG7 in cell lines and CD34+ cells	160
4.1.2	Optimisation of the lentivirus-mediated shRNA delivery method for the knock-down of ATG7 in CP CML CD34+ primary cells	166
4.2	Investigation of ATG7 knock-down in combination with TKIs on CP CML CD34+ cells.....	178
4.2.1	Analysis of CP CML CD34+ cell proliferation following ATG7 knock-down and TKI treatment	178
4.2.2	Analysis of CP CML CD34+ cell apoptosis following ATG7 knock-down and TKI treatment	180

4.2.3	Analysis of CML committed progenitor cell potential and differentiation following ATG7 knock-down and TKI treatment.....	182
4.3	Investigation of ATG7 knock-down in combination with TKIs on Ph- CD34+ cells	194
4.3.1	Analysis of Ph- CD34+ cell proliferation following ATG7 knock-down and TKI treatment	194
4.3.2	Analysis of Ph- CD34+ cell apoptosis following ATG7 knock-down and TKI treatment	196
4.3.3	Analysis of Ph- committed progenitor cell potential following ATG7 knock-down and exposure to TKIs.....	198
4.3.4	Transcriptional analysis of key autophagy genes in Ph+ and Ph- CD34+ cells	200
5	Results (III): Investigation of the role of ATG7 and autophagy in the fate decision of leukaemic cells.....	202
5.1	Characterisation of BC CML cells following ATG7 knock-down	203
5.1.1	Assessment of KCL22 viability following ATG7 knock-down	204
5.1.2	Characterisation of K562 cells following ATG7 knock-down.....	207
5.2	Characterisation of CLL cells following ATG7 knock-down.....	225
5.2.1	Assessment of HG3 proliferation and cell viability following ATG7 knock-down..	227
5.2.2	Effect of ATG7 knock-down in the differentiation of HG3 cells.....	231
5.3	Effect of Atg7 knock-down in mouse c-kit enriched MLL-ENL transformed cells .	236
6	Discussion.....	238
6.1	Autophagy in cancer	241
6.2	Is autophagy a survival factor for CML?	243
6.3	Summary and future directions	257
	Appendix	260
	List of References	263

List of Tables

Table 1-1: Human haemopoietic system lineage marker phenotypes.....	23
Table 1-2: Staging system for CML according to the World Health Organisation (WHO) Classification 2008.....	27
Table 1-3: ABL binding proteins and substrates	29
Table 1-4: BCR-ABL substrates	31
Table 1-5: Criteria of treatment responses in CML	41
Table 1-6: Autophagy genes in mammals.....	52
Table 1-7: Clinical trials investigating autophagy inhibition using HCQ or CQ in combination with anti-cancer therapies	62
Table 2-1: Small molecule inhibitors.....	66
Table 3-1: Recommended methods for monitoring autophagy in higher eukaryotes.....	117
Table 3-2: Methods used for measuring autophagic elements' volume and autophagic flux	120

List of Figures

Figure 1-1: The haemopoietic hierarchy	20
Figure 1-2: BCR, ABL structure and different fusion products	30
Figure 1-3: Signal transduction pathways in BCR-ABL transformed cells.....	32
Figure 1-4: IM resistance mechanisms	43
Figure 1-5: Overview of the autophagy process in vertebrates	53
Figure 1-6: Autophagosome elongation.....	56
Figure 1-7: The role of autophagy in cancer.....	60
Figure 1-8: Proposed mechanism for the role of autophagy in TKI-induced CML treatment	63
Figure 2-1: Trypan blue method for cell counting and viability assessment with improved Neubauer counting chamber	81
Figure 2-2: Sorting the CD34+CD38- subpopulation from primary human CD34+ samples	85
Figure 2-3: Assemble of sandwich for transfer of proteins to PVDF membrane	91
Figure 2-4: The Fluidigm [®] 48.48 Dynamic Array [™]	98
Figure 2-5: The LTC-IC assay	100
Figure 2-6: Strategy for cloning the shATG7 hairpin into the pLKO.1-GFP backbone ...	106
Figure 2-7: Isolation of ten pLKO.1-GFP-shATG7 clones (circa; ca.)	108
Figure 3-1: Effect of TKI treatment on BCR-ABL activity, measured by phosphorylation of downstream effectors CrKL and STAT5, in K562 cells	112
Figure 3-2: Comparison of IM, DAS and PON treatment in the proliferation of K562 cells	115
Figure 3-3: Accumulation of autophagosome-associated LC3-II upon IM or DAS treatment of K562 cells	123
Figure 3-4: Accumulation of autophagosome-associated LC3-II upon IM, DAS or PON treatment of CP CML CD34+ cells.....	127
Figure 3-5: Formation of LC3-positive punctae in DAS- and PON-treated K562 cells....	129
Figure 3-6: Formation of LC3-positive punctae in IM-, DAS- and PON-treated CP CML CD34+ cells.....	131
Figure 3-7: Induction of autophagy in K562 cells upon TKI treatment measured by FACS	133
Figure 3-8: CQ-mediated autophagy inhibition enhances TKI-induced apoptosis in K562 cells	135

Figure 3-9: CQ/HCQ enhance TKI-induced inhibition of the colony forming ability of K562 cells	137
Figure 3-10: TKIs in combination with HCQ in the proliferation of CP CML CD34+ cells	139
Figure 3-11: HCQ-mediated autophagy inhibition enhances TKI effect against the clonogenic ability of CP CML CD34+ cells.....	141
Figure 3-12: Comparison of PON treatment in BaF3 ^{WT} , BaF3 ^{T315I} and BaF3 ^{Parental} cells..	144
Figure 3-13: The PI3K/AKT/mTOR pathway in cell survival	145
Figure 3-14: Comparison of BEZ treatment in KCL22 ^{WT} and KCL22 ^{T315I} cells.....	147
Figure 3-15: Comparison of RAPA treatment in KCL22 ^{WT} and KCL22 ^{T315I} cells.....	149
Figure 3-16: Formation of LC3-positive punctae in RAPA- and BEZ-treated CP CML CD34+ cells.....	151
Figure 3-17: CQ-mediated autophagy inhibition improves the apoptotic effect of PON and BEZ treatment in KCL22 ^{T315I} cells	153
Figure 3-18: Treatment with DAS or PON does not induce autophagy in Ph- CD34+ cells	156
Figure 4-1: Assessment of the siRNA nucleofection method in the viability, transfection efficiency and mRNA knock-down in K562 cells	163
Figure 4-2: Assessment of the siRNA nucleofection method in the viability, transfection and knock-down efficiency in Ph- CD34+ progenitor cells	165
Figure 4-3: Assessment of the use of concentrated HIV-based lentiviral virus in the viability, and transduction efficiency in CD34+ progenitor cells.....	167
Figure 4-4: Assessment of the use of unconcentrated HIV-based lentiviral virus in the viability, and transduction efficiency in CD34+ cells.....	169
Figure 4-5: Measurement of ATG7 and LC3-II protein levels in K562 cells that stably express ATG7-targeting hairpins carried by pGIPZ vector	171
Figure 4-6: Measurement of DAS effect on the autophagic activity of K562 cells in the presence of ATG7 knock-down	173
Figure 4-7: The CMV promoter of the pGIPZ vector is methylated in K562 cells.....	175
Figure 4-8: Measurement of ATG7 and LC3-II protein levels in CD34+ primitive cells that stably express an ATG7-targeting hairpin carried by the pLKO.1 vector	177
Figure 4-9: Comparison of NIL, DAS and PON treatments in combination with ATG7 knock-down in CP CML CD34+ cells.....	179
Figure 4-10: Analysis of TKI-induced apoptosis in the presence of ATG7 knock-down in CP CML CD34+ cells	181

Figure 4-11: ATG7 knock-down-mediated autophagy inhibition enhances 3 day TKI treatment effect against the clonogenic ability of CP CML CD34+ cells	183
Figure 4-12: ATG7 knock-down-mediated autophagy inhibition enhances 6 day TKI treatment effect against the clonogenic ability of CP CML CD34+ cells	185
Figure 4-13: Ablation of the clonogenic ability of CD34+CD38- cells from a CP CML patient upon ATG7 knock-down.....	187
Figure 4-14: ATG7 knock-down-mediated autophagy inhibition enhances prolonged TKI treatment effect against the clonogenic ability of CP CML CD34+ cells	189
Figure 4-15: ATG7 knock-down-mediated autophagy inhibition is associated with reduced erythroid colony-formation potential in CP CML CD34+ cells	191
Figure 4-16: Assessment of GFP expression in cells from CML CD34+ progenitor colonies surviving ATG7 knock-down	193
Figure 4-17: Comparison of NIL, DAS and PON treatments in combination with ATG7 knock-down in Ph- CD34+ cells.....	195
Figure 4-18: Analysis of TKI-induced apoptosis in the presence of ATG7 knock-down in Ph-CD34+ cells	197
Figure 4-19: ATG7 knock-down-mediated autophagy inhibition alone or in the presence of TKI treatment does not affect the clonogenic ability of Ph- CD34+ cells.....	199
Figure 4-20: Transcriptional analysis of key autophagy genes in Ph+ and Ph- CD34+ cells	201
Figure 5-1: CML development and disease progression	203
Figure 5-2: Cell death analysis in KCL22 cells upon ATG7 knock-down.....	206
Figure 5-3: ATG7 and LC3 monitoring in K562 cells that stably express an ATG7-targeting hairpin carried by pLKO.1 vector.....	209
Figure 5-4: Analysis of K562 cell proliferation upon ATG7 knock-down.....	211
Figure 5-5: Cell death analysis in K562 cells upon ATG7 knock-down.....	213
Figure 5-6: Analysis of the erythroid differentiation potential of K562 cells upon ATG7 knock-down.....	215
Figure 5-7: Analysis of the morphology and the mitochondrial profile of K562 cells upon ATG7 knock-down	217
Figure 5-8: Analysis of the morphology K562 cells surviving prolonged ATG7 knock-down.....	219
Figure 5-9: Measurement of superoxide levels within K562 cells surviving prolonged ATG7 knock-down	221

Figure 5-10: Analysis of clone-initiating potential of single-sorted ATG7 knock-down K562 cells	223
Figure 5-11: Measurement of ATG7 protein levels in HG3 cells that stably express an ATG7-targeting hairpin carried by pLKO.1 vector	226
Figure 5-12: Analysis of HG3 cell proliferation upon ATG7 knock-down.....	228
Figure 5-13: Cell death analysis in HG3 cells upon ATG7 knock-down	230
Figure 5-14: Increase in the cell size of HG3 cells upon ATG7 knock-down.....	232
Figure 5-15: Morphological analysis of HG3 cells surviving ATG7 knock-down	234
Figure 6-1: The BCR-ABL/PI3K/AKT/FOXO4/ATF5/mTOR-mediated autophagy-inhibition pathway.....	247
Figure 6-2: Induction of cytoprotective autophagy upon TKI-treatment of CML cells	248
Figure 6-3: Autophagy takes part in many cellular processes	254
Figure 6-4: Overview of the observed effects upon ATG7 knock-down in CP and BC CML cells	259

Acknowledgements

I am extremely grateful to my principal supervisor, Professor Tessa Holyoake, for directing this project and supporting me throughout the PhD. I am very privileged to have been able to work under the guidance of someone so charismatic and inspirational. I would also very much like to thank my co-supervisor, Dr Guðmundur Vignir Helgason, for his invaluable guidance and help during the last three years. I am indebted to him for the scientific training I have received.

This thesis would not have been possible without the help from many individuals. Firstly, I would like to thank Ms Elaine Allan and Dr Arunima Mukhopadhyay for the enormous technical support they have offered me, and for all the helpful discussions. I would also like to thank Ms Amy Sinclair and Dr Milica Vukovic for being the best colleagues and friends I could have ever wished for; I am looking forward to Amy becoming “Dr” and both of you “Mrs”. I also owe my gratitude to Dr Alan Hair for his endless assistance in the lab, and for making me smile every morning, even on the rainy days. A huge thanks to Ms Diane Verrechia for all the help she has offered me. I am very appreciative to all my past and present colleagues at the Paul O’Gorman Leukaemia Research Centre who have helped me in any respect at the PhD.

I am indebted to my advisor, Professor Kevin Ryan, for his guidance, and for many useful discussions throughout the project.

I would also like to acknowledge the University of Glasgow, the Medical Research Council, and all patients who have donated blood samples and made this work possible.

Special thanks to Alex; gracias por tu apoyo y paciencia - y recuerda que siempre serás mi trucho.

Finally, I would like to thank my family and friends for supporting me. Μαμά, μπαμπά και Χρήστο, σας ευχαριστώ για όλες τις θυσίες που κάνατε για εμένα-όπου και αν είμαι, σας κουβαλάω στην σκέψη μου.

Author's Declaration

Unless otherwise stated, I declare that all the work presented in this thesis is my own.

Abbreviations

§	Section
3-MA	3-Methyladenine
4E-BP1	Eukaryotic Translation Initiation Factor 4E-Binding Protein 1
7-AAD	7 aminoactinomycin D
a-1-GP	a-1-Acidglycoprotein
AAP-1	ABL Associated Protein 1
ABC	ATP-Binding Cassette Sub-Family
ABCB1	ATP-Binding Cassette Sub-Family B Member 1
ABL	v-abl Abelson Murine Leukaemia Viral Oncogene Homolog
AGM	Aorta, Gonads and Mesonephros
aka	Also Known As
AKT/PKB	Protein kinase B
ALBA®	Human Albumin Solution
ALL	Acute Lymphoblastic Leukemia
ALOX5	Arachidonate 5-Lipoxygenase
AMBRA1	Activating Molecule In BECLIN1-Regulated Autophagy Protein 1
AML	Acute Myeloid Leukaemia
AP	Accelerated Phase
APC	Allophycocyanin
ATG	Autophagy-Related Genes
ATM	Ataxia Telangiectasia Mutated
ATP	Adenosine Triphosphate
AZA	5-Azacytidine
BAD	BCL-2-Associated Death Promoter
BAP-1	BCR-Associated Protein 1
BARKOR	BECLIN1-Associated Autophagy-Related Key Regulator
BC	Blast Crisis
BCA	Bicinchoninic Acid
BCL-XL	B-Cell Lymphoma-Extra Large
BCR	Breakpoint Cluster Region
BEZ	NVP-BEZ235
BFU-E	Burst Forming Unit-Erythroid
BIT	BSA /Insulin/Transferrin
BM	Bone Marrow
BMT	Bone Marrow Transplantation
bp	Base Pair
BSA	Bovine Serum Albumin
ca.	Circa
CB	Cord Blood
CBL	Casitas B-Lineage Lymphoma
CC	Coiled-Coil
CD	Cluster of Differentiation
CFC	Colony-Forming Cell
CFU-E	Colony-Forming Unit Erythroid
CHOICES	Chloroquine And Imatinib Combination To Eliminate Stem cells

CHR	Complete Haematologic Response
CLI	Clindamycin
CLPs	Common Lymphoid Progenitors
CML	Chronic Myeloid Leukaemia
CMPs	Common Myeloid Progenitors
CMR	Complete Molecular Response
CNL	Chronic Neutrophilic Leukaemia
CP	Chronic Phase
CQ	Chloroquine
CrK	Avian Sarcoma Virus CT10 Oncogene Homolog
CrKL	CrK-Like Protein
CrTX	Crotoxin
CSCs	Cancer Stem Cells
Ct	Threshold Cycle
CXCR4	CXC-Chemokine Receptor 4
CYP3	Cytochrome P450, Family 3, Subfamily A
CyR	Cytogenetic Response
DAPI	4',6-diamidino-2-phenylindole
DAS	Dasatinib
DEPTOR	DEP Domains Interactor of mTOR
dH ₂ O	Distilled Water
DMEM	Dulbecco's Modified Eagle Medium
DMSO	Dimethyl Sulfoxide
DNA	Deoxyribonucleic Acid
dNTPs	Deoxyribonucleotide Triphosphates
DRAM	Damage-Regulated Autophagy Modulator
dsH ₂ O	distilled sterile water
EDTA	Ethylenediaminetetraacetic Acid
EFS	Event-Free Survival
ELISA	Enzyme-Linked Immunosorbent Assay
ELN	European Leukaemia Net
EM	Electron Microscopy
EOS	Estimated Overall Survival
EPIC	Evaluation Of Ponatinib Versus Imatinib In Chronic Myeloid Leukaemia
ER	Endoplasmic Reticulum
EtOH	Ethanol
FACS	Fluorescence-Activated Cell Sorting
FAK	Focal Adhesion Kinase
FCS	Foetal Calf Serum
FDA	Food And Drug Administration
FIP200	Focal Adhesion Kinase Family-Interacting Protein Of 200Kd
FISH	Fluorescent <i>In Situ</i> Hybridisation
FITC	Fluorescein Isothiocyanate
FLT3L	Flt-3 Ligand
FoxO	Forkhead Box Class O
FSC	Forward-Angle Light Scatter
FT	Farnesyl Transferases
G-CSF	Granulocyte Colony Stimulating Factor
G-proteins	Guanine-Nucleotide-Binding Proteins

GeoMean	Geometrical Mean
GF	Growth Factor
GM-CSF	Granulocyte Macrophage Colony-Stimulating Factor
GRB2	Growth Factor Receptor Bound Protein 2
GβL	G-Protein β-Subunit Like Protein
HATs	Histone Acetyltransferases
HBS	HEPES-Buffered Saline
HBSS-CMF	Hank's Buffered Salt Solution – Calcium And Magnesium Free
HCK	Haemopoietic Cell Kinase
HCl	Hydrochloric Acid
HCQ	hydroxychloroquine
HDACs	Histone Deacetylases
HEPES	4-(2-hydroxyethyl)-1-Piperazineethanesulfonic Acid
HLAI	Human Leukocyte Antigen Class I
hOCT-1	Human Organic Cation Transporter-1
HPC	Haemopoietic Progenitor Cell
HRP	Horseradish Peroxidase
HSCs	Haemopoietic Stem Cells
IC50	Half Maximal Inhibitory Concentration
IFC	Integrated Fluidic Circuit
IFNα	Interferon α
IL-3	Interleukin-3
IM	Imatinib
IMDM	Isocove's Modified Dulbecco's Medium
iPSCs	Induced Pluripotent Stem Cells
IRIS	International Randomized Study Of Interferon And STI571
JAKs	Janus Kinases
kb	Kilobase Pairs
KCl	Potassium chloride
Kd	Kilodaltons
KO	Knock-Out
LB	Luria Broth
LC3	Microtubule-Associated Protein 1 Light Chain 3
Lin	Lineage Cocktail 1
LIR	LC3-Interacting Region
LREC	Local Research And Ethics Committee
LSCs	Leukaemic Stem Cells
LSI	Locus Specific Identifier
LT-HSCs	Long-Term Haemopoietic Stem Cells
LTBMC	Long-Term Bone Marrow Culture
LTC-IC	Long-Term Culture Initiating-Cell
M-bcr	Major BCR Region
m-bcr	Minor BCR Region
MAP	RAS–Mitogen Activated Protein
MAPK	Mitogen-Activated Protein Kinase
MCL-1	Myeloid Leukaemia Cell Differentiation Protein 1
MCyR	Major Cytogenetic Response
MDM2	murine double minute 2
MDR1	Multidrug Resistance- Associated Membrane Transporter

MFI	Mean Fluorescence Intensity
MIP-1 α	Macrophage Inflammatory Protein 1 α
mLST8	Mammalian LST8
MMR	Major Molecular Response
MNC	Mononuclear Cell
MOI	Multiple Of Infection
MPPs	Multipotent Progenitors
MRD	Minimal Residual Disease
mRFP	Monomeric Red Fluorescence Protein
MSCs	Mesenchymal Stem Cells
mSIN1	Mammalian Stress-Activated Protein Kinase Interacting Protein 1
mTOR	Mammalian Target Of Rapamycin
mTORC1	mTOR Complex 1
mTORC2	mTOR Complex 2
NA	Not Applicable
NBR1	Neighbor Of BRCA1 Gene 1
NCCN	National Comprehensive Cancer Network
NIL	Nilotinib
No of colonies	Number Of Colonies
NOD/SCID	Non-Obese Diabetic/Severe Combined Immunodeficient
NRF2	Nuclear Factor-Erythroid 2-Related Factor-2
NS	Not Significant
PACE	Ponatinib Ph+ ALL And CML Evaluation
PAGE	Polyacrylamide Gel Electrophoresis
PARK2	E3 Ligase Parkin
PBS	Phosphate Buffered Saline
PCD	Programmed Cell Death
PDGFR	Platelet-Derived Growth Factor Receptor
PDPK1	Phosphoinositide Dependent Kinase 1
PE	Phosphatidylethanolamine
PE	Phycoerythrin
PerCP	Peridinin Chlorophyll Protein
Ph	Philadelphia Chromosome
PH	Pleckstrin-Homology
PI3K	Phosphatidylinositol 3- Kinase
PINK1	PTEN-Induced Putative kinase 1
PiP3	Phosphatidylinositol-3,4,5-Trisphosphate
PKC α	Protein Kinase C α
PLC γ	Phospholipase C γ
PN	Product Number
PON	Ponatinib
PPP	Proline-Rich Region
PURO	Puromycin
PVDF	Polyvinylidene Fluoride
qRT-PCR	Quantitative RT-PCR
Rac-GAP	Rac GTPase activating protein
RAF	RAS-Activated Factor
RAPA	Rapamycin
RAPTOR	Regulatory-Associated Protein Of mTOR

RAS	Rat Sarcoma
RAS-GAP	RAS GTPase-Activating Protein
Rho-GEF	Rho guanine-nucleotide exchange factor
RICTOR	Rapamycin-Insensitive Companion Of mTOR
RIPA	Radio-Immunoprecipitation Assay
RNAi	RNA interference
ROS	Reactive Oxygen Species
RPS6	Ribosomal Protein S6
RPS6K	Ribosomal Protein S6 Kinase
RSV	Resveratrol
RT-PCR	Reverse Transcriptase Polymerase Chain Reaction
RT-STA	Reverse Transcriptase Specific Target Amplification
SAHA	Suberoylanilide Hydroxamic Acid
SAP	Shrimp Alkaline Phosphatase
Sca	Stem Cell Antigen 1
SCF	Stem Cell Factor
SCT	Stem Cell Transplantation
SDS	Sodium Dodecyl Sulfate
SEM	Standard Error Of The Mean
SFKs	SRC Family Kinases
SFM	Serum Free Medium
SH1	SRC Homology Domain 1
SHC	SRC Homology Containing Protein
shRNA	Short-Hairpin RNA
siRNA	Small Interfering RNA
SMO	Smoothed
SNP	Single Nucleotide Polymorphism
SoS	Son Of Sevenless
SQSTM1	Sequestosome 1
SSC	Side-Angle Light Scatter
ST-HSCs	Short-Term Haemopoietic Stem Cells
STAT	Signal Transducer And Activator Of Transcription
SYP	Synaptophysin
tATG5	Truncated ATG5
TBE	Tris/Borate/EDTA
TBS	Tris-Buffered Saline
TBST	TBS-Tween
TEMED	Tetramethylethylenediamine
TIE2	Immunoglobulin-Like And EGF-Like Domains 2
TKIs	Tyrosine Kinase Inhibitors
TPO	Thrombopoietin
TSC2	Tuberous Sclerosis Protein 2
UBA	Ubiquitin-Associated
UBL	Ubiquitin-Like
ULK1/2	Unc-51- Like Kinase 1/2
UV	Ultraviolet
UVRAG	UV Irradiation Resistance-Associated Gene
VPS34	Vacuolar Protein Sorting 34
WHO	World Health Organisation

WM	Wortmannin
WT	Wild Type
μ -bcr	μ BCR Region

1 Introduction

1.1 Haemopoiesis and haemopoietic stem cells

Haemopoiesis is the process that refers to the production of the blood cellular components. In 1961, Till and McCulloch demonstrated the existence of clonogenic bone marrow (BM) cells that could give rise to multilineage haemopoietic colonies in the spleen of lethally irradiated mice. Some of these colonies contained a subset of clonogenic cells that could reconstitute haemopoiesis of irradiated mice at secondary transplants [1]. It was proposed that these cells are haemopoietic stem cells (HSCs), i.e. cells that at single cell level have the properties of self-renewal and multilineage differentiation [2-5].

During mammalian embryonic development the sites of haemopoietic potential are constantly shifting and sequentially include the yolk sac, the aorta, gonads and mesonephros (AGM) region, the placenta and the foetal liver. Based on mouse transplantation experiments, it has been suggested that the first HSCs bearing the characteristic hallmarks (self-renewal, multipotency, migration and apoptosis), appear at the AGM region of the embryo 11 days post coitum [6]. Shortly before birth, the HSCs migrate from the primary foetal haemopoietic centre, the liver, to the primary adult haemopoietic centre, the BM, where they engraft and self-renew.

HSCs are relatively rare, accounting for approximately 0.05% of the total BM cells [7]. They are multipotent cells that can differentiate into all types of mature blood cells by residing on top of a hierarchy of progenitors that progressively commit to several or one lineage (Figure 1-1) [8]. However, terminally differentiated blood cells are predominantly short lived within the circulation and, therefore, need to be constantly replaced. In order to prevent exhaustion of the BM cell pool, the HSCs proliferate and self-renew. Through asymmetric division, an HSC gives rise to a non-self-renewing oligolineage haemopoietic progenitor cell (HPC) and an identical daughter cell that retains all the primitive stem cell features [9]. HSCs can also self-renew through symmetrical division, generating two identical HSCs that will contribute towards the maintenance of the HSC compartment. During or after the division of an HSC, each of the daughter cells has to decide its fate and it is believed that this decision largely depends on the environment, known also as the stem cell niche [10].

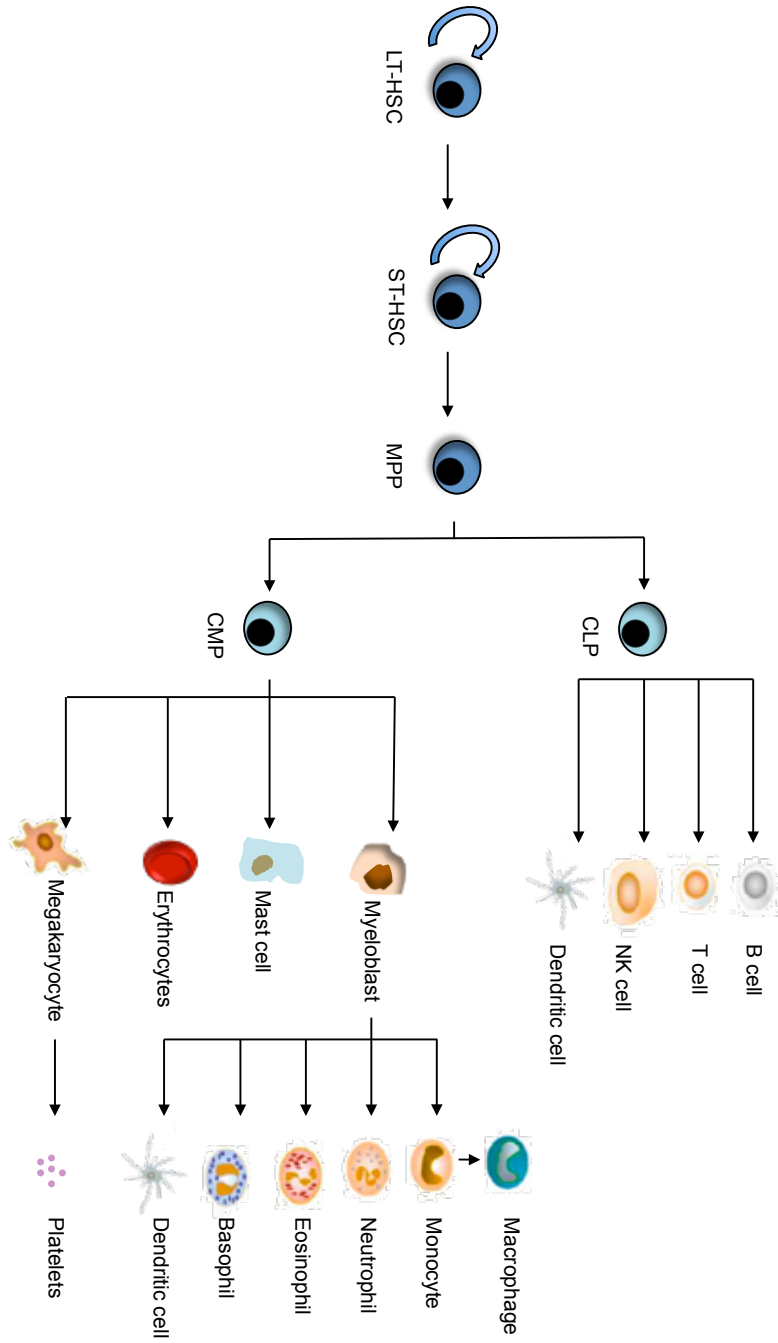


Figure 1-1: The haemopoietic hierarchy

Long-term HSCs (LT-HSCs) sit at the top of the hierarchy and have unlimited self-renewal capacity, unlike the short-term HSCs (ST-HSCs), which have limited self-renewal capacity. Upon activation, HSCs divide and generate multipotent progenitors (MPPs) that can further differentiate to common lymphoid progenitors (CLPs) or common myeloid progenitors (CMPs). Subsequently, CLPs can differentiate into lymphoid lineages and CMPs into myeloid lineages, as shown above.

Functional analyses of HSCs can be performed by *in vitro* or *in vivo* experiments. The colony-forming cell (CFC) and long-term culture initiating-cell (LTC-IC) are *in vitro* assays used to evaluate the potential of HPCs and HSCs respectively [11, 12]. *In vivo* experiments involve mainly the BM engraftment of non-obese diabetic/severe combined immunodeficient (NOD/SCID) mice to demonstrate the ability of HSCs to reconstitute haemopoiesis [13]. One of the most important advances for *in vivo* functional analyses was the enablement of the isolation of HSCs by fluorescence-activated cell sorting (FACS) depending on the cell surface marker profile. In 1988, Sprangrude and colleagues isolated HSCs from the BM of mice, and concluded that the phenotype of the HSCs that could reconstitute haemopoiesis long-term was Thy1^{low} [also known as (aka) cluster of differentiation 90 (CD90)], Lin^- (lineage cocktail 1), and Sca1^+ (stem cell antigen 1) [2]. Transplantation experiments focusing on the ability of HSCs subpopulations to engraft the BM of lethally irradiated mice showed that the population Sprangrude and colleagues had identified contained different HSC subsets, all capable of differentiating into lymphoid and myeloid lineages but with different self-renewal and reconstitution capability [3, 14]. In 1996, Osawa and colleagues first demonstrated that injection of a single HSC could reconstitute the long-term the haemopoiesis of a lethally irradiated recipient [5] and based on this foundation, following studies classified HSCs into three functional subsets: (i) the LT-HSCs, that reside in BM niches and can provide life-long haemopoiesis due to their ability of indefinite self-renewal, (ii) the ST-HSCs that have the ability to self-renew for a defined interval and can transiently reconstitute haemopoiesis [3], and (iii) the MPP cells which have undetectable or no ability to self-renew [14]. It should also be mentioned that the cycle status among these subsets differs as well; the majority of LT-HSCs are quiescent (G_0 phase) [15-17] while a significant fraction of ST-HSCs and MPPs are in cycle under homeostatic conditions [1]. Using mathematical model analysis it was predicted that a HSC divides about once every year, with the limit of 70 divisions throughout its lifetime [18]. This extended cell cycle arrest represents a homeostatic mechanism to ensure that the stem cell pool will not be severely depleted and also allows for repair of any DNA damage that may occur.

Human HSCs were isolated and validated by similar techniques previously used for mouse HSCs with the help of antibodies targeting cell surface markers. The CD molecules have been extensively used as markers because they feature different cell types and stages of differentiation. In the early 1990s it was noticed that during maturation the levels of CD34 antigen expression in cells from adult BM were decreasing while simultaneously increasing for the CD38 [19]. A few years later, DiGiusto and colleagues reported in foetal BM, that CD34 expression decreases with the commitment of HPCs to specific lineages and cells expressing higher levels of CD34 were more primitive [20]. Therefore, the first cell surface marker used for the enrichment of human HSCs was the CD34 antigen, a 115-kilodaltons (Kd) type I transmembrane glycoprotein. The CD34⁺ compartment contains multilineage primitive HSCs that have the ability to reconstitute haemopoiesis [21]. Despite its indisputable significance as a marker for stem cells, little is known about the function and regulation of CD34. It has been suggested that it may play a role in adhesion of leukocytes and haemopoietic cells, cell localisation, and signal transduction, including prevention of terminal differentiation [22]. Another marker used for the characterisation of HSCs is the CD38 antigen, a transmembrane glycoprotein used initially as a marker of lymphoid differentiation [23]. Its expression correlates with differentiation since levels of CD38 increase progressively during the process of maturation [19]. The use of CD38 as a marker allows for further identification of the HSC subpopulations; the CD34⁺CD38⁺ compartment includes the ST-HSCs, while the CD34⁺CD38⁻ the LT-HSCs [24]. The cell surface profile of HSCs is also defined by the presence of receptors that promote quiescence and help the anchorage in the niche. Such receptors include the tyrosine kinase c-KIT (aka CD117), immunoglobulin-like and EGF-like domains 2 (TIE2) receptors, the CXC-chemokine receptor 4 (CXCR4), that via binding niche cell-secreted ligands, ultimately, promote cell cycle arrest (Table 1-1) [25]. The quiescence of HSCs is also regulated by intracellular proteins and transcription factors [25].

Cell Type	Phenotype
HSC	CD34 ⁺ Lin ⁻ CD38 ⁻ CD33 ⁻ HLA-DR ^{low} c-Kit ⁺ CD133 ⁺ CD90 ⁺
MPP and lineage committed progenitors	CD34 ⁺ Lin ^{+/-} CD38 ⁺ CD33 ⁺ HLA-DR ^{high}
Mature	CD34 ⁻ Lin ⁺

Table 1-1: Human haemopoietic system lineage marker phenotypes

It has been suggested that HSCs can shift among three phases; (i) the dormant phase, where cells are arrested in G₀ and have very low metabolism, (ii) the homeostatic phase, where cells are able to cycle, and (iii) the injury-activated phase, where cells are continuously cycling and have high metabolism. Even if the molecular events underlying these phases have not been elucidated so far, it has become apparent during recent years that decisions made regarding the fate of a stem cell depend on interactions with the niche. The HSCs reside within various sub-regions in the BM and their function may actually depend on their exact localisation. Intravital microscopy has revealed that HSCs appear to be inherent in the periosteal region of calvarium marrow [26]. Stem cell niches include several cellular components, including osteoblasts, osteoclasts, CXCL12-abundant reticular cells, and vascular endothelial-cadherin⁺ sinusoidal endothelial cells [25]. It has been proposed that gradients from osteoblast-secreted factors may regulate the niche and its size [27, 28], as well as the quiescence status of the HSCs [29]. On the other hand, there are studies underlining the importance of the vascular niche and the CXCL12-regulated migration of the HSCs to it [30]. Nevertheless, in the calvarium the osteoblastic and vascular niches are not anatomically separated; therefore, arguments regarding which niche is more influential may be only semantic [31].

1.2 The cancer stem cell hypothesis

In 1997 Bonnet and Dick provided the first conclusive evidence for the existence of cancer stem cells (CSCs). They isolated different subpopulations of human acute myeloid leukaemia (AML) stem and progenitor cells and evaluated their capacity to initiate cancer after transplantation to NOD/SCID mice. Surprisingly, they observed that the target cells responsible for the initiation of AML resided exclusively within the CD34⁺CD38⁻ compartment of HSCs and not the CD34⁺ or CD34⁺CD38⁺ subpopulations [32]. Hence, the primitive stem cells are the target of transforming events rather than committed progenitors. This concept gave rise to the CSC theory; it supports that, due to similarities that CSCs and HSCs present by means of phenotype and function, the CSCs must originate from HSCs that have accumulated mutations. Following studies on other haemopoietic and solid tumours [33] provided further evidence for the presence of a small number of CSCs that have normal stem cell characteristics, such as stable self-renewal properties, but are accountable for the initiation of cancer, metastasis and resistance to treatment [34]. However, it is still unclear if CSCs share more normal stem cell features, such as the ability to undergo asymmetric and symmetric divisions and how stable their phenotype is. On the other hand, controversies arose regarding the potential of CSCs and their origin. A number of scientists have been questioning the interpretation of the data generated from xenotransplantation experiments. They support that the proposed CSCs may not be responsible for the initiation of the disease but actually reflect populations of cells that have the ability to engraft overriding cross-species differences within stem cell niches, cytokine profiles or residual innate immunity [35]. Another hypothesis questioning the notion of CSCs, suggests that these cells could originate from progenitor or more differentiated cells that acquired mutations leading to the gain of self-renewal capacity prior or after being transformed [36]. In samples from acute promyelocytic leukaemia, a subtype of AML, the transforming oncogene PML-RARA was detected in CD34⁻CD38⁺ populations but not in the CD34⁺CD38⁻ fraction [37]. Retroviral transduction of CMPs with the oncogene MLL-ENL conferred properties of self-renewal and induced AML following transplantation into irradiated mice [38]. Similar studies in other types of leukaemia have also suggested that in some cases the leukaemia initiating cells originate from progenitors rather than primitive HSCs [39-41]. In a study performed by Huntly and colleagues, following transduction with the MOZ-TIF2 oncogene, CMPs gained capacity of serial replating and AML initiation after serial transplantation [42]. However, the authors did not record gain of similar properties in BCR-ABL-transduced GMPs.

Therefore, it seems that some, but not all, oncogenes can confer leukaemia initiating properties in committed progenitor cells.

Nevertheless, a constantly emerging list of papers keeps providing evidence in support of the CSC theory. A recent study conducted by the research group of Carlos Cordon-Cardo identified a subpopulation of cells expressing markers of embryonic development in prostate cancer patient samples that consist the core of drug resistance and tumour progression [43]. These cells had CSC properties, including tumour initiating potential, however, lacked differentiation markers and human leukocyte antigen class I (HLAI) antigens. They were also in higher percentages in patients with more aggressive or metastatic tumours. Regardless of the disputes about the origin of these cells, it is widely accepted that targeting these treatment-resistant cancer initiating cells would attack the foundation of tumour growth, and potentially offer a curative option.

1.3 CML

1.3.1 Historical overview

In 1960, Peter Nowell and David Hungerford opened a new era in cancer research by providing the first evidence for a genetic link to cancer. They discovered the hallmark of CML; a minute abnormal chromosome present in leukocytes from CML patients [44]. This chromosome, designated as Philadelphia chromosome (Ph) after the city at which it was discovered, was not found in normal leukocytes but only in malignant cells from CML patients. Since then, CML has served as a paradigm disease not only for haemopoietic malignancies but also for other types of cancer.

Interestingly, in 1973 Janet Rowley demonstrated that the Ph is the product of a translocation between chromosomes 9 and 22 [45] and a decade afterwards, it was determined that the genes involved were the breakpoint cluster region (*BCR*), whose product's function is still not clear, and the v-abl Abelson murine leukaemia viral oncogene homolog (*ABL*), coding for a tyrosine kinase. The t(9;22) translocation generated a fusion BCR-ABL protein that had lost appropriate regulation of ABL and was constitutively active and therefore, could be the cause of CML. The most rigorous evidence validating this hypothesis came from *in vivo* experiments in mice, when a series of publications demonstrated that BCR-ABL is the cause and not the result of CML, it has the ability to transform cells and is both necessary and sufficient for the development and maintenance of the disease [46-49].

The first evidence that CML is a clonal disease of stem cell origin came from Fialkow and colleagues in 1967 [50]. Following studies by the same group on female CML patients heterozygous for the X-linked gene coding for glucose-6-phosphate dehydrogenase further established the CML stem cell theory; the disease originates from Ph⁺ HSCs that have the capacity to self-renew and constitute the disease [51, 52].

1.3.2 Disease incidence, course and progression

CML has an incidence of about 1 in 50,000 per year, accounts for 15% of all adult leukaemias, and does not present with significant ethnic or geographical predisposition [53]. The median age of onset is 45 to 55 years, with the majority of patients being asymptomatic during diagnosis and discovered after routine blood tests. Presenting symptoms include weight loss, fever, splenomegaly, purpura, night sweats, abdominal fullness and gout.

CML is characterised by evolution through a biphasic or triphasic course. The majority of the cases (approximately 85%) are diagnosed during the asymptomatic chronic phase (CP) where the cells are mainly differentiated, minimally invasive and maintain their functionality [53]. If left untreated, the disease inevitably progresses after three to five years to an intermediate accelerated phase (AP) and later to BC [54]. Nevertheless, up to a quarter of patients progress directly to BC without developing the intermediate AC [55]. AC and BC are characterised by differentiation arrest and accumulation of blast cells in the blood and BM (Table 1-2) [56]. Especially during BC, there is a clonal expansion of immature population of blasts that may have developed additional cytogenetic abnormalities, and exhibit enhanced proliferation and reduced susceptibility to apoptosis. The BC transformation can be myeloid, lymphoid or both, with median survival measured in months [57].

The progression of the disease is a complex and gradual process that represents the accumulation of genetic and epigenetic alterations; these may include enhanced BCR-ABL activity following gene amplification, increased promoter activity or other less direct mechanisms, such as decreased miR-203 levels, inhibition of SHP-1 phosphatase and inactivation of PP2A [58]. Interestingly, BCR-ABL may contribute to the progression process by activating mitogenic, anti-apoptotic and anti-differentiation mediators (e.g. MYC, JAK2, hnRNP-E2, MDM2, STAT5, BMI1 and BCL2), inhibiting tumour suppressors (e.g. p53 or CEBPa), or through aberrant splicing of modulators like glycogen synthase kinase 3 beta and PYK2 [58].

Feature	CP	AP	BC
Blast % in blood or BM	<10%	10–19%	≥ 20%
Basophil % in blood	<20%	≥ 20%	NA
Thrombocytosis (×10 ⁹ /L)	≤1000 or responsive to therapy if >1000	>1000, unresponsive to therapy	NA
Thrombocytopenia (×10 ⁹ /L)	≥100 or related to therapy if <100	<100, unrelated to therapy	NA
Splenomegaly	Responsive to therapy	Persistent or increasing, unresponsive to therapy	NA
Extramedullary blast tumour (chloroma)	Absent	Absent	Present
New cytogenetic changes that develop after the initial BM karyotype	Absent	Present	NA

Table 1-2: Staging system for CML according to the World Health Organisation (WHO) Classification 2008 (NA; not applicable)

1.3.3 Diagnosis and monitoring

The disease hallmark, Ph, is found in 90-95% of CML patients, but can be also detected in patients with acute lymphoblastic leukemia (ALL) or AML [53]. Cytogenetic analysis for CML diagnosis is the gold standard method that allows for simultaneous identification of possible clonal evolution; however, it is a laborious and time-consuming technique. Moreover, 5-10% of CML patients present with cryptic rearrangements, i.e. the Ph cannot be demonstrated by cytogenetic analysis. In these cases the *BCR-ABL* fusion gene can be detected by fluorescent *in situ* hybridisation (FISH) analysis or by reverse transcriptase polymerase chain reaction analysis (RT-PCR). FISH and quantitative RT-PCR (qRT-PCR) are also used to assess the response after stem cell transplantation (SCT) or the efficacy of treatment monitoring minimal residual disease (MRD) in remission patients.

1.3.4 BCR-ABL structure

The *BCR* gene (130 kilobases; kb) codes for a 160Kd cytoplasmic protein proposed to be taking part in the antimicrobial defense of myeloid cells [59]; however, its function is still not well-defined [60]. It contains a coiled-coil (CC) oligomerisation domain [61] and a serine/threonine domain that is retained in all BCR-ABL fusion proteins. It also contains a Rho guanine-nucleotide exchange factor (Rho-GEF) homology domain, a calcium-dependent lipid-binding site, and a Rac GTPase activating protein (Rac-GAP) domain [62, 63].

The *ABL* gene (280kb) is transcribed into two alternative mRNA transcripts of 7kb (exon Ib, 2–11) and 6kb (exon Ia, 2–11) length and translated into a 145Kd protein that belongs to the non-receptor family of tyrosine kinases. ABL can be found mainly in the cytoplasm, and at lower levels in the nucleus [64, 65]. Its N-terminus includes three domains with homology to the SRC kinases (they regulate signal transduction in cell growth, differentiation and survival pathways): (i) the SRC homology domain 1 (SH1) that holds the tyrosine kinase activity and is absolutely essential for transformation and (ii) the SH2 and SH3 domains that bind phosphotyrosine and proline-rich regions respectively. It also includes sites that facilitate the binding with DNA, adaptor proteins, and actin [66-69].

Interacting proteins (Table 1-3) include amongst other the CrKL adaptor proteins and the SHPTP1 tyrosine phosphatase, a protein that interplays with the regulation of cytokine pathways [66, 70].

Binding proteins	Description
p53	Tumour suppressor protein
Rb	Tumour suppressor protein
3BP-1	SH3 domain-containing protein
3BP-2	SH3 domain-containing protein
AAP-1	ABL associated protein 1
ATM	Ataxia telangiectasia mutated protein
DNA-PK	Kinase involved in DNA repair

Binding proteins and substrates	Description
CrK-1/CrKL	SH2 and SH3 domain-containing protein
ABL-1	ABL interactor-1 protein
ABL-2	ABL interactor-2 protein
SHPTP-1	Protein tyrosine phosphatase
RNA Pol II	Large subunit of RNA polymerase II
CAS	Crk binding protein
P62-DOK	RAS-GAP associated phosphotyrosine protein

Table 1-3: ABL binding proteins and substrates

(Adapted from [71])

The native ABL activity is very low compared to the oncogenic BCR-ABL [72] and has been proposed to be enhanced by DNA damage [73, 74], progression of cell cycle to S phase [75], and cellular adhesion mediated by integrins [76].

The malignant transformation ability of BCR-ABL is related to the type of fusion. Depending on where the breakpoints occur within the *BCR* and *ABL* genes, different-sized mRNA and protein isoforms are produced (Figure 1-2). *BCR* breakpoints may occur within the major (M-bcr), minor (m-bcr) or a third region designated as the μ region (μ -bcr). In general, the longer the sequence of *BCR* is retained in the fusion, the more preferable the prognosis is. The breakpoints are widely spread at *ABL*; nonetheless, due to splicing of the primary mRNA, *BCR* is almost always fused to the *ABL* exon 2. Therefore, depending on where the breakpoints occur within the *BCR*, different sized proteins are produced that have diverse capacity to transform the haemopoietic cells and lead to different phenotypes. In CML the dominant fusion protein is the BCR-ABL^{p210}, while in ALL it is the BCR-ABL^{p185} and in chronic neutrophilic leukaemia (CNL) BCR-ABL^{p230}.

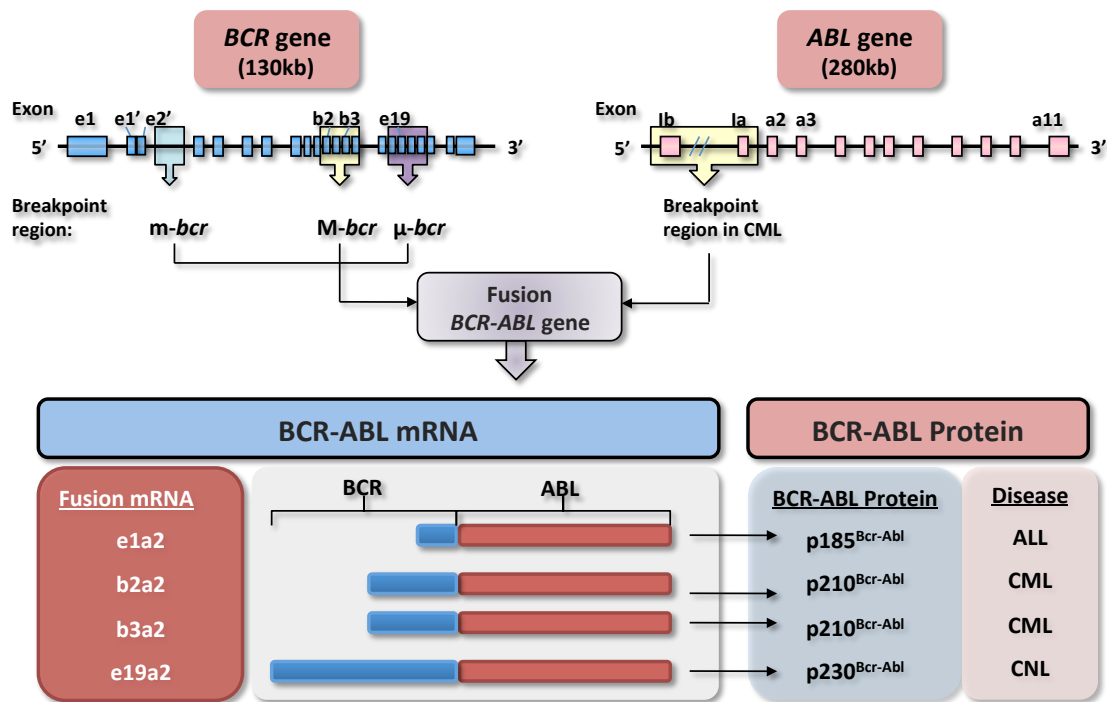


Figure 1-2: *BCR*, *ABL* structure and different fusion products

(Original figure, compiled from information within [77, 78])

1.3.5 *BCR-ABL* function

Upon demonstration that *BCR-ABL* is the cause of the leukaemogenic transformation, extensive efforts have been undertaken in order to identify its molecular mechanism of action. The constitutively active tyrosine kinase *BCR-ABL* has a large variety of targets (Table 1-4), and activates a plethora of pathways that protect the cell from undergoing apoptosis and lead to transformation, such as the RAS, PI3K, and Janus kinases (JAK)-signal transducer and activator of transcription (STAT) pathways (Figure 1-3). The apoptotic effects of cytotoxic agents are abrogated in a *BCR-ABL* positive background, not only in cell lines but also in CD34⁺ patient cells [79]. Ultimately, the combined effect of *BCR-ABL* activity results in deregulated proliferation, and inhibition of apoptosis that promote BM hypercellularity, growth factor (GF) independence and genomic instability. Moreover, the altered cellular adhesion within the compartment of Ph⁺ HSCs and HPCs lead to abnormal entry of immature cells into the peripheral blood and extramedullary tissues.

Substrate	Full Name	Function
AKT/PKB	Protein kinase B	Serine/Threonine kinase
BAD	BCL-2-associated death promoter	Pro-apoptotic
BAP-1	BCR-associated protein 1	14-3-3 protein
BCL-X_L	B-cell lymphoma-extra large	Anti-apoptotic
CBL	Casitas B-lineage lymphoma	E3-ubiquitin ligase
CrK	Avian sarcoma virus CT10 oncogene homolog	Adaptor molecule
CrKL	CrK-like protein	Adaptor molecule
FAK	Focal adhesion kinase	Cytoskeleton
GRB2	Growth factor receptor bound protein 2	Adaptor molecule
PI3K	Phosphatidylinositol 3- kinase	Phospholipid kinase
PLCγ	Phospholipase C γ	Phospholipase
RAF	RAS-activated factor	Serine/Threonine kinase
RAS	Rat sarcoma	Small G-protein
RAS-GAP	RAS GTPase-activating protein	Ras-GTPase activating
SHC	SRC homology containing protein	Adaptor molecule
SoS	Son of sevenless	Guanine nucleotide exchange factor
STAT1/5	Signal transducer and activator of transcription 1/5	Transcriptional activator
SYP	Synaptophysin	Protein phosphatase

Table 1-4: BCR-ABL substrates

(Adapted from [71] and [57])

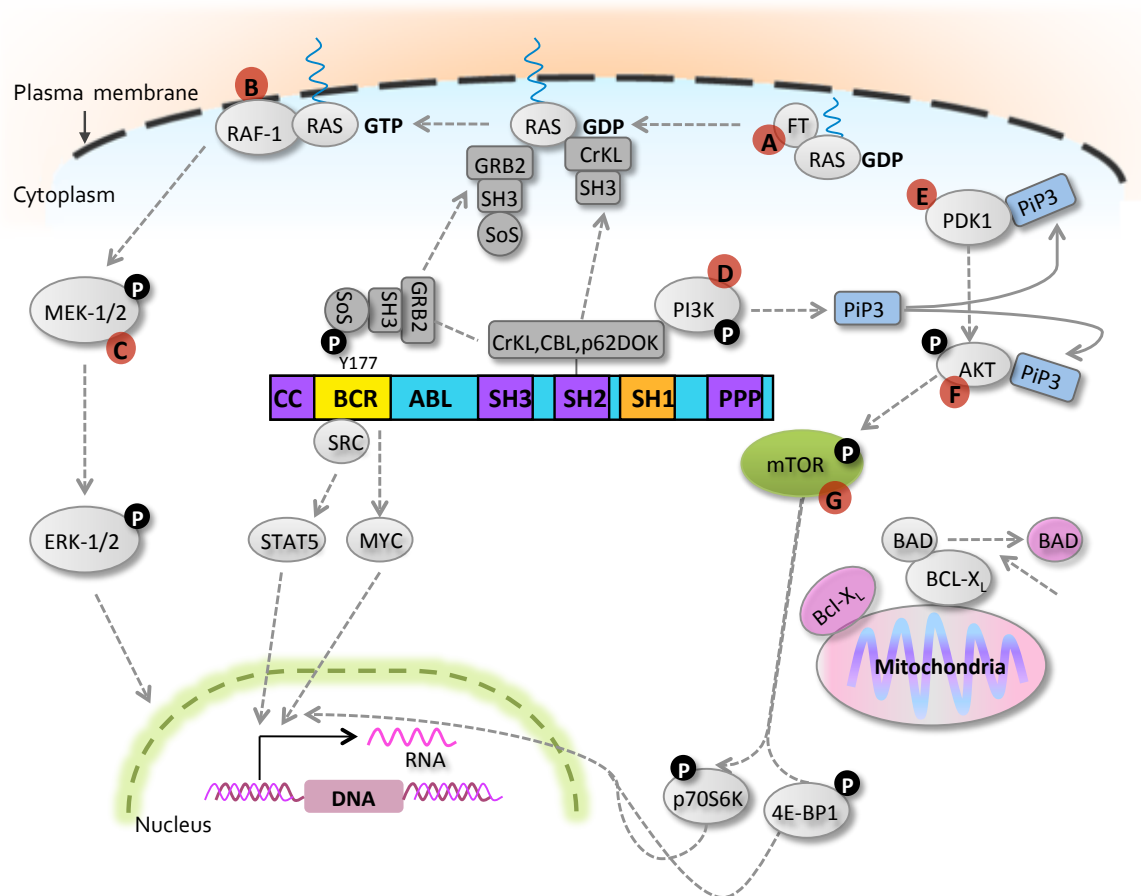


Figure 1-3: Signal transduction pathways in BCR-ABL transformed cells

BCR N-terminus includes a CC domain necessary for dimerisation, while SH2, SH3 and proline-rich region (PPP) of ABL interact with other proteins and bind adaptor proteins, such as the CrKL, forming a multiprotein complex. BCR-ABL has many downstream targets; the most important one includes the RAS–mitogen activated protein (MAP) kinase signaling cascade, which is important for the transforming activity of BCR-ABL. Other targets include PI3K, STAT5, and the MYC transcription factor that is a protooncogene. Farnesyl transferases (FT) transfer a farnesyl to the C-terminal cysteine of RAS (A), promoting its binding to the cell membrane so as to activate the serine kinase RAF (B) that subsequently activates the MAP pathway (C). PI3K produces phosphatidylinositol-3,4,5-trisphosphate (PiP3); the latter is essential for the localisation of PDK1 and AKT to the inner side of the cell membrane. Subsequently, PDK1 activates AKT (E) and AKT activates the mammalian target of rapamycin (mTOR) (F), which activates the p70S6 kinase and 4E-BP1 (G), two major global regulators of gene transcription in response to growth stimuli. *Note:* this is a simplified diagram; many more associations between BCR-ABL and other signaling proteins have been reported. (Redrawn from [77]).

1.3.5.1 The GRB2 adaptor

One of the critical events in the BCR-ABL transformation is the autophosphorylation of tyrosine 177 (Y177), a site emanating leukaemogenic signals through a mediator known as GRB2, an adaptor molecule that plays an important role in human haemopoietic progenitor transformation [80]. Mice carrying a mutation changing the 177 amino-acid from tyrosine to phenylalanine (T177F) present attenuated BCR-ABL transforming capacity and have extended life expectancy [81].

1.3.5.2 Activation of the RAS pathway

Y177 binds to GRB2 via its SH2 domain and facilitates the formation of complexes between GRB2 and SoS, leading to activation of RAS [82]. RAS refers to a family of small guanine-nucleotide-binding proteins (G-proteins) that are active when bound to GTP and inactive when bound to GDP. Chang and colleagues identified the two first members of the family, HRAS and KRAS, while studying two cancer-causing viruses, the Harvey sarcoma virus and Kirsten sarcoma virus [83]. RAS proteins sit at the beginning of a cascade of kinases known as RAS-RAF-MEK-MAPK pathway, and are deregulated in many cancers, promoting tumour growth and disease progression. GTP-bound RAS activates the serine/threonine-selective protein kinase RAF, which then phosphorylates MEK and ultimately, leads to the activation of the MAP kinase (MAPK). MAPK regulates cellular transcription and translation via indirect activation of the ribosomal protein S6 (RPS6) and interaction with a range of transcription factors.

1.3.5.3 Activation of the PI3K/AKT/mTOR pathway

The Y177/GRB2 interaction facilitates the binding of a scaffolding adaptor protein, GAB2. BCR-ABL mediated phosphorylation of the YXXM motif of GAB2 allows for interaction of the molecule with PI3K regulatory subunits and activation of the PI3K/AKT/mTOR pathway [84]. Interestingly, BCR-ABL transformation was diminished in mice lacking expression of GAB2 [84]. A recent study by Wöhrle and colleagues, provided data supporting that GAB2-mediated resistance to conventional CML treatment is partially attributed to constitutive phosphorylation of a PI3K recruitment site within GAB2 [85].

The PI3K/AKT/mTOR pathway partakes in the regulation of cellular functions such as growth, proliferation, differentiation, motility, metabolism and survival, in response to

extracellular cues mediated by cell surface receptors and G-proteins. Additionally, this pathway is activated in various cancers [86]. PI3K is an intracellular signal transducer enzyme and contains a regulatory subunit with an SH2 domain, and a catalytic subunit that catalyses the addition of a phosphate to PiP2 at the 3 position, generating PiP3. PiP3 recruits plasma pleckstrin-homology (PH) domain-containing proteins, and acts as key signaling molecule [87]. AKT is a serine/threonine-specific protein kinase that contains a PH domain and, hence, can bind to PiP3. The localisation of AKT to the membrane after binding to PiP3 allows for its activation by phosphoinositide dependent kinase 1 (PDK1) following phosphorylation at threonine 308 [88, 89].

Activated AKT phosphorylates a variety of substrates that play a vital role in BCR-ABL mediated transformation including mTOR, a serine/threonine kinase that acts as a hub for signals from insulin, GFs and amino-acids [90]. It regulates a variety of processes, including cell growth, survival, motility, protein transcription and synthesis, as well as autophagy (discussed later) [91, 92].

mTOR is the catalytic core in two complexes, mTOR complex1 (mTORC1) and 2 (mTORC2). mTORC1 contains the mTOR, the regulatory-associated protein of mTOR (RAPTOR), the mammalian LST8/G-protein β -subunit like protein (mLST8/G β L), PRAS40 and the DEP domains interactor of mTOR (DEPTOR) [93, 94]. Two important effectors of mTORC1 that mediate protein synthesis are the RPS6 kinase (RPS6K) and the eukaryotic translation initiation factor 4E-binding protein 1 (4E-BP1). Upon AKT activation, mTORC1 phosphorylates RPS6K and this facilitates its further phosphorylation and activation by PDK1 [95]. The activated RPS6K activates RPS6 to initiate protein synthesis [96] and via a positive feedback loop, it also activates mTORC1 [97]. Moreover, mTORC1 enhances protein translation by phosphorylating 4E-BP1 and promoting disassociation from the eIF4E and activation of the cap-dependent translation [98]. Recent models suggest that cancer cells dependent on AKT, actually are mTORC1 “addicted” and rely on its activity to drive tumourigenesis [99].

mTORC2 consists of the mTOR, the rapamycin (RAPA; aka sirolimus)-insensitive companion of mTOR (RICTOR), mLST8/G β L and the mammalian stress-activated protein kinase interacting protein 1 (mSIN1) [100, 101]. mTORC2 activates AKT via phosphorylation of the serine 473 [102] and also, has an important influence on the cytoskeleton by regulating actin, the focal adhesion proteins, protein kinase C α (PKC α) and the small GTPases (RHOA, CDC42 and RAC1) .

In the past it was believed that RAPA could target only the mTORC1 but not the mTORC2 or AKT. Nevertheless, a study from Sarbassov and colleagues suggests that prolonged

exposure to RAPA targets mTORC2 assembly and mTORC2-mediated AKT phosphorylation in some cell types, by reducing the amounts of available mTOR [103]. Currently, RAPA and its analogues – temsirolimus, everolimus and deforolimus- are tested in many cancer clinical trials. NVP-BEZ235 (BEZ; LC Laboratories, MA, USA) is another compound currently tested in clinical trials as a potential anti-cancer treatment. BEZ is a quinoline derivative that targets the activity of both PI3K and mTOR kinases via binding to the adenosine triphosphate (ATP)-binding cleft of these enzymes [104]. PI-103 is also a very promising dual kinase inhibitor of PI3K and mTOR [105].

Another significant substrate of AKT is the group of forkhead box class O (FoxO) transcription factors that regulate the cell cycle. Phosphorylation by AKT deactivates FoxOs and promotes cell survival, growth and proliferation [106]. Furthermore, AKT may inhibit apoptosis by phosphorylating BAD, causing it to dissociate from the BCL2/BCL-X complex [107].

The murine double minute 2 (*MDM2*) oncogene is translated into an E3 ubiquitin ligase that negatively regulates the tumour suppressor p53. It has been suggested that upon AKT phosphorylation, MDM2 represses the transcription of p53, allowing for cell death evasion [108-110].

1.3.5.4 The CrKL adaptor

In 1994, Hovee and colleagues identified CrKL, a 38Kd adaptor protein of BCR-ABL in CML cells, that could also interact with native ABL [111]. CrKL contains an SH2 domain, two SH3 domains and has no catalytic domain [112], and was shown to be the major BCR-ABL phosphorylated protein in neutrophils from CML patients' peripheral blood samples [113]. Later on, it was demonstrated that BCR-ABL phosphorylated CrKL on tyrosine 207 (T207) [114]. Subsequently, the phosphorylated CrKL can form different complexes; through its SH2 domain it binds the CBL protein, and with its SH3 domain the BCR-ABL [115]. Even if the function of CrKL has not been elucidated yet, it has been proposed that it can bind through its SH3 domain to PI3K [116] and, in that way, exert its leukaemogenic effects. It has been also proposed that it contributes in integrin-mediated cell adhesion through binding focal adhesion proteins such as paxillin [117].

CrKL is a prominent substrate of BCR-ABL [118] and has been extensively used as a marker of BCR-ABL activity in western blot [119] and FACS assays in primitive CML cells from patients [120].

1.3.5.5 Activation of the JAK-STAT pathway

JAKs are intracellular tyrosine kinases that mediate signals from receptors activated by cytokines. Upon binding of the ligand to the receptor, JAKs are activated and subsequently, activate the receptor. Phosphorylation of the receptor's tyrosine residues by JAK allows for interaction with SH2 domain containing proteins, such as the STAT family. These proteins bind to the receptors and after JAK-mediated activation, form dimers and translocate to the nucleus where they regulate the transcription of their target genes [121].

The JAK-STAT pathway is highly upregulated in CML cells [122, 123] and one of its mediators, STAT5, has been suggested to be an essential factor in the BCR-ABL mediated leukaemogenesis [124, 125] partially by inhibiting apoptosis via regulation of BCL2 family members, such as the induced myeloid leukaemia cell differentiation protein (MCL-1) and BCL-X_L [126, 127]. *In vivo* experiments in mice underline the critical role of Stat5 in Bcr-Abl mediated CML initiation and maintenance [124, 125]. Interestingly, apart from its role in cell transformation, STAT5 may also contribute to the development of resistance and disease progression in a JAK-independent manner [128]. Introduction of dominant-negative JAK mutants in BCR-ABL expressing cells did not suppress phosphorylation of STAT5, proposing that BCR-ABL could activate STAT5 through other mediators [122], such as the haemopoietic cell kinase (HCK) [129].

1.3.5.6 BCR-ABL growth factor mimicking

Interleukin-3 (IL-3) and the granulocyte colony stimulating factor (G-CSF) are GFs that bind to HSC receptors and, following activation of pathways such as the RAS, PI3K and JAK-STAT, promote differentiation and proliferation [130, 131]. While normal HSCs cannot survive and proliferate in the absence of GFs [16, 17], transformed quiescent primitive cells from CML patients can grow and proliferate *in vitro* in a GF-independent manner [132]. BCR-ABL positive cells override dependence on external supplementation of GFs for their survival and proliferation by promoting an aberrant autocrine loop production of IL-3 and G-CSF [132, 133] in early progenitor cells that could deregulate critical cell cycle mediators [134] and lead to exit from quiescence [133]. Transplantation of BM cells genetically manipulated to produce IL-3 lead to the development of myeloproliferative disorders in a mouse model [135-137], highlighting the consequences of GF deregulations. Hence, the BCR-ABL mimicking of physiologic GF stimulation

could be responsible for a significant part of the leukaemic transformation, potentially through activation of STAT5 [134].

1.3.5.7 BCR-ABL alteration of the niche

As described earlier, normal HSCs express on their surface receptors that bind ligands secreted from niche cells and, following adhesion to the niche, promote cell cycle arrest [25]. For instance, mice carrying mutations within the tyrosine kinase domain of TIE2 receptors that bind angiopoietin, or the myeloproliferative leukaemia virus oncogene receptor that binds thrombopoietin (TPO), lead to HSCs detachment from the niche, increased cycling, and finally, HSC exhaustion [29, 138]. Integrins refer to another class of receptors that mediate the adhesion of HSCs to the stroma [139] and simultaneously, promote cell cycle arrest [140]. A possible explanation for the increased proliferation and circulation of CML stem and progenitor cells could be that they have altered adhesion properties compared to normal HSCs [2, 141, 142]. In support of this hypothesis are data that demonstrate suppression of CXCR4 expression in BC CML patient samples and evasion of adhesion [143]. Drug-mediated inhibition of the kinase activity of BCR-ABL in primitive CML cells co-cultured with mesenchymal stem cells (MSCs) leads to upregulation of CXCR4, followed by migration of the CML cells to the BM, cell cycle arrest and, ultimately, survival of quiescent CML progenitor cells [144].

1.3.6 CML treatment

1.3.6.1 Historical treatment of CML

One of the first attempts to treat CML was published by Sir Arthur Conan Doyle in 1882, when he was a practising physician in Birmingham. He administered iron and quinine to a 29-year-old patient with “leucocythaemia”, the term used for CML at the time, because he thought that the symptoms were attributed to a previous attack of malaria. After seeing no effect, he used arsenic; 1% solutions of arsenic trioxide, aka Fowler’s solution, that had been used since 1786 for malaria patients and diseases involving fever and shivering [145]. However, arsenic was used for the treatment of leukaemias since ancient times; it was used by Hippocrates (460-370 before Christ), who gave cancer its name from the Greek word “καρκίνος” (carcinus) for crab [146]. The Fowler’s solution was reported to improve the clinical condition of CML patients but the effects lasted only for a short period of time [145]. In 1903, with the introduction of radiotherapy, treatment of CML patients included

frequent X-ray sessions, with or without the oral administration of benzene. The therapeutic response to radiotherapy was great, nevertheless, soon after radiation was linked to the development of leukaemia.

Surprisingly, the way to chemotherapy was opened by a warfare agent used during World War I, known as “mustard gas”; soldiers exposed to this gas presented very low white blood cell counts. Analogues of the sulphur compound contained in the gas were then produced for the treatment of CML. Their clinical use showed improvement of the treatment but not prolongation of survival [145]. Additionally, such compounds had substantial toxic effects. In 1953, busulphan, an oral alkylating agent, was introduced for the treatment of CML. Nonetheless, it was also associated with severe side effects [147]. By that time, CML was regarded as a fatal and incurable disease. Nevertheless, in the 1980s the scene changed when allogeneic BM transplantation (BMT) and SCT, that had been previously proven effective for acute leukaemia patients [148], were used as a curative potential for CML patients [149]. Despite their auspicious effects, BMT and SCT could be offered only to 20% of CML patients due to limitations such as age, physical condition and matched donor availability [150]. Additionally, up to 72% of low-risk CML patients had a 5-year survival but this percent dropped dramatically to 20% in high-risk patients that had approximately 73% mortality [151]. Additionally, due to the nature of the procedure, allogeneic SCT patients were facing an increased risk of morbidity and mortality due to infections, mucositis, graft failure or graft-versus-host disease [152, 153]. In the 1980s, the cytokine interferon α (IFN α) offered an alternative less toxic treatment for the management of CML, attenuating the disease symptoms, and prolonging life expectancy. Moreover, many patients appeared to be Ph negative following IFN α treatment and presented with a lower rate of blastic transformation [154]. Later, it was suggested IFN α mediated restoration of haemopoiesis could be attributed to recovery of adhesion of CML progenitors to the BM stroma [155].

1.3.6.2 The development of IM

In the 1990s Nicholas Lydon and Brian Druker, based on rational drug design, developed a BCR-ABL TKI called IM (STI571, Gleevec®, Glivec®, formerly CGP 57148B; Novartis, USA). IM binds competitively to the N-terminal region of the ATP-binding pocket of the inactive form of ABL [156]. IM binding to BCR-ABL stabilises the inactive conformation and inhibits autophosphorylation. Therefore, IM blocks the kinase activity and the subsequent phosphorylation of key downstream substrates. Moreover, IM targets the c-KIT and PDGF receptors [157]. The specificity of IM against BCR-ABL positive cell lines and

patients samples was demonstrated *in vitro* and *in vivo*, with minimal toxicity to BCR-ABL negative cells [156, 158]. With half maximal inhibitory concentration (IC50) IM within the range of 0.1–0.5 μ m, IM inhibits BCR-ABL activity and proliferation, promoting apoptosis of CML cells [46].

In 1998 an IM dose-escalating phase I trial was initiated with doses ranging from 25 to 1000mg per day; out of the 54 patients receiving doses higher than 300mg/day, 53 achieved complete haematologic response (CHR), 29 cytogenetic response (CyR), 17 of which presented major responses (0-35% Ph+ metaphase cells) [119]. Furthermore, a phase II clinical trial evaluated the effect of IM on late CP CML patients that had previously failed IFN α ; 95% of the patients achieved major cytogenetic response (MCyR) and, after a median follow-up of 18 months, in 89% of the patients disease had not progressed to AP or BC [159]. In order to assess the efficacy of IM versus the standard therapy for CML CP patients at the time, a combination of IFN α with cytarabine (a chemotherapeutic agent that inhibits DNA synthesis), a phase III International Randomized Study of Interferon and STI571 (IRIS) was launched in 2000, recruiting 1106 patients from 16 countries [160]. In this randomised trial, patients in the IM group were receiving 400mg/day while patients in the IFN α group received gradually increasing doses of IFN α , and once the maximum tolerated dose was achieved (up to 5×10^6 U / m² body surface area / day), patients received subcutaneously cytarabine (up to 40 mg / day) for 10 days every month. A median follow-up of 19 months revealed that McyR rates were higher in the IM group (IM; 87.1% versus IFN α plus cytarabine; 34.7%), as well as complete CyR (IM; 76.2 versus IFN α plus cytarabine; 14.5). IM was also better tolerated, and was associated with decreased rates of disease progression. In May 2001, IM received approval by the United States Food and Drug Administration (FDA) for the treatment of Ph+ CML [161].

The 6-year data from the IRIS study further underlined the supremacy of IM; patients on IM had an estimated event-free survival (EFS) rate of 83%, estimated rate of freedom from progression to AP and BC of 93%, and estimated overall survival (EOS) of 88%, or 95% when only CML-related deaths were taken into account [162]. The importance of achieving a quick IM response (within the first 24 months after initiation of treatment) has been highlighted during recent years since it has been associated with increased life expectancy, comparable to the general population [163]. Therefore, it could be disheartening that almost a quarter of newly CP diagnosed patients in the IRIS trial did not achieve complete CyR within the first 18 months of treatment [160]. Nevertheless, the efficacy of IM was superior to any previous treatment, taking into account BMT and SCT

[164]. Hence, IM is since then used as a first-line treatment for newly diagnosed CP CML [161, 162, 165].

1.3.6.3 IM responses

Even if IM has an effect on the majority of CP patients, once the disease progresses to AP or BC, it has little or no effect. Another major drawback of IM involves the development of resistance. Data from 5-year follow up of CML patients receiving IM, showed that in 7% of the patients the disease had progressed to AP or BC, 2% of which had initially achieved a complete CyR response and a reduction of <3 -log in levels of BCR-ABL transcripts at 18 months [166].

A framework of guidelines and recommendations by the European LeukaemiaNet (ELN) [80] and National Comprehensive Cancer Network (NCCN) [82] has been provided for the evaluation and classification of patient responses to optimal, suboptimal or failure. Criteria refer mainly to the achievement of endpoints based on haematological, cytogenetic and molecular responses within specific time after the initiation of treatment (Table 1-5). An optimal response usually refers to a 2-log reduction in BCR-ABL transcripts by 3 months [167] and/or major molecular response (MMR) (3-log reduction in BCR-ABL transcripts), by 12 months [168]. However, responses from patients on 400mg IM daily that do not achieve CHR by 3 months or complete CyR by 12 months are classified as failure, or primary resistance. Secondary resistance refers to patients that initially responded to IM but later lost established CHR, complete CyR, or the disease progressed to AP or BC [77], and can be caused by various reasons, with most prominent the development of point mutations within the BCR-ABL kinase domain [169].

In the past, a suboptimal response was described as the failure to achieve 1-log reduction of BCR-ABL transcripts by 6 months or a 2-log reduction by 12 months [167]. On the other hand, recently it was demonstrated that the frequency of suboptimal responders may be higher than initially estimated; 4, 8 and 40% of CML patients on 400mg/day after 6, 12 and 18 months, respectively, fulfilled the suboptimal response criteria [170]. Nonetheless, identification and classification of suboptimal responses still remains unclear. By 6 months of treatment, suboptimal responders have EFS comparable to patients with primary resistance. Therefore, it is harder to decide in clinic the best treatment alternative for suboptimal responders.

Response	Criteria
CHR	Complete normalisation of peripheral blood count; Leukocyte count $<10 \times 10^9$ cells/L Platelet count $<450 \times 10^9$ cells/L No immature cells in the peripheral blood No signs or symptoms of disease including splenomegaly
Partial haematologic response	Same as those for CHR, except: Persistence of immature cells, or Platelet count $<50\%$ of the pre-treatment count but $>450 \times 10^9$ cells/L, or Persistent splenomegaly but $>50\%$ of the pre-treatment extent
Complete CyR	No Ph+ cells detectable by cytogenetics in the BM
Partial CyR	1-34% Ph+ cells detectable in the BM
MCyR	$<35\%$ Ph+ cells detectable in the BM (includes complete and partial CyR)
Minor CyR	35-90% Ph+ cells detectable in the BM
Complete molecular response (CMR)	Undetectable BCR-ABL transcript by qRT-PCR, or ≥ 4.5 log reduction compared to starting level
MMR	≥ 3 log reduction of BCR-ABL transcript, or $<0.1\%$ BCR-ABL transcript by qRT-PCR

Table 1-5: Criteria of treatment responses in CML

1.3.6.4 Molecular persistence

Despite the superiority of IM versus the combination of IFN α with cytarabine in achieving complete CyR, only 4% of the IM treated patients achieved CMR [168]. The majority of the patients in the IM arm had detectable BCR-ABL transcripts, which means that a leukaemic clone managed to escape treatment and lead to MRD. The question that subsequently arose was, if IM had eradicated all leukaemic clones in patients with CMR. Therefore, the STIM [171] and the Australian [172] studies were launched. In the STIM study IM was discontinued in 69 patients who had been in CMR for at least 2 years.

Approximately 58% of these patients relapsed within the first 6 months. Similarly, in the Australian study, it was demonstrated that even patients that maintained CMR after IM cessation, harboured residual leukaemia. These observations support the hypothesis that a fraction of leukaemic stem cells (LSCs) is refractory to IM and replenishes the disease upon drug withdrawal, leading to relapse.

The inability of IM to target the persistent fraction of LSCs can be attributed to the quiescent status of these cells. It has been suggested that CD34+ Ph+ cells could be inherently insensitive to IM, since they manage to survive 10 times higher concentration (10 μ M) than the inhibitory concentration (1 μ M), unlike more differentiated cells [173]. Analysis of the reduction rates of BCR-ABL transcripts with a mathematical model suggests that this process is biphasic [174]. During the first phase there is a rapid decrease in transcripts, representing the elimination of Ph+ progenitors and more committed cells. However, the following second phase is much slower and illustrates the inaccessibility of LSCs to IM. Hence, the restored haemopoiesis upon IM treatment seems to be attributed to the suppression of the proliferative capacity of these cells rather than their elimination [175].

1.3.6.5 Mechanisms of resistance

The diverse mechanisms of resistance development against IM were first studied in BCR-ABL positive cell lines following prolonged treatment to progressively increasing doses, from suboptimal concentrations up to 1mM [176-178]. Resistance mechanisms can be versatile, as depicted in Figure 1-4.

1.3.6.5.1 Mutations affecting the BCR-ABL kinase domain

The major cause of IM resistance involves the development of point mutations that prevent efficient IM binding [179]. More than 100 mutations have been identified so far, the development of which is attributed to the genomic instability that BCR-ABL is promoting via DNA damage and impairment of the repair mechanisms [180]. These mutations can affect directly IM contact positions or indirectly, by occurring within sites that destabilise the inactive conformation of BCR-ABL, and impair access of IM to the ATP-binding site [181]. Depending on their proximity to the kinase domain and other factors, these mutations can induce from moderate to severe resistance with significantly increased IM IC50 values compared to native BCR-ABL positive cells [182, 183]. The first identified

IM resistance mutation leads to an exchange of threonine at position 315 to isoleucine (T315I), and until today, BCR-ABL^{T315I} remains the most troublesome mutant, associated with a highly aggressive phenotype and poor outcome [184-186].

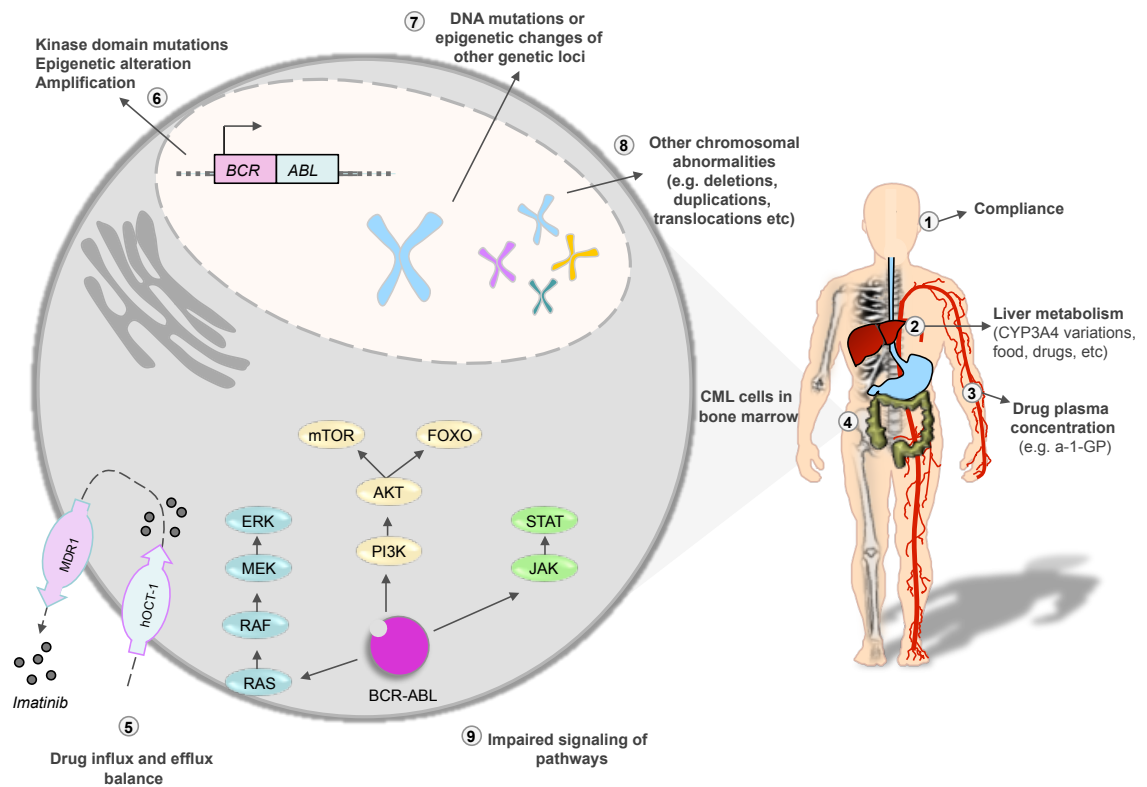


Figure 1-4: IM resistance mechanisms

IM resistance can be attributed to a plethora of causes that vary from patient compliance (1) to the metabolism and bioavailability of the drug (2,3,5), as well as the development of genetic modifications (6,7,8) and alterations in the signaling pathways downstream of BCR-ABL (9). (a-1-GP: a-1-acidglycoprotein; hOCT-1: human organic cation transporter-1; MDR1: multidrug resistance-associated membrane transporter). (Redrawn from [187])

1.3.6.5.2 BCR-ABL overexpression

BCR-ABL gene amplification and protein overexpression were demonstrated to cause IM resistance in cell lines [176-178] and patient samples [184, 188]. A possible explanation could be that the amount of IM within the cell is not sufficient for the inhibition of BCR-ABL, and this residual activity allows the clone to survive and proliferate. On the other

hand, it has been suggested that high levels of BCR-ABL promote genomic instability and this, leads to the development of mutations that ultimately lead to the development of resistance. In a study performed by Tang and colleagues it was observed that BCR-ABL overexpression is essential for the development of mutations within the kinase domain [189]. However, such observations were not made in CML patient samples; out of the 66 patients only two were identified with *BCR-ABL* gene amplification and the rest carried kinase domain mutations [190]. Nevertheless, it should be underlined that high levels of BCR-ABL are toxic for the cells. The first step in the development of resistance could be overexpression of BCR-ABL that subsequently, leads to the development of a kinase domain mutation. Therefore, the initial overexpressing clone would die and would not be detected in the samples, while a lower BCR-ABL expressing clone carrying the mutation would have a growth advantage and drive the resistance [189].

1.3.6.5.3 BCR-ABL-related epigenetic modifications

BCR-ABL has been proposed to promote epigenetic alterations by hyperacetylating histone H4 [191]. Moreover, IM resistant cell lines have been proposed to have distorted balance between histone deacetylases (HDACs) and histone acetyltransferases (HATs) that subsequently, lead to abnormal acetylation of key proteins, like Hsp90 and p53 [192].

Another hypothesis supports that IM may be able to target Ph⁺ cells only when in a specific epigenetic differentiated cell state. Carette and colleagues generated induced pluripotent stem cells (iPSCs) from a *BCR-ABL* oncogene addicted CML cell line and, surprisingly, after reprogramming the cells became resistant to IM and did not depend on BCR-ABL on survival [193].

1.3.6.5.4 Clonal evolution & activation of alternative signaling pathways

BCR-ABL independence implies that the cells have acquired additional mutations and do not exclusively rely on BCR-ABL for survival. The development of chromosomal abnormalities in addition to the Ph, known as clonal evolution, is considered to be a poor prognostic factor. Such abnormalities are associated with genomic instability and include, for instance, inactivation of p53 and overexpression of c-MYC and BCR-ABL as a result of isochromosome 17, trisomy 8 and duplication of the Ph, respectively [179, 194, 195].

Alterations in various cellular pathways and mechanisms can also be responsible for BCR-ABL-independent aberrant growth and survival. SRC activation has been suggested to

have a significant impact on disease progression, even in cases where IM has effectively suppressed BCR-ABL protein expression to undetectable levels [196]. For instance, LYN, an SRC related kinase, has been found to be abnormally overexpressed and activated in IM resistant cells that carry native, unmutated *BCR-ABL* and IM is efficiently suppressing BCR-ABL activity. Interestingly, inhibition of LYN in these IM-resistant cells reduced proliferation and survival while it didn't have an effect on IM sensitive cells [197].

Another counter-regulatory mechanism relevant to BCR-ABL independent IM resistance involves the adaptive autocrine secretion of the granulocyte macrophage colony-stimulating factor (GM-CSF) via activation of the antiapoptotic JAK2/STAT5 pathway. JAK2 inhibition managed to override GM-CSF-induced IM resistance [198]. Additionally, it has been suggested that high levels of STAT5 can drive TKI resistance in a JAK2 independent manner [128]. It has been also proposed that extended IM treatment can lead to epigenetic silencing of *PTEN*, followed by aberrant activation of the PI3K/AKT pathway and STAT5 signaling [199, 200].

1.3.6.5.5 Pharmacokinetics & drug delivery issues

Changes with regards to the distribution of IM, such as diminished delivery, can result in suboptimal intracellular drug concentrations and development of resistance. This can be attributed to dysfunctioning drug import and export pumps on the target cell membrane, as well as deregulated plasma proteins and enzymes.

ATP-binding cassette sub-family B member 1 (ABCB1) transporter, aka MDR1, is a transmembrane glycoprotein that belongs to the ATP-binding cassette sub-family (ABC). ABC transporters use the energy of ATP hydrolysis to open/close ion channels of proteins, including themselves, and have also been suggested to carry out other functions, such as translation of RNA and DNA repair [191]. It was proposed that ABCB1 upregulation could lead to the development of resistance due to increased drug efflux [201]. Nevertheless, later studies from our lab demonstrated that ABCB1 inhibition did not lead to increased intracellular IM concentrations [202]. Moreover, it was illustrated that ABCB1 activity is very low within the CD34+ fraction, and this could explain why inhibition of ABCB1 did not sensitize these cells to IM.

It has been suggested that concentrations of bioavailable IM can be significantly reduced after binding to plasma proteins, such as the α -1-GP. This displacement affects the pharmacological efficiency of IM and reduces its antileukaemic activity in mouse models [203]. A positive correlation between α -1-GP and IM plasma levels was also established in

the total of 19 CP, AP and BC CML patients. Clindamycin (CLI) is an antibiotic that can compete with IM for binding to a-1-GP *in vitro*, and its administration to five CML patients resulted in rapid decrease of IM plasma levels [204]. Nevertheless, published data from our lab support that normal a-1-GP at supra-physiological concentrations, or CML-derived a-1-GP, do not inhibit the IM effect on the proliferation of Ph⁺ cells *in vitro* [205]. Another membrane transporter that has been associated with IM resistance is the hOCT-1. In 2004, Thomas and colleagues first demonstrated that inhibition of hOCT-1, but not hOCT-2 or hOCT-3, reduced IM uptake in CML cells [206]. Furthermore, it was illustrated that patients with high hOCT-1 expression levels before the initiation of IM treatment, presented higher responses associated with higher rates of complete CyR, EFS and EOS [207]. Recently, the same group identified that the hOCT-1 single nucleotide polymorphism (SNP) M420del is associated with less favorable IM responses, further supporting the importance of hOCT-1 in IM treatment [208].

The amount of IM available depends not only on the equilibrium between influx and efflux, but also on the rate of its biotransformation. CYP3A (cytochrome P450, family 3, subfamily A) is a hepatic enzyme that metabolises IM to its active form via N-demethylation. Data from a pilot study on *in vivo* CYP3A activity in 14 CML patients support that elevated levels of CYP3A are associated with better responses, probably because this allows for higher amounts of bioavailable IM [209]. Factors that alter CYP3A levels or function, such as gene polymorphisms, interaction with other drugs or food habits, may affect IM responses.

1.3.6.5.6 Compliance

Patient compliance is another crucial parameter affecting IM responses. A study on 169 CML patients revealed that there is a strong correlation between patient adherence and the achievement of MMR and CMR [210]. Poor compliance has been associated with suboptimal response since patients with adherence < or = 80% did not respond at molecular level. This hypothesis has been further validated in a following study on 87 patients, where compliance was monitored by a microchip incorporated at the prescription bottle for pill counting, over a period of 3 months [211]. Data supported the direct association between adherence and treatment response; strong compliance has been linked to high rates of achieving CMR, while poor compliance with suboptimal responses.

1.3.6.6 Strategies to override resistance

1.3.6.6.1 IM dose escalation

A first approach in order to overcome resistance issues was escalation of IM doses. Such an escalation could be beneficial in cases of BCR-ABL overexpression and/or *BCR-ABL* amplification, as well as mutations that are susceptible to higher doses of IM. Moreover, during the phase 1 dose-escalating trial of IM, a dose-response effect was noticed. In 2003 Kantarjian and colleagues published a study based on 54 CML CP patients that had been previously treated with IM at 400mg/day and had developed resistance or relapsed [212]. These patients were treated with up to 800mg/day; 65% of the patients with haematologic resistance or relapse and 56% of those with cytogenetic resistance or relapse achieved partial or complete haematologic and cytogenetic responses, respectively. In another study, IM dose was increased to 800mg/day in 84 CML CP patients that had failed IM at 400mg/day [213]. Complete CyR was achieved in 52% of the patients with cytogenetic failure and 5% of those with haematologic failure, and maintained in 88% of the patients beyond 2 years.

1.3.6.6.2 Second-generation TKIs

In an effort to override IM resistance, second generation TKIs were developed. DAS and NIL allow for more effective binding with BCR-ABL and can target mutant BCR-ABL forms that are not inhibited by IM.

1.3.6.6.2.1 *DASATINIB*

DAS (Sprycel®; formerly BMS-354825, Bristol-Myers Squibb, NY, USA) is a multi-targeted kinase inhibitor with specificity against the SRC and ABL kinases, as well as c-KIT and PDGF-R [214]. DAS has much higher affinity for ABL than IM and can target both its active and inactive conformations [169]. DAS is >300-fold times more potent than IM against cells expressing native BCR-ABL, and can target the majority of the IM-resistant BCR-ABL isoforms harbouring mutations, with the exception of the T315I [215, 216].

In 2008, Hochhaus and colleagues released the data from a phase II trial evaluating the efficacy of DAS in 387 CML CP patients resistant or intolerant to IM [217]. After a median follow-up of 15.2 months, 91% of patients receiving 70mg DAS twice daily

attained or maintained a CHR, 59% attained or maintained a MCyR, from which 49% achieved complete CyR. Following, the clinical efficacy of DAS in newly diagnosed CML patients was evaluated in the DASISION trial [218]. In DASISION, 519 CML CP patients were recruited and randomised between two treatment arms, 100 mg DAS versus 400 mg IM per day. After a minimum follow-up of 12 months, patients on DAS achieved significantly higher and faster rates of complete CyR (DAS 77% vs IM 66%; $p = 0.007$) and MMR (DAS 46% vs IM 28%; $p < 0.0001$). In 2006, DAS gained approval from FDA for the treatment of newly diagnosed adult Ph⁺ CML and ALL patients and patients who have previously found to be resistant or intolerant to prior therapy.

Nevertheless, the efficacy of DAS at more progressed disease stages, in AP and BC patients, was limited; responses were poor and not long lasting [219, 220]. Additionally, like IM, DAS was efficient in targeting CML progenitors and more differentiated cells, however, failed to eliminate the persistent fraction of the quiescent leukaemic stem cells [221].

1.3.6.6.2.2 NILOTINIB

NIL (AMN107; Tasisa, Novartis, Switzerland), is a BCR-ABL TKI, that structurally resembles to IM, but carries a modification in a methylpiperazinyl group that allows for higher affinity to the inactive conformation of ABL [222]. NIL exhibits >20 times higher potency than IM [223], and can target *in vitro* all the BCR-ABL mutants whose conformations are inaccessible to IM, with the exception of the BCR-ABL^{T315I} isoform [215, 224].

The clinical efficacy of NIL was underlined in the ENESTnd trial, where NIL at 300mg or 400mg twice daily was associated with better responses compared to IM at 400mg daily. A median 24-month follow up revealed that 71% patients at the NIL arm achieved MMR versus 44% at the IM arm [225]. In 2010, NIL received FDA approval for the treatment of adult patients with newly diagnosed Ph⁺ CP CML. However, NIL, like IM and DAS, cannot eliminate the persistent population of LSCs [226].

1.3.6.6.3 Third-generation TKIs

1.3.6.6.3.1 Ponatinib

PON (AP24534; ARIAD, MA, USA) is a third generation pan-BCR-ABL inhibitor that can target all BCR-ABL mutants, including the BCR-ABL^{T315I}, as well as FLT3 and SRC kinases [227]. The toxicity and safety of the clinical use of PON were explored in a phase I trial focused on CML patients that had previously failed a minimum of two TKIs. PON was well tolerated and associated with superior responses; 98% of the CML CP patients had a complete haematologic response, 72% had a MCyR, and 44% had a MMR [228]. Therefore, a phase II Ponatinib Ph+ ALL and CML Evaluation (PACE) trial was launched in September 2010 [229]. During the PACE trial, CP (271 patients) and AP (79 patients) CML patients that resistant or intolerant to DAS or NIL or harbouring the T315I mutation were receiving PON 45mg daily and the results were very encouraging. In July 2012, ARIAD announced the initiation of the phase III Evaluation of PON versus IM in CML (EPIC) trial that will compare the efficacy of PON with that of IM in the treatment of adult patients with newly diagnosed CP CML [230].

1.3.6.6.3.2 Bosutinib

Bosutinib (SKI-606; Pfizer, NY, USA) is a dual inhibitor of ABL and SRC, targeting simultaneously c-KIT and some PDGF receptor members. Bosutinib is currently tested in a phase III clinical trial.

1.3.6.6.4 Investigational agents

Aurora kinases are serine/threonine kinases that play an active role in mitosis and their deregulation has been associated with many cancers. These enzymes are being considered for treatment of CML since they inhibit, among many targets, ABL. Allosteric inhibitors that selectively target BCR-ABL, like GNF-5, are also under investigation [231]. A novel approach in inhibiting ABL refers to a class of molecules, known as “switch pocket inhibitors”, such as DCC-2036 (Deciphera, KS, USA) [232]. DCC-2036 exerts its effects by binding to two amino acids in the switch pocket of ABL that are necessary for the shift of BCR-ABL from the inactive to the active form.

Anti-CML vaccines have also been tested for the treatment of patients. Recent studies suggest that BCR-ABL is not a strong immunogen; therefore, research is focused on developing vaccines from other immunogens, such as WT1, PRTN3, HMMR, PRAME, SPAG9, AURKA, IL1RAP and BMI1 [233].

1.3.6.6.5 Combination approaches for the elimination of the persistent CML stem cells

As described above, TKIs fail to eradicate the fraction of primitive LSCs that persist and replenish disease. Recent studies by our lab and others, demonstrated that the LSCs may not be oncogene addicted [234, 235]. In such a scenario, TKIs will be completely ineffective in targeting these cells since their survival will not be affected by the absence of BCR-ABL initiated signals. Therefore, rational strategy would involve the combinational targeting of these cells with TKIs and other agents that target vital pathways for the survival of LSCs. Combinational approaches could also have an inhibitory effect on disease progression since this process is mainly relying on the development of secondary BCR-ABL independent changes such as, activation of alternative pathways and epigenetic alterations [58].

There is a series of studies investigating the benefits from the combination of IM with alternative reagents. For instance, HDAC inhibitors in combination with IM have been demonstrated to induce apoptosis in quiescent IM resistant CML progenitors *in vitro*, while *in vivo* administration of IM and HDAC inhibitors eradicated the LSC population in a mouse model [236]. Moreover, Preudhomme and colleagues demonstrated that the combination of peginterferon α -2a (90 μ g weekly) and IM (400mg daily) was superior to IM treatment alone (at 400mg daily) [237]. Patients presented significantly higher rates of superior molecular response (reduction of 4 log units or more from the baseline level) in the combination arm (30%) versus IM alone (14%) (P=0.001).

Metabolic modulators have also been tested in combination with IM. Arachidonate 5-lipoxygenase (ALOX5) is an enzyme that takes part in transforming essential fatty acids into leukotrienes and has been proposed to be essential for the maintenance of LSCs. *In vivo* experiments in a murine model demonstrated that BCR-ABL could not induce CML in an Alox5 deficient background [238]. Based on these data, a phase I trial has been launched in order to evaluate the clinical efficacy of IM in combination with zileuton, an ALOX5 inhibitor.

Another pathway that has been suggested to be vital for the self-renewal of LSCs is the Hedgehog pathway. Loss of Smoothened (SMO), a vital Hedgehog pathway mediator,

leads to targeting of the leukaemia initiating CML stem cells and targets their ability to proliferate and induce the disease [239]. A phase II trial is currently investigating the combination of a SMO inhibitor with DAS in CML CP patients.

1.4 Autophagy

In 1963, de Duve introduced the term autophagy - from the Greek words *αυτό* (self) and *φαγία* (eating) - a cell survival lysosomal pathway used by eukaryotes to degrade and recycle cellular components, such as aged proteins and organelles, in order to recoup ATP and essential building blocks during nutrient and/or oxygen deprivation [240]. For a long time autophagy was regarded solely as a stress-induced cellular recycling mechanism. Nevertheless, research during the last 10 years has revealed the multifaceted role of autophagy; this process takes place in virtually all mammalian cells, from oocytes to neurons, and ensures homeostasis and quality control. Autophagy can target bulk cytoplasm or selective cargo, clearing damaged mitochondria (mitophagy) or peroxisomes (pexophagy). Additionally, autophagy takes part in various cellular processes such as ageing, inflammation, innate and acquired immunity, as well as differentiation [241]. Impairment of autophagy has been associated with the development of many diseases, including cancer.

There are three different types of autophagy. Chaperone-mediated autophagy is a secondary response to nutrient starvation; cytosolic proteins tagged with a pentapeptide motif are transferred to the lysosomes and afterwards unfolded with chaperones' mediation. On the other hand, during microautophagy cytoplasmic components are recruited directly on the lysosomal membrane, which subsequently gets introverted and/or segmented.

Macroautophagy, is the most efficient autophagic clearance mechanism and the most common type of autophagy, therefore, hereafter macroautophagy will be referred to as autophagy. Through this process, cytoplasmic components are being delivered to the lysosomes for degradation after inclusion in *de novo* constructed double-membrane vesicles, the autophagosomes [242]. These formations are derived from the phagophores (aka isolation membranes), cup-shaped membranes, which are generated after the induction of autophagy. As the phagophores expand, they segregate cytoplasm and finally isolate it upon their structural completion [243]. The autophagosomes slide along cytoskeletal structures and fuse with lysosomes, generating the autophagolysosomes. Degradation of the included components and the inner autophagosomal membrane follows.

Autophagy is regulated by the autophagy-related genes (*Atg*) that have been discovered in *S. cerevisiae*. From these 31 genes, 15 are mainly required for the autophagic machinery, and only 11 of them have unambiguous orthologues in mammals (Table 1-6). Most of these “core” *Atg*’s mediate the autophagosome formation [243].

Autophagy genes in mammals		
Gene	Protein function	Chromosomal location
<i>ATG1, ULK1</i>	Serine/threonine protein kinase; it may be involved in induction/membrane recycling	12q24.3 17p11.2
<i>ATG3</i>	Ubiquitin-conjugating E2-like enzyme; covalently attaches ATG8/LC3 to PE	3q13.2
<i>ATG4</i>	Cysteine protease; cleavage of ATG8	Xq22.1–q22.3 (<i>ATG4A</i>) 2q37.3 (<i>ATG4B</i>) 1p31.3 (<i>ATG4C</i>) 19p13.2 (<i>ATG4D</i>)
<i>ATG5</i>	Conjugated to ATG12; binds AT16 as part of a tetrameric complex of unknown function	6q21
<i>ATG6, BECN1</i>	Component of the class III PI3K complex that is required for autophagy	17q21
<i>ATG7</i>	Homolog of the ubiquitin-activating enzyme; it activates both ATG8/LC3 and ATG12	3p25.3
<i>ATG8, MAP1LC3</i>	Ubiquitin-like protein conjugated to PE; formation and expansion of the autophagosome	
<i>ATG9</i>	Transmembrane protein; it may be involved in delivering membrane to the forming Autophagosome	2q35 (<i>ATG9A</i>) 7q36.1 (<i>ATG9B</i>)
<i>ATG10</i>	Functions as an ubiquitin-conjugating-like enzyme; covalently attaches ATG12 to ATG5	5q14.1–q14.2
<i>ATG12</i>	Structural similarity to ubiquitin; it is conjugated to an internal lysine of ATG5	5q21–q22
<i>ATG16</i>	Binds ATG5 and homo-oligomerizes to form a tetrameric complex	2q37.1 (<i>ATG16L1</i>) 11q13.4 (<i>ATG16L2</i>)

Table 1-6: Autophagy genes in mammals

(Table compiled from information within [244] and [240])

1.4.1 Molecular mechanism

Basal autophagy occurs constantly within the majority of mammalian cells at low levels. Nevertheless, under conditions of starvation or stress [endoplasmic reticulum (ER) stress, hypoxia or oxidative stress], autophagy is induced [245]. The autophagic process can be divided into the following steps: initiation, autophagosome formation, fusion and degradation (Figure 1-5).

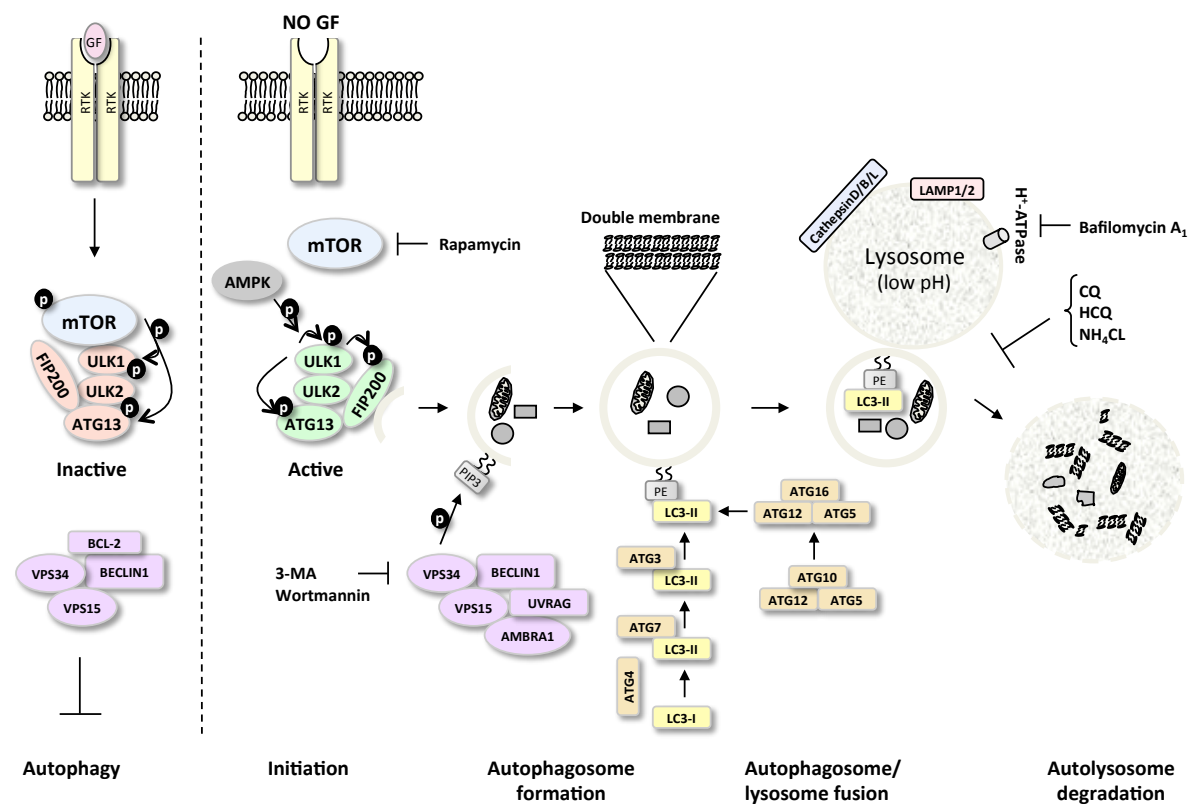


Figure 1-5: Overview of the autophagy process in vertebrates

(Adapted from [246])

Initiation: The mediator that sits atop the hierarchy of the autophagy initiation cascade is the Unc-51-like kinase 1 (ULK1), which along with the Unc-51-like kinase 2 (ULK2), consist the Atg1 yeast homologs. Kim and colleagues recently offered an insight about the regulation of ULK1 by AMPK and mTORC1 [247]. During energy sufficient conditions, mTORC1 is active in a RHEB-dependent manner and phosphorylates ULK1 on Ser757, prohibiting its interaction with AMPK. Nevertheless, upon glucose starvation, the energy sensor AMPK, phosphorylates tuberous sclerosis protein 2 (TSC2) and RAPTOR thus, inhibiting mTORC1 and mTORC1-mediated ULK1 phosphorylation. Hence, ULK1 is free to interact with AMPK, which phosphorylates ULK1 at Ser317 and Ser777 and activates it. It should be underlined however, that ULK1-mediated autophagy induction upon RAPA treatment or amino-acid starvation, occurs in an AMPK-independent manner.

Regardless of nutrient conditions, the ULKs form a complex with the mammalian ATG13 (Atg13 homolog) and the focal adhesion kinase family-interacting protein of 200Kd (FIP200) (Atg17 homolog) [248, 249]. Active ULKs, phosphorylate and activate the ATG13 and FIP200, and the activated ULK-ATG13-FIP200 complex is recruited to the phagophores [250]. Nonetheless, mTOR has been also suggested to directly phosphorylate and inactivate ATG13 under nutrient rich conditions [249]. Hence, phosphorylation of ATG13 by ULKs and mTOR must occur within different sites, having opposite effects.

Autophagosome formation: The first step of this process refers to the nucleation of the phagophore. In order to achieve this, a complex comprising of the class III PI3K vacuolar protein sorting 34 (VPS34), the regulatory unit VPS15 (previously known as p150 in mammalian cells) [251, 252] and BECLIN1 (ATG6; Vps30 or Atg6 yeast homolog) [253, 254]. Recently, a new interactor of this complex was identified; this molecule, known as BECLIN1-associated autophagy-related key regulator (BARKOR), has a sequence that is 18% identical and 32% similar to the yeast Atg14 [255]. Therefore, mammalian BARKOR is also known as autophagy-related protein 14-like (ATG14L) protein. In yeast, there are two PI3K complexes; the [Vps34-Vps15-Atg6]-Atg14, which takes part in autophagy, and the [Vps34-Vps15-Atg6]-Vps38, which takes part in the vacuolar protein-sorting pathway [256]. It is believed that Atg14 and Vps38 “tag” the complexes and determine their function and localisation. Accordingly, in mammals the core of the PI3K complex consists of the VPS34-VPS15-BECLIN1 and, depending on the binding of specific interactors, such as ATG14L or the UV irradiation resistance-associated gene (UVRAG; Vps38 yeast homolog) protein, the complex gains specific functions regarding membrane trafficking. In the mammalian autophagy machinery, ATG14L is believed to target the PI3K complexes

to an ER subdomain that is essential for the autophagy [257, 258]. Hence, in both yeast and mammals, ATG14L is mediating the localisation of the PI3K complexes to the site of the autophagosome formation.

Furthermore, the function of the PI3K complex can be regulated via interaction of BECLIN1 with its binding partners. The apoptosis regulator protein BCL2 can inhibit autophagy through interaction with the BH3-like domain in BECLIN1 [259]. This interaction is, however, reversed during starvation, allowing BECLIN1 to induce autophagy [260]. BECLIN1 has also been demonstrated to interact with UVRAG and activate autophagy [261]. Another BECLIN1 interactor is the activating molecule in BECLIN1-regulated autophagy protein 1 (AMBRA1). The PI3K core complex is docked to the cytoskeleton via dyneins through a BECLIN1/AMBRA1 interaction. Di Bartolomeo and colleagues demonstrated that upon autophagy induction, ULK1 phosphorylates AMBRA1, disrupting the interaction with BECLIN1 [262]. This allows the PI3K complex to de-attach from dyneins and reach the ER in order to initiate the autophagosome nucleation.

The origin of the autophagosomal membrane still remains unclear. Some studies suggest that either the ER or the Golgi is the source, however, others propose both ER and mitochondria, or a *de novo* membrane generation [263].

The expansion of the phagophore and, ultimately, the formation of the autophagosome, depend on two ubiquitin-like (UBL) conjugation systems; the ATG12–ATG5 and the ATG8–PE (phosphatidylethanolamine) [ATG8 is also known as microtubule-associated protein 1 light chain 3 (LC3); Atg8 yeast homolog]. The proteins with UBL activity, ATG12 and ATG8, undergo a cascade of conjugation with different ATG interactors (Figure 1-6).

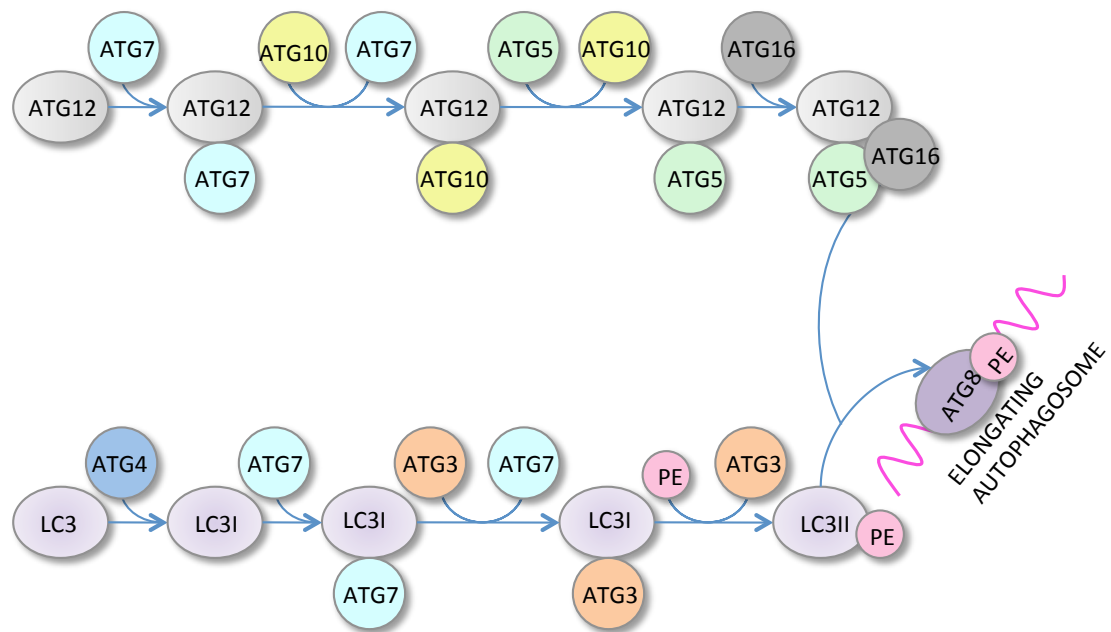


Figure 1-6: Autophagosome elongation

(Original figure, compiled from information within [244] and [243]).

ATG12-ATG5 system: ATG7, a homodimeric E1-like enzyme, activates ATG12. Following, ATG7 covalently conjugates ATG12 to ATG10 (E2-like enzyme) and then to ATG5. The ATG12-ATG5 complex associates then to ATG16-like (ATG16L; Atg16 yeast homolog), which mediates the attachment of the complex to the phagophore [264]. Subsequently, the ATG12-ATG5-ATG16L facilitates the loading of the ATG8-PE on the nascent autophagosomal membrane [243].

LC3-PE system: In humans there have been identified three LC3 isoforms (LC3A, -B, and -C) and four additional Atg8 yeast homologs (GABARAP, GEC1/GABARAPL1, GATE16/GABARAPL2, and GABARAPL3) [265, 266]. LC3 is post-translational modified by the ATG4, a cysteine protease. ATG4 removes 22 amino acids from the C-terminal of LC3, leading to the exposure of a glycine residue, and generates the cytosolic form (LC3-I) [267, 268]. Once autophagy is induced, ATG7 activates LC3 and transfers it to ATG3 (E2-like enzyme). Finally, ATG12-ATG5 covalently binds PE to LC3-I [269, 270], generating the lipidated form, LC3-II [268]. Autophagosomes have double membrane, and the composition of the inner and the outer membranes are different. LC3-II

seems to be the most indispensable building block for both inner and outer autophagic membranes [126].

It is believed that the expanding autophagosomes engulf bulk cytoplasmic contents in a non-specific manner. Nonetheless, this process can also be selective; cargo receptors deliver ubiquitinated substrates for autophagic degradation. Such a receptor is the mammalian protein p62/sequestosome 1 (SQSTM1), which contains a C-terminal ubiquitin-associated (UBA) domain that binds ubiquitin, and a conserved 22-amino acid acidic peptide motif LC3-interacting region (LIR) that allows for direct binding to human LC3 family members [271]. The selective recognition and degradation of p62 through autophagy were demonstrated by its accumulation in autophagy deficient cells [272, 273]. NBR1 (neighbor of BRCA1 gene 1) is another autophagy receptor containing a UBA domain and a LIR region [274]. NBR1 and p62 can work independently, or interact and form oligomers.

Fusion and degradation: Upon formation of the complete autophagosome, ATG4 releases the outer membrane LC3 from the PE by cutting the amide bond that links them [275]. The mechanistic details of the autophagosome fusion with the lysosomes in order to form the autolysosomes or autophagolysosomes, are still not clear. Nevertheless, in mammals, it has been demonstrated that this process requires the presence of lysosomal membrane protein LAMP-2, the small GTPase RAB7 and UVRAG [276-278].

Following fusion, the cargo is lysed mainly by cathepsins [279]. The macromolecules have been digested to their monomeric units, and released to the cytosol for reuse. Nevertheless, this process has to be further investigated; especially, the process of the autophagic recycling of carbohydrates and lipids remains vastly unknown.

1.4.2 Autophagy in cancer

1.4.2.1 Autophagy and cell death

Apoptosis, aka programmed cell death (PCD) type I, is a highly ordered process that recruits proteases and caspases for the dismantling of a cell. Accordingly, the extended vacuolisation of the cytoplasm accompanied by Golgi, ER and polyribosomes degradation before nuclear destruction, has been considered by many as an autophagic cell death, or PCD type II [280]. Along with necrosis, which is a non-ordered accidental type of death induced usually by external factors, apoptosis and autophagy cell death consist the three pathways of cell death [281]. Nevertheless, there have been arguments regarding the

contribution of autophagy in the process of cell death. More specifically, the Nomenclature Committee of Cell Death 2009 underlined that the “autophagic cell death” term “*may misleadingly suggest a form of death occurring through autophagy, as this process often promotes cell survival*” [241]. Hence, the use of a broader definition, such as “cell death occurring with autophagy” may be more suitable.

It has now been established that disruption of apoptosis can lead to tumour initiation, progression or metastasis. p53 is an extensively investigated transcription factor that acts as a tumour suppressor and is deregulated in more than 50% of all cancers [282-284]. p53 is involved in many cancer prevention mechanisms, including DNA repair, cell cycle regulation and initiation of apoptosis. In 2006, it was demonstrated that, DRAM (damage-regulated autophagy modulator), a p53 target, is required for DNA-damage induced autophagy and is indispensable for p53-mediated apoptosis [284, 285]. It has been suggested that the p53 regulation of autophagy depends on its localisation; nuclear p53 appears to induce autophagy at transcriptional level, whereas cytosolic p53 suppresses autophagy [286]. Recently, Lee and colleagues provided the first evidence for a direct interaction between p53 and ATG7 and a non-autophagic role for ATG7 [287]. ATG7 was essential during starvation for initiation of cell cycle arrest by binding to p53 and inducing expression of the cell cycle inhibitor p21. During starvation conditions, absence of ATG7 resulted in increased DNA damage and reactive oxygen species (ROS), as well as transcriptional increase of the proapoptotic genes *PUMA*, *NOXA*, and *BAX* and, ultimately, p53-dependent apoptosis.

Another autophagy gene interplaying with apoptosis is the ATG5, which is considered to be the “molecular switch” between autophagy and apoptosis. Cellular death stimulation and other stress factors (e.g. anticancer drugs) activate the calpains, a family of proteases, which cleave ATG5. The truncated ATG5 product (tATG5) triggers the release of mitochondrial cytochrome c and leads to an autophagosome-independent cell death [288].

1.4.2.2 The autophagy paradox

In 1999, experiments on Beclin1 haplodeficient mice associated for the first time an autophagy gene with tumorigenesis [254]. Following, it was demonstrated that BECLIN1 was monoallelically deleted in 40-70% of sporadic human breast or ovarian cancers cases [254], and haploinsufficient Beclin1 mice were prone to tumour development, including lymphoma, lung cancer and hepatocellular carcinoma [289, 290]. *ATG* genetically modified mice with compromised autophagy at whole body or tissue-specific level,

presented neurodegeneration, muscle and liver damage, chronic inflammations and frequent infections, as well as the development of spontaneous tumours [291, 292]. Tissue cells from such $ATG^{-/-}$ mice had abnormal mitochondria, increased number of polyubiquitinated protein aggregates, lipid droplets, ribosomes, peroxisomes, as well as autophagy receptors p62 and NBR1 [291-293]. These data support the notion that autophagy acts as a tumour suppressor mechanism, most probably through its role in homeostasis and quality control. Autophagy ablation leads to ER stress and accumulation of dysfunctional proteins' aggregates that have been suggested to favour tumourigenesis [294]. Furthermore, impairments in mitophagy lead to the accumulation of dysfunctional mitochondria and subsequent oxidative stress due to increased number of ROS. PINK1 and PARK2 (aka parkin) take part in the ubiquitination of the outer mitochondrial membrane so as to target damaged mitochondria for autophagic degradation [295]. These proteins are mutated in Parkinson's disease, and their inactivation causes hepatocellular carcinoma in mice [296]. Increased ROS due to an autophagy-deficient background promote deoxyribonucleic acid (DNA) damage, and lead to genetic instability [287]. Interestingly, accumulation of p62 due to impaired autophagy has been suggested to drive tumourigenesis by aberrantly increased ROS and oxidative DNA damage that enhance the development of acquired mutations and the activation of tumour-promoting pathways [297]. p62 has been proposed to activate the transcriptional nuclear factor-erythroid 2-related factor-2 (NRF2), which regulates cellular defense upon oxidative stress [298, 299]. Autophagy suppression in the liver of mice has been demonstrated to lead to increased p62 levels, overexpression, activation and translocation of Nrf2 to the nucleus, followed by transcription of the Nrf2 gene targets and tumourigenesis [298, 300, 301]. NRF2 has been suggested to have a dual role in cancer; from the one hand, it protects from oxidative stress, from the other hand, its overexpression had been proposed to give a survival and growth advantage to tumour cells [302]. Finally, it has been suggested that increased ROS levels could reduce immunity against cancer antigen by promoting apoptosis of T-cells.

Another potential contribution of autophagy deficiency towards development of cancer is through inflammatory responses. The aforementioned effects of compromised autophagy on oxidative and ER stress, genomic instability etc, induce prolonged tissue damage and an inflammatory environment [303]. Autophagy defects lead to inflammation in Crohn's disease [304] and pancreatitis [305], and chronic inflammation supports cancer development. Loss of Beclin1 allele in mice has been shown to promote liver inflammation and hepatocellular carcinoma [289, 290, 306].

On the other hand, autophagy has been considered as a survival mechanism since its discovery and increasing evidence suggest that autophagy acts also as a survival mechanism within cancer cells. Cells in the core of the tumour or highly proliferating cancer cells that have surpassed the potential of their vascular niche, have to overcome adverse conditions such as hypoxia and limited access to nutrients and GFs [307, 308]. Unlike normal cells that have low basal autophagy levels, cancer cells seem to be “addicted” to high levels of autophagy under nutrients replete conditions [307].

In support of the cancer cell “autophagy addiction” hypothesis are studies demonstrating the autophagy dependence of RAS-driven cancers [309-311]. Data showed that autophagy is required for the maintenance of mitochondrial integrity, which is necessary for the survival of RAS-expressing cells during starvation [309]. Most importantly, tumourigenic ability of RAS was ablated in an autophagy deficient background [309, 311].

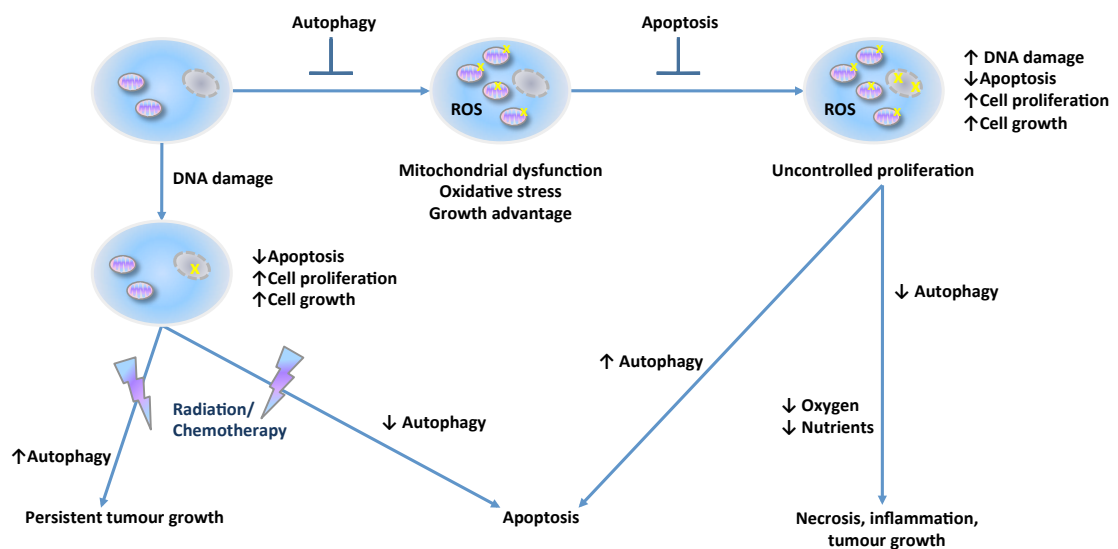


Figure 1-7: The role of autophagy in cancer

(Adapted from [240]).

Taken altogether, autophagy seems to have a dual role in cancer; it can act as a tumour suppressor by ensuring cellular integrity, however, in established tumours it seems to support the survival of cancer cells [307]. Therefore, modulation of autophagy for cancer therapy should be context-specific and take into account the type of tumour, the stage of disease and the nature of the treatment [244].

1.4.2.3 Inhibition of autophagy in CML

The most commonly used autophagy inhibitors nowadays include chloroquine (CQ), and its derivative hydroxychloroquine (HCQ), which is associated with lower retinal toxicity [312, 313]. CQ has been extensively used in the clinic for malaria, as well as for autoimmune diseases, such as rheumatoid arthritis and systemic lupus. Both CQ and HCQ inhibit autophagy at a late stage, by inhibiting lysosomal acidification and preventing the fusion between autophagosomes and lysosomes. CQ and HCQ are not exclusive autophagy inhibitors and affect other cellular pathways as well. However, since these drugs are FDA-approved, they can be used in the clinic for the inhibition of autophagy, and a number of clinical trials are investigating their effects in combination with other anti-cancer agents (Table 1-7).

Early stage pharmacological autophagy inhibitors target the PI3K-kinases, such as the 3-methyladenine (3-MA), a PI3K-III inhibitor, and wortmannin (WM), a pan-PI3K inhibitor [314]. Nonetheless, PI3K inhibitors may also suppress class I PI3K kinases upstream of mTOR, and, partially, induce autophagy. Moreover, like CQ and HCQ, PI3K inhibitors are not targeting autophagy solely, and some of them are associated with high toxicity at clinically relevant doses [315].

Chemical autophagy inhibitors can block autophagy at the fusion stage, such as vinblastine and nocodazole [316], or at the degradation stage, such as ammonium chloride or lysosomal protease inhibitors E64d and pepstatin [279]. Another late autophagy stage inhibitor is bafilomycin A1, which inhibits lysosomal acidification [317]. It should also be mentioned, that none of these chemical inhibitors is specific to autophagy.

Drug	Phase	Drug target	Clinical trial	Cancer type
Hydroxychloroquine (Plaquenil)	0, I, II	Autophagy	NCT00771056, NCT00962845, NCT00726596, NCT01144169, NCT01144169, NCT00726596	Multiple
Along with HCQ				
Sunitinib (Sutent)	I	Multiple receptor tyrosine kinases	NCT00813423	Solid tumors
Temozolomide (Temodar/Temodal)	I	DNA	NCT00714181	Solid tumors
Temsirolimus (Torisel)	I	mTOR	NCT00909831	Solid tumors
Vorinostat (Zolinza)	I	Histone deacetylase	NCT01023737	Metastatic breast cancer
Ixabepilone (Ixempra)	I/II	Microtubules	NCT00765765	Metastatic breast cancer
Imatinib mesylate (Gleevec)	II	Tyrosine kinases	NCT01227135	Chronic myelogenous leukemia
Capecitabine (Xeloda)	II	DNA	NCT01006369	Metastatic colorectal cancer
5-fluorouracil (5-FU)				
Oxaliplatin (Eloxatin)				
Bevacizumab (Avastin)		VEGF		
5-fluorouracil (5-FU)	I/II	DNA	NCT01206530	Colorectal cancer
Leucovorin (Folic acid)		Thymidylate synthase		
Oxaliplatin (Eloxatin)		DNA		
Bevacizumab (Avastin)		VEGF		
Radiation therapy	I/II		NCT00486603	Glioblastoma multiforme
Temozolomide (Temodar, Temodel)		DNA		
Carboplatin (Paraplatin)	I/II	DNA	NCT00933803	Lung cancer (non-small cell)
Paclitaxel (Abraxane, TaxolB)		Microtubules		
Bevacizumab (Avastin)		VEGF		
Erlotinib (Tarceva)	II	Tyrosine kinases	NCT00977470	Lung cancer (non-small cell)
Gefitinib (Iressa)	I/II	Tyrosine kinases	NCT00809237	Metastatic lung cancer (non-small cell)
Bortezomib (Velcade)	I/II	Proteasome	NCT00568880	Multiple myeloma
Gemcitabine (Gemzar)	I/II	DNA	NCT01128296	Pancreatic cancer
Docetaxel (Taxotere)	II	Microtubules	NCT00786682	Prostate cancer
Along with CQ				
Chloroquine (Aralen)	III	Autophagy	NCT00224978	Glioblastoma multiforme
Tamoxifen (Novaldex, Istabal, Valadex)	I/II	Estrogen receptor	NCT01023477	Ductal carcinoma <i>in situ</i>
Cisplatin (Cisplatin)	I/II	DNA	NCT00969306	Lung cancer (extensive small cell)
Etoposide (Eposin, Etopophos, Vepesid)				
Radiation therapy	I/II		NCT00969306	Lung cancer (limited small cell)
Cisplatin (Cisplatin)		DNA		
Etoposide (Eposin, Etopophos, Vepesid)				
Cyclophosphamide	II	DNA	NCT01438177	Multiple myeloma
Bortezomib (Velcade)		Proteasome		
Cyclophosphamide	0	DNA	NCT01396200	Multiple myeloma

Table 1-7: Clinical trials investigating autophagy inhibition using HCQ or CQ in combination with anti-cancer therapies

(Reproduced from [318])

1.4.3 Autophagy in CML

In 2006, Yan and colleagues demonstrated that crotoxin (CrTX), a neurotoxin with antitumour activity, induces apoptosis and autophagy in BC CML cell line K562 [319]. Inhibition of the CrTX-induced autophagy with 3-MA or ammonium chloride enhanced the neurotoxin's cytotoxicity. Additionally, Carew and colleagues suggested a year later that CQ-mediated inhibition of autophagy potentiated the effects of the HDAC inhibitor suberoylanilide hydroxamic acid (SAHA) in IM-resistant CML cell lines and primary cells

[320]. In 2008, inhibition of BCR-ABL by bafetinib, a dual BCR-ABL/LYN TKI, or IM, was shown to induce protective autophagy [321, 322].

In 2009, our lab provided for the first time rigorous evidence demonstrating that TKIs induces autophagy in CML primary cells and its inhibition augments TKI effects [323]. IM treatment induced autophagy in CML cell lines and primary cells; inhibition of the IM-induced autophagy either with CQ enhanced the effects of IM (Figure 1-8). Furthermore, CQ potentiated the effects of second generation TKIs, DAS and NIL. Importantly, induction of autophagy was demonstrated to be specific to inhibition of BCR-ABL activity, since IM treatment did not enhance autophagic activity in the cells carrying the resistant clone BCR-ABL^{T315I}. Nevertheless, these data do not clarify if the observed effect on stem/progenitor cells is due to the inhibition of cellular autophagy or lysosomal activity, or other CQ-associated off-target effects.

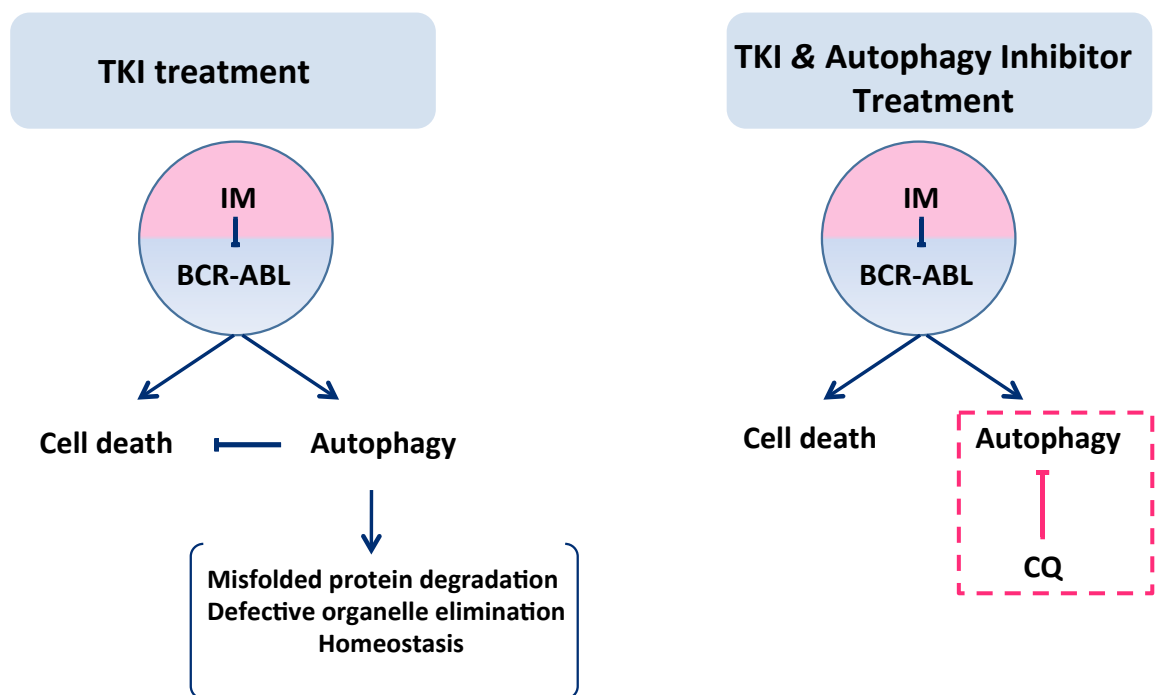


Figure 1-8: Proposed mechanism for the role of autophagy in TKI-induced CML treatment

Sheng and colleagues recently shed more light regarding the mechanism by which inhibition of BCR-ABL is leading to induction of autophagy [324]. Oncogenic BCR-ABL mimicks the effects of GF and activates the PI3K/AKT pathway, which inhibits FoxO4. Inhibition of FoxO4 leads to increased levels of the transcription factor ATF5 and its target, mTOR. Subsequently, mTOR suppresses autophagy. Upon BCR-ABL inhibition, for example during TKI treatment, decreases PI3K/AKT signaling and FoxO4 is free to inhibit ATF5, leading to decreased transcription of mTOR and increase in autophagy.

Our data regarding the protective role of autophagy in CML were supported by the following studies [325-329]. Most importantly, in 2011, Altman and colleagues demonstrated that autophagy is necessary for Bcr-Abl transformation; deletion of Atg3 in a mouse model prevented Bcr-Abl-mediated leukaemogenesis [330]. However, there are studies supporting the induction of autophagy in combination with targeting of non-BCR-ABL related pathways for the treatment of CML [331, 332]. Resveratrol (RSV), a phytoalexin, has been proposed to induce apoptosis and autophagy in an AMPK-dependent manner, and inhibition of RSV-induced autophagy partially rescued RSV-mediated apoptosis within CML cells sensitive or resistant to IM [331]. Additionally, it has been proposed that treatment with arsenic trioxide, an autophagy inducer, has antileukaemic effects that are partially attributed to the autophagic degradation of BCR-ABL [333].

1.4.3.1 The CHOICES clinical trial

The findings from the study of Bellodi and colleagues provided the foundation for the initiation of the phase II clinical trial CHOICES (CQ and IM Combination to Eliminate Stem cells) clinical trial. CHOICES is a randomised trial investigating the effects of IM versus HCQ and IM for CML patients that have been on IM for >1 year and are in MCyR with residual disease detectable by qRT-PCR.

Primary objectives include determining if the combination HCQ plus IM versus IM alone is more effective in terms of lowering BCR-ABL levels in CML patients with MCyR and residual disease detectable by qRT-PCR after at least 1 year of IM treatment, as well as evaluating the safety and tolerability of this regimen in these patients.

Patients are randomised to 1 of 2 treatment arms:

Arm A: Patients receive oral IM daily. Treatment repeats every 4 weeks for up to 12 months in the absence of disease progression or unacceptable toxicity.

Arm B: Patients receive oral IM daily and oral HCQ twice daily. Treatment repeats every 4 weeks for up to 12 months in the absence of disease progression or unacceptable toxicity.

In both arms, patients may then receive oral IM daily for another 12 months during the follow up period of this study. Consenting patients undergo blood sample and BM collection at baseline, during, and after completion of study therapy for pharmacologic and other laboratory studies. After completion of study treatment, patients are followed up at 3, 6, 9, and 12 months.

2 Materials and Methods

2.1 Materials

2.1.1 Small molecule inhibitors

IM was provided as a white powder under a Materials Transfer Agreement from Novartis Pharma (Basel, Switzerland). DAS was provided as a white powder under a Materials Transfer Agreement from Bristol-Myers Squibb (Princeton, NJ, USA). PON was provided as a white powder under a Materials Transfer Agreement from ARIAD Pharmaceuticals Inc. (Massachusetts, USA).

Details of the suppliers, stock concentrations, and diluents of all drugs and inhibitors used are listed in Table 2-1. All stock aliquots were stored at -20°C, with the exception of HCQ and CQ, which were stored at 4°C. All small molecule inhibitors were made up fresh for each experiment and diluted to the appropriate concentration with appropriate medium prior to use.

Molecule	Solvent	Stock Concentration	Supplier
CQ	Water	100mM	Sigma-Aldrich
DAS	DMSO	20mM	Bristol-Myers Squibb
HCQ	PBS	100mM	Sigma-Aldrich
IM	Water	100mM	Novartis
NIL	DMSO	10mM	Novartis
BEZ	DMSO	1mM	LC Laboratories
PON	DMSO	10mM	ARIAD Pharma
RAPA	EtOH	2mM	Sigma-Aldrich

Table 2-1: Small molecule inhibitors (dimethyl sulfoxide; DMSO, phosphate buffered saline; PBS, ethanol; EtOH)

2.1.2 Tissue culture materials

Abbot Diagnostics, Maidenhead, UK	Locus specific identifier (LS1) BCR-ABL Dual Colour FISH probe
Baxter Healthcare, Nottingham, UK	Sterile water
BD Biosciences, Oxford, UK	Annexin binding buffer (10X) Anti-human IgG allophycocyanin (APC) isotype control Anti-human IgG fluorescein isothiocyanate (FITC) isotype control Anti-human IgG phycoerythrin (PE) isotype control BD BioCoat™ - Collagen I 12-well plates FACS flow/FACS clean Mouse anti-human-annexin-V-FITC antibody Mouse anti-human-annexin-V-PE antibody Mouse anti-human-CD34-APC Mouse anti-human-CD38-FITC Mouse anti-human-annexin-V-peridinin chlorophyll protein (PerCP)-Cy™5.5 PE anti-human CD235a Via-Probe™ - 7 aminoactinomycin D (7-AAD)
Chugai Pharma, London, UK	Recombinant human G-CSF
Enzo Life Sciences, Exeter, UK	Cyto-ID® Autophagy detection kit
Gilson, Middleton, USA	Yellow and blue pipette tips
Greiner Bio-One, Gloucestershire, UK	Cryo.s™ cryotubes Tissue culture flasks (25cm ² , 75cm ² and 175cm ²) Tissue culture plates (6-well, 12-well, 24-well and 96-well) Pipettes (5mL, 10mL and 25mL)
Invitrogen, Paisley, UK	2-mercaptoethanol Foetal calf serum (FCS) L-glutamine (200mM) Isocove's modified dulbecco's medium (IMDM) Dulbecco's modified eagle medium (DMEM) RPMI 1640 Dulbecco's PBS MitoTracker® Red CMXRos MitoSOX™ Red
Miltenyi Biotec, Bisley, UK	CliniMACS CD34 reagent CliniMACS PBS/ ethylenediaminetetraacetic acid (EDTA) buffer

	CliniMACS tubing set CD34 MicroBead kit
Nalgene Labware, Roskilde, Denmark	25 and 75cm ³ non-adherent tissue culture flasks Cryo freezing container “Mr. Frosty” Vacubottles
Scottish National Blood Transfusion, Glasgow, UK	20% Human serum albumin 4.5% Human albumin solution (ALBA®)
Sigma-Aldrich, Dorset, UK	5-Azacytidine (AZA) Bovine serum albumin (BSA) Carbonate-bicarbonate buffer DMSO Ficoll/histopaque solution (1.077g/mL) G418 Gelatin Hank’s buffered salt solution – calcium and magnesium free (HBSS-CMF) Hydrochloric acid (HCl) Hygromycin B Magnesium chloride (MgCl ₂) Poly-L-lysine Potassium chloride (KCl) Puromycin (PURO) Sodium azide Trisodium citrate Trypan blue Trypsin-EDTA
Startorius, Hannover, Germany	Minisart 0.2µM sterile filters Minisart 0.45µM sterile filters
Stem Cell Technologies, British Columbia, Canada	Methocult® H4434 Methocult® H4230 Bovine pancreatic deoxyribonuclease (DNase 1) 1mg/mL BSA/insulin/transferrin (BIT) Serum substitute Flt-3 ligand (FLT3L) IL-3 IL-6 Stem Cell Factor (SCF) TPO GM-CSF Macrophage inflammatory protein 1α (MIP-1α)
Sterilin Ltd, Hounslow, UK	Pastettes Disposable pipettes (5mL, 10mL and 25mL) Sterile plastic falcon tubes (15 and 50mL)

Thermo-Scientific, Hertfordshire, UK	ON-TARGETplus SMARTpool-human ATG7 ON-TARGETplus non-targeting pool
---	--

2.1.3 Molecular biology materials

Abcam, Cambridge, UK	Mouse anti-human-p62 antibody Mouse anti-human-actin antibody
Applied Biosystems, Foster City, CA, USA	GeneAmp® RNA PCR core kit High capacity complimentary DNA (cDNA) reverse transcription kit Nuclease free water TaqMan® probes Deoxyribonucleotide triphosphates (dNTPs)
Bio-Rad Hercules, CA, USA	Combs for gel casting Gel casting trays Immuno-Blot™ polyvinylidene fluoride (PVDF) membrane Immuno-Star™ WesternC™ Kit
Bioline, London, UK	HyperPAGE prestained protein marker
Cell Signalling, New England Biolabs Hitchin, UK	Anti-rabbit IgG horseradish peroxidase (HRP)-linked secondary antibody Rabbit anti-human-ATG7 antibody Rabbit anti-human-p-CrkL antibody Rabbit anti-human-LC3b antibody Rabbit anti-human-p-RPS6 antibody Rabbit anti-human-β-Tubulin antibody
Chemical Store, University of Glasgow Glasgow, UK	EtOH Methanol
Chemicon International, Temecula, CA, USA	10X Re-Blot™ plus strong antibody Stripping solution
Eurofins MWG Operon, Wolverhampton, UK	PCR primers
Helena Biosciences, Gateshead, UK	Agarose powder
Invitrogen, Paisley, UK	Novex® Sharp™ pre-stained protein standard NuPage® MES sodium dodecyl sulfate (SDS) running buffer (20X) CellsDirect™ One-Step qRT-PCR kit Nupage® Novex® Bis-Tris 4-12% gel NuPage® transfer buffer (20X) XCell II™ Blot module Miller's Luria Broth (LB) base®

Lonza, Basel, Switzerland	Amaxa® cell line nucleofector® kit V Amaxa® human CD34+ cell nucleofector® kit
New England Biolabs (NEB), Hertfordshire, UK	NdeI restriction enzyme SpeI restriction enzyme
Promega, Southampton, UK	100 base pair (bp) DNA ladder PCR loading dye (6X) CellTiter-Glo® luminescent cell viability assay Shrimp alkaline phosphatase (SAP)
Qiagen, West Sussex, UK	RNeasy mini kit QIAshredder kit HiSpeed® plasmid midi kit
SG Wasseraufbereitung und Regenerierstation GmbH, Barsbittel, Germany	Ultra pure water system (sterile water)
Sigma-Aldrich, Dorset, UK	0.1% Ponceau S solution 2-glycerophosphate Aprotinin Boric acid CaCl ₂ *2H ₂ O EDTA Formaldehyde solution (36.5%) Leupeptin NP-40 PMSF Protein A-sepharose® Sodium chloride Sodium fluoride Sodium orthovanadate Sodium pyrophosphate Tris base TWEEN 20 for electrophoresis Tetramethylethylenediamine (TEMED) 4-(2-hydroxyethyl)-1-piperazineethanesulfonic acid (HEPES)
Thermo-Scientific, Hertfordshire, UK	BCA™ protein assay kit

2.1.4 TaqMan® probes

Gene	Product No	Gene	Product No
18S	Hs99999901	E2F1	Hs00153451
ABL1	Hs01104728	GABARAP L1	Hs00740588
APOBEC3B	Hs00358981	GAPDH	Hs99999905
ATG12	Hs01047860	GUSB	Hs99999908
ATG13	Hs00207186	HES1	Hs00172878
ATG3	Hs00223937	HES5	Hs01387463
ATG4B	Hs00367088	HIF1A	Hs00936371
ATG5	Hs00169468	MAP1LC3B	Hs00797944
ATG7	Hs00197348	MCL1	Hs03043899
ATM	Hs01112307	MDM2	Hs00234753
BAK1	Hs00940250	p21	Hs00355782
BAX	Hs00180269	p53	Hs01039246
BECN1	Hs00186838	RB	Hs01078066
BID	Hs00609630	SIRT1	Hs01009006
BIM	Hs00708019	SIRT6	Hs00213036
BIRC5	Hs04194392	TBP	Hs99999910
BRCA1	Hs01556193	TGFB1	Hs00998129
CDKN1B	Hs00153277	TGFBR1	Hs00610320
CHEK2	Hs00200485	ULK1	Hs00177504
CHK1	Hs00967506	ULK2	Hs00206622
CXCL1	Hs00236937	WNT4	Hs00229142
CYCLIN D1	Hs00765553	WNT5A	Hs00998537

2.1.5 Fluorescence microscopy supplies

Abcam, Cambridge, UK	Mouse IgG2a isotype control Rabbit F(ab') ₂ -IgG-isotype control
Carl Zeiss, Jena, Germany	AxioVision software
Cell Signalling, New England Biolabs, Hitchin, UK	Rabbit anti-human-LC3B antibody
Hendley, Essex, UK	Multi-spot microscope slides
Invitrogen, Paisley, UK	Alexa Fluor® 488 cholera toxin subunit B conjugate Alexa Fluor® 488 goat anti-rabbit IgG Alexa Fluor® 594 goat anti-mouse IgG Alexa Fluor® 488 phalloidin
Sigma-Aldrich, Dorest, UK	Poly-L-lysine solution 0.1 % (w/v) Triton-X100
Vector Laboratories Ltd, Peterborough, UK	VECTASHIELD® mounting medium with 4',6-diamidino-2-phenylindole (DAPI)

2.1.6 PCR primer sequences

TAT Forward	GAAGCATCCAGGAAGTC AGCC
TAT Reverse	GCTGTCTCCGCTTCTTCC TGCC
Human U6 Promoter Forward	GACTATCATATGCTTACCGT
pLKO.1 Backbone Reverse	AAACCCAGGGCTGCCTTGGAAAAG

2.1.7 Equipment

Kell-Strom, Wethersfield, USA	Branson 200 Ultrasonic cleaner
Epson (UK), Hertfordshire, UK	Epson perfection 4490 photo scanner
BD Biosciences, San Jose, CA	FACSAria II FACSCalibur
Gilson, Middleton, USA	Gilson pipetman single channel pipettes
Weber Scientific International, West Sussex, UK	Hawksley Neubauer counting chamber
Carestream Health, Rochester, NY, USA	Kodak X-OMAT 1000

Thermo Fisher Scientific, Loughborough, UK	Multiscan EX photometer
Lonza, Basel, Switzerland	Nucleofector® II device
Bio-Rad Hercules, CA, USA	PowerPac300
Schutron, Reutlingen, Germany	Thermoshaker
Bio-Rad Laboratories Ltd., UK	Trans-Blot® SD cell Molecular Imager® ChemiDoc™ XRS
Carl Zeiss, Jena, Germany	Fluorescence microscope Light microscope
Labtech International East Sussex, UK	NanoDrop ND-1000 spectrophotometer
Invitrogen, Paisley, UK	XCell SureLock™ mini-cell electrophoresis system

2.1.8 Preparation of medium and solutions

2.1.8.1 Tissue culture mediums and solutions

2.1.8.1.1 RPMI++

RPMI 1640	440mL
FCS	50mL
L-glutamine (200mM)	5mL
Penicillin/streptomycin solution (10,000U/mL ⁻¹ /10,000gmL ⁻¹)	5mL

2.1.8.1.2 DMEM++

DMEM	440mL
FCS	50mL
L-glutamine (200mM)	5mL
Penicillin/streptomycin solution (10,000U/mL ⁻¹ /10,000gmL ⁻¹)	5mL

2.1.8.1.3 20% FCS DMEM[^]

DMEM	390mL
FCS	100mL
L-glutamine (200mM)	5mL
Penicillin/streptomycin solution (10,000U/mL ⁻¹ /10,000gmL ⁻¹)	5mL

2.1.8.1.4 DMEM* for maintenance of stromal cell line SI/SI for LTC-IC

DMEM	500mL
FCS	75mL
L-glutamine	10mL
Penicillin/streptomycin solution (10,000U/mL ⁻¹ /10,000gmL ⁻¹)	10mL

2.1.8.1.5 RPMI* for maintenance of stromal cell line M2-10B4 for LTC-IC

RPMI 1640	500mL
FCS	50mL
L-glutamine	10mL
Penicillin/streptomycin solution (10,000U/mL ⁻¹ /10,000gmL ⁻¹)	10mL

2.1.8.1.6 IMDM/2% FCS

IMDM	98mL
FCS	2mL

2.1.8.1.7 Myelocult

Myelocult™	100mL
Hydrocortisone hemisuccinate (1x10 ⁻⁴ M)	1mL

2.1.8.1.8 DAMP solution [for thawing cryopreserved CD34+ or mononuclear cell (MNC) aliquots from -150°C]

DNase I (2 vials at approximately 2500U/1mL/vial)	2mL
Magnesium chloride (400X, 1.0M stock)	1.25mL
Trisodium citrate (0.155M)	53mL
Human serum albumin (20%, SNBTS)	25mL
Dulbecco's PBS (magnesium/calcium free)	418.75mL

2.1.8.1.9 Serum free medium (SFM)

BIT	25mL
L-glutamine (200mM)	1.25mL
Penicillin/streptomycin solution (10,000U/mL ⁻¹ /10,000gmL ⁻¹)	1.25mL
2-mercaptoethanol (50mM)	250µL
Low density lipoprotein (10mg/mL)	500µL
IMDM	97.25mL

2.1.8.1.10 SFM supplemented with five growth factors (SFM+5GFs)

SFM	10mL
IL-3 (50µg/mL)	4µL
IL-6 (50µg/mL)	4µL
G-CSF (20µg/mL)	10µL
FLT3L (50µg/mL)	20µL
SCF (50µg/mL)	20µL

2.1.8.1.11 SFM supplemented with physiological growth factors (SFM+PGFs)

SFM	10mL
SCF (0.5µg/mL)	4µL
G-CSF (2µg/mL)	5µL
GM-CSF (0.1µg/mL)	20µL
IL-6 (5µg/mL)	2µL
LIF (0.1µg/mL)	5µL
MIP-1α (0.1µg/mL)	20µL

*Filter through 0.22µM filter

2.1.8.1.12 20% DMSO/4.5% ALBA

DMSO	20mL
4.5% ALBA	80mL

2.1.8.1.13 PBS/2% FCS

PBS	490mL
FCS	10mL

2.1.8.1.14 Annexin binding buffer

Annexin binding buffer (10X)	1mL
distilled water (dH ₂ O)	9mL

2.1.8.1.15 Fix perm wash – PBS/1% BSA

BSA	10g
PBS	to 1L

2.1.8.1.16 IMDM^{m+} for the maintenance of mouse c-kit enriched cells

IMDM	
FCS	10%
mouse SCF	40 ng/ml
mouse IL-6	20 ng/ml
mouse IL-3	20 ng/ml

2.1.8.2 Western blotting solutions

2.1.8.2.1 Lysis buffer for protein lysates (radio-immunoprecipitation assay; RIPA)

distilled sterile water (dsH ₂ O)	7.75mL
1.5M NaCl	1mL
1M Tris-HCl	0.5mL
150mM EDTA	333 μ L
NP-40	50 μ L
10% (w/v) Sodium deoxycholate	250 μ L

*Immediately prior to use, one protease inhibitor tablet added per 10mL of buffer

2.1.8.2.2 2X SDS Sample buffer (Laemmli)

1.5M Tris-HCl, pH6.8	10mL
Glycerol	30mL
20% (w/v) SDS	6mL
Bromophenol blue	1.8mg
2-mercaptoethanol	15mL
dsH ₂ O	to 100 mL

2.1.8.2.3 10X TBS buffer

NaCl	876.6g
Tris	121.1g
dH ₂ O	10L

2.1.8.2.4 1X TBS-Tween (TBST) buffer

10X Tris-buffered saline (TBS) buffer	1L
TWEEN 20	10mL
dH ₂ O	8.99L

2.1.8.2.5 Homemade gels

2.1.8.2.5.1 10% Resolving gel

dsH ₂ O	4mL
30% Acrylamide	3.3mL
1.5M Tris (pH8.8)	2.5mL
10% SDS	0.1mL
10% APS	0.1mL
TEMED	0.01mL

2.1.8.2.5.2 15% Resolving gel

dsH ₂ O	2.3mL
30% Acrylamide	5.0mL

1.5M Tris (pH8.8)	2.5mL
10% SDS	0.1mL
10% APS	0.1mL
TEMED	0.01mL

2.1.8.2.5.3 *Stacking gel*

dsH ₂ O	1.4mL
30% Acrylamide	0.33mL
1.0M Tris (pH6.8)	0.25mL
10% SDS	0.02mL
10% APS	0.02mL
TEMED	0.01mL

2.1.8.2.6 1X NuPAGE® Running buffer

NuPAGE® MES SDS Running Buffer (20X)	50mL
dH ₂ O	to 1L

2.1.8.2.7 1X NuPAGE® Transfer buffer

NuPAGE® Transfer Buffer (20X)	30mL
dH ₂ O	510mL
Methanol	60mL

2.1.8.2.8 10X Running buffer (homemade)

Glycine	144.1g
Tris	30.3g
SDS	10g
dH ₂ O	to 2L
pH to 8.3	

2.1.8.2.9 1X Running buffer (homemade)

10X Running buffer (homemade)	100mL
dH ₂ O	900mL

2.1.8.2.10 10X Transfer buffer (homemade)

Glycine	144.1g
Tris	30.3g
dH ₂ O	to 2L
pH to 8.3	

2.1.8.2.11 1X Transfer buffer (homemade)

10X Transfer buffer (homemade)	100mL
--------------------------------	-------

Methanol	200mL
dH ₂ O	700mL

2.1.8.2.12 5% BSA/TBST blocking buffer	
1X TBST buffer	100mL
BSA	5g

2.1.8.3 Immunofluorescence solutions

2.1.8.3.1 3.65% Formaldehyde	
36.5% Formaldehyde solution	1mL
PBS	9mL

2.1.8.3.2 0.5% Triton-X-100	
Triton-X-100	250mL
PBS	50mL

2.1.8.4 PCR-based assays solutions

2.1.8.4.1 2X RT-PCR Master Mix (10μL/assay)	
10X Reverse transcription buffer	2μL
25X dNTPs Mix	0.8μL
10X Reverse transcripton random primers	2μL
Reverse transcriptase	1μL
Nuclease free dsH ₂ O	4.2μL

2.1.8.4.2 PCR Mix (50μL)	
10X PCR Buffer	5μL
dNTPs mix (1000μM)	10μL
Taq polymerase	0.25μL
Forward primer (100μM)	0.25μL
Reverse primer (100μM)	0.25μL
MgCl ₂ (25mM)	5μL
cDNA	1μL
Nuclease free dsH ₂ O	28.25μL

2.1.8.4.3 10X Tris/Borate/EDTA (TBE) buffer	
Boric acid	55g
EDTA (0.5M, pH8.0)	40mL
Tris base	108g
dsH ₂ O	1L

2.1.8.4.4 2X Reverse Transcriptase Specific Target Amplification (RT-STA) mix

For one well:

0.2X TaqMan® probes mix	1.4µL
Cells direct 2X reaction	2.8µL
SUPERase-In	0.056µL
SuperscriptIII RT	0.112µL
TE buffer	0.672µL

2.1.8.5 Transfection solution

2.1.8.5.1 2X HEPES-buffered saline (HBS)

NaCl	8g
KCl	0.37g
Na ₂ HPO ₄	106.5mg
Dextrose	1.0g
HEPES	5g
dsH ₂ O	to 500mL

pH to 7.05

*Sterile filter through 0.45µm filter

2.1.8.5.2 2M CaCl₂

CaCl ₂ *2H ₂ O	147g
dsH ₂ O	to 500mL

2.1.8.5.3 Transfection solution/10cm² petri dish

dsH ₂ O	440µL
2X HBS	500µL
2M CaCl ₂ (dropwise)	60µL

2.1.8.6 Microbiology solutions

2.1.8.6.1 LB

Miller's LB base®	25g
dsH ₂ O	to 1L

Autoclave

Ampicillin (100mg/mL)	1mL
-----------------------	-----

2.1.8.6.2 Glycerol solution (30%)

Glycerol	3mL
dsH ₂ O	to 10mL

2.2 Methods

2.2.1 Cell Culture

2.2.1.1 Culture of cell lines

The BC CML wild type (WT) cell lines K562 and KCL22 and the CLL cell line HG3, were all available “in-house”, and grown in suspension culture in RPMI++ medium (2.1.8.1.1) in tissue culture flasks. KCL22 cells expressing BCR-ABL^{T315I} were kindly donated by Professor Bruno Calabretta and maintained in RPMI++. BaF3 cells (murine IL-3 dependent pro-B cells) that stably expressed BCR-ABL, either the native p210 isoform or carrying the T315I kinase domain mutation, were donated as a kind gift from Professor Junia Melo and were also grown in RPMI++. M2-10B4 and SI/SI murine fibroblast cell lines were cultured in RPMI* (2.1.8.1.5) and DMEM* (2.1.8.1.4), respectively. Mouse c-kit enriched MLL-ENL transformed cells were kindly donated by Dr Deniz Gezer, and maintained in IMDM^{m+} (2.1.8.1.16).

All cell lines were maintained at 37°C with 5% CO₂ in 25 or 75cm³ tissue culture flasks, counted and passaged every two days with warm fresh medium, to maintain a density of between 1x10⁵-1x10⁶ cells/mL.

2.2.1.2 Cell proliferation assays

2.2.1.2.1 Trypan blue dye exclusion method

Background: The trypan blue dye exclusion method was used for cell counting and assessment of viability. Cells with damaged membranes are porous and absorb the trypan blue dye, appearing dark blue under a light microscope; viable cells with an intact membrane do not absorb the dye. For cell counting only the unstained cells were counted and the remaining stained dead cells were deemed non-viable.

Method: Trypan blue dye was first diluted 1:10 with PBS and 90µL was added to 10µL of cell suspension to give a 1:10 dilution of cells. Approximately 10µL of the mixture was transferred to a counting chamber (improved Neubauer haemocytometer) and the four squares (a,b,c and d) were counted to give a statistically significant count. Number of cells and percent of viability were determined by using the formulas shown in Figure 2-1.

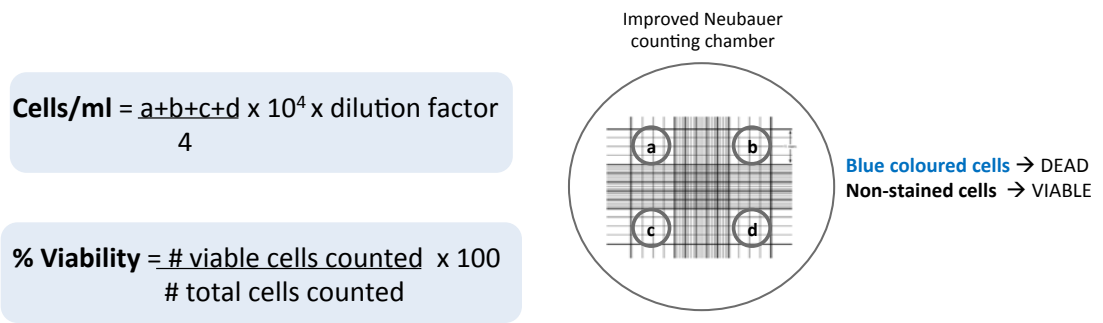


Figure 2-1: Trypan blue method for cell counting and viability assessment with improved Neubauer counting chamber

2.2.1.2.2 CellTiter-Glo® Luminescent Cell Viability Assay

Background: The CellTiter-Glo® luminescent cell viability assay [Promega, product number (PN) G7570] determines the number of viable cells in culture based on quantitation of the ATP present, which is directly proportional to the number of cells present in culture. The reagents generate a luminescent signal with extended half-life (>5h).

Method: Culture volume containing 5000 cells was centrifuged (400 x g for 5mins) and resuspended in 100 μ L medium. The suspension was transferred to an opaque-walled 96-well plate along with several ATP solutions (concentrations ranging from 1 μ M to 10nM ATP) for the generation of a standard curve. Medium containing no cells was used as a background control. The plate and its contents were equilibrated at room temperature for 30mins, and following 100 μ L of reagent (prepared according to the manufacturer's guidelines) was added to each well. The contents of the plate were mixed for 2mins on an orbital shaker, and incubated at room temperature for 10mins. Following incubation, the signal was recorded by a luminometer.

2.2.1.3 Primary samples' collection and enrichment

All samples were collected with the approval of the Local Research and Ethics Committee (LREC) and all human participants gave written informed consent.

2.2.1.3.1 CML samples

Leukapheresis samples from newly diagnosed untreated patients with CP CML were enriched to more than 90% CD34⁺ progenitors, by positive selection with CliniMACS, and cryopreserved. CML samples were determined to be Ph⁺ by FISH by Ms Elaine Allan. Purification of the MNC fraction from whole blood cell samples and selection of CD34⁺ cells from MNC samples were performed by Dr Alan Hair.

2.2.1.3.2 non-CML samples

Peripheral blood samples were obtained from patients undergoing autologous stem cell collection for either non-Hodgkin's lymphoma or multiple myeloma. Patient stem cells were mobilised with G-CSF following chemotherapy and the excess CD34⁺ cells remaining after those required for clinical use were donated for research purposes.

2.2.1.3.3 Cord blood (CB) samples

CD34⁺ cells were isolated from fresh or cryopreserved CB samples using human MACS CD34 MicroBeads according to the manufacturer's protocol (Miltenyi Biotec, Surrey, UK). After separation, CD34⁺ purity was assessed by flow cytometry.

2.2.1.4 Cryopreservation of cells

Primary CML/non-CML/CB CD34⁺ cells, as well as cell lines, were cryopreserved in liquid nitrogen at -150°C for long-term storage.

Isolated CML/non-CML/CB CD34⁺ cells from fresh samples were suspended in 4.5% ALBA® and aliquoted in cryotubes; an equal volume of 20% DMSO in 4.5% ALBA® (2.1.8.1.12) was added to give a final DMSO concentration of 10%.

Cell lines in exponential growth phase were collected and resuspended with 10% DMSO in FCS (5-10x10⁶ cells/mL), and aliquoted into cryotubes. The cryotubes were transferred to a cryofreezing container ("Mr Frosty") and kept at -80°C overnight to achieve a controlled

temperature reduction. The next day the cryotubes were transferred to a -150°C liquid nitrogen freezer for long-term storage.

2.2.1.5 Recovery of frozen samples

Primary CML/non-CML/CB CD34⁺ cells were removed from liquid nitrogen and immediately thawed at 37°C in a water bath until ice crystals disappeared. The cells were transferred to a 15mL sterile tube and recovered by adding dropwise 10mL of prewarmed at 37°C DAMP (2.1.8.1.8) thawing solution over a 20mins period. This step was performed at room temperature to enhance the activity of the DNase I, with constant agitation to avoid clumping of the cells. After centrifugation ($120 \times g$ for 10mins), the supernatant was removed and the pellet was washed twice more in DAMP (to get rid of remaining traces of DMSO). Subsequently, the cells were transferred to appropriate volume of SFM+PGFs medium (2.1.8.1.11) for CML and CB samples, or SFM+5GFs medium (2.1.8.1.10) for non-CML samples. The cells were seeded in a 25cm^3 non-adherent tissue culture flask at a density of approximately 1.5×10^6 cells/mL for overnight recovery.

Cell lines were thawed in a 37°C water bath and recovered slowly as above but in PBS instead of DAMP. The cells were then washed twice with PBS ($400 \times g$ for 5mins) and transferred to RPMI⁺⁺. Cells were plated in a 75cm^3 tissue culture flask at a density of 2×10^5 cells/mL (unless otherwise stated).

2.2.1.6 Culture of CD34⁺ cells

Following recovery from long-term liquid nitrogen storage, CML/CB cells were cultured in SFM+PGFs and non-CML cells in SFM+5GF, in 25 or 75cm^3 non-adherent tissue culture flasks. The cells were seeded at an initial concentration of approximately 1.5×10^6 cells/mL and maintained in an incubator at 37°C , 5% CO_2 . Drugs were added to each experiment as appropriate to the described conditions. The cells were harvested at indicated time-points, washed in PBS/2% FCS and aliquots were removed for performing cell counts, FACS analysis and RNA preparation. Wherever cell number was not restrictive, aliquots were taken for protein lysates.

2.2.2 Flow cytometry

FACS is a quantitative technique that permits the characterisation and sorting of cells depending on their phenotype after staining with fluorochrome-labelled antibodies. A flow cytometer is equipped with lasers that supply excitation energy, as well as filters and detectors that detect the fluorescent emissions from the cells. Moreover, flow cytometers can measure the size of a cell, using forward-angle light scatter (FSC), and the granularity of a cell, using side-angle light scatter (SSC). All the flow cytometric analyses herein described were carried out on a Becton Dickinson FACSCanto. Data was analysed using FlowJo software.

2.2.2.1 Selection of CD34+38- cells from total CD34+ samples

CD34+ cells, prior or post transduction, were centrifuged (400 x g for 5mins) and resuspended in 100µl PBS/2% FCS (2.1.8.1.13). Aliquots of cells (2×10^4 cells per tube) were removed for appropriate isotype controls and used to set the detectors, so that the negative isotype population was placed in the first log decade for each flow cytometry channel. CD34-APC and CD38-PerCP positive controls (5µL of antibody per tube) were also set up. The remaining test cells were stained with 15µL of CD34-APC and 15µL of CD38-PerCP antibody and incubated for 20mins at room temperature in the dark. Following incubation, samples were washed twice with PBS/2% FCS (1000rpm for 5mins). The controls were resuspended in 100µL PBS/2% FCS and the test cells were resuspended in 2mL PBS/2% FCS. All samples were sterile filtered through a mesh filter before sorting. The controls were run first and the compensation between fluorochromes with emission spectra overlap was adjusted. The population of CD34+CD38+ and CD34+38- cells were then sorted using a Becton Dickinson FACSAria.

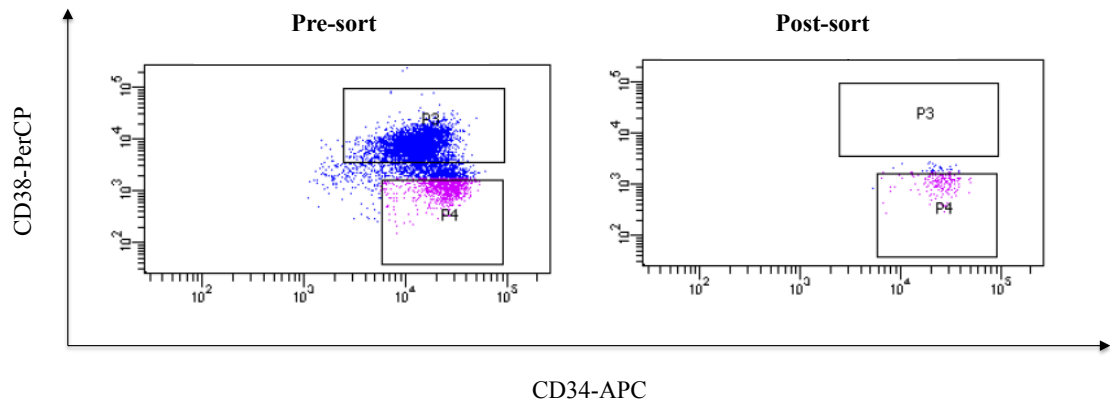


Figure 2-2: Sorting the CD34+CD38- subpopulation from primary human CD34+ samples

The P3 gate represents the CD34+CD38+ cells and the P4 the more primitive CD34+CD38- subpopulation.

2.2.2.2 Surface antibody staining

1×10^5 primary cells were collected, washed in PBS/2% FCS (400 x g for 5mins) and resuspended in 100 μ L PBS/2% FCS with appropriate antibody solution. Subsequently, the samples were incubated in the dark for 15mins. After incubation, the cells were washed twice in PBS/2% FCS (400 x g for 5mins) and analysed by FACS immediately, or kept at 4°C until analysis. Appropriate isotype controls were used as negative controls.

2.2.2.3 Apoptosis and necrosis assessment

Background: Apoptosis and necrosis were assessed by FACS analysis after annexin V staining based on the principle that during early apoptosis phosphatidylserine translocates from the inner layer of plasma membrane to the outer layer and therefore, is available for binding by annexin V. Nonetheless, cells in late apoptosis continue to bind annexin V after loss of plasma membrane integrity. Hence, in order to differentiate between early and late apoptosis, cells were stained with 7-AAD, a nucleic acid dye. Late apoptotic cells were 7-AAD positive since the integrity of plasma membrane was lost. Staining cells simultaneously with annexin V and 7-AAD enabled distinguishing of viable, early apoptotic and late apoptotic (or necrotic cells) by flow cytometry (annexin V- 7AAD-, annexin V+ 7AAD- and annexin V+ 7AAD+, respectively).

Method: Cells were incubated with 5µL annexin-V-FITC (BD, PN 560931) - or annexin-V-PE (BD, PN560930)/ annexin-V-PerCP-CyTM5.5 (BD, PN 561431) for cells that have been transduced and are expressing GFP - and 10µL 7-AAD in 100µL annexin binding buffer (2.1.8.1.14) for 15mins in the dark. The cells were then topped with 300µL annexin binding buffer and analysed by FACS within an hour, to identify percentages of necrotic and apoptotic cells.

2.2.2.4 Cyto-ID® autophagy detection kit

Background: Cyto-ID® autophagy detection kit (Enzo Life Sciences, PN 51031K200) offers evaluation of autophagic activity in live cells by FACS. It relies on the development of a novel dye, Cyto-IDTM green autophagy detection reagent, which selectively labels green vacuoles associated with the autophagy pathway, with minimal background lysosomal staining. The probe is a cationic amphiphilic tracer dye that rapidly partitions into cells in a similar manner as drugs that induce phospholipidosis.

Method: Cell culture medium containing 10⁵ cells was centrifuged (400 x g for 5mins) to pellet the cells and the supernatant was discarded. The cells were washed with PBS, centrifuged as before, and the supernatant was discarded. The cells were resuspended in 95µL 1X assay buffer (1:10 dilution of 10X assay buffer in dsH₂O) provided in the kit, and transferred to a FACS tube. 5 µL of Cyto-IDTM green autophagy detection reagent were added to the cell suspension and gently vortexed, followed by 15mins incubation at room temperature in the dark. The samples were analysed by FACS using a 488nm laser with the FL-1 channel for the detection of the Cyto-IDTM green autophagy detection reagent. Autophagic activity was estimated measuring the mean fluorescence intensity (MFI) value.

2.2.2.5 Evaluation of mitochondrial membrane potential

Background: MitoTracker® Red CMXRos (Invitrogen, PN M7512) is a commercially available cell-permeant fluorescent dye that labels active mitochondria within live cells, utilizing the mitochondrial membrane potential.

Method: Target cells were washed with PBS and incubated with 200nM MitoTracker® Red CMXRos in PBS at 37°C in the dark for 30mins. Cells took up the dye at this stage since it is cell-permeable. Following, cells were centrifuged (400 x g for 5mins) and

resuspended in prewarmed medium. Fluorescence was detected by FACS (excitation wavelength approximately 590nm).

2.2.2.6 Mitochondrial superoxide measurement

Background: Superoxide is the main form of ROS within mitochondria, produced as a by-product during oxidative phosphorylation. MitoSOX™ Red (Invitrogen, PN M36008) is a cationic dye that targets specifically superoxide within mitochondria and not other ROS, emitting fluorescence at 599nm.

Method: Target cells were washed with PBS and incubated with 5µM MitoSOX™ Red in PBS at 37°C in the dark for 30mins. Cells took up the dye at this stage since it is cell-permeable. Following, cells were centrifuged (400 x g for 5mins) and resuspended in prewarmed medium. Fluorescence was detected by FACS (excitation wavelength approximately 590nm).

2.2.3 Western blotting

Western blotting (aka protein immunoblotting) is a robust protein analysis technique that identifies with specific antibodies proteins that have been separated according to their size by gel electrophoresis. The gel is placed then next to the membrane and application of an electrical current induces the proteins in the gel to move to the membrane made of nitrocellulose or PVDF. Therefore, the membrane represents a replica of the gel's protein pattern, and allows visualisation of the protein(s) of interest after staining with a specific antibody coupled to an easily detectable enzyme such as HRP, a radioactive isotope or fluorescent dye.

2.2.3.1 Protein lysate preparation

In order to analyse the proteins of interest within a sample, the cells need to be lysed. There are many recipes for lysis buffers but a few will serve for most western blotting experiments. In brief, they differ in their ability to solubilise proteins, with those containing SDS and other ionic detergents considered to be the harshest and therefore most likely to give the highest yield. For the herein described experiments, two different lysis buffers were used.

2.2.3.1.1 RIPA buffer lysis method

As soon the cells are lysed, proteolysis, dephosphorylation and denaturation also initiate. These events can be significantly inhibited by: 1) keeping the samples on ice, or at 4°C, at all times, and 2) by adding appropriate protease inhibitors fresh to the lysis buffer. Therefore, RIPA buffer (2.1.8.2.1) was prepared immediately prior to use and samples were processed while keeping on ice.

Equal cell numbers from different treatment conditions were washed twice with ice cold PBS (400 x g for 5mins). The cells were then transferred to a 1.5mL eppendorf and washed again in ice cold PBS. The lysis buffer was added to the cells (50µL per 1-3x10⁵ cells), mixed by pipetting up and down and incubated for 15mins on ice. Subsequently, the cell lysates were centrifuged (21,000 x g for 10mins at 4°C) to pellet chromatin and debris. The supernatants were transferred to new eppendorf tubes and stored at -20°C until use.

2.2.3.1.2 2X SDS sample buffer/ Laemmli method

Background: SDS denatures proteins by binding around their polypeptide backbone in a mass ratio of 1.4:1, assigning a negative charge that is proportional to their length. Hence, in denaturing SDS-polyacrylamide gel electrophoresis (PAGE) separations, migration is determined not by intrinsic electrical charge but by molecular weight. 2-mercaptoethanol is used as a reducing agent in the lysis buffer; it reduces disulphide bridges in proteins before they adopt the random-coil configuration so that all the constituent polypeptides can be analysed separately. Glycerol is added to the buffer to increase the density of the sample to be loaded and keep it at the bottom of the well, restricting overflow and uneven gel loading. Bromophenol blue is a small anionic dye molecule that enables the visualisation of the migration of proteins.

Method: 1x10⁶ cells from each treatment condition were washed twice with PBS (120 x g for 5mins) and the supernatant was carefully removed. The cell pellet was resuspended with 2X SDS sample/Laemmli lysis buffer (2.1.8.2.2) (200µL per 1x10⁶ cells), mixed by pipetting up and down and cell lysates were stored at -20°C. Prior to use, protein samples were thawed, mixed by vortexing, heated at 95°C for 10mins and vortexed again before the loading step for best resolution.

2.2.3.2 Protein quantification

Background: Bicinchoninic acid (BCA) protein assay was used to quantify RIPA-lysed protein samples' concentrations according to the manufacturer's instructions. This assay utilises the reduction of Cu^{2+} to Cu^{1+} by protein in an alkaline medium and detects Cu^{1+} by a reagent containing BCA in a colorimetric way. The purple product generated by this reaction is formed by the chelation of one Cu^{1+} ion with two molecules of BCA. The water-soluble complex absorbs strongly at 562nm and its absorbance linearly correlates with increasing concentrations from 20 to 2000 $\mu\text{g}/\text{mL}$.

Method: BSA standards were prepared by serially diluting 2000 $\mu\text{g}/\text{mL}$ BSA in dH_2O . The following BSA concentrations were prepared: 2000, 1500, 1000, 750, 500, 250, 125, 50, 25 and 5 $\mu\text{g}/\text{mL}$ and a blank (dH_2O). These BSA standards were stored at -20°C and used in multiple times.

The BCATM Protein Assay Kit (Thermo-Scientific, PN 23227) was used for protein quantification. BCA working solution was prepared according to manufacturer's instructions, by mixing thoroughly reagents A and B (50:1). 200 μL of this solution was then added to each well of a 96-well plate. 10 μL of each BSA standard concentration was added to each well in triplicate, and 10 μL of protein samples was added in duplicate. The 96-well plate was incubated at 37°C for 30mins and read by an enzyme-linked immunosorbent assay (ELISA) plate reader for absorbance at 562nm. Protein concentrations were calculated according to the BSA standards and equal amounts of protein lysates were loaded for western blotting.

Note: The aforementioned procedure was not followed for the 2X SDS sample buffer-lysed protein samples since the buffer contains bromophenol blue that does not allow the colorimetric detection of the protein content. For these samples, equal number of cells from each treatment was lysed in equal amount of lysis buffer, assuming, thus, that the protein lysates should contain equal amounts of protein.

2.2.3.3 SDS-PAGE

Background: SDS-PAGE is a denaturing separation method used for the analysis of protein samples. As described above, the protein samples are in an SDS containing solution (used either as loading buffer for RIPA-lysed samples or as lysis sample buffer for Laemmli-lysed samples), which binds to hydrophobic regions of the protein molecules, forcing them to unfold into long negatively charged polypeptide chains and become freely soluble in the

solution. Following the application of an electric current, the proteins migrate towards the positive electrode. The size and shape of the polypeptides as well as the pore-size of the gel matrix determine the direction, distance, and speed of migration with smaller polypeptides travelling more rapidly through the gel. Common gel materials are agarose (a polysaccharide) and acrylamide (a 3-carbon amide which is polymerised to form long chains with cross-links between the chains). The pore size of the gel is influenced by the percentage of gel material used and, in the case of acrylamide, the amount of cross-linking.

Method: SDS-PAGE method was utilised for the separation of the proteins based on their size. After short centrifugation, protein samples were loaded into a Nupage® Novex® Bis-Tris 4-12% (Invitrogen, PN NP0321BOX) gradient gel or a homemade 10% or 15% non-gradient gel (2.1.8.2.5). 10µL of Novex® Sharp™ Pre-stained protein standard (Invitrogen, PN LC5800) or HyperPAGE prestained protein marker (Bioline, PN BIO33066) was loaded into a well so as to determine the molecular weight of the proteins within the samples. Gels were run in 1X NuPAGE® MES SDS running buffer (2.1.8.2.6) for the precast gels, or homemade 1X running buffer (2.1.8.2.9) for the homemade gels, at 80V for the first 30mins and at 120V for the remaining time, in a Invitrogen XCell SureLock™ mini-cell electrophoresis system.

2.2.3.4 Transfer to PVDF membrane

Following gel electrophoresis, proteins were transferred from the gel to a PVDF membrane. PVDF membrane was activated by brief soaking into methanol, followed by soaking in transfer buffer until completely wet. The sponges and paper towels were all soaked carefully in 20% methanol transfer buffer (2.1.8.2.7 or 2.1.8.2.11) before use. Methanol was included in the transfer buffer, for two main reasons; firstly, to maintain dimensional stability of gels and minimise gel swelling, and secondly, to remove SDS from proteins and increase protein binding to the membrane.

The transfer sandwich was assembled as shown in Figure 2-3. Proteins were transferred at 30V for 80mins in an XCell II™ blot module.

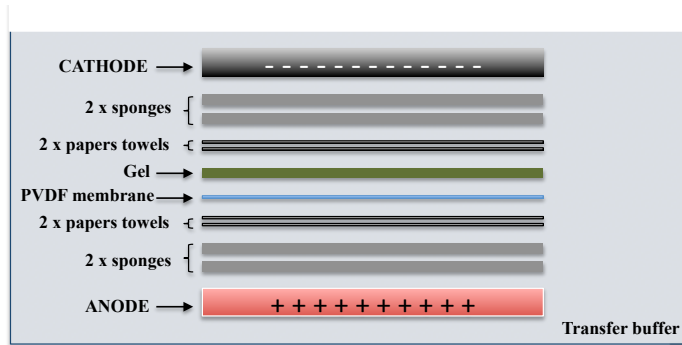


Figure 2-3: Assemble of sandwich for transfer of proteins to PVDF membrane

2.2.3.5 Immunolabelling

In order to verify the efficiency of the proteins' transfer onto the membrane, the transfer membrane was stained with 0.1% Ponceau S for a min. Ponceau S destaining of the membrane occurred with careful washes with dH₂O. Subsequently, the membrane was blocked in 5% BSA/TBST blocking buffer (2.1.9.2.12) at room temperature for 30mins with constant agitation. After blocking, the membrane was incubated with primary antibody solution diluted in the blocking buffer (e.g. p-CrkL, LC3B, GAPDH, p-RPS6K; 1:1000 dilution) overnight at 4°C with gentle rotation. The next day, the membrane was washed in the 1X TBST buffer (2.1.8.2.4) 3x15mins to get rid of unbound primary antibody and reduce background. After washes, the membrane was incubated with HRP-conjugated secondary antibody solution (1:3000 dilution) for 1h at room temperature with agitation. Following secondary antibody incubation, the membrane was washed in the 1X TBST buffer 3x15mins to remove unbound secondary antibody. Finally, the Immuno-Star™ WesternC™ kit (Bio-Rad, PN 170-5070) was used according to the manufacturer's instructions for development of the membrane. Just before the development, the membrane was incubated with the mixture of equal amounts of luminol/enhancer solution and peroxide solutions for 3mins. HRP oxidises luminol in the presence of hydrogen peroxide and when oxidised luminol goes back to its initial state, and light is emitted. The enhancer increases signal intensity and length. At last, digital pictures of protein bands were taken by the Molecular Imager® ChemiDoc™ XRS machine.

2.2.3.6 Stripping

In order to incubate the PVDF membrane with a different primary antibody, the membrane was incubated in Re-Blot™ Plus Strong Antibody Stripping Solution (Chemicon, PN 2504) (1mL of the 10X buffer was diluted with 9mL distilled water) for about 15mins with constant agitation at room temperature. The stripping buffer can remove antibodies bound to the membrane without removing proteins. The membrane was washed briefly in TBST and re-blocked in 5% BSA/TBST blocking buffer for 30mins before incubation with another primary antibody.

2.2.4 Immunofluorescence microscopy

Poly-L-lysine coated multi-spot microscope slides were prepared in advance; poly-L-lysine is adhesive and it facilitates suspension cells binding to glass microscope slides. Poly-L-lysine solution (Sigma-Aldrich, PN P8920) was diluted 1:10 in distilled water, and multi-spot microscope slides were immersed in the dilution in a coplin jar for 10mins. Excessive poly-L-lysine solution was removed, and the slides were air-dried and kept in a box for future use.

30,000 cells per treatment were added to each well of a poly-L-lysine-coated multi-spot slide. Samples were allowed to adhere to the slides for 90mins in a tissue culture incubator. Following, the excess medium was gently removed by blotting carefully with tissue paper and the cells were fixed by cross-linking protein molecules with the addition of 30 μ L of the 3.65% formaldehyde solution (2.1.8.3.1) per well. The slides were incubated for 20mins at room temperature and washed 2x5mins in PBS. Permeabilisation was performed by incubating the cells with 30 μ L of 0.5% Triton-X-100 solution (2.1.8.3.2) per well for 10mins. Triton-X-100 solution can dissolve cellular lipid membranes to allow antibody access of internal proteins. After washing in PBS 2x5mins, the slides were dried and each spot was blocked with 30 μ L blocking buffer (2.1.8.2.12) for 1h at room temperature. LC3B antibody (Cell Signaling, PN 2775) at a concentration of 0.5 μ g/mL in blocking buffer was added to each well. 30 μ L of rabbit F(ab')₂-IgG-isotype (Abcam, PN ab37416; 0.5 μ g/mL in blocking buffer) was used as a control. The slides were incubated for 90mins at room temperature. Following incubation, the slides were washed 4x5mins with PBS. Subsequently, the slides were incubated with Alexa Fluor® 488 goat anti-rabbit IgG secondary antibody (Invitrogen, PN a-11008) (1 μ g/mL in blocking buffer; 30 μ L per spot) for 1h at room temperature in the dark. The slides were washed 4x5mins with PBS and

then air-dried. Two drops of VECTASHIELD® mounting medium with DAPI (Vector, PN H-1200) were added to the centre of each slide and a coverslip placed on the top. The coverslip was carefully pushed down, so that the mounting medium spread over each well of the slide and then sealed with nail varnish. The slides were stored at 4°C until analysis.

All slides were analysed using a Zeiss Imager M1 microscope at 100x magnification using oil immersion and Axiovision software. Images were captured with multiple layers from the top to the bottom of cells with optimal distance (0.25µM) between adjacent layers. Captured images were subjected to deconvolution to remove non-specific fluorescence and sharpen images. Deconvolution was performed by utilising the deconvolution module of the AxioVision software; the iterative algorithm and clip normalisation methods were used.

2.2.5 PCR-based assays

PCR is a technique used to amplify a single or a few copies of a DNA piece to millions of copies. Usually, it includes 20-40 thermal cycles, with each cycle consisting of three steps including 1) denaturation of the double-stranded DNA into single strands, 2) annealing of primers to the single-stranded DNA and 3) extension of primers by the Taq polymerase. Nowadays, PCR has widespread application.

2.2.5.1 Primer design

Primers were designed with Vector NTI ® software and were verified by using the NCBI/Primer-Blast. The cDNA sequences were identified by searches on the Pubmed website, and used to design appropriate primers. The primers were about 20bp with similar melting temperatures between forward and reverse primers, excluding internal loops or primer dimers.

2.2.5.2 RNA extraction

Cells were harvested, washed in ice-cold PBS, and pelleted by centrifugation at 500 x g for 3mins at 4°C prior to RNA extraction. The RNeasy Mini Kit (Qiagen, PN 74106) was used according to the manufacturer's instructions for the extraction of the total cellular RNA. The concentration and quality of extracted RNA were measured with a NanoDrop ND-

1000 spectrophotometer (Labtech International Ltd). Absorbance at 260nm quantified nucleic acid concentration, and RNA purity was determined by the ratio of 260/280 (1.8 to 2.0) and 260/230 (1.8 or greater). This is because nucleic acid is detected at 260nm, while solvents, salts and protein are detected at 230nm and 280nm. RNA was stored diluted in RNase free dsH₂O at -80°C.

2.2.5.3 cDNA synthesis by reverse transcription

RNA was reverse transcribed into cDNA by the High Capacity cDNA Reverse Transcription Kit (Applied Biosystems, PN 4374966) according to the manufacturer's instructions. RNA samples were prepared to a concentration of 1µg per 10µl in nuclease-free dsH₂O and mixed with 10µL of 2X Reverse Transcription Master Mix (2.1.8.4.1) in a PCR tube to give a final concentration of 1 x RT-buffer, 4mM dNTP mix, 1xRT random primers, and 2.5IU/ml MultiScribe reverse transcriptase (Applied Biosystems, PN 4311235). The 20µL mixture was run in a MastercyclerTM PCR machine (Eppendorf UK Ltd.). The program was 25⁰C for 10mins, 37⁰C for 120mins and 85⁰C for 5secs. Synthesised cDNA was kept at 4⁰C for short-term storage or at -20⁰C for long-term storage.

2.2.5.4 Single-cell preamplification

CellsDirectTM One-Step qRT-PCR Kit (Invitrogen, PN 11753) was used for the amplification of 1-300 sorted cells. Initially, a 0.2X probe mix was prepared by adding 1µL of each of the 20X TaqMan® probes to be used on the chip (can preamplify up to 100 targets even if the 48.48 dynamic array chip can accommodate up to 48 probes) and appropriate TE volume up to 100µL total mix volume. The 0.2X probe mix was stored at -20⁰C up to 6 weeks. The RT-STA mix (2.1.8.4.4) was prepared each time just before the sort. 1 up to 300 target cells were sorted into a well with 5µL, vortexed and briefly centrifuged. The preamplification mixture was run in a MastercyclerTM PCR machine. The program was 50⁰C for 10mins, 95⁰C for 12mins, 95⁰C for 15secs and 65⁰C for 4mins, for a total of 18 cycles. Synthesised cDNA was kept at 4⁰C for short-term storage or at -20⁰C for long-term storage. The amplified cDNA was diluted 5X with TE buffer (20µL per well), vortexed and briefly centrifuged. Samples were stored at -20⁰C until analysis.

2.2.5.5 qRT-PCR

qRT-PCR uses the linearity of DNA amplification to determine absolute or relative amounts of a known sequence in a sample by monitoring DNA amplification through each cycle. When the DNA is in the log linear phase of amplification, the amount of fluorescence increases above the background. Threshold cycle (Ct) is the point at which the fluorescence becomes measurable. By using multiple dilutions of a known amount of standard DNA, a standard curve can be generated of log concentration against Ct. The amount of DNA or cDNA in an unknown sample can then be calculated from its Ct value.

2.2.5.6 TaqMan® qRT-PCR

Background: This method uses dual-labelled probes, which are oligonucleotides designed to hybridise to a complementary region of the cDNA of interest, and contain (i) a fluorescent reporter dye on the 5' base, and (ii) a quencher located on the 3' base. When irradiated, the excited fluorescent reporter dye transfers energy to the nearby quencher molecule rather than fluorescing, resulting in a non-fluorescent substrate. However, during PCR, when the polymerase extends the PCR product from the upstream primer, the 5' exonuclease activity of the polymerase cleaves the probe. This separates the fluorescent quencher and reporter dyes and fluorescence resonance energy transfer no longer occurs. The increase in fluorescence intensity is proportionate to the number of probe molecules that are cleaved.

Method: TaqMan® qRT-PCR was performed using TaqMan® Gene Expression Assays (Applied Biosystems), as follows. The TaqMan® Gene Expression Assay probes (2.1.4) were all carrying a FAM reporter; GAPDH, GUSB, 18S and TBP were used as endogenous controls. In a MicroAmp™ Optical 96-well reaction plate (Applied Biosystems) a total volume of 25µl/reaction was prepared, containing 1X TaqMan® Gene Expression Mastermix (AmpliTaq Gold® DNA Polymerase, Uracil-DNA glycosylase, dNTPs with deoxyuridine triphosphate, ROX™ Passive Reference, in addition to buffer components), 1X TaqMan® Gene Expression Assay and 1µl cDNA diluted in nuclease free dsH₂O. For each sample, each gene was assayed in triplicate, and a negative control containing nuclease free dsH₂O in place of cDNA was included. Plate wells were capped and the plate centrifuged briefly. The plate was inserted into an Applied Biosystems 7900 Fast Real-Time PCR System thermal cycler, and programmed to complete 40 cycles as follows: 50°C for 2mins, 95°C for 10mins, 95°C for 15secs, and 60°C for 1min. Reactions

were analysed using Sequence Detections Systems software version 2.3 (Applied Biosystems). Results for each sample were analysed by using the 2^{-DDCt} method [334].

2.2.5.7 PCR amplification

PCR Mix (2.1.8.4.2) was prepared in a PCR tube with GeneAmp® RNA PCR Core Kit according to the manufacturer's instruction. The PCR tube was heated to 94°C for 5mins at first to denature all the double stranded cDNA, and then 35 cycles of 94°C for 30secs, 52°C for 1min and 72°C for 1min were set in a PCR Thermo Cycler. After all cycles finished, the tubes were heated to 72°C for 5mins for final extension, and then held at 4°C.

2.2.5.8 Gel electrophoresis

The PCR products were ran in agarose gels in order to visualise individual DNA bands. 1% agarose gels were prepared by diluting 0.5g agarose powder in 50mL of 1X TBE buffer (10X TBE buffer -2.1.8.4.3- diluted in dH₂O). The mixture was heated in a conical flask in a microwave until the agarose powder had completely dissolved. When the gel cooled down, 1µL ethidium bromide (10mg/mL) was added and mixed well. Subsequently, the gel was poured into a casting tray with a comb inserted to create loading wells. The gel was left to set for about 30mins. The comb was removed and the gel was placed in a gel tank filled with 1X TBE buffer so as to cover completely the gel. 10µL of PCR product mixed with 2µL loading dye (6X) was loaded into each well of the gel (2µL of 100bp DNA ladder was loaded in a separate lane), and then the gel was run at 50V constant voltage. After running, the gel was viewed by an ultraviolet (UV) transilluminator (ChemiDoc) and photographed.

2.2.5.9 High-throughput qRT-PCR (Fluidigm®)

Background: Fluidigm® introduced in 2006 the first commercial system for digital PCR using nanolitre volumes, based on integrated fluidic circuits (chips) having integrated chambers and valves for partitioning samples. The Fluidigm® 48.48 Dynamic Array™ chip allows the validation of up to 48 genes in each of the 48 samples simultaneously. With a dynamic array chip, high-throughput multiplexing is easy because the integrated fluidic

circuit (IFC) does the work of combining samples and primer-probe sets into 2,304 PCR assays (48 real-time curves for each of 48 samples).

Method: Initially, the 48.48 the dynamic array was primed in order to close the interface valves and prevent premature mixing of samples and assays. A plate “assays” (BioMark®) was prepared by loading into each well a mixture containing 3.0µl assay loading reagent (Fluidigm, PN 85000736) and 3.0µl of each TaqMan® gene expression assay. A ‘samples’ plate (BioMark®) was prepared by mixing in each well 3.0µl Taqman® Universal PCR Master Mix, 0.3µl 20X GE sample loading reagent (Fluidigm, PN 85000735) and 2.7µl from the pre-amplified cDNA mix (2.2.5.4). 5µl from each well in plate “arrays” and plate “samples” were loaded into separate array and sample inlets on the left and right frames of the chip respectively, as shown in Figure 2-4. Note that the in the number 22 sample inlet, the RT-STA water control was loaded. Following, the dynamic array was placed on the IFC controller, and software interface was used to pressure load the assay components into reaction chambers. Assay components were automatically combined on-chip. Subsequently, the dynamic array was transferred to a BioMark Real-Time PCR System for thermal cycling and fluorescence detection. Amplifications were carried out at 95°C for 10mins, followed by 40 PCR cycles at 95°C (15secs) and 60°C (4mins) on the BioMark System. qRT-PCR analysis software was used to visualise and interact with amplification curves performed analysis, colour-coded heat maps, and Ct data for the run. Data was analysed as for qRT-PCR using GAPDH rRNA as the housekeeping gene (GUSB, 18S and TBP were also tested).

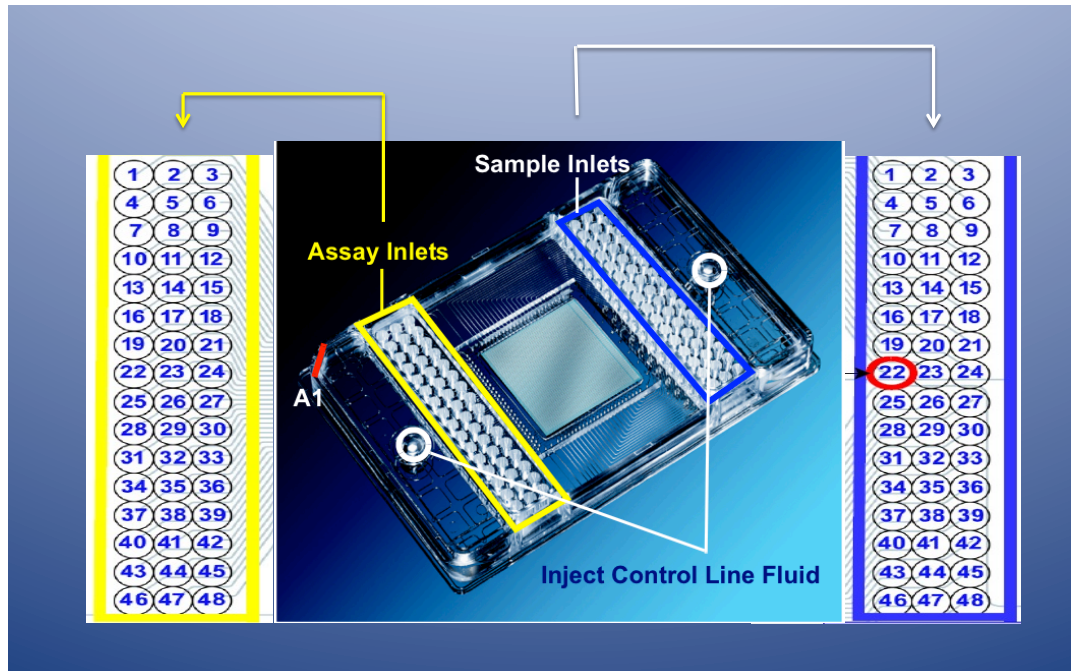


Figure 2-4: The Fluidigm[®] 48.48 Dynamic Array[™]

2.2.6 Statistics

All statistical analyses were performed either with the Microsoft Office Excel software using the two-sided unpaired or paired Student's t-test or the GraphPad Prism Software. P-values less than 0.05 were considered statistically significant. The results are shown as the mean \pm standard error of the mean (SEM).

2.2.7 Cellular techniques

2.2.7.1 LTC-IC

Background: Primitive haemopoietic cells with proliferative potential can be maintained in long-term bone marrow culture (LTBMC) for extended periods of time in microenvironment formed by supportive stromal layer. An application of LTBMC is an assay that measures the number of LTC-IC.

In this assay, the cells of interest are overlaid on a supportive irradiated stromal cell monolayer and cultured for 5 weeks before being transferred to a CFC. The number of colonies counted at the end of the assay correlated with the number of LTC-IC within the initial test cell sample. Figure 2-5 shows a schematic diagram for the method used in the LTC-IC assay.

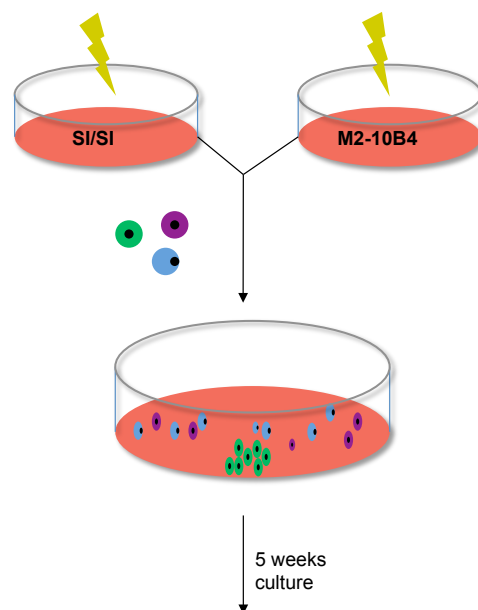
Step 1 : Establishment of feeders

Supportive stromal cell layer consisting of two irradiated cell lines:
 SI/SI → express SCF and IL-3
 M2-10B4 → express G-CSF and IL-3

Step 2 : Addition of known number of test cells

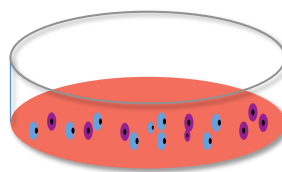
Step 3: Maintenance of the culture

The total cultivating time is 5 weeks with weekly change of $\frac{1}{2}$ of the medium



Step 4: Harvest and plate

Harvest endline dish, including adherent and non-adherent cells, and plate appropriate aliquot in methylcellulose cultures.

**Step 4: Count total number of colonies**

Calculate number of LTC-IC in test cell suspension based on the average output of CFC per LTC-IC as determined by a limiting dilution assay.

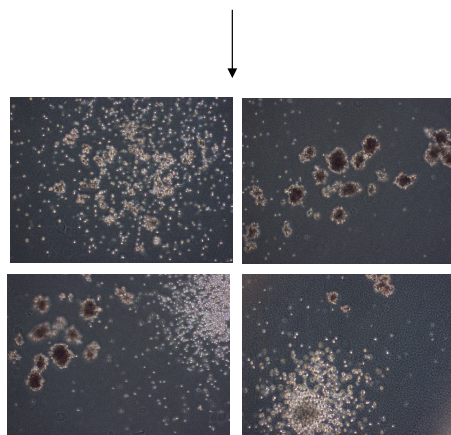


Figure 2-5: The LTC-IC assay

Method: LTC-IC stromal support was provided by two genetically modified murine fibroblast cell lines, M2-10B4 (expressing G-CSF and IL-3) and SI/SI (expressing SCF), which were kindly provided by the Terry Fox Laboratories (Vancouver, BC, Canada). Following thawing the cell lines were maintained in culture and when the monolayer was semi-confluent, the cells were trypsinised and passaged to allow for propagation of sufficient cells for LTC-IC. Proliferation of untransduced cells was minimised but supplementing the cultures on alternate weeks with hygromycin B (final concentration 62.5µg/mL for M2-10B4 and 125µg/mL for SI/SI fibroblasts) and G418 (final concentration 400µg/mL for M2-10B4 and 800µg/mL for SI/SI fibroblasts). Moreover, in order to render them incapable of proliferation, M2-10B4 and SI/SI cells were irradiated at 80gray prior to being seeded with the test cells. Afterwards, M2-10B4 and SI/SI fibroblasts were mixed in a 1:1 ratio and resuspended in hydrocortisone supplemented Myelocult™ to a final cell concentration of 3×10^5 cells/mL. 2mL of this suspension was then aliquoted into the required number of wells of a BD BioCoat™ - Collagen I 12-well plate (BD, PN 354500). After 24h of incubation, the test cells were inoculated in duplicates onto the stromal monolayers. The cells were incubated for a total of 5 weeks at 37°C, 5% CO₂ with weekly replacement of 1mL Myelocult™, in order to achieve a half medium change. After 5 weeks, LTC-IC were harvested and set up in CFC assay. Culture supernatant from each LTC-IC well was collected in a sterile 15mL centrifuge tube. Each well was washed with

2mL HBSS-CMF (to remove any serum-containing Myelocult™ medium), which was also transferred to the collection tube. Adherent cells were detached after incubation with 1mL 0.25% trypsin-EDTA for a maximum of 5mins and transferred to the harvest tube. Immediately, 2mL of IMDM/2% FCS were added to the LTC-IC well, swirled gently and transferred to the harvest tube. A further 2mL of HBSS-CMF was used to wash the well and then transferred to the harvest tube. The harvest tubes were then centrifuged (400 x g for 10mins). Finally, the supernatant was gently poured off and the cells were resuspended in the remaining supernatant. The volume of the remaining cell suspension was noted and a cell count was performed.

2.2.7.2 CFC assay

Duplicate committed progenitor cell assays were set up for each cell volume of each treatment condition at a cell concentration of 2.5×10^4 /mL. Appropriate volume of cell suspension for duplicate wells was added to 3mL of Methocult™ H4434 medium for committed progenitor cell assays and vortexed for 15secs. After 10mins (in order to allow for the formed bubbles to go to the surface), 1.5mL of this mixture was transferred to a 35mm tissue culture dish in duplicate. Each dish was gently swirled, so as to coat the whole surface, and then incubated for 14 days at 37°C, 5% CO₂. At the end of this time, the number of viable colonies was counted in each dish and this allowed a comparison of the LTC-IC present in the different treatment conditions.

In experiments where CFC assays were performed alone (without LTC-IC), 5000 cells were added to 3mL of Methocult™ methylcellulose medium and split into two 35mm tissue culture dishes in duplicate. The rest of the procedure was the same as described directly above.

For CFC experiments with cell lines, the Methocult™ H4230 medium was used.

2.2.7.3 Isolation of cell line sub-clones

Background: In theory, all cells within a cell line are clones and therefore, should be genetically uniform. Nevertheless, spontaneous mutations giving a proliferation advantage can occur in single cells and lead to a mixed population of sub-clones carrying different genetic defects. In order to validate that the phenotype observed after ATG7 knock-down was attributed to the knock-down and not the selection of a mutation carrying K562 sub-clone, the following approach was followed.

Method: K562 cells were transduced three times with virus carrying an ATG7 or control short hairpin, as described at section (§) 2.2.8.1.1. 48h after the last incubation with virus, successfully transduced cells were sorted based on the expression of the GFP marker. Single control or ATG7 knock-down GFP⁺ cells were sorted in individual wells of 96-well plates with 100 μ L RPMI⁺⁺. The presence of a single cell was verified after examination under a microscope.

2.2.8 Gene knock-down

A widely used approach in order to study the function and regulation of a specific gene or to explore its therapeutic applications, is by knocking it down, i.e. depleting/deleting the gene's product, and investigating the effects it has on the cells' phenotype. This can be carried out either by editing the organism's DNA, e.g. by deleting the gene itself, or by degrading the gene's product at mRNA level before it matures into a functional protein. The latter technique utilises small interfering RNA (siRNA) that via the RNA interference (RNAi) technology silence the target gene in a sequence-specific manner. These siRNAs can be stably introduced even to a non-dividing cell in the form of short hairpin RNA (shRNA)—which will be processed within the cells into siRNA- through lentiviral delivery and they will be integrated to the host's genome. In order to knock-down a gene transiently, processed siRNA molecules can be introduced directly into the cells nucleus by electroporation.

2.2.8.1 Lentiviral transduction

pLKO.1-GFP-shATG7_E, pGIPZ-GFP-shATG7_1 and pGIPZ-GFP-shATG7_2 vectors carrying hairpins targeting *ATG7* were used along with the packaging vectors psPAX2 and pCMV-VSV-G (see Appendix for plasmid maps). For murine samples, the pLKO.1-PURO-shAtg7 vector was used. Vectors pLKO.1-GFP-shCtrl and pGIPZ-GFP-shCtrl carried scrambled - non-targeting- hairpins and were used as control.

The plasmids pGIPZ-GFP-shATG7_1 and pGIPZ-GFP-shATG7_2, were donated by Professor Ravi Bhatia. The plasmid pCMV-VSV-G was kindly donated by Professor John Rossi. pLKO.1-PURO-shATG7 and pLKO.1-PURO-shAtg7 were donated by Professor Kevin Ryan. Plasmids pLKO.1-GFP-shCtrl and psPAX2 were donated by Dr Kamil Kranc. As described below (§2.2.9), the shATG7 hairpin was cloned into the pLKO.1-GFP backbone in order to be able to select by FACS the transduced cells.

2.2.8.1.1 Transfection of HEK293 cells

For the production of the virus, HEK293 cells were transfected using the CaCl₂ method. The cells were set up two days before the transfection as 2x10⁶ cells/ 10cm² petri dish in 10ml DMEM++ to allow them to adhere. In order to facilitate the attachment, the petri dishes were coated with 0.1% gelatin in dsH₂O. 10µg of the shRNA vector, 6.5µg psPAX2, and 3.0µg pCMV-VSV-G were diluted in the transfection solution (2.1.8.5). The transfection mixture was incubated at 37⁰C for 30mins and then, transferred dropwise to the HEK293 cells. The following morning, the medium was replaced with 20% FCS DMEM[^] (2.1.8.1.3) (to wash off the CaCl₂ precipitate) and the flasks were examined under inverted fluorescent microscope for the presence of green cells. After 24h, the virus was collected as supernatant and used either directly for the transfection of primary CML/non-CML/cord blood CD34+ cells or it was ultracentrifuged, as described below.

2.2.8.1.2 Transduction of CML cells with fresh virus

After 24h of incubation, virus-containing 20% FCS DMEM[^] medium was collected from the HEK293 cells and used for the transduction of primary CML/non-CML/CB samples or cell lines. The cells were spinoculated in 5mL or 20mL of virus containing medium in 25cm² or 75cm² flasks respectively (approximately 5x10⁵ cells/mL) at 400 x g for 90mins. Virus transduction reagents Transdux™ (Lonza, PN LV850A-1) and polybrene (Sigma-Aldrich, PN 107689; dilution 1:2000) were used for primary samples and cell lines, respectively, in order to facilitate the entrance of the virions in the target cells and increase the efficiency of the transduction. 15mL of fresh medium were placed on the HEK cells so as to produce more rounds of virus. Spinoculations were repeated at 32h, 48h and 56h. 72h after the first transduction, the cells were centrifuged (400 x g for 5mins) and the viral containing supernatant was removed. The cells were resuspended in SFM+5GFS (for non-CML samples) or SFM+PGFs (for CML and CB samples). Transduced cells were sorted 48h after the last incubation with virus, based on the presence of GFP, and used as described per experiment.

2.2.8.1.3 Transduction of CML cells with concentrated virus

Concentrated virus was produced after 24h of incubation by ultracentrifuging the supernatant 20% FCS DMEM[^] medium of the transfected HEK293 cells in Beckman tubes at 625,000 x g for 2h in vacuum, at 4⁰C. The supernatant was removed carefully and the pellet, which contained the virus particles, was resuspended in 200μL SFM. Titration of the virus was carried out by adding small aliquots of the concentrated virus solution (from 2μL to 20 μL) on HT1080 cells (10⁵ cells/well in a 6-well plate). Polybrene (dilution 1:2000), a cationic polymer, was used to enhance the transduction of the cells. Four days post-transduction, the HT1080 cells were analysed by FACS and the virus titre was estimated by using the following formula:

$$(10^5 \text{ seeded cells} \times \% \text{GFP+ cells}) \times 1000 / \mu\text{L virus}$$

Equation 2-1

200μL of unconcentrated virus were also titrated in order to evaluate the efficiency of the ultracentrifugation.

Primary samples were transduced with multiple of infection (MOI) 10 in the presence of Transdux™. This procedure was repeated after 24h. 48h after the last incubation with virus, the cells were centrifuged (400 x g for 5mins) and the viral containing supernatant was removed. The cells were resuspended in SFM+5GF (for non-CML) or SFM+PGFs (for CML and CB samples). Transduced cells were sorted the day after, based on the presence of GFP, and used as described per experiment.

2.2.8.1.4 Amaxa® nucleofection

Culture volume containing 1x10⁶ cells was centrifuged (400 x g for 5mins) at room temperature. The supernatant was completely removed and the cell pellet was washed twice in 5mL PBS. Subsequently, the pellet was resuspended with 100μl room temperature Cell Lines Nucleofector® Solution V (Lonza, PN VCA-1003) - for cell lines- or Human CD34+ Cell Nucleofector® Solution (Lonza, PN VPA-1003) - for primary CD34+ samples- that included 2μg pmaxGFP® vector and 50nM control (Thermo-Scientific, PN D-001810-01) or ATG7 targeting siRNA pool (Thermo-Scientific, PN L-020112-00). A pool of four siRNAs was preferred over single siRNAs in order to mimic the natural silencing pathway and reduce the off-target effects. The suspension was transferred into a certified cuvette and sealed with a cap provided with the kit. The cuvette was inserted into

the Nucleofector® Cuvette Holder of a Nucleofector®II Device and the appropriate transfection program was chosen from the menu (T-020 for cell lines or U-008 for CD34+ cells). Once the program finished, the solution was transferred to 5mL of prewarmed medium in a 6-well plate by using the supplied pipettes. The cells were stored in a humidified 37°C/5% CO₂ incubator until analysis. Transfected cells were sorted 48h later, based on the expression of GFP, and used as described per experiment.

2.2.9 Cloning

Background: In order to be able to select the successfully transduced cells, the shRNA vectors carry selection markers, such as genes coding for fluorescent proteins or antibiotics resistance. The pLKO.1-PURO-shATG7 vector carried the selection market of resistance to puromycin. This means that selection of the successfully transduced cells would have to be carried out by growing the total number of cells for 3 days in medium supplemented with puromycin, a technique that has mainly two drawbacks; firstly, the transduced cells would not be able to be selected by FACS and secondly, we do not know if the phenotype or biochemistry of the cells would be affected by the process selection in the presence of PURO. Therefore, it was decided to clone the hairpin of the pLKO.1-PURO-shATG7 in a pLKO.1 backbone that carried as selection gene GFP, a marker that allows for FACS selection and it is not relatively toxic to the cells (Figure 2-6). The shATG7 hairpin was “cut” from the pLKO.1-PURO-shATG7 vector and cloned into the backbone of the pLKO.1-GFP-shCtrl.

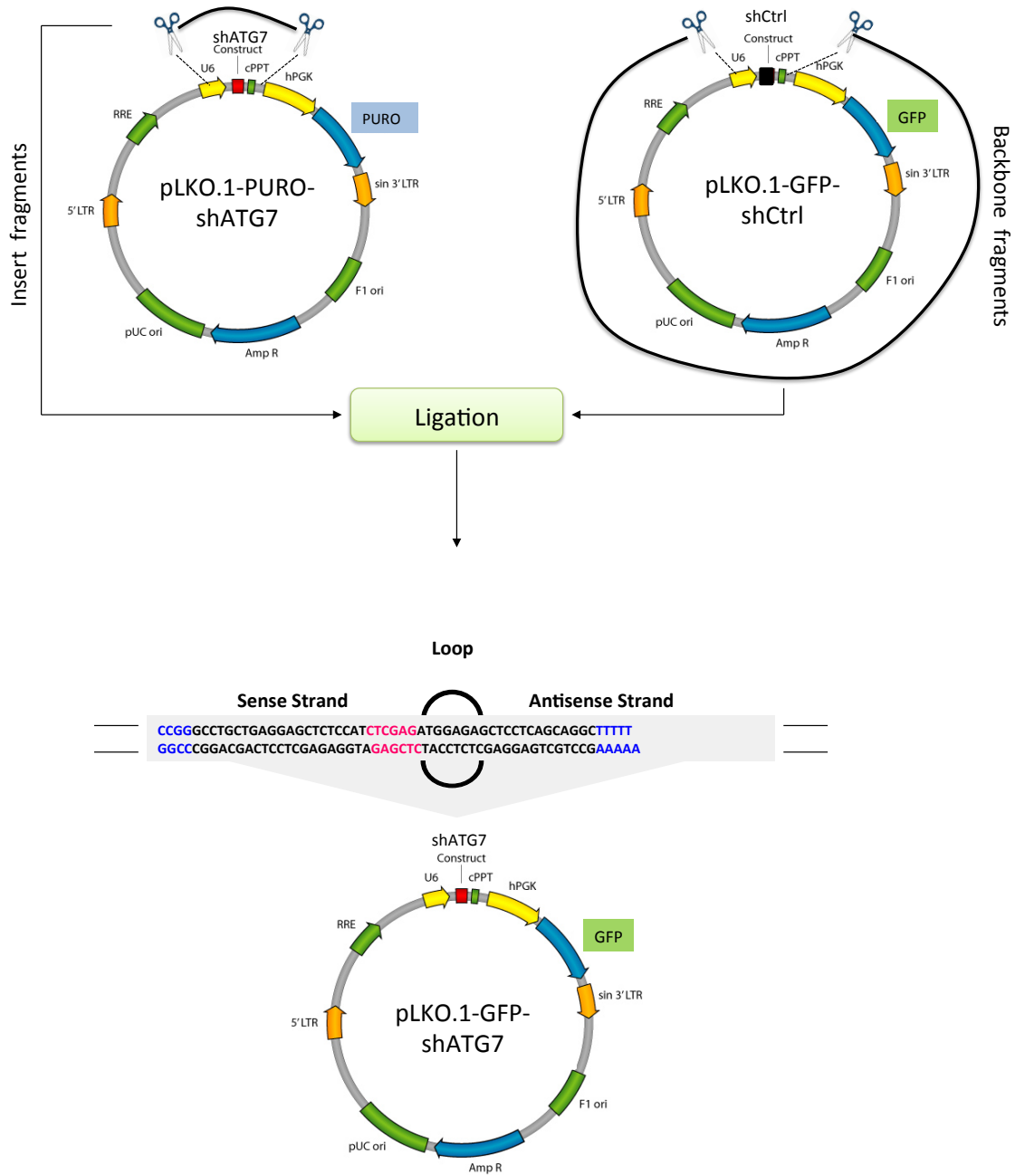


Figure 2-6: Strategy for cloning the shATG7 hairpin into the pLKO.1-GFP backbone

Method: In order to generate bacterial stocks carrying the plasmids of interest, competent bacteria were transformed with plasmids pLKO.1-PURO-shATG7 or pLKO.1-GFP-shCtrl and incubated overnight at 37°C on agar plates supplemented with ampicillin. The following day, a starter culture was formed by inoculating a single colony from each plate into 5mL LB (2.1.8.6.1), and incubated overnight at 37°C with constant agitation. After 24h, each starter culture was moved to 250mL of LB and incubated at 37°C with constant agitation. The plasmids were collected from the cells 24h later by using the HiSpeed® Plasmid Midi Kit (Qiagen, PN 12643) as described by the manufacturer's instructions; 2mL of each culture were stored as bacterial glycerol stock (30% glycerol in dsH₂O). Subsequently, both pLKO.1-PURO-shATG7 and pLKO.1-GFP-shCtrl were double-digested with the restriction enzymes *SpeI* (NEB, PN R0133) and *NdeI* (NEB, R0111) at 37°C for 3h in order to cut both plasmids in two fragments; the backbone fragments (which included the selection marker) and the insert fragments (which included the short hairpin). Following, the double-digested vector pLKO.1-GFP-shCtrl was incubated for 45min with SAP (Promega, PN M8201) in order to dephosphorylate its overhanging complementary ends and inhibit annealing between them. Hence, each plasmid was cut in two fragments; the approx. 6.5kb vector backbone (pLKO.1-GFP or pLKO.1-PURO) and the approximately 600bp insert fragment that contained the shRNA hairpin (shATG7 or shCtrl). Afterwards, the digestion products were separated on a 1% agarose gel. The fragments of interest, pLKO.1-GFP backbone and shATG7 insert, were isolated under long-wave UV light using a clean scalpel (short-wave UV light is not recommended because it may break DNA). The products were gel-purified by using the QIAquick Gel Extraction Kit according to manufacturer's instructions. The concentration and quality of extracted DNA were measured with a NanoDrop ND-1000 spectrophotometer. Following, the pLKO.1-GFP backbone and shATG7 insert fragments were ligated overnight at room temperature. As dephosphorylation control, pLKO.1-GFP backbone fragments were ligated but without adding the insert fragments. The ligation products were used for bacterial transformation. The dephosphorylation control presented with no colony growth, which confirmed that the dephosphorylation step was successful. On the other hand, bacteria that were transformed with the ligation product from the pLKO.1-GFP backbone and the shATG7 insert presented with hundreds of colonies. From these, 10 single colonies were randomly selected and grown overnight in 5mL LB for an initiation colony. After 24h, plasmid was extracted from 3mL of each starter culture by using the QIAprep Spin Miniprep Kit according to manufacturer's instructions. The remaining 2mL were stored as bacterial glycerol stock (30% glycerol dsH₂O). Following isolation, the 10 plasmid clones

were double digested with the *SpeI* and *NdeI* restriction enzymes in order to verify the presence of the insert and after electrophoresis, all of them appeared to have an insert (Figure 2-7). Three random clones were sent for sequencing analysis with primer that were flanking the shRNA area, where it was verified that all of them carried the shATG7 sequence, without the presence of any mutations or alterations.

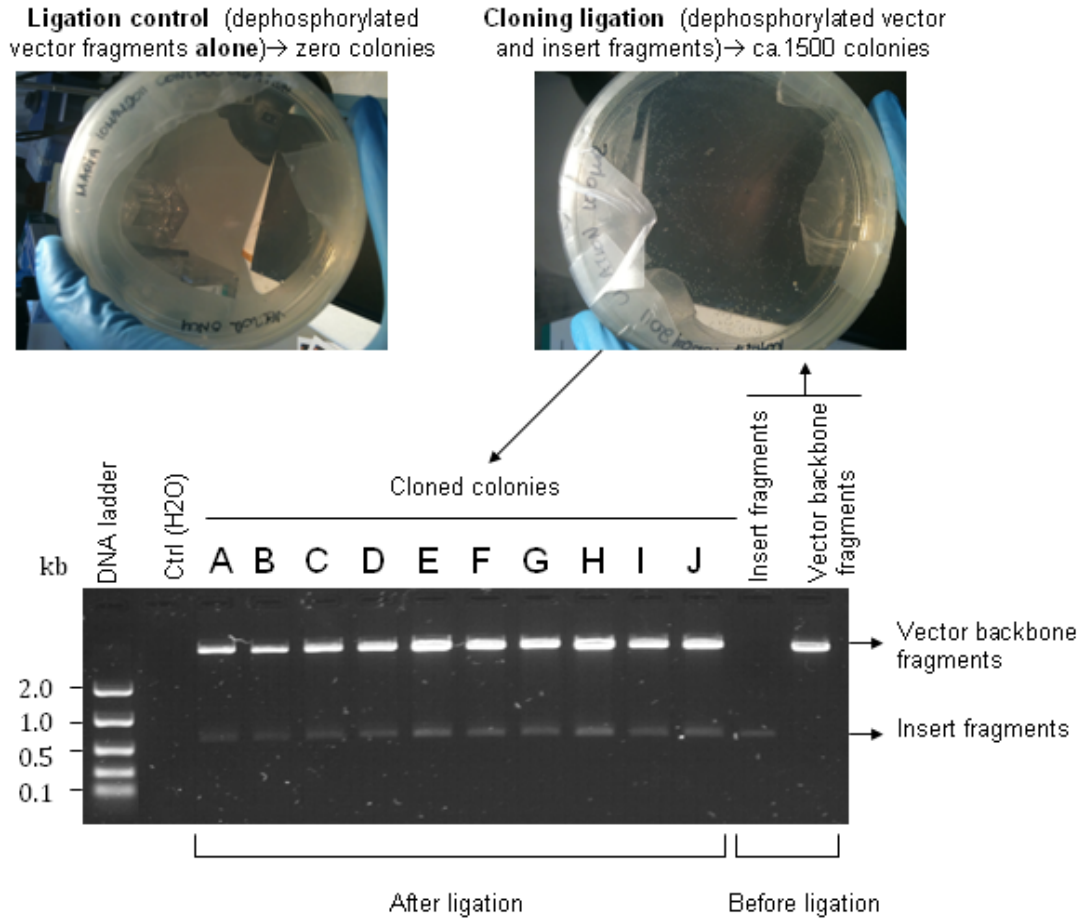


Figure 2-7: Isolation of ten pLKO.1-GFP-shATG7 clones (circa; ca.)

2.2.10 Morphological analysis of CML cells

Background: Morphological analyses of CML cells was performed by staining with the "Diff-Quik" staining kit (DADE Behring, PN130832) and examination under a light microscope. "Diff-Quik" is a product based on the Romanowski group of stains; the variants of the Romanowski group differ in the degree of oxidation of the methylene blue stain prior to the precipitation. The staining system incorporates an acidic red dye that targets the basic parts of a cell, and a dark blue/purple basic dye that is attracted to the acidic parts of a cell. Hydrophobic structures, like the Golgi zone, remain unstained.

Method: $2-5 \times 10^4$ cells were harvested and adhered onto a slide using a Shandon Cytospin 3 centrifuge. Following, the cells were fixed for 1min with the fixative "Diff-Quik" and sequentially incubated for 1min with the dye A and dye B supplied in the kit. Finally, slides were briefly washed, air-dried and examined under a light microscope.

3 Results (I): Effects of first, second, and third generation TKIs on proliferation, survival and autophagy in CML cell lines and primary cells

TKIs have revolutionised the treatment of CML patients, nevertheless fail to cure the disease due to persistence of a fraction of LSCs. Recent studies by our lab and others [234, 235] suggest that these cells may not be oncogene addicted and, therefore, survive and proliferate even upon complete BCR-ABL inhibition. A new strategy in eliminating the refractory fraction of CML stem cells includes the combination of TKIs with agents that target other survival mechanisms, such as autophagy.

In this chapter, the effects of first (IM), second (DAS) and third (PON) generation TKIs were investigated with regards to cell proliferation, viability, clonogenic ability and induction of autophagy in CML cells. In order to monitor effects induced upon exposure to TKIs, established human CML BC cell line models were used; these included the K562 cell line, which carries the *BCR-ABL1* e14-a2 (b3-a2) fusion gene, and the KCL22 cell line, that carries the *BCR-ABL1* e13-a2 (b2-a2) fusion gene. KCL22 cells carrying the BCR-ABL^{T315I} (KCL22^{T315I}) mutant were utilised in order to evaluate the TKI efficacy in the presence of the T315I mutation, and compared to KCL22 cells carrying the native BCR-ABL^{p210} (KCL22^{WT}). IL-3 dependent murine pro B cell line BaF3 (BaF3^{Parental}) that had been transfected with BCR-ABL^{p210} (BaF3^{WT}) or BCR-ABL^{T315I} (BaF3^{T315I}) – thus rendering their growth IL-3 independent- were also used for the monitoring of TKI effects in combination with CQ. Finally, the efficacy of PI3K/AKT/mTOR inhibitors against CML cells carrying the native or mutant BCR-ABL was investigated in the presence and absence of CQ.

Experiments described in this chapter were designed with the aim to:

- 1) investigate the effects of IM, DAS and PON on BCR-ABL inhibition, cell proliferation, viability and clonogenic ability of CML cell lines, and CD34+ human CML cells
- 2) investigate if TKI-mediated BCR-ABL inhibition leads to induction of autophagy
- 3) investigate if pharmacological inhibition of autophagy with CQ or HCQ enhances the efficacy of TKIs and mTOR inhibitors

3.1 TKIs in the proliferation, survival and autophagy of CML cells expressing native BCR-ABL

3.1.1 Optimisation of IM, DAS and PON treatment to maximise targeting of BCR-ABL activity in K562 cells

The aim of this section was to identify by western blot TKI concentrations that fully inhibit BCR-ABL activity, and to investigate the effects on the proliferation of CML cells.

Previous studies on K562 cells have identified a proliferation half minimal inhibitory concentration (IC₅₀) for IM at 400nM, for DAS at 1.5nM [335], and for PON at 4nM [227]. Based on these observations, it was decided to investigate the levels of BCR-ABL inhibition upon 24h treatment with the following TKI concentrations; 125 to 8000nM IM, 2.5 to 160nM DAS, and 1.0 to 10000nM PON. The inhibitory effect of TKI treatment on BCR-ABL activity was measured by monitoring the phosphorylation levels of downstream effectors STAT5 and/or CrKL. Protein lysates were analysed by western blot and β -tubulin was included as a protein loading control.

As illustrated in Figure 3-1A, phosphorylation of STAT5 was not affected until treatment with 4 μ M IM. Shah and colleagues [336] have reported that phosphorylation of STAT5 is a more sensitive marker of BCR-ABL activity compared to phosphorylation of CrKL, potentially due to the difference within the non-phosphorylated/phosphorylated ratio of the proteins at steady state. This could explain why 4 μ M of IM did not inhibit as effectively the phosphorylation of CrKL. Hence, for all subsequent experiments, it was decided to use IM at 5 μ M which is the highest clinically achievable concentration [337].

DAS was more potent than IM, and doses \geq 20nM had a significant inhibitory effect on BCR-ABL, as reflected by reduced CrKL phosphorylation (Figure 3-1B). Nevertheless, even upon exposure to 160nM, BCR-ABL activity was not completely inhibited. Based on these observations it was decided to use DAS at 150nM, which is close to the maximal achievable plasma concentration *in vivo* [221].

Finally, treatment with \geq 100nM PON almost completely inhibited BCR-ABL activity and abolished phosphorylation of CrKL (Figure 3-1C). Therefore, for subsequent experiments, PON was used at the clinically achievable concentration of 100nM [228].

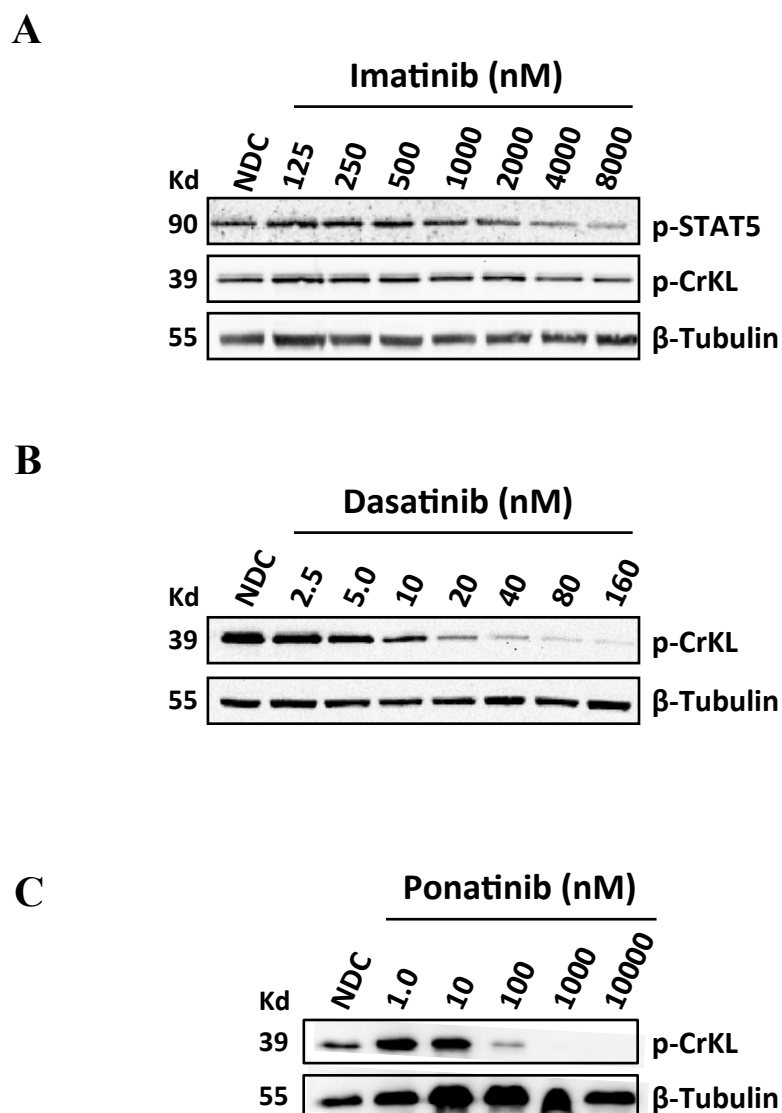


Figure 3-1: Effect of TKI treatment on BCR-ABL activity, measured by phosphorylation of downstream effectors CrKL and STAT5, in K562 cells

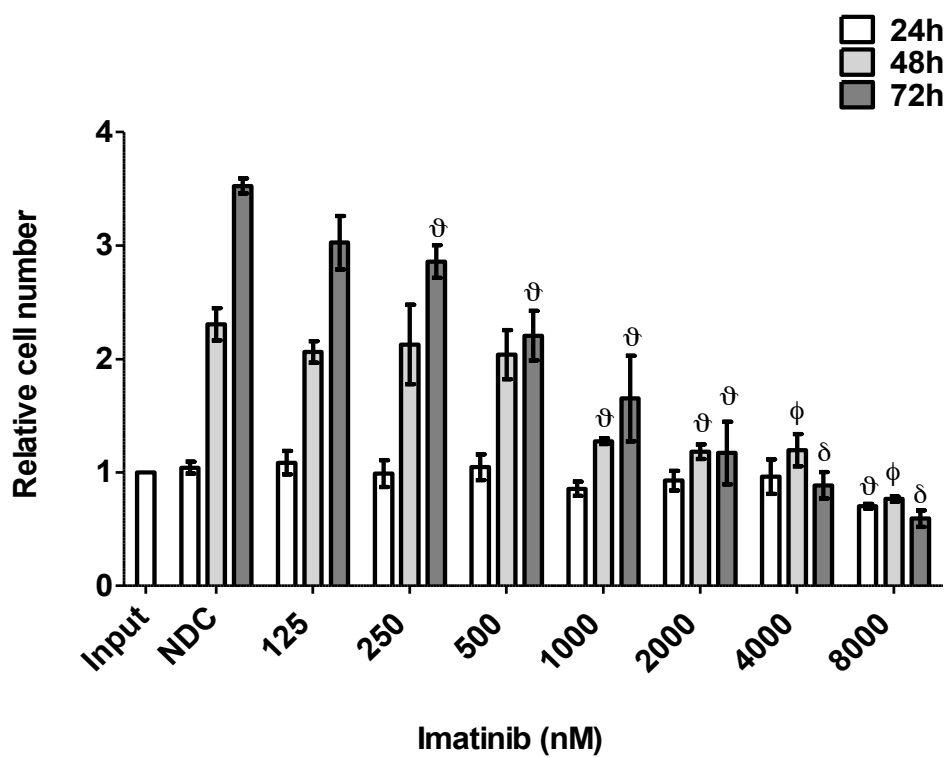
Western blot analysis on lysates from K562 cells treated for 24h with IM (A), DAS (B) or PON (C). B-tubulin measured as loading control.

The effectiveness of IM, DAS and PON was also assessed with regards to cell proliferation potential. K562 cells were exposed to different concentrations of IM (125 to 8000nM), DAS (0.625 to 40nM) or PON (1 to 10000nM) and cell counts were performed every 24h for a total of 72h. Cell viability was established by using the trypan blue exclusion method. Figure 3-2 demonstrates the relative proliferation of K562 cells over 72h under continuous exposure to IM (A), DAS (B) and PON (C).

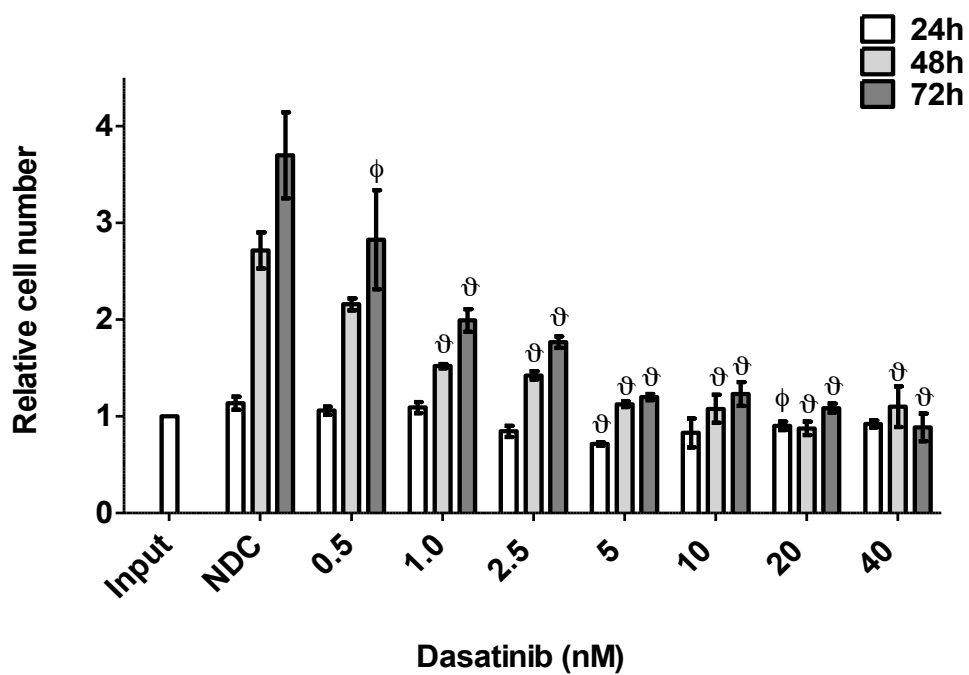
Our data illustrate that IM had an antiproliferative effect on K562 cells, which became apparent after 48h of treatment with doses higher than 1 μ M. However, IM had a cytotoxic effect only at 8 μ M ($p=0.03$ versus input), a dose higher than the clinically achievable concentration. Likewise, DAS suppressed the proliferation of K562 cells following 48h of treatment at doses higher than 2.5nM but did not have a cytotoxic effect up to 40nM. This could be attributed to incomplete inhibition of BCR-ABL (see Figure 3-1B). On the other hand, PON was associated with strong antiproliferative and cytotoxic effects in K562 cells; continuous exposure for 72h to as low as 10nM reduced the number of viable cell by >60% compared to the input ($p=0.001$).

Figure 3-2D presents the proliferation IC₅₀ values for IM, DAS and PON (based on the cell count data following 72h of treatment), and are in agreement with previously published studies [227, 338]. Our experiments demonstrate that amongst the three TKIs tested, DAS and PON were more effective in inhibiting BCR-ABL activity and proliferation in K562 cells. IM treatment up to 8 μ M (higher than the clinically achievable concentration) did not completely inhibit phosphorylation of CrKL, unlike DAS and PON. Furthermore, DAS and PON presented similar proliferation IC₅₀ and were >100fold more potent compared to IM. It should also be highlighted that IM and DAS were mostly antiproliferative, reaching maximum effect at approximately 2 μ M for IM and 5nM for DAS; drug concentration increase beyond these doses did not confer cytotoxicity up to 8 μ M for IM and 40nM for DAS. On the other hand, PON had an apparent cytotoxicity at doses ≥ 10 nM. It should be mentioned that IM, DAS and PON also have an inhibitory effect on other non-BCR-ABL kinases such as KIT, platelet-derived growth factor receptor (PDGFR) and others. Hence, the observation that these TKIs show different antiproliferative/cytotoxic effects may reflect the different effect they have on BCR-ABL-independent targets. For instance, unlike IM, low doses of DAS have been reported to inhibit SRC family kinases (SFKs), including SRC, LCK, LYN, FGR, BLK, FYN, YES, HCK [338], and this may explain why DAS has a stronger antiproliferative effect compared to IM. In a similar manner, the cytotoxic effect of PON may be superior due to inhibition of kinases that are not targeted by IM and DAS, such as Aurora A [227].

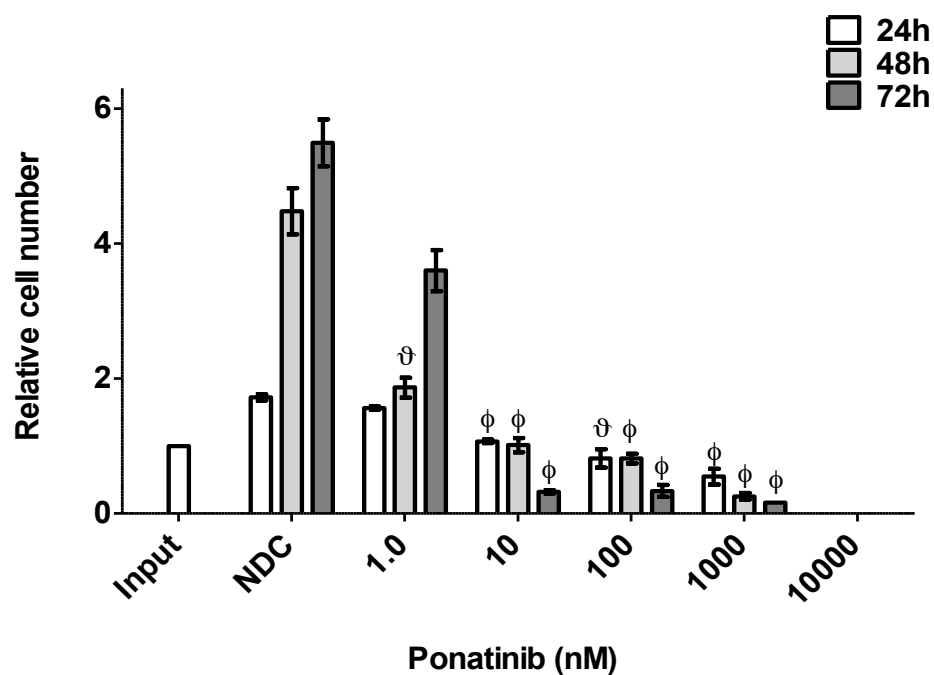
A



B



C



D

Drug	IC50 (nM)
IM	303.6
DAS	2.5
PON	1.59

Figure 3-2: Comparison of IM, DAS and PON treatment in the proliferation of K562 cells

K562 cells were treated with IM (A), DAS (B) or PON (C). Cell counts were performed at 24, 48 and 72h following treatment initiation and viability was determined by using the trypan blue exclusion method. The number of viable cells in each treatment was compared to the input and the relative numbers are presented as mean±SEM (n=3). (D) Proliferation IC50 values were estimated based on the proliferation data after 72h of TKI treatment. (θ; p≤0.05, φ; p≤0.01, δ; p≤0.001, NDC; no drug control)

3.1.2 Effects of TKI-mediated BCR-ABL inhibition on autophagy

It has been suggested that TKI-mediated BCR-ABL inhibition leads to induction of autophagy. In order to investigate this hypothesis, a series of experiments were designed for the monitoring of autophagy upon treatment of CML cells with IM, DAS or PON.

3.1.2.1 Autophagy monitoring assays

The most common mammalian autophagy marker is LC3; this is the only validated protein so far that stably associates with the autophagosome membranes. LC3 is cleaved at the C-terminus by ATG4, forming the LC3-I cytosolic form. Upon induction of autophagy, through a cascade of reactions, LC3-I is lipidated by covalent binding to PE, generating the LC3-II form. LC3-II is then utilised for the construction of the inner and outer autophagosomal membranes. Following fusion with lysosomes, LC3-II in the inner membrane is degraded by lysosomal enzymes, while outer membrane-bound LC3-II is cleaved off by ATG4 and re-used for lipidation and loading to autophagosomes upon autophagy stimulation.

Despite the continuously increasing number of publications focusing on the investigation of autophagy (PubMed search for “autophagy” retrieves >11,500 publications; website last accessed 6th of March 2013), there is still confusion regarding the acceptable methods of monitoring autophagy, especially in multicellular eukaryotes. Autophagy assays can be divided into two categories (i) assays that measure the volume of autophagic elements (e.g. autophagosomes or autophagolysosomes) at any stage of the process, and (ii) assays that monitor the flux through the pathway (i.e. complete process) (Table 3-1). It should be underlined that autophagy is a multi-step, highly dynamic process, described better by the term “autophagic flux”. Hence, increase in autophagosomes/LC3-II levels may reflect (i) autophagy induction with increased formation of autophagosomes, or (ii) reduced/blocked autophagy turnover, perhaps due to delayed trafficking to the lysosomes, reduced fusion between compartments or impaired lysosomal proteolytic activity. Therefore, accumulation of autophagosomes or LC3-II does not simplistically imply an induction in autophagy. The experimental and the biological context are parameters that have also to be taken into account when choosing upon suitable autophagy monitoring assays. Hence, it becomes apparent that for rigorous autophagy monitoring no single assay can be the most appropriate, since each method is associated with different advantages and limitations, and more than one assay have to be performed in order to obtain robust data.

Criteria	Methods
Monitoring Phagophore and Autophagosome Formation	
Electron microscopy (increase in autophagosome quantity)	Quantitative electron microscopy, immunoelectron microscopy
LC3 western blotting and ubiquitin-like protein conjugation systems (increase in the amount of LC3-II, and ATG12-ATG5 conjugation)	Western blot
Fluorescence microscopy (increase in LC3 punctae)	Fluorescence, immunofluorescence and immunoelectron microscopy
mTOR and ULK1 kinase activity	Western blot, immunoprecipitation or kinase assays
Transcriptional regulation	Northern blot or qRT-PCR
Monitoring Autophagy by Flux Measurements	
Autophagic protein degradation	Turnover of long-lived proteins
Turnover of LC3-II	Western blot \pm lysosomal fusion or degradation inhibitors
GFP-LC3 lysosomal delivery, and proteolysis (to generate free GFP)	Fluorescence microscopy, FACS, western blot \pm lysosomal fusion or degradation inhibitors
p62 western blot	Western blot with qRT-PCR or northern blot to assess transcription
Autophagic sequestration assays	Lysosomal accumulation by biochemical or multilabel fluorescence techniques
Turnover of autophagic compartment	Electron microscopy morphometry/stereology
Autophagosome-lysosome colocalisation and dequenching assay	Fluorescence microscopy
Tandem mRFP-GFP fluorescence microscopy	Fluorescence microscopy of tandem mRFP-GFP-LC3
Tissue fractionation	Centrifugation, western blot and electron microscopy
Analyses <i>in vivo</i>	Fluorescence microscopy and immunohistochemistry

Table 3-1: Recommended methods for monitoring autophagy in higher eukaryotes (Modified from [339])

For the purposes of this study, a detailed set of guidelines [339] about autophagy monitoring was taken into account when deciding upon the assays that better fit the CML system, and multiple assays were tested in order to validate autophagic responses.

In the 1950s, autophagy was first described by electron microscopy (EM) [340]. Nowadays, EM remains the most informative method used for the morphological analysis and evaluation of selective and non-selective autophagic activity, allowing for the direct visualisation of the autophagic elements (e.g. autophagosomes and autophagolysosomes) (Table 3-2A). However, EM data interpretation can be misleading due to methodological/sampling artefacts, apart from being a laborious and expensive technique.

Herein, two methods were used for the measurement of the volume of autophagic elements: (i) measurement of LC3-positive punctae per cell after staining with anti-LC3 antibody and analysis by immunofluorescence (Table 3-2B), and (ii) measurement of LC3-II levels by western blot (Table 3-2C).

Currently, commercially available anti-LC3 antibodies stain both LC3-I and LC3-II. In an immunofluorescence assay LC3-I is diffused in the cytoplasm, whereas LC3-II appears punctate since it is bound on autophagic membranes.

In an immunoblot, incubation with anti-LC3 antibody reveals two bands: the cytosolic LC3-I with a size of 16Kd, and the autophagosome membrane-bound LC3-II with size of 14Kd. Since LC3-II is PE-conjugated, its molecular weight is greater than LC3-I. However, due to the hydrophobic nature of PE, LC3-II migrates faster in SDS-PAGE, displaying a lower molecular weight compared to its actual size.

As mentioned earlier, autophagy is a dynamic process and an increase in LC3-positive punctae or LC3-II levels may reflect an increase in autophagosome synthesis or a reduction/defect in autophagosome turnover. Therefore, we also performed autophagic flux assays.

In order to monitor LC3-turnover by western blot (Table 3-2D) we included in our analyses control lysates harvested from cells that had been treated with inhibitors of the autophagic flow [341]. CQ and HCQ disrupt the completion of autophagy at late stages by increasing the pH within lysosomes, inhibiting the fusion between autophagosomes and lysosomes. In order to evaluate the autophagic flux in our samples under basal conditions, we compared LC3-II levels between untreated samples and samples that had been treated with CQ or HCQ; accumulation of LC3-II in the CQ or HCQ-treated cells would indicate efficient autophagic flux, while similar LC3-II levels between NDC and CQ or HCQ-treated cells would suggest a delay or block of autophagy at a stage before autolysosome degradation.

Likewise, LC3-II levels were detected not only in TKI-treated samples, but also in cells treated with the combination TKI/CQ or HCQ. Similar LC3-II levels between the CQ- or HCQ-treated cells and the combination TKI/CQ or HCQ-treated cells would suggest that the treatment has no effect on the autophagic activity, while an increase in LC3-II levels in the combination TKI/CQ or HCQ-treated cells compared to the CQ- or HCQ-treated cells would indicate that the TKI treatment is inducing autophagy.

Since (i) LC3 antibodies present different affinity for LC3-I and LC3-II, (ii) LC3-I and LC3-II present different expression patterns in different cell lines and tissues, and (iii) LC3-II has a shorter half-time life compared to LC3-I due to degradation of autolysosomes, determining autophagy changes based on the western blot ratio between LC3-I and LC3-II can give false results. Hence, in this study we decided to assess autophagy activity by normalising the total LC3-II levels to a loading control, such as actin or β -tubulin [342].

The autophagic flux was also monitored by FACS, following staining with the Cyto-ID® dye that fluoresces after incorporation to autophagic elements, in the absence or presence of CQ or HCQ-mediated autophagy inhibition.

Transient transfection or stable transduction of target cells with the mRFP-GFP-LC3 construct is a very useful tool in monitoring of autophagy (Table 3-2F). LC3 protein is tagged with both monomeric red fluorescence protein (mRFP) and GFP. Since mRFP has a relatively lower pKa value (approximately 4.8) than GFP (approximately 6.2), mRFP fluorescence remains more stable in acidic compartments whereas GFP fluorescence is rapidly quenched [343]. This difference on the properties of mRFP and GFP enables monitoring of the autophagic turnover. Upon induction of the flux, early autophagosomes are synthesized (yellow-tagged as they co-express mRFP and GFP) and late autophagosomes undergo degradation following fusion with lysosomes (red-tagged as they express only mRFP; GFP is quenched). On the other hand, disrupted turnover is associated with increase only in yellow-tagged autophagosomes due to delay or blockade of the latter autophagic stages.

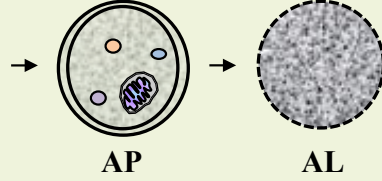
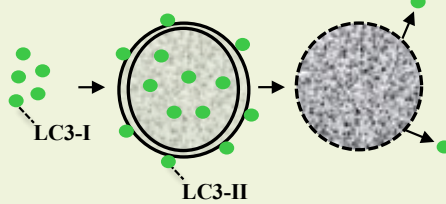
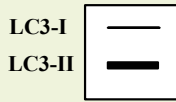
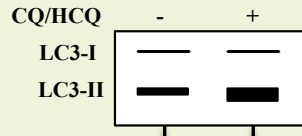
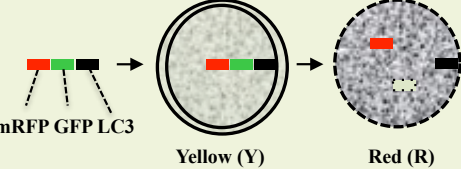
Assays		Method	Typical Results				
			Basal	Induction	Suppression (early)	Suppression (late)	
Conventional morphology	A. AP/AL detection 	EM	→ AP	↑↑ AP	↓ AP	↑↑ AP	
			→ AL	↑↑ AL	↓ AL	↓ AL	
Number of autophagosomes	B. Number of LC3 puncta per cell 	FM	→	↑↑	↓	↑↑	
	C. LC3-II amount 		WB	→	↑↑	↓	↑↑
Autophagic flux	D. LC3 turnover assay  Difference in LC3-II levels	WB	→	↑↑	↓	↓	
	E. FC after CytoID®±CQ/HCQ 		FC	→	↑↑	↓	↓
	F. mRFP-GFP-LC3 colour change 		FM	→ R	↑↑ R	↓ R	↓ R
	→ Y	↑↑ Y		↓ Y	↑↑ Y		

Table 3-2: Methods used for measuring autophagic elements' volume and autophagic flux (AP; autophagosome, AL; autophagolysosome, EM; electron microscopy, FM; fluorescence microscopy, WB; western blot, FC; flow cytometry) (Modified from [344])

3.1.2.2 Accumulation of autophagosome-bound LC3-II in K562 cells upon treatment with IM and DAS

In order to investigate if TKIs induce autophagy in CML BC cells upon BCR-ABL inhibition, K562 cells were treated with IM and DAS at concentrations previously shown to inhibit BCR-ABL activity (see §3.1.1 for more details). Cells were exposed for 4h to 5 μ M IM or 150nM DAS \pm 10 μ M CQ in order to assess the autophagic flow. As explained in §3.1.2.1, if TKIs induced autophagy, the TKI/CQ combination-treated cells should present higher levels of LC3-II compared to CQ treatment alone. Whole cell lysates were analysed by western blot and LC3-II protein levels were determined after densitometry and normalisation to β -tubulin. Calibration was performed towards the NDC arm.

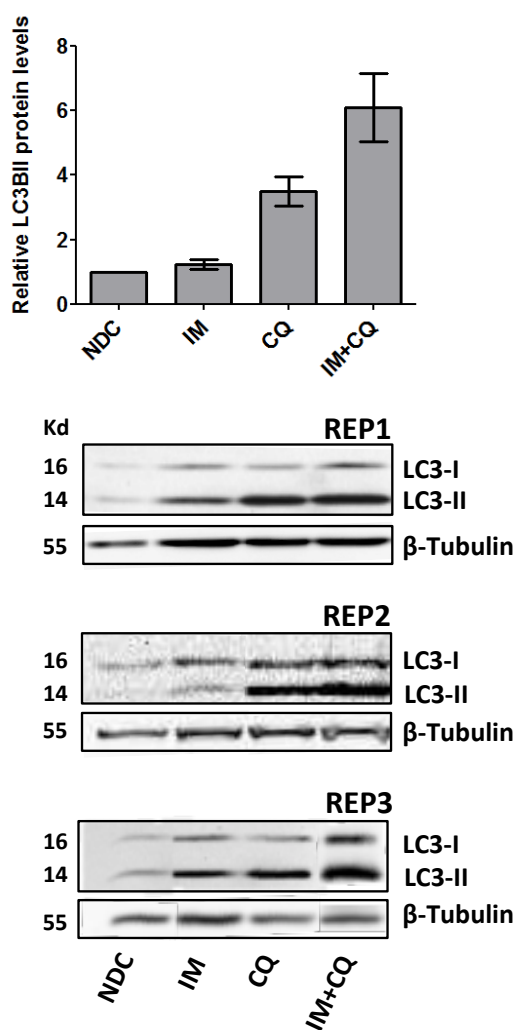
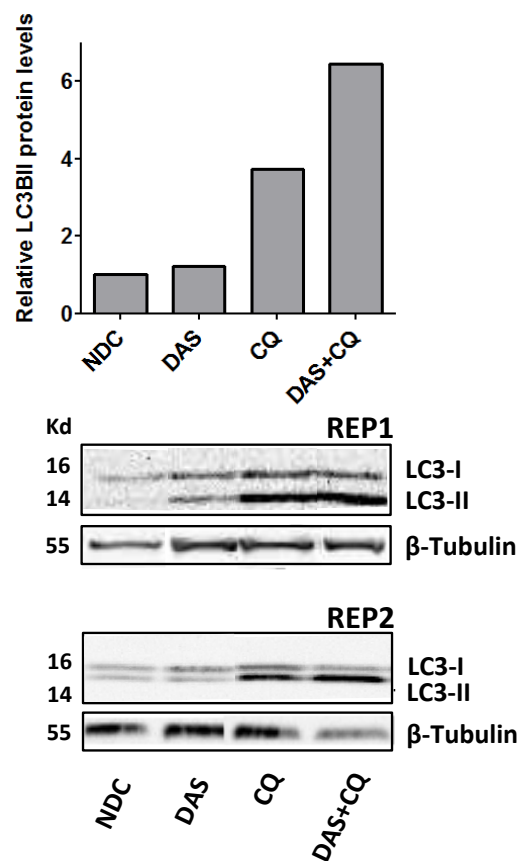
Figure 3-3 suggests that IM (A) induced synthesis of autophagosomes and promoted autophagy in BC K562 cells. Cells treated with IM/CQ presented higher levels of LC3-II (6-fold increase compared to NDC) versus CQ-alone treated cells (3.5-fold increase compared to NDC) (n=3). Even if this increase was not statistically significant (p=0.08), induction of autophagy at this level within an IM-treated cell may significantly support its survival in the absence of BCR-ABL signalling.

Likewise, Figure 3-3B illustrated that LC3-II protein levels were higher in K562 cells treated with DAS/CQ combination (6.4-fold increase compared to NDC) compared to cells that had been treated with CQ only (3.7-fold increase compared to NDC) (n=2). This observation suggests that lipidation of LC3 is enhanced following treatment with DAS.

Since both IM and DAS have the same mechanism of action (targeting BCR-ABL kinase activity), the densitometry data presented in Figure 3-3A and 3-3B were combined and analysed so as to further evaluate the effect of TKIs on the autophagic flux.

As Figure 3-3C reveals, TKI-mediated BCR-ABL-inhibition led to a significant increase in the autophagic flow. The combination of TKI/CQ presented higher levels of LC3 lipidation (6-fold increase relative to the NDC) compared to CQ treatment alone (4-fold increase relative to the NDC), and this increase was statistically significant (p=0.02).

Taken together, these data suggested that inhibition of BCR-ABL activity, mediated either by IM or DAS, is associated with an increase in the autophagic flow in K562 BC cells.

A**B**

C

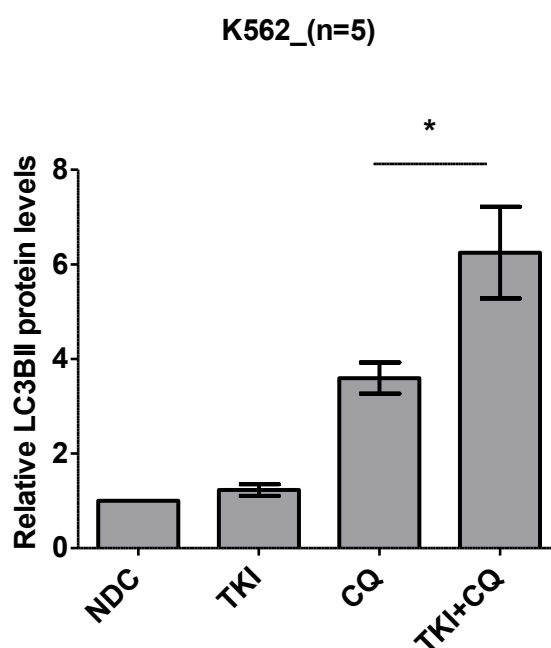


Figure 3-3: Accumulation of autophagosome-associated LC3-II upon IM or DAS treatment of K562 cells

Western blotting was used for the analysis of LC3-II levels following 4h treatment of K562 with (A) 5 μ M IM \pm 10 μ M CQ or (B) 150nM DAS \pm 10 μ M CQ. Combined analysis of the data presented in (A) and (B) is depicted in (C). Densitometry calculations for western blot data shown were performed by using the Quantity One software (verifying for non-saturation and subtracting background). The graphs represent relative LC3-II levels (normalised to β -tubulin levels) compared to the no drug control (NDC) as mean \pm SEM of n=3 for IM and mean of n=2 for DAS. (ns; not significant, *; p \leq 0.05)

3.1.2.3 Accumulation of autophagosome-bound LC3-II in CP CML CD34+ cells upon treatment with IM, DAS or PON

Having demonstrated that treatment with IM or DAS induces autophagy in the BC CML cell line K562 (§3.2.2), we investigated if TKIs induce autophagy upon inhibition of BCR-ABL in CD34+ cells from CP CML patients.

Primary CP CML CD34+ cells were cultured in SFM+PGFs, and treated with TKIs at clinically achievable concentrations that had been previously shown to effectively inhibit BCR-ABL activity (see §3.1.1). Cells were treated for 4h with 5 μ M IM, 150nM DAS, or 100nM PON, in the absence or presence of 10 μ M CQ. Whole cell lysates were analysed by western blot and LC3-II protein levels were determined after densitometry and normalisation to β -tubulin. Calibration was performed towards the NDC arm.

IM induced autophagy in CD34+ cells from a CML patient; LC3-II levels were significantly higher in the cells that were exposed to IM in the presence of CQ (28-fold increase), compared to CQ-treated alone cells (14-fold increase) (Figure 3-4A).

Accumulation of LC3-II was also observed in CD34+ cells (n=2) upon treatment with DAS (Figure 3-4B). Inhibition of BCR-ABL activity was verified by complete inhibition of CrKL phosphorylation in both samples. This observation further highlights the efficacy of DAS in the inhibition of BCR-ABL activity even after short exposure time. Interestingly, DAS-mediated inhibition of BCR-ABL signalling was associated with induction of autophagy and increase in LC3 lipidation; while CQ-treated cells had a 1.98-fold increase in LC3-II levels, DAS/CQ-treated cells presented a 2.24-fold increase.

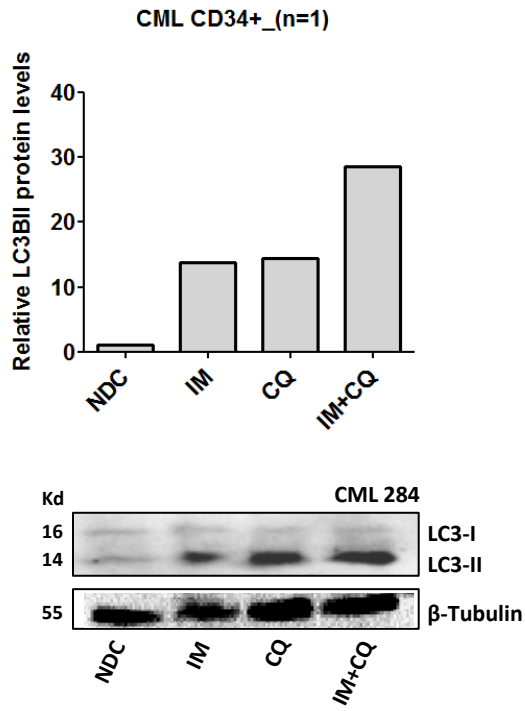
PON has been reported to be active against a variety of BCR-ABL mutants that are refractory to first and second generation TKIs [227]. However, no published study so far has investigated the role of PON treatment on autophagy. We first report here that inhibition of BCR-ABL activity upon treatment with 100nM PON, induced autophagy in CD34+ cells of CP CML patients (Figure 3-4C); LC3-II levels were significantly higher in the PON/CQ arm (1.46-fold increase) compared to CQ alone treated cells (1.31-fold increase), suggesting increased autophagosome synthesis.

Densitometry data from the above mentioned protein analyses on CP CML CD34+ cells treated with TKIs \pm CQ were combined in order to evaluate overall effect of TKIs on autophagy. Figure 3-4D demonstrates that TKIs induced autophagy upon inhibition of BCR-ABL; the TKI/CQ arm was associated with higher levels of LC3-II (2.18-fold increase relative to the NDC) compared to CQ treatment alone (1.72-fold increase relative to the NDC), suggesting an approximately 27% increase of the autophagic activity

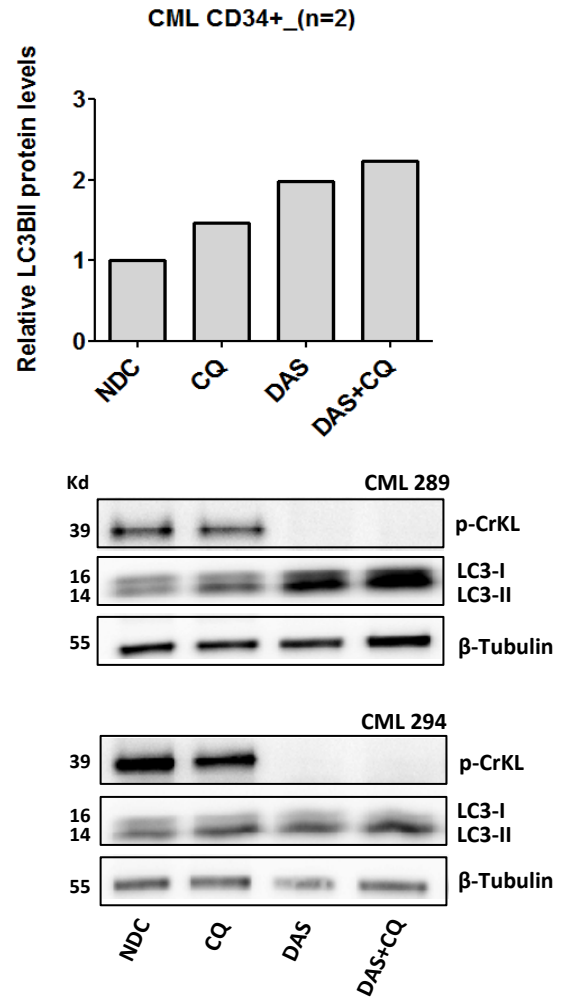
(average of $n=4$). Even if this increase is not significant by the statistical point of view ($p=0.07$), it does not necessarily mean that this level of induction in the autophagic flux does not have a significant effect on the biological system.

Taken together, our results demonstrate that TKI-mediated inhibition of BCR-ABL activity leads to induction of autophagy. In a CP CML CD34+ sample, IM increased the autophagic flux by approximately 50% compared to the basal autophagy levels (IM/CQ versus CQ alone). On the other hand, in CP CML CD34+ cells, DAS increased approximately 13% the autophagic activity (average from $n=2$), while PON approximately 11.4% (average from $n=2$). Based on the observations from the LC3-II protein analysis, IM induced the highest levels of autophagy, while DAS and PON exhibited similar effects. However, this could be sample-specific; the IM-treated CD34+ cells (sample CML284) demonstrated a high autophagic flux under basal conditions (comparison of LC3-II levels between NDC and CQ arms). The effect of IM on LC3 lipidation should be further investigated by protein analysis on more primary CML samples. Finally, even if combined data analysis from all TKIs (Figure 3-4D) did not reveal a significant increase of the autophagic flow upon TKI treatment, inclusion of more samples could statistically increase the significance of the autophagic induction since this trend is always observed after TKI treatment.

A



B



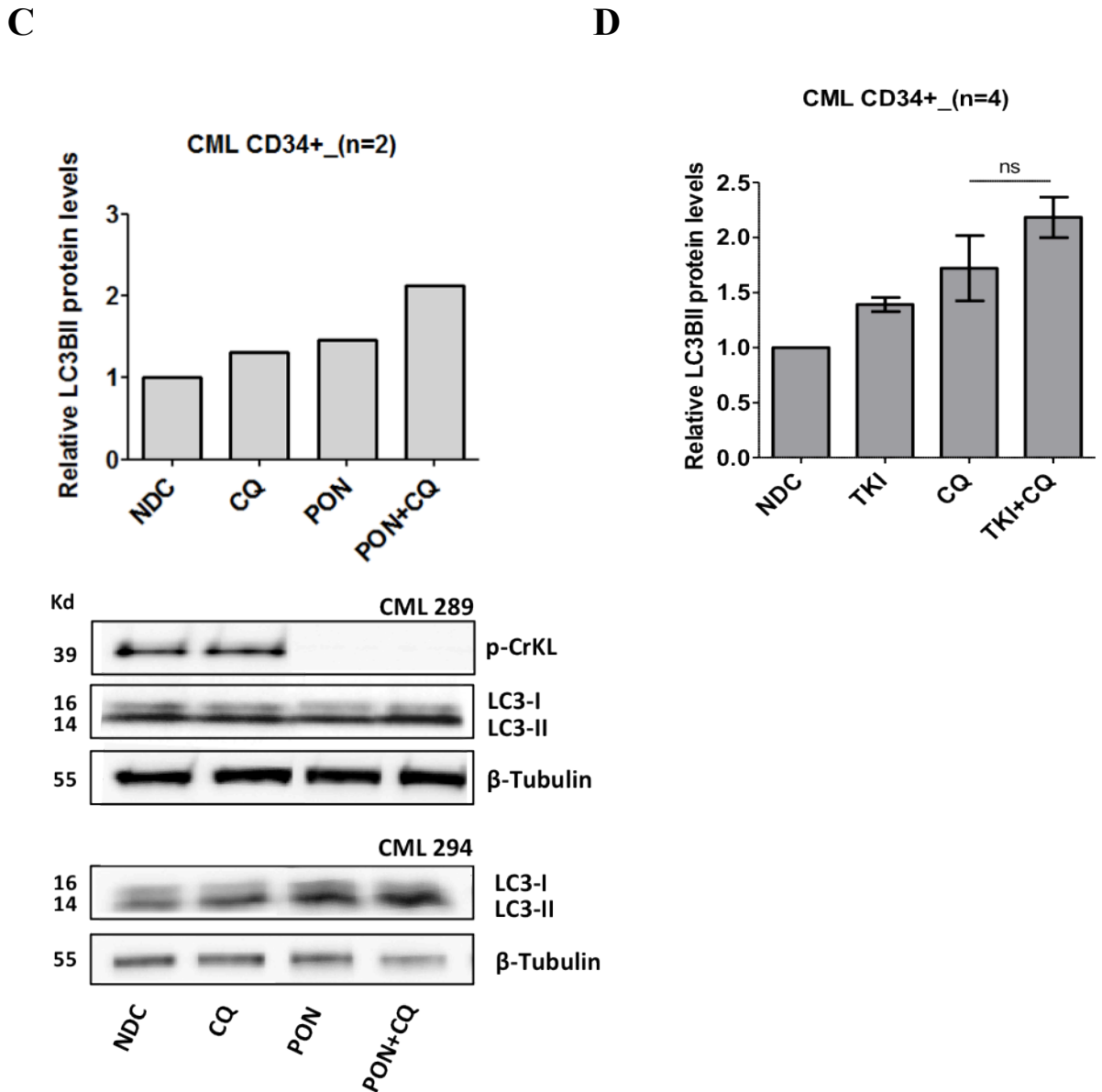


Figure 3-4: Accumulation of autophagosome-associated LC3-II upon IM, DAS or PON treatment of CP CML CD34+ cells

Western blotting was used for the analysis of LC3-II levels following 4h treatment of CML CD34+ cells with (A) 5 μ M IM \pm 10 μ M CQ, (B) 150nM DAS \pm 10 μ M CQ, or (C) 100nM PON \pm 10 μ M CQ. Combined analysis of the data presented in (B) and (C) is depicted in (D). Densitometry calculations for western blot data shown were performed by using the Quantity One software (verifying for non-saturation and subtracting background). The graphs represent the relative LC3-II levels (normalised to β -tubulin levels) compared to the NDC. (ns; not significant)

3.1.2.4 Increased synthesis of LC3-positive punctae in K562 BC CML cells upon treatment with TKIs

The most rigorous autophagy monitoring assays rely on two autophagy hallmarks, (i) lipidation of LC3, and (ii) changes in the subcellular distribution of LC3. As mentioned earlier, upon induction of autophagy, LC3 is lipidated and associated with autophagosome membranes; hence, coinciding with its lipidation, LC3 is redistributed within the cell into cytoplasmic punctae that can be visualised by immunofluorescence microscopy.

In order to validate our protein analysis data demonstrating increased LC3 lipidation following TKI treatment, we performed immunofluorescence microscopy analysis on endogenous LC3 in TKI-treated CML BC cells. K562 cells were treated for 4h with 150nM DAS or 100nM PON, followed by fixation onto slides and sequential staining with primary anti-LC3 antibody and Alexa-fluorochrome conjugated secondary antibody. DAPI was used for the counterstaining of nuclei.

Figure 3-5A demonstrates the accumulation of LC3-positive punctae in the presence of DAS or PON. Enumeration of the LC3-positive punctae revealed that DAS- or PON-treated cells presented >3-fold increase compared to the NDC (99 and 109 punctae/cell for DAS and PON respectively, versus 30 punctae/cell for the NDC) (Figure 3-5B). At this point it should also be mentioned that PON treatment was associated with accumulation of larger LC3-positive punctae (size $>0.5\mu\text{m}^2$) compared to DAS-treated or NDC cells (size $<0.5\mu\text{m}^2$). This could potentially indicate that PON affects kinases that regulate the size of the autophagosomes, such as the Rho-kinase 1 [345].

These data are in agreement with previous western blot data (§3.2.2), suggesting induction of autophagy within BC CML cells upon treatment with either of these TKIs.

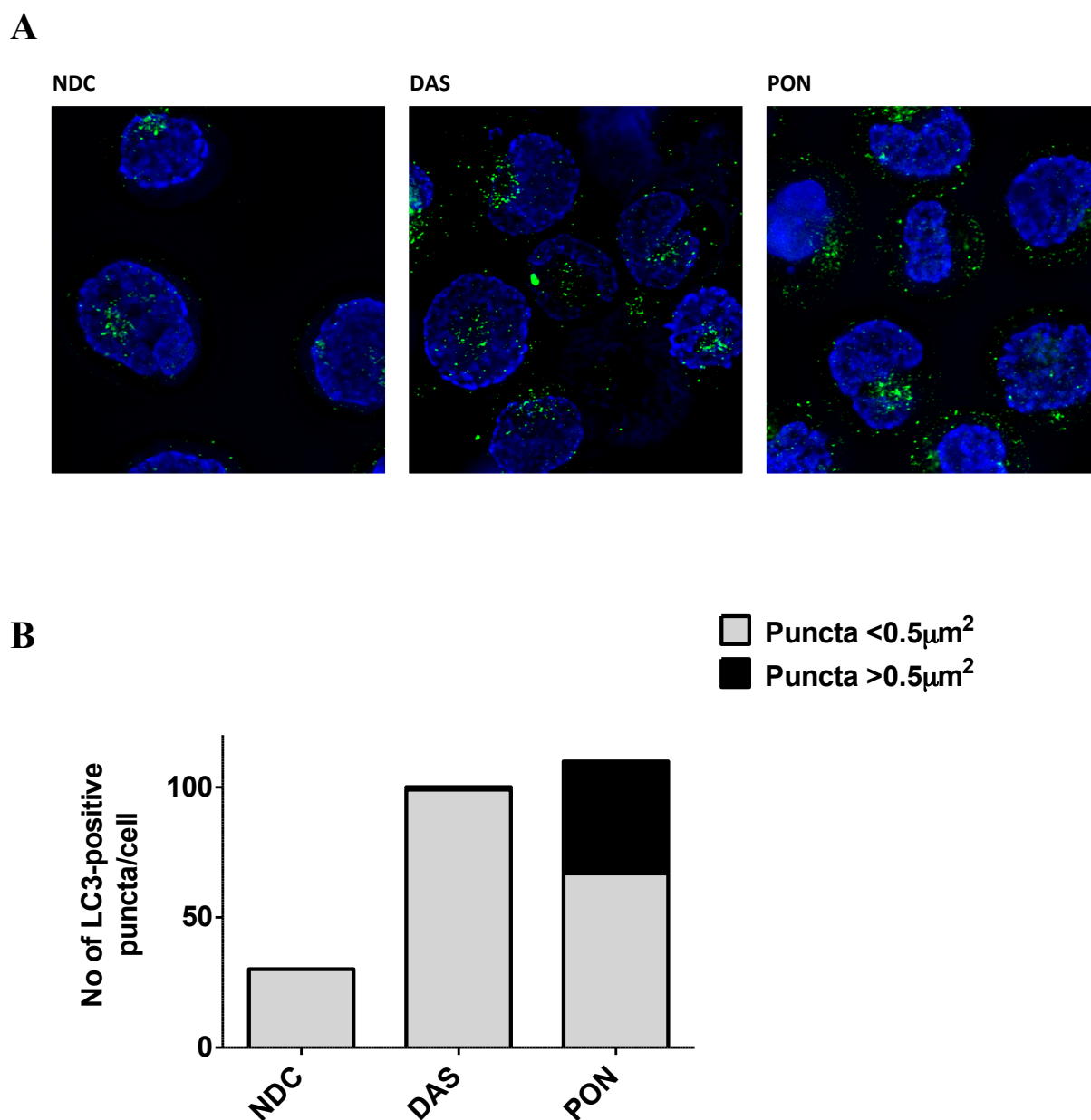


Figure 3-5: Formation of LC3-positive punctae in DAS- and PON-treated K562 cells

Immunofluorescence imaging on K562 cells treated for 4h with 150nM DAS, 100nM PON or NDC. Cells were stained with primary anti-LC3B antibody and secondary Alexa-fluorochrome conjugated antibody. (A) Photos represent Z-stack overlay after deconvolution by using the AxioVision software. Captions presented at 1000X magnification, DAPI used for nuclei staining. (B) Enumeration of the LC3-positive punctae was carried out by using the AxioVision 4 Module AutoMeasure software ($n \geq 30$ cells).

3.1.2.5 Increased synthesis of LC3-positive punctae in CP CML CD34+ cells upon treatment with TKIs

The question that next arose was if TKIs enhance the formation of LC3-positive punctae in CML CD34+ cells upon inhibition of BCR-ABL.

Human CP CML CD34+ cells were cultured in SFM+PGFs and treated for 24h with 5 μ M IM, 150nM DAS, 100nM PON or NDC. Formation of LC3-positive punctae was assessed by immunofluorescence microscopy.

Figure 3-6 demonstrates that treatment with IM (A), DAS or PON (B) resulted in an increase in LC3-positive punctae, suggesting enhanced synthesis of autophagosomes. Among the three TKIs, IM had the most moderate effect, whereas DAS and PON led to higher levels of autophagy induction. This could be attributed to more effective BCR-ABL targeting with 150nM DAS or 100nM PON compared to 5 μ M IM.

Overall, these experiments illustrated visually the induction of autophagy in human primary CP CML stem and progenitor cells upon treatment with TKIs.

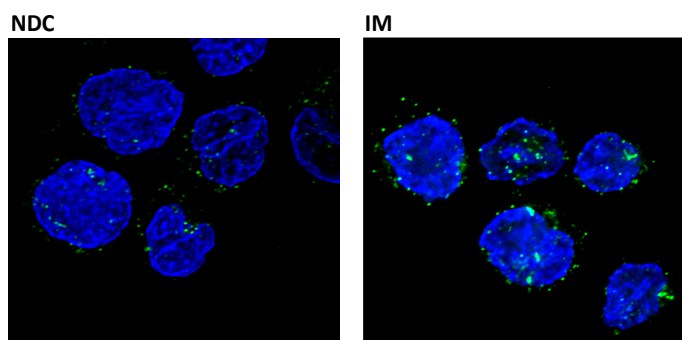
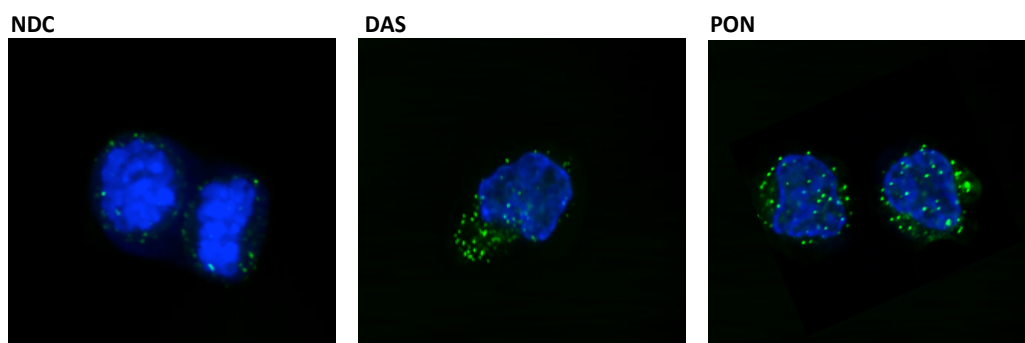
A**B**

Figure 3-6: Formation of LC3-positive punctae in IM-, DAS- and PON-treated CP CML CD34+ cells

Immunofluorescence imaging on CP CML CD34+ cells treated for 24h with 5 μ M IM (A), 150nM DAS, 100nM PON (B) or NDC. Cells were stained with primary anti-LC3 antibody and secondary Alexa-fluorochrome conjugated antibody. Photos represent Z-stack overlay after deconvolution by using the AxioVision software. Captions presented at 1000X magnification, DAPI used for nuclei staining.

3.1.2.6 Autophagy increase in K562 BC cells following TKI treatment measured by FACS

Another approach in monitoring the effect of TKI-induced autophagy was by FACS analysis following staining with the Cyto-ID® Autophagy Detection Kit. The kit includes a dye that, according to the manufacturer's instructions, stains specifically pre-autophagosomes, autophagosomes, and autolysosomes, with minimal lysosomal staining. Incorporation of the dye to autophagic structures leads to bright fluorescence that can be detected by FACS analysis at the FL-1 channel (readout as FITC).

K562 cells were treated for 4h with 5 μ M IM, 150nM DAS or 100nM PON, in the absence or presence of 10 μ M CQ or HCQ. Cells were then analysed by FACS for the detection of fluorescent Cyto-ID® dye (procedure described at §2.2.24). The geometrical mean (GeoMean) of FITC (log scale) among different treatments was calibrated towards the NDC.

Figure 3-7 demonstrates that all TKIs tested -IM (A), PON (B) and DAS (C) - induced autophagy upon BCR-ABL inhibition, since fluorescence was higher in the cells incubated with any TKI combined with autophagy inhibitor (CQ or HCQ) compared to treatment with autophagy inhibitor alone (n=2 for IM and PON and n=1 for DAS).

An aliquot of the cells treated with 150nM DAS \pm 10 μ M CQ was lysed and analysed by western blot. Figure 3-7D demonstrates the densitometry analysis on LC3-II protein levels measured by immunoblot. Comparison of the analysis of the same sample by CytoID®/FACS (Figure 3-7C) and immunoblot (Figure 3-7D) revealed an inconsistency in the data produced by these assays. Significant changes in LC3 lipidation at protein level (measured by immunoblot analysis) appeared as a subtle autophagy increase by CytoID® via FACS. For instance, a 36-fold increase in LC3-II protein levels between NDC and CQ, by CytoID®/FACS appeared as 1.78-fold relative increase.

Our results suggest that monitoring autophagy via FACS following staining with CytoID® may be suitable for samples where a very low number of cells is available for experimenting (such as HSCs). Nevertheless, this assay appeared to be less sensitive compared to previously described methods. This should be kept in mind when analysing CytoID® data, since subtle changes by FACS could reflect significant changes at protein level.

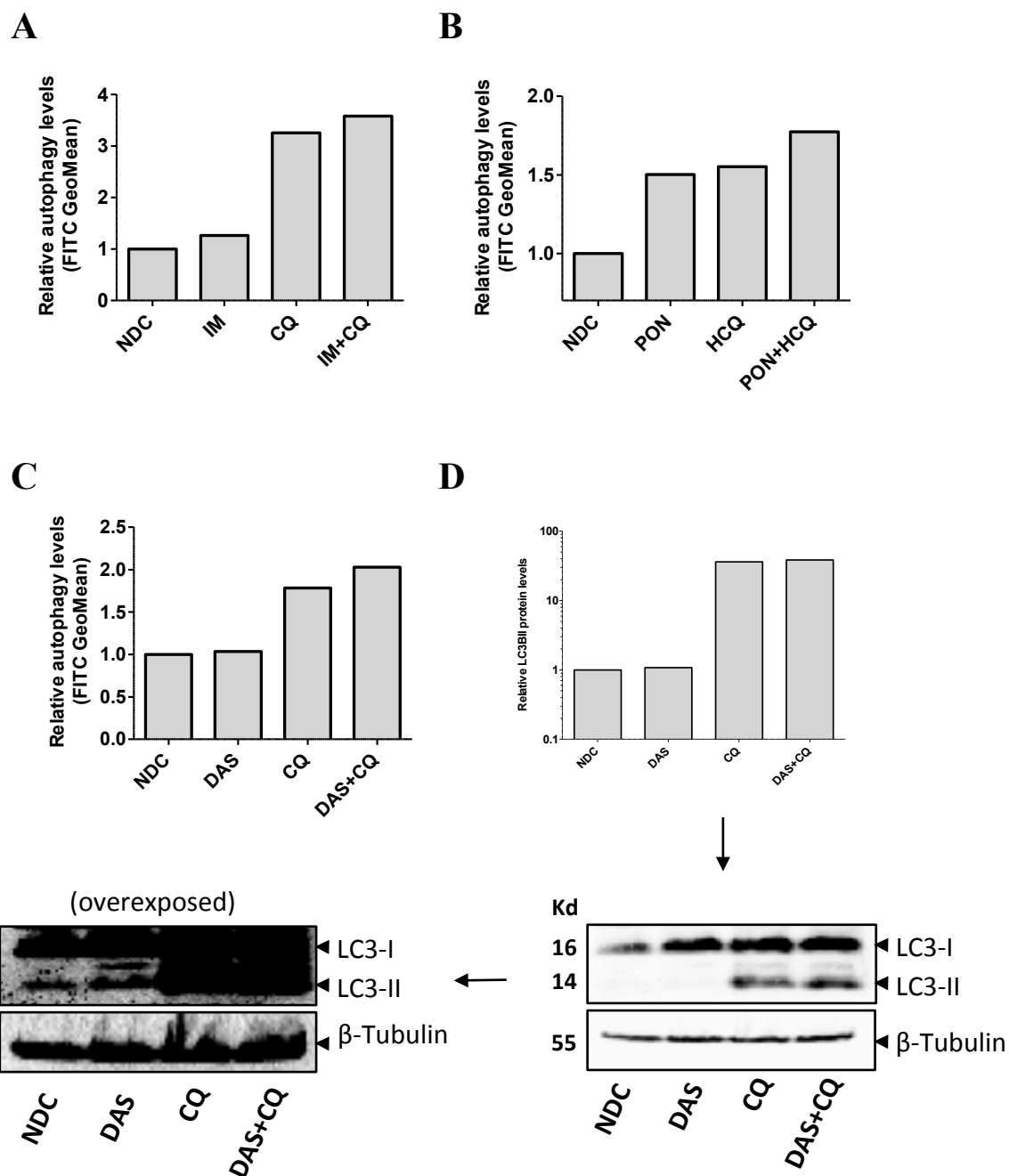


Figure 3-7: Induction of autophagy in K562 cells upon TKI treatment measured by FACS

K562 cells were treated for 4h with $5\mu\text{M}$ IM, 150nM DAS or 100nM PON $\pm 10\mu\text{M}$ CQ or HCQ. Cells were then stained with the CytoID® Autophagy dye. Fluorescence was measured by FACS at the FL-1 channel as FITC. The graphs represent the GeoMean FITC of $n=2$ relative to the NDC for IM (A), PON (B) and $n=1$ for DAS (C). Western blot analysis was performed on an aliquot of the DAS \pm CQ-treated cells and densitometry analysis is presented at (D). Densitometry calculations for western blot data shown were performed by using the Quantity One software (verifying for non-saturation and subtracting background). The graphs represent the relative LC3-II levels (normalised to β -tubulin levels) compared to the NDC. (ns; not significant)

3.1.3 Pharmacological inhibition of autophagy enhances TKI-induced effects in CML cells

Experiments above demonstrated that TKIs induce autophagy in BC and CP CML cells upon inhibition of BCR-ABL. Hence, our next target was to explore if autophagy has a cytoprotective role within CML cells.

In this series of experiments autophagy was suppressed in TKI-treated cells pharmacologically, by using inhibitors CQ or HCQ. Subsequently, it was investigated if TKIs are more effective with regards to apoptosis induction and suppression of the clonogenic ability of CML cells in an autophagy-inhibited background.

3.1.3.1 TKI treatment in combination with CQ-mediated autophagy inhibition in K562 BC cells

3.1.3.1.1 Analysis of apoptosis in K562 cells following TKI treatment in combination with CQ-mediated autophagy inhibition

The apoptotic effect of the TKI/CQ combination versus single agent TKI was investigated in CML BC cells. K562 cells were treated for 72h with TKIs (5 μ M IM, 150nM DAS or 100nM PON) \pm 10 μ M CQ. Apoptosis was analysed by FACS following annexin V/Viaprobe staining.

Figure 3-8 demonstrates that CQ does not affect the apoptosis of K562 as a single agent, unlike TKIs that are targeted anti-CML drugs. Among the three TKIs tested, IM was the least potent in terms of apoptosis induction; despite increasing the mean levels of apoptosis (23.6 \pm 3.6% versus 11.6 \pm 2.2% in the NDC arm), statistical analysis revealed that this induction was not significant (p=0.13). However, CQ augmented the apoptotic effect of IM and the combination IM/CQ induced apoptosis at significant levels (49.2 \pm 8.4; p=0.04).

DAS was more effective than IM, and as a single agent significantly induced the apoptotic rate within K562 cells (28.1 \pm 4.4%; p=0.04). CQ-mediated autophagy inhibition further promoted the apoptotic effect of DAS (58.8 \pm 11.4%; p=0.03).

PON presented the highest activity among the three TKIs tested, targeting as a single agent almost half of the cells (43.7 \pm 4%; p=0.019). However, there was an obvious increase in the apoptotic percentage in the PON/CQ-treated arm (67.8 \pm 8.9%; p=0.006).

Overall, these data suggest that TKI-induced apoptosis is enhanced in the presence of CQ-mediated autophagy inhibition, with PON/CQ combination having the greatest effect.

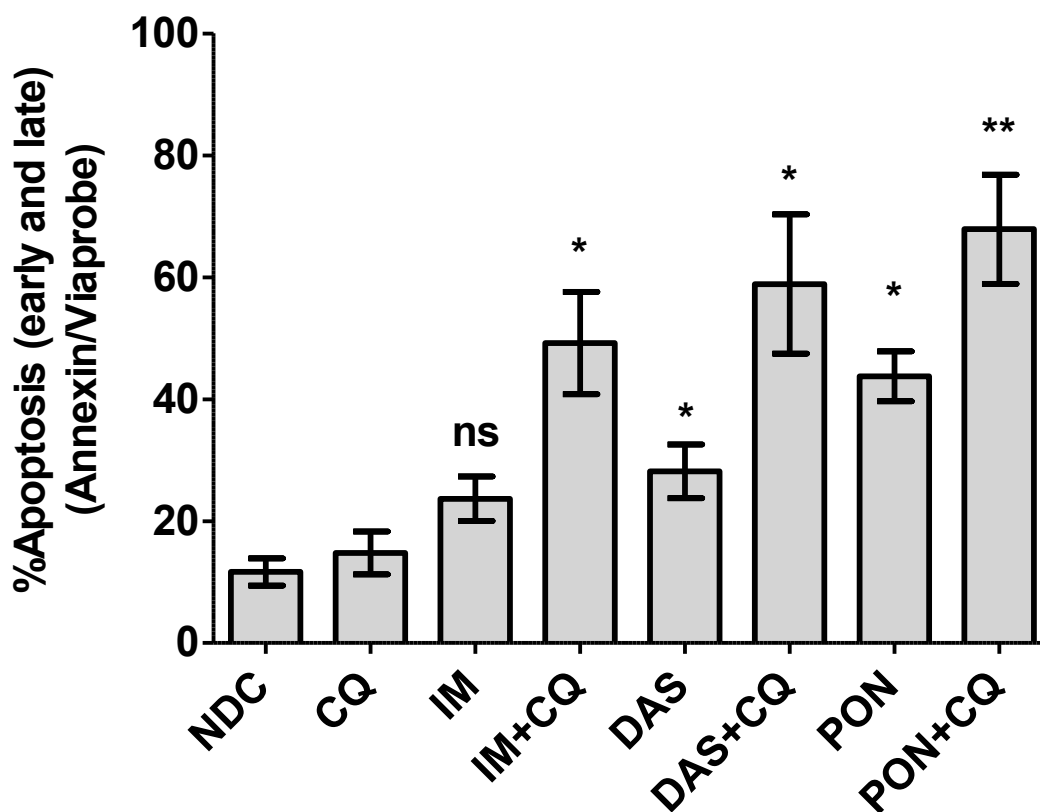


Figure 3-8: CQ-mediated autophagy inhibition enhances TKI-induced apoptosis in K562 cells

K562 cells were treated for 72h with 5 μ M IM or 150nM DAS or 100nM PON, with or without 10 μ M CQ, and analysed by FACS following annexin V/Viaprobe staining. Graph represents apoptosis (early and late) relative to NDC and numbers are presented as mean \pm SEM (n=3). Statistical analysis was performed by using paired t-test. Annotation above a bar refers to statistical significance between the bar and the NDC. (ns; not significant, *, p \leq 0.05, **, p \leq 0.01)

3.1.3.1.2 Analysis of K562 clonogenic ability following TKI treatment in combination with CQ/HCQ-mediated autophagy inhibition

The effect of CQ/HCQ-mediated autophagy inhibition in combination with TKIs was investigated by measuring the clonogenic ability of K562 cells.

1000 K562 cells/treatment (in duplicate) were grown for two weeks in Methocult® that had been supplemented with 500nM IM or 5nM DAS or 1nM PON, in the absence or presence of 10 μ M CQ or HCQ.

Figure 3-9A illustrates that 500nM IM significantly suppressed the clonogenic ability of the cells compared to NDC ($p=0.0219$). CQ significantly enhanced IM effect ($p=0.0223$ IM/CQ versus IM), with the combination IM/CQ reducing colony numbers >50% ($p=0.0131$ IM/CQ versus NDC).

Likewise, 5nM DAS inhibited efficiently the ability of K562 to form colonies ($p=0.0028$ versus NDC). However, the combination DAS/CQ was much more potent in suppressing the clonogenicity of the cells ($p=0.0032$ DAS/CQ versus NDC).

Figure 3-9B demonstrates that 1nM PON was not efficient in suppressing colony formation ability as a single agent ($p=0.1195$ PON versus NDC) (Figure 3-16B). Nevertheless, HCQ dramatically enhanced its effect ($p=0.0159$ PON/HCQ versus PON) and the combination of PON/HCQ was highly effective, suppressing >95% the clonogenic ability of K562 cells ($p=0.0030$ PON/HCQ versus NDC).

In this experiment IM, DAS and PON were used in 10, 30 and 100 times, respectively, lower concentrations compared to the ones we previously identified to efficiently inhibit BCR-ABL activity (i.e. 5 μ M IM, 150nM DAS and 100nM PON). In all cases, CQ/HCQ-mediated inhibition of autophagy enhanced the efficacy of the drugs against the clonogenicity of the K562 cells. This could suggest that cytoprotective autophagy is induced even upon incomplete BCR-ABL inhibition, allowing the cells to survive and proliferate.

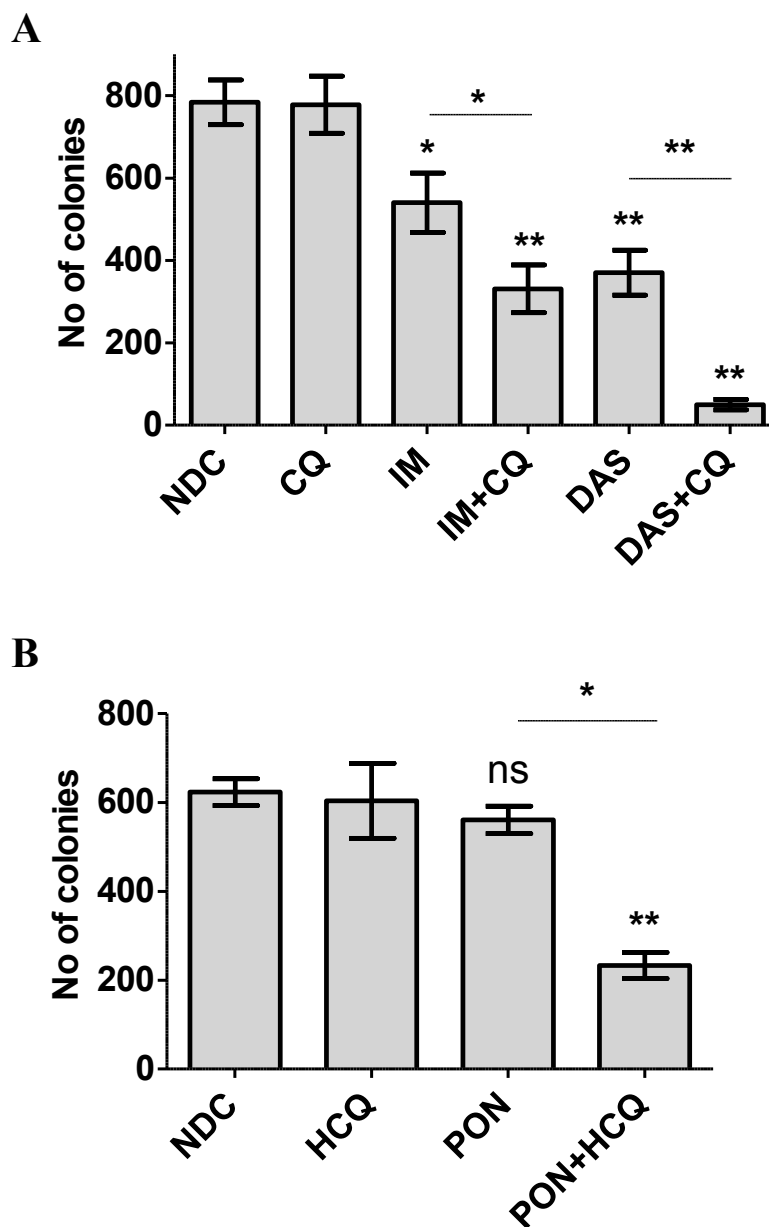


Figure 3-9: CQ/HCQ enhance TKI-induced inhibition of the colony forming ability of K562 cells

1000 K562 cells/treatment (in duplicate) were grown for two weeks in Methocult® that contained 500nM IM or 5nM DAS (A) or 1nM PON (B), with or without 10 μ M CQ. Colonies were counted after 14 days under light microscope. Number of colonies (No of colonies) /arm is presented as mean \pm SEM (n=3). Statistical analysis was performed by using paired t-test. Annotation above a bar refers to statistical significance between the bar and the NDC. (ns; not significant, *, $p \leq 0.05$, **, $p \leq 0.01$)

3.1.3.2 HCQ-mediated inhibition of autophagy enhances TKI-induced effects in CML CD34+ cells

Having observed that CQ enhances TKI effects in Ph⁺ cell lines, the efficacy of the combination was investigated in human CML CD34⁺ cells.

3.1.3.2.1 Analysis of CP CML CD34⁺ cell viability following TKI treatment in combination with HCQ-mediated autophagy inhibition

CD34⁺ cells from CP CML patients were treated with 5 μ M IM, 150nM DAS or 100nM PON, in the presence or absence of 10 μ M HCQ and cell counts were performed after 3 and 6 days. Cell viability was established by using the trypan blue exclusion method.

Figure 3-10 demonstrates that 3 days following treatment initiation all TKIs mildly suppressed cell proliferation. HCQ-mediated inhibition did not enhance the antiproliferative effect of TKIs at significant levels at this time point. Nevertheless, the combination DAS/HCQ had a significant antiproliferative effect ($p=0.02$ versus NDC), which was associated with cytotoxicity (23% reduction of cell number compared to the input).

Day 6 cell counts were performed on $n=2$ for IM and IM/HCQ; one of the biological triplicates for these treatment arms was contaminated with fungi and therefore, it was not taken into account for analysis. Statistical analysis at that time point revealed that DAS and PON were effective as single agents in suppressing the expansion of CP CML CD34⁺ cells ($p=0.03$ and $p=0.04$ respectively). Nevertheless, the combination of DAS or PON with HCQ revealed only slight enhancement of the TKI-mediated antiproliferative effect of the TKIs ($p=0.03$ for both DAS/HCQ and PON/HCQ versus NDC). A similar trend was observed in the IM versus IM/HCQ treatment arms as well.

Overall, HCQ did not enhance the antiproliferative effect of IM, DAS and PON after 3 or 6 days of treatment. In order to investigate if HCQ-mediated autophagy inhibition affects the long-term survival of CP CML CD34⁺ cells, the experiment in §3.1.3.2.2 was designed.

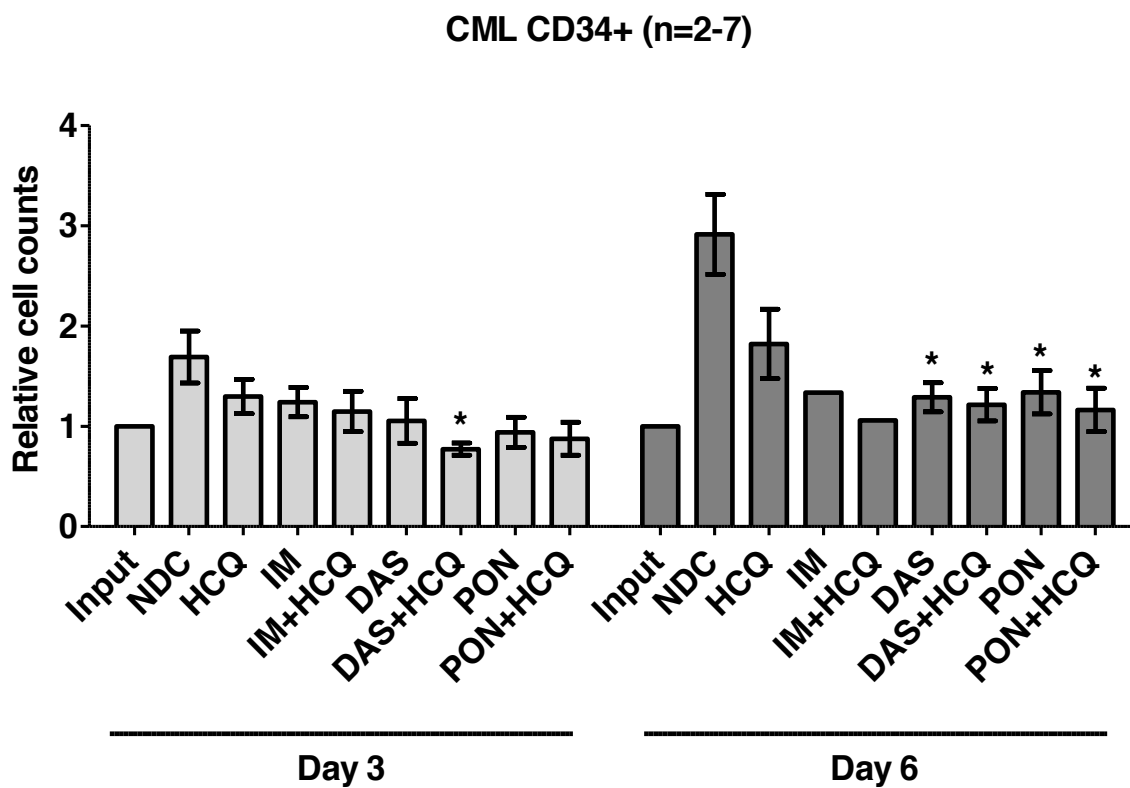


Figure 3-10: TKIs in combination with HCQ in the proliferation of CP CML CD34+ cells

CML CD34+ cells were cultured in SFM+PGFs. Cell counts were performed at 3 and 6 days after treatment initiation and viability was determined by using the trypan blue exclusion method. The number of viable cells in each treatment was compared to input and the relative numbers are presented as mean \pm SEM (n=3-7), apart from IM and IM/HCQ (mean of n=2). Annotation above a bar refers to statistical significance between the bar and the NDC. (*; $p \leq 0.05$)

3.1.3.2.2 Analysis of CP CML CD34+ CFC potential following TKI treatment in combination with HCQ-mediated autophagy inhibition

The committed progenitor potential of CP CML CD34+ cells was tested following TKI treatment, in the presence or absence of HCQ-mediated autophagy inhibition.

CD34+ cells from three CP CML patients were treated *in vitro* with 150nM DAS or 100nM PON, with or without 10 μ M HCQ. 3 days later, drugs were washed out and 2500 cells/arm were transferred to Methocult®. Cell potential was measured by colony counts 14 days later.

Figure 3-11A provides data suggesting that HCQ potentiates the TKI-induced reduction of committed progenitor cell potential. DAS as a single agent did not significantly inhibit the cells' clonogenic ability ($p=0.1$); however, the combination DAS/HCQ was significantly more effective ($p=0.03$). Similarly, PON was not potent in reducing the number of colonies ($p=0.08$), but HCQ enhanced its effect and the combination treatment resulted in significantly lower numbers of colonies ($p=0.03$).

In order to assess the effect of prolonged HCQ-mediated exposure in the presence of TKIs, the following experiment was performed. 2500 CD34+ CP CML cells were transferred to Methocult® containing 5 μ M IM or 2 μ M NIL or 150nM DAS or 100nM PON, in the presence or absence of 10 μ M HCQ. Cell potential under prolonged TKI and HCQ exposure was measured by colony counts 14 days later.

Figure 3-11B demonstrated that all TKIs significantly suppressed the clonogenic ability of the CML cells ($p=0.04$ for IM, $p=0.01$ for NIL, $p=0.07$ for DAS, $p=0.01$ for PON). However, the efficacy of all TKIs was enhanced by HCQ and all TKI/HCQ combinations were associated with superior effect compared to TKI-alone treatment ($p=0.01$ for IM/HCQ, $p=0.009$ for NIL/HCQ, $p=0.006$ for DAS/HCQ, $p=0.009$ for PON/HCQ).

Taken together, these data support that pharmacological inhibition of autophagy augments the efficacy of TKIs against the colony-forming potential of CP CML cells.

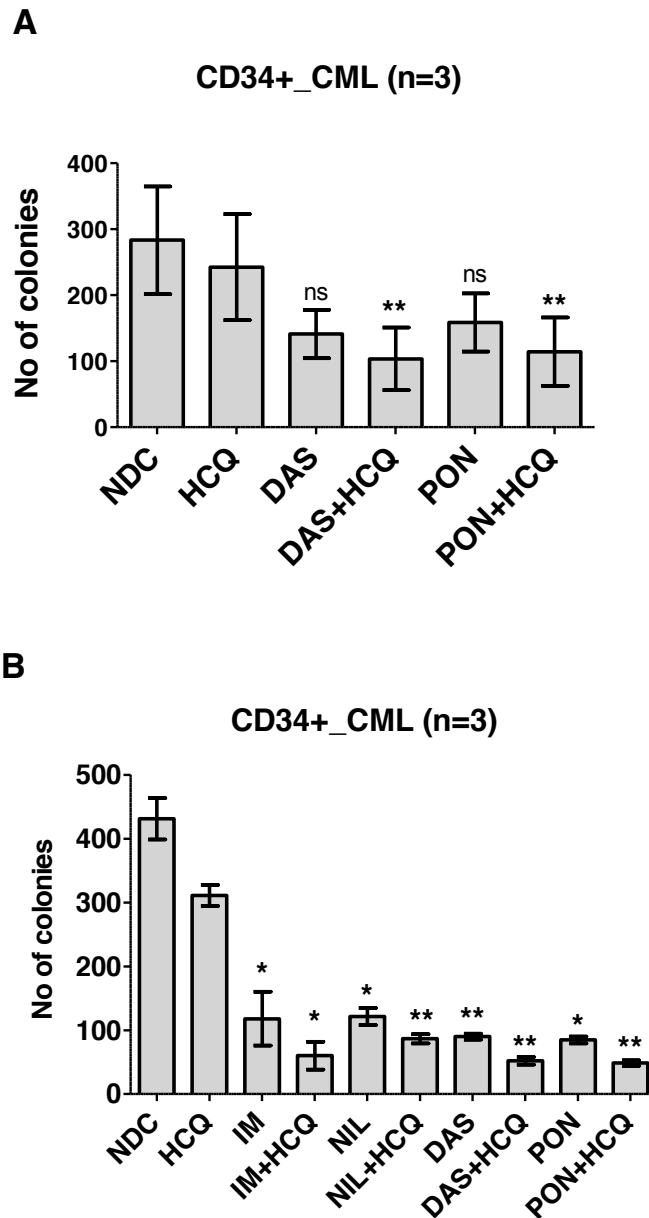


Figure 3-11: HCQ-mediated autophagy inhibition enhances TKI effect against the clonogenic ability of CP CML CD34+ cells

CP CML CD34+ cells were cultured in SFM+PGFs. (A) Cells were treated for 3 days with 150nM DAS or 100nM PON, with or without 10 μ M HCQ. Drugs were washed out and 2500 cells/arm were transferred to Methocult®. (B) 2500 CD34+ CP CML cells were transferred to Methocult® containing 5 μ M IM or 2 μ M NIL or 150nM DAS or 100nM PON, in the presence or absence of 10 μ M HCQ. Colony counts were performed after 14 days under light microscope. No of colonies are presented as mean \pm SEM (n=3). Statistical analysis was performed by using paired t-test. Annotation above a bar refers to statistical significance between the bar and the NDC. (ns; not significant, *, $p \leq 0.05$, **, $p \leq 0.01$)

3.2 PON and mTOR inhibitors in the treatment of CML cells expressing BCR-ABL^{T315I}

CML clones carrying the T315I mutation are resistant to all first and second generation TKIs. More specifically, it has been suggested that BCR-ABL^{T315I} clones are “selected” by sequential treatment with first and second generation TKIs due to their inherent resistance [346]. In this section we aimed to investigate TKI- and non-TKI drugs for the targeting of CML cells carrying the T315I mutation.

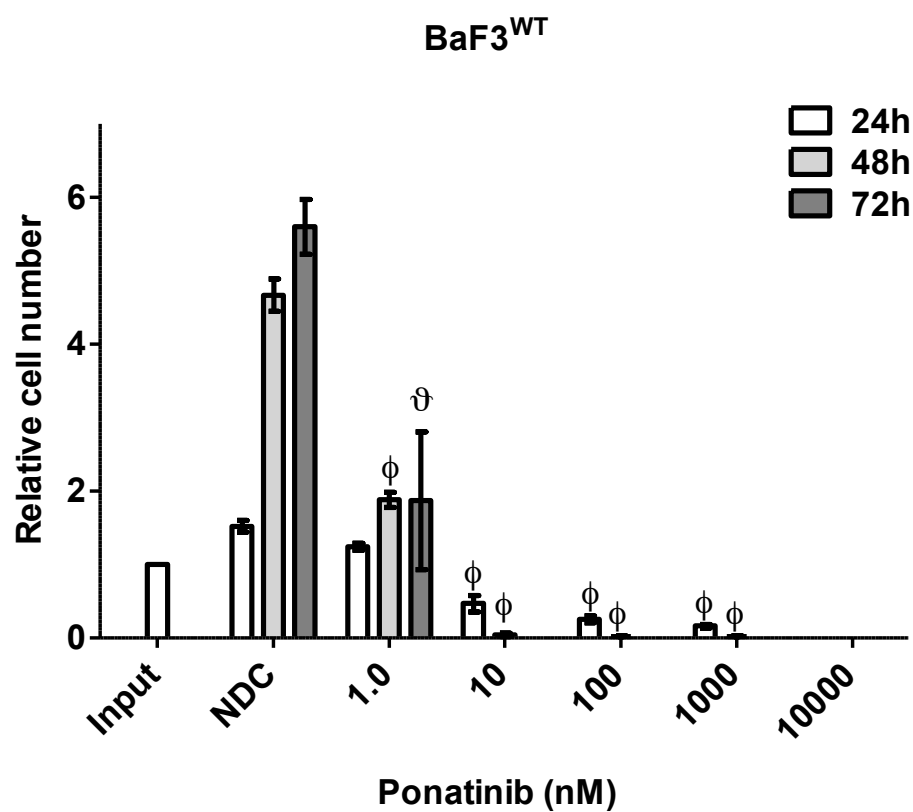
3.2.1 Effect of PON on the proliferation of CML cells carrying BCR-ABL^{T315I}

So far, PON is the only FDA approved TKI that has been reported to be active against BCR-ABL^{T315I}. Hence, we designed a series of experiments in order to evaluate the efficacy of PON in inhibiting the proliferation of CML cells carrying the T315I mutation. BaF3^{T315I} cells were treated with 0.1 to 10000nM PON and proliferation was evaluated by cell counts performed every 24h, for a total of 72h. Cell viability was established by using the trypan blue exclusion method.

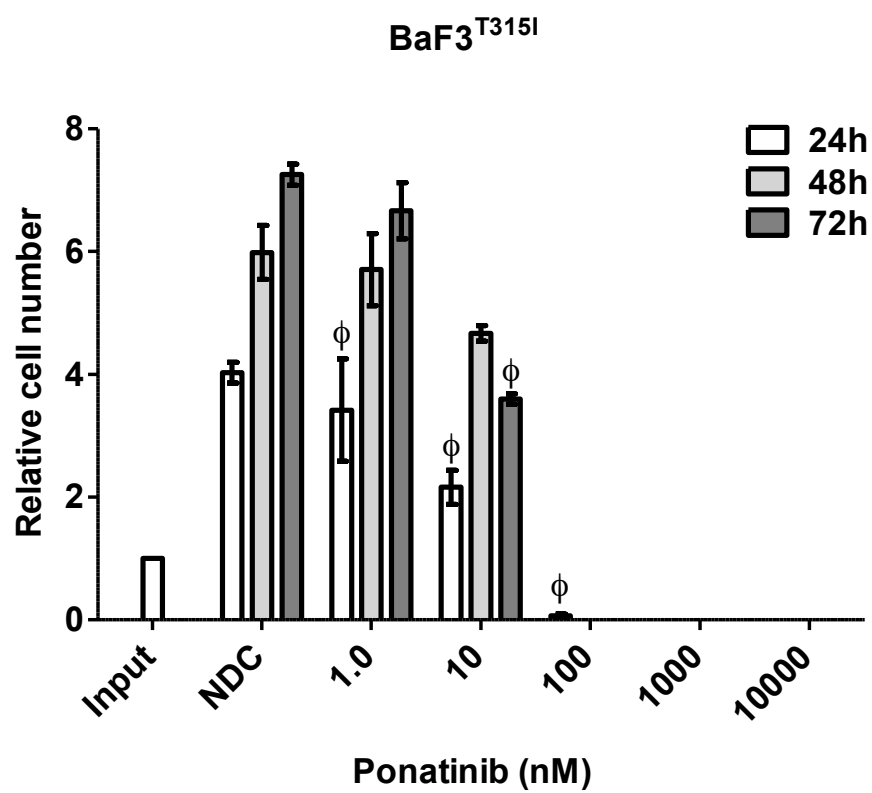
Figure 3-12 clearly demonstrates that PON concentrations within the range of 1 to 10nM effectively inhibited the proliferation of BaF3 cells carrying either native (A), or mutated BCR-ABL (B). PON was associated with increased cytotoxicity and concentrations ≥ 10 nM in BaF3^{WT} cells and ≥ 100 nM in BaF3^{T315I} cells reduced the number of viable cells below the input ($p=0.04$ and $p=0.001$, respectively). Nevertheless, BaF3^{Parental} cells were not significantly affected by PON and continued to proliferate even after exposure to increased concentrations of PON (Figure 3-12C).

Based on the 72h cell counts, the proliferation IC₅₀ of PON was evaluated in BaF3 cells. As depicted in Figure 3-12D, IC₅₀ values were similar between BaF3^{WT} (0.95nM) and BaF3^{T315I} (7.6nM) cells, underlining the efficacy of the drug in cells carrying the T315I mutation. Nonetheless, these drug concentrations had no effect on BaF3^{Parental} cells, which presented ≥ 100 -fold increased IC₅₀ value (177.7nM), highlighting the specificity of the drug. Overall, our data demonstrate the anti-proliferative/cytotoxic effect of PON against CML cells carrying the T315I mutation.

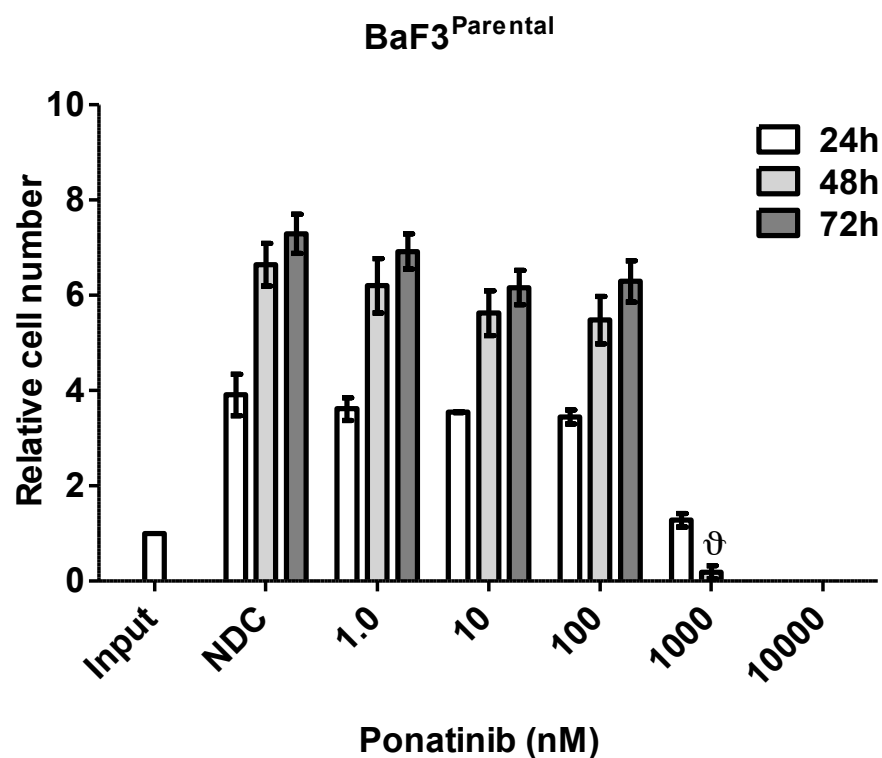
A



B



C



D

Drug	IC ₅₀ (nM)
BaF3 ^{WT}	0.95
BaF3 ^{T315I}	7.6
BaF3 ^{Parental}	177.7

Figure 3-12: Comparison of PON treatment in BaF3^{WT}, BaF3^{T315I} and BaF3^{Parental} cells

BaF3^{WT} (A), BaF3^{T315I} (B) and BaF3^{Parental} (C) cells were treated with increasing concentrations of PON. Cell counts were performed at 24, 48 and 72h after treatment initiation, and viability was determined by using the trypan blue exclusion method. The number of viable cells in each treatment was compared to the input and the relative numbers are presented as mean±SEM (n=3). (D) Proliferation IC₅₀ values were estimated based on the proliferation data after 72h of TKI treatment. (θ; p≤0.05, φ; p≤0.01, δ; p≤0.001)

3.2.2 Effects of mTOR inhibitors' treatment in CML cells

During recent years a constantly growing number of studies has underlined the significance of the PI3K/AKT/mTOR pathway in the survival of cancer cells, making it a target for the development of potential anti-cancer drugs. Agents inhibiting the PI3K/AKT/mTOR pathway are currently being tested for the treatment of leukaemic patients, including CML [347]. These agents act downstream of BCR-ABL and hence, could benefit patients that do not respond to or are resistant to first and second generation TKIs (Figure 3-13).

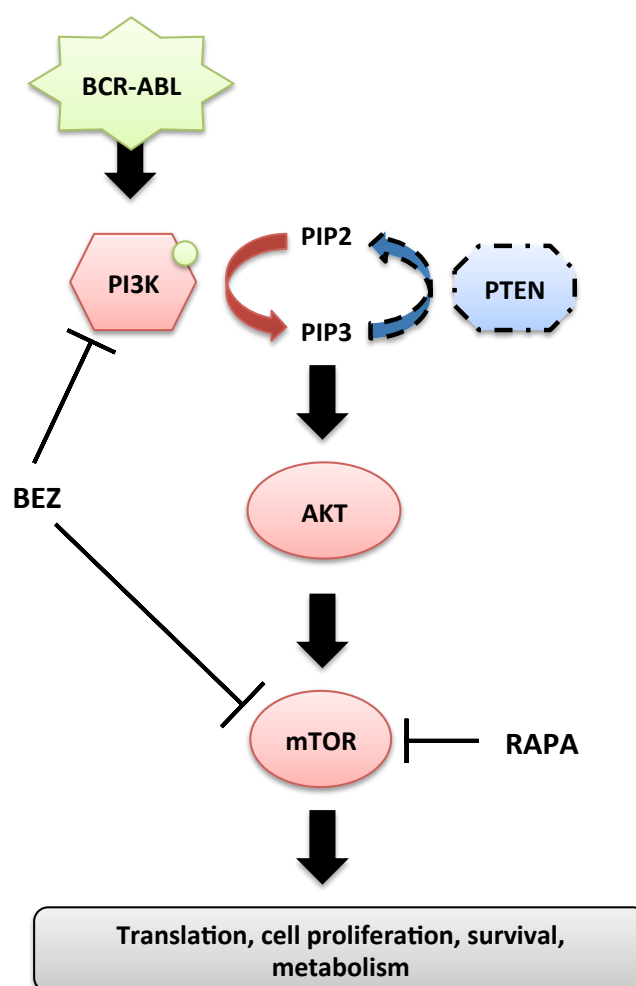


Figure 3-13: The PI3K/AKT/mTOR pathway in cell survival

3.2.2.1 Effect of mTOR inhibitors in the proliferation of BCR-ABL^{T315I}-expressing CML cells

In order to investigate the effects of mTOR inhibition in the proliferation of resistant T315I cells, two inhibitors were used: (i) RAPA, which inhibits mTORC1 activity, and (ii) BEZ, a dual ATP-competitive PI3K and mTOR inhibitor.

KCL22^{T315I} cells were treated with 0.1 to 1000nM BEZ and proliferation was evaluated by cell counts performed every 24h, for a total of 72h. Cell viability was established by using the trypan blue exclusion method.

Figure 3-14 demonstrates that within the first 48h of treatment, 100nM BEZ inhibited 50% the size of the viable population of KCL22 cells carrying either native (44.6±4.8%; p=0.007) (A), or BCR-ABL^{T315I} (48±6.3%; p=0.01) (B). Number of viable cells was further reduced within the next 24h of 100nM BEZ treatment; approximately 80% of the KCL22^{WT} and KCL22^{T315I} were eradicated, suggesting that the BEZ concentrations ≥100nM had a cytotoxic effect. Hence, it was decided for subsequent experiments to use BEZ in the IC50 proliferation dose of 100nM.

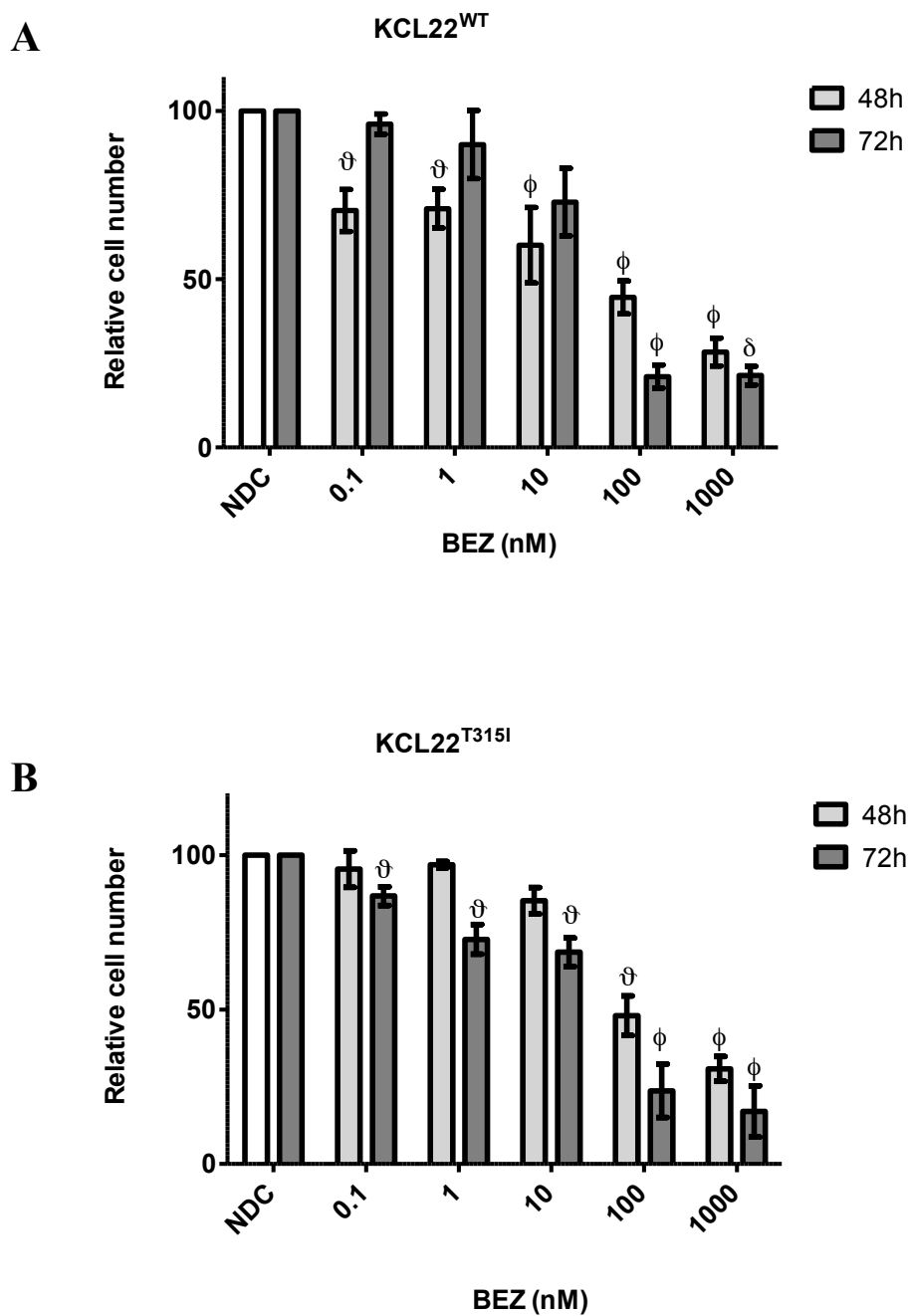


Figure 3-14: Comparison of BEZ treatment in KCL22^{WT} and KCL22^{T315I} cells

KCL22^{WT} (A) and KCL22^{T315I} (B) cells were treated with increasing concentrations of BEZ. Cell counts were performed at 48 and 72h after treatment initiation, and viability was determined by using the trypan blue exclusion method. The number of viable cells in each treatment was compared to the NDC and the relative numbers are presented as mean±SEM (n=3). (θ; p≤0.05, φ; p≤0.01, δ; p≤0.001)

KCL22^{T315} cells were also treated with 0.1 to 1000nM RAPA and proliferation was evaluated by cell counts performed every 24h, for a total of 72h. Cell viability was established by using the trypan blue exclusion method.

Figure 3-15 illustrates that RAPA had an antiproliferative effect against both KCL22^{WT} (A) and KCL22^{T315} (B) cells. Following 72h of treatment with 10nM RAPA the proliferation of KCL22^{T315} was reduced approximately 50% ($53.7 \pm 2.8\%$; $p=0.003$), suggesting that this is the IC50 concentration of the drug. Nevertheless, treatment with 10- and 100-fold increased concentration did not achieve higher antiproliferative effects ($50.4 \pm 2.9\%$ for 100nM and $51.7 \pm 3.3\%$ for 1000nM treatment). Hence, it was decided to use RAPA in the concentration of 10nM for subsequent experiments.

Overall, these data suggest that mTOR inhibitors RAPA and BEZ suppress proliferation of KCL22 cells carrying the T315I mutation.

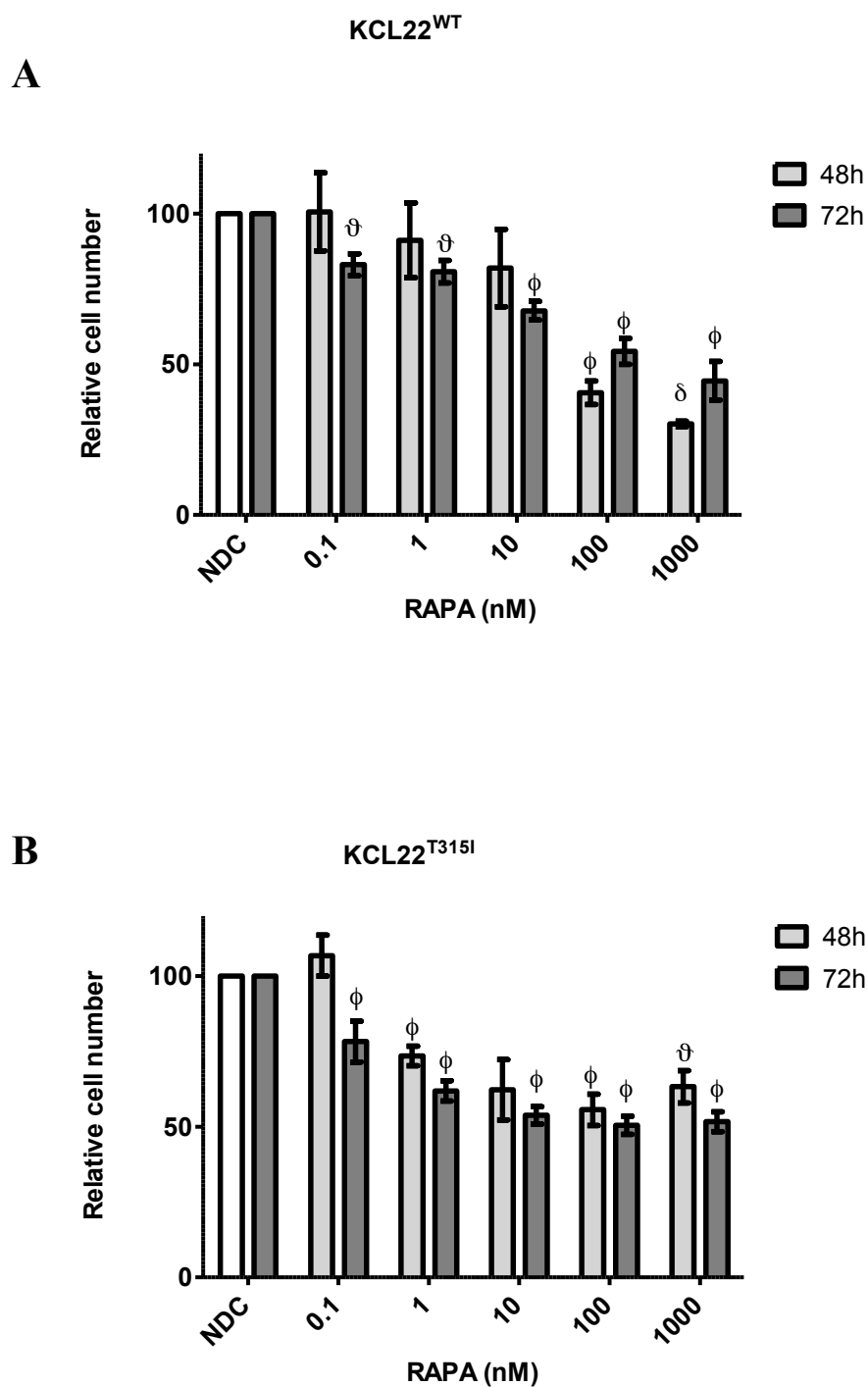


Figure 3-15: Comparison of RAPA treatment in KCL22^{WT} and KCL22^{T315I} cells

KCL22^{WT} (A) and KCL22^{T315I} (B) cells were treated with increasing concentrations of RAPA. Cell counts were performed at 48 and 72h after treatment initiation, and viability was determined by using the trypan blue exclusion method. The number of viable cells in each treatment was compared to the NDC and the relative numbers are presented as mean±SEM (n=3). (θ; p≤0.05, φ; p≤0.01, δ; p≤0.001)

3.2.2.2 Effect of mTOR inhibitors in the autophagic flow of CML cells

In §3.2.2.1 we demonstrated that BEZ and RAPA had antiproliferative effects against CML BC cells carrying either native or BCR-ABL^{T315I}. Nevertheless, since these agents suppress mTOR, the major negative regulator of autophagy, they could induce autophagy. In order to further investigate the effect of BEZ and RAPA on the autophagic flow of CML cells, we performed the following experiment.

Human CP CML CD34+ cells were cultured in SFM+PGFs and treated for 24h with 10nM RAPA or 100nM BEZ. Assessment of autophagy was carried out by immunofluorescence microscopy analysis on endogenous LC3 levels, following fixation of the treated cells onto slides and sequential staining with primary anti-LC3 antibody and Alexa-fluorochrome conjugated secondary antibody. DAPI was used for the counterstaining of nuclei.

Figure 3-16 demonstrates the accumulation of LC3-positive punctae in the presence of RAPA or BEZ, suggesting the induction of autophagy upon treatment with these mTOR inhibitors.

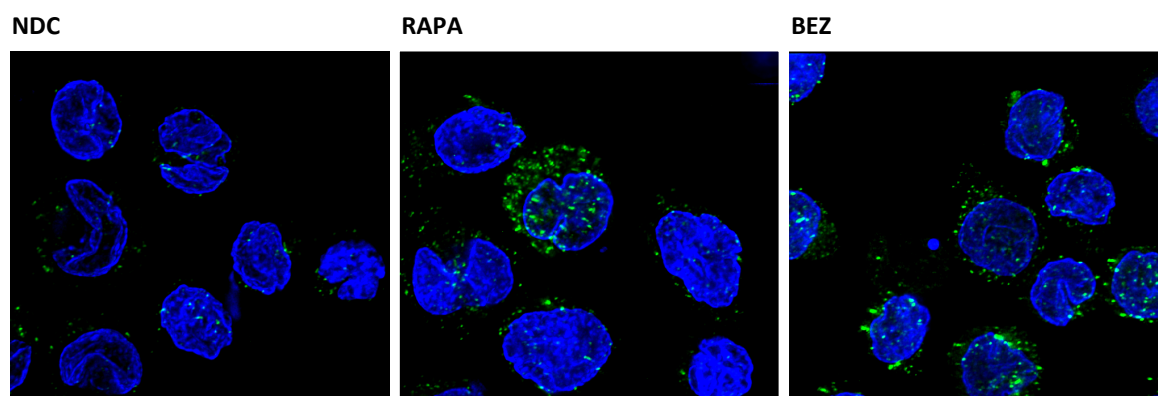


Figure 3-16: Formation of LC3-positive punctae in RAPA- and BEZ-treated CP CML CD34+ cells

Immunofluorescence imaging on CP CML CD34+ cells treated for 24h with 10nM RAPA or 100nM BEZ or NDC. Cells were stained with primary anti-LC3B antibody and secondary Alexa-fluorochrome conjugated antibody. Photos represent Z-stack overlay after deconvolution by using the AxioVision software. Captions presented at 1000X magnification, DAPI used for nuclei staining.

3.2.2.3 Analysis of apoptosis in KCL22^{T315I} cells following treatment with TKIs or mTOR inhibitors, in combination with CQ-mediated autophagy inhibition

In order to evaluate if autophagy inhibition augments the effect of PON or mTOR pathway inhibitors, RAPA and BEZ, on CML cells carrying the T315I mutation, the following experiments were performed.

KCL22^{WT} and KCL22^{T315I} were treated for 72h with 150nM DAS, 100nM PON, 10nM RAPA, 100nM BEZ or NDC, in the presence or absence of 10 μ M CQ. Apoptosis was measured by FACS after annexinV/Viaprobe staining.

According to data presented in Figure 3-17A, PON (47.7 \pm 2.7%) was more effective than DAS (39.9 \pm 1.6%) in inducing apoptosis in KCL22^{WT} cells, but none of these TKIs induced apoptosis at statistically significant levels as a single agent (p=0.056 and p=0.12, respectively). Nevertheless, CQ-mediated inhibition enhanced the apoptotic effect of PON at significant levels (p=0.02 PON/CQ versus NDC). RAPA did not induce significant levels of apoptosis, alone (22.9 \pm 9.2%; p=0.4) or in combination with CQ (33.6 \pm 10.1; p=0.36), but its effect was enhanced in the presence of CQ-mediated autophagy inhibition. Interestingly, our data underline the significance of mTOR signalling in cancer cells since BEZ (41.5 \pm 6.1; p=0.09) as single agent induced similar levels of apoptosis compared to DAS. Likewise, CQ enhanced the effect of BEZ (44.4 \pm 5.1%; p=0.06).

As expected, DAS, alone (9.3 \pm 5.2%; p=0.6) or in combination with CQ (11.8 \pm 6.7%; p=0.9), did not affect the apoptosis of KCL22^{T315I} cells since it is not active against the BCR-ABL^{T315I} (Figure 3-17B). However, PON that has been suggested to target BCR-ABL^{T315I} activity, significantly induced apoptosis in KCL22^{T315I} cells (30.9 \pm 7.3%; p=0.02). The apoptotic effect of PON was further boosted upon CQ-mediated autophagy inhibition with the PON/CQ combination (40.1 \pm 8.3%; p=0.01). RAPA (19.4 \pm 8%; p=0.09) was associated with higher levels of apoptosis in KCL22^{T315I} cells compared to DAS, and CQ-mediated inhibition of autophagy enhanced its apoptotic effect (27.4 \pm 13.8%; p=0.17). BEZ, as a single agent was potent in inducing apoptosis in KCL22^{T315I} cells (30.6 \pm 8.2%; p=0.04), to similar levels to PON. Interestingly, the BEZ/CQ combination induced the highest levels of apoptosis in these cells (45.6 \pm 4.3; p=0.0005), highlighting the significance of mTOR for the survival of these leukaemic blast cells.

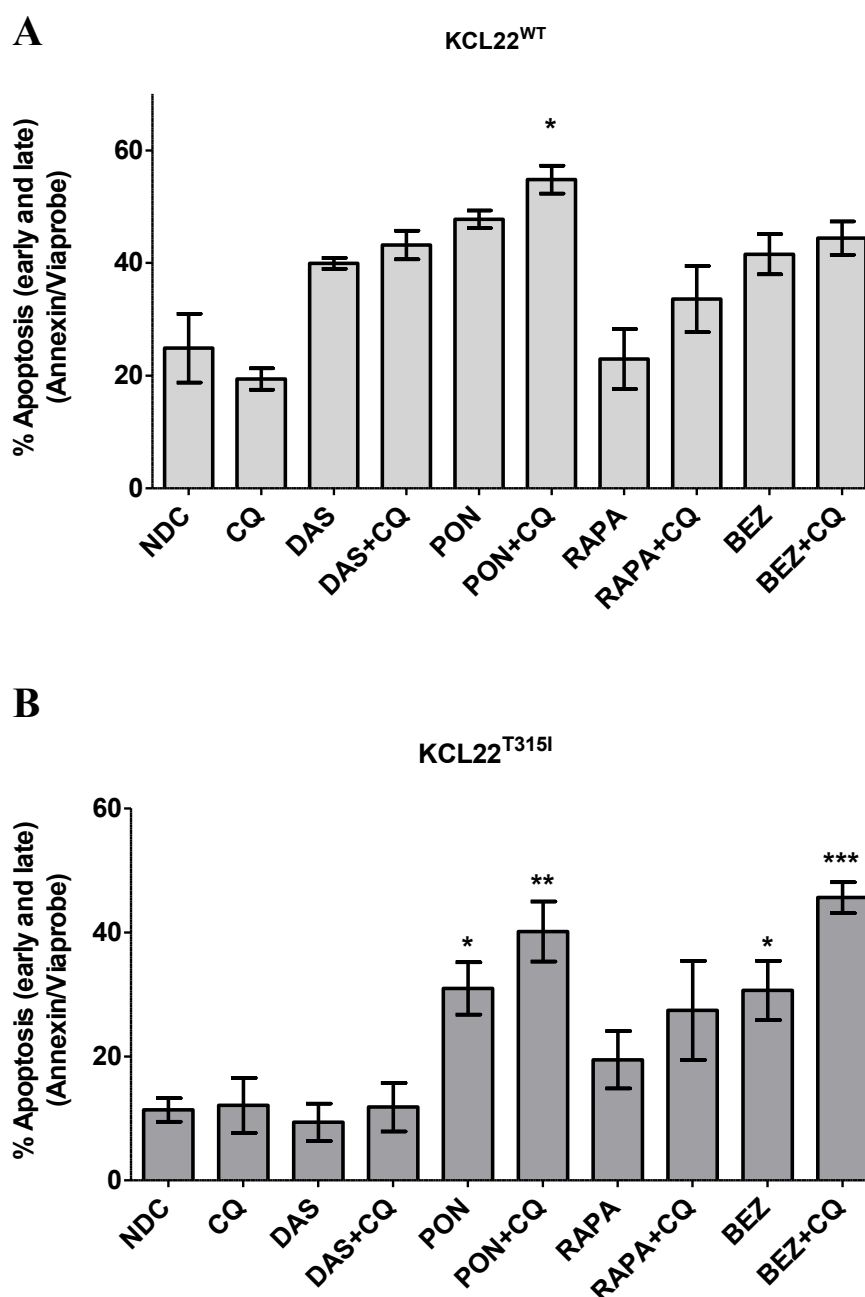


Figure 3-17: CQ-mediated autophagy inhibition improves the apoptotic effect of PON and BEZ treatment in KCL22^{T315I} cells

KCL22^{WT} (A) and KCL22^{T315I} (B) were treated for 72h 150nM DAS, 100nM PON, 10nM RAPA, 100nM BEZ or NDC, in the presence or absence of 10 μ M CQ. Apoptosis was measured by FACS after annexinV/Viaprobe staining. Graphs represent apoptosis percentages as mean \pm SEM (n=3). Statistical analysis was performed by using unpaired t-test. Annotation above a bar refers to statistical significance between the bar and the NDC. (*; p \leq 0.05, **; p \leq 0.01; ***; p \leq 0.001)

3.3 TKI treatment in the autophagy and survival of Ph- cells

3.3.1.1 Treatment with IM, DAS or PON does not induce autophagy in Ph- CD34+ primary cells

Experiments previously described, demonstrated that first (IM), second (DAS) and third (PON) generation TKIs induced autophagy upon treatment of Ph+ cells. In order to exclude that this was attributed to targeting of non-BCR-ABL related pathways, Ph- cells were treated with TKIs±CQ and the effect on the autophagic flux was monitored.

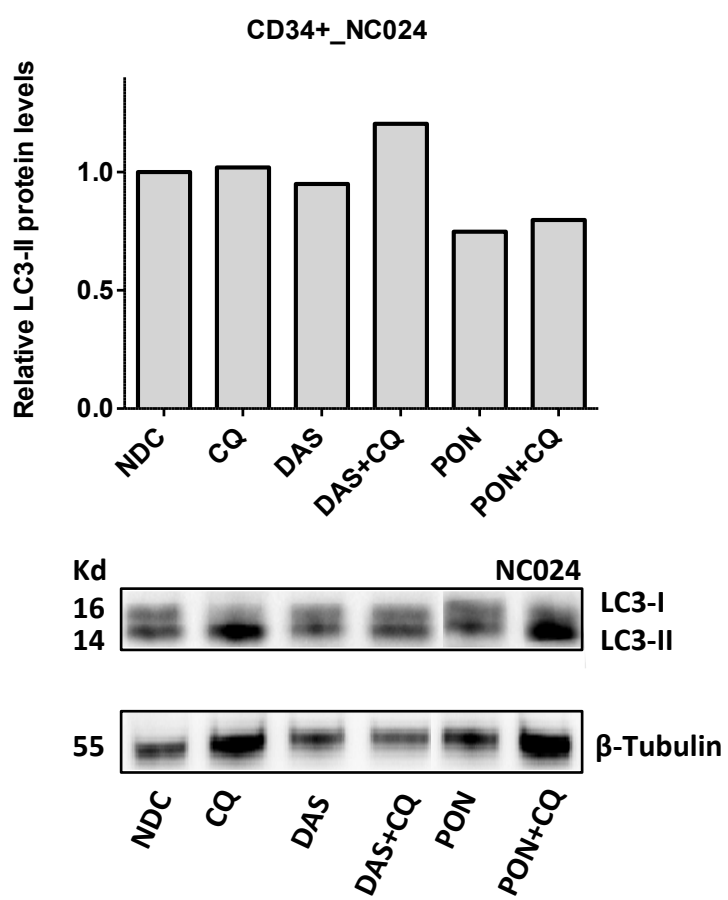
Ph- CD34+ cells from a donor were cultured in SFM+5GFs and treated for 4h with 150nM DAS or 100nM PON, in the absence or presence of 10µM CQ. Cell aliquots from each treatment arm were used for (i) lysis and analysis by western blot for the measurement of LC3-II protein levels, and (ii) staining with CytoID® and analysis by FACS, for the detection of the autophagic activity.

Figure 3-18A demonstrates that treatment with PON did not affect the levels of LC3 lipidation in Ph-CD34+ cells; the PON/HCQ combination presented a 21% decrease in LC3-II compared to HCQ treatment arm. Nevertheless, DAS had a mild effect on autophagy; cells treated with DAS/HCQ combination presented a 20% increase in LC3 lipidation compared to HCQ-treated cells. This may be attributed to the inhibition of non-BCR-ABL targets, such as the SFKs.

Furthermore, autophagy was monitored in the same samples by FACS after staining with CytoID®, as described in §2.2.2.4.

Data presented in Figure 3-18B, illustrate that autophagy was not induced upon TKI treatment of Ph- CD34+ cells since the FITC GeoMean was not increased in the TKI/HCQ combination compared to HCQ treatment alone. However, as discussed in §3.1.2.6, these data on their own could be inconclusive, but in combination with the protein analysis results, they demonstrate that TKIs do not induce autophagy in Ph- CD34+ cells. This observation further supports the notion that autophagy is induced in Ph+ cells upon TKI treatment due to BCR-ABL inhibition.

A



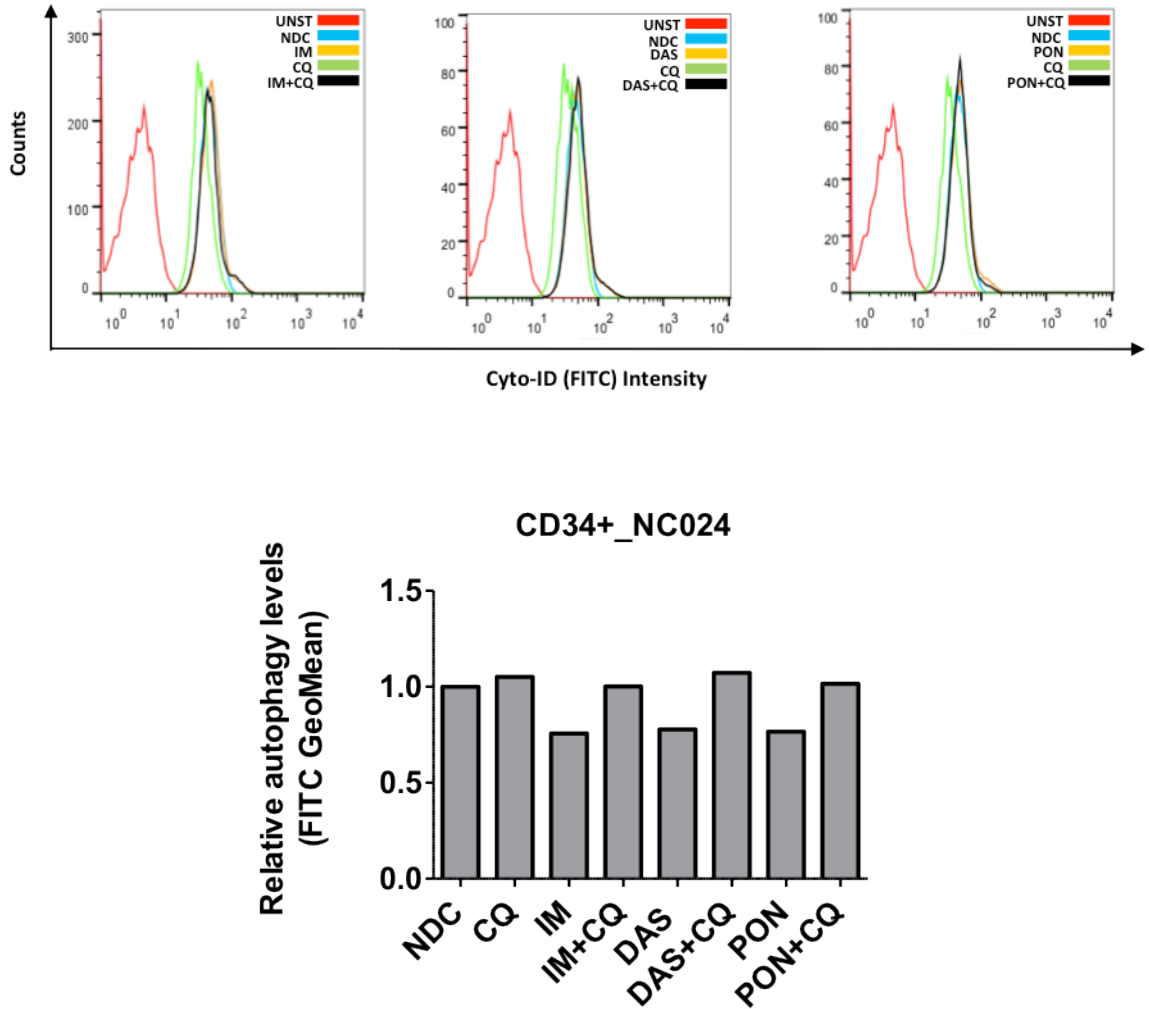
B

Figure 3-18: Treatment with DAS or PON does not induce autophagy in Ph- CD34+ cells

(A) LC3-II levels were measured in Ph- CD34+ cells by western blot, following 4h treatment with 150nM DAS or 100nM PON, \pm 10 μ M CQ. Densitometry calculations for western blot data shown were performed by using the Quantity One software (verifying for non-saturation and subtracting background). The graph represents the relative LC3-II levels (normalised to β -tubulin) compared to the NDC (n=1). (B) Cell aliquots from the same treatment arms were stained with the CytoID® Autophagy dye and FITC levels were determined by FACS analysis. The overlay of the logFITC FACS profiles is shown at the top, while the graphs below represent the FITC geometrical mean relative to the NDC (n=1).

3.3.2 Analysis of the effect of DAS/CQ combination treatment on a co-culture of Ph-/Ph+ cells

In order to investigate if CQ-mediated autophagy inhibition in combination with TKIs could potentially have a cytotoxic effect on Ph- cells, the following experiment was performed on IL-3-dependent BaF3^{Parental} cells (Ph-) and BaF3 cells that had been previously transfected with GFP-BCR-ABL^{p210} (BaF3^{p210}) and could grow independently of the presence of IL-3.

Equal amounts of BaF3^{Parental} and BaF3^{p210} cells were used to initiate a co-culture where both populations were represented equally. Cells were maintained in RPMI⁺ supplemented with IL-3, and treated with or without 150nM DAS, in the presence or absence of 10 μ M CQ. The size of each population within the co-culture was monitored via FACS for a total of 96h following treatment initiation, based on the selection marker GFP expressed only by BaF3^{p210} cells. The experiment was repeated for n=3.

As illustrated in Figure 3-19, FACS analysis verified that both BaF3^{p210} and BaF3^{Parental} were equally represented at all time points examined in the NCD, underlining that both populations had the same viability under culture conditions. CQ-mediated inhibition of autophagy did not affect the BaF3^{Parental} cells in the co-culture; however, it appeared to have a slight inhibitory effect on the growth kinetics of the BaF3^{p210} population. Exposure to DAS targeted specifically the BaF3^{p210} cells and significantly reduced their survival from the first 24h of treatment (p=0.03), leading to almost complete eradication of the population after 96h (p=0.004). Most importantly, the combination of DAS/CQ did not have any effect on the survival and proliferation of the BaF3^{Parental} population, while it completely abolished the BaF3^{p210} population.

Overall, these experiments demonstrate that the highest clinically achievable DAS concentration in combination with CQ has no cytotoxic effects on Ph- cells, and effectively targets only Ph+ cells in an *in vitro* co-culture.

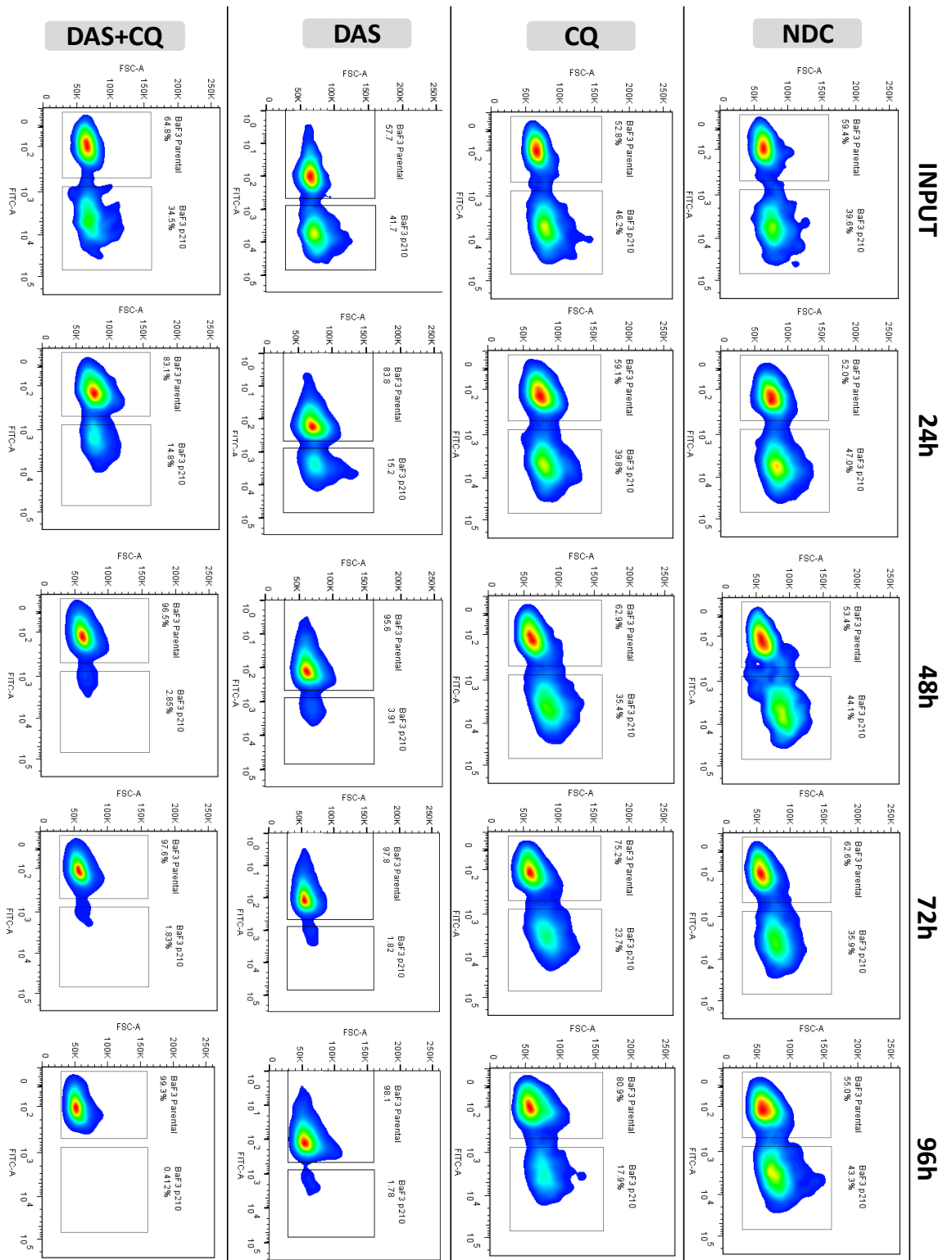


Figure 3-19: DAS/CQ treatment is specifically targeting Ph⁺ cells and is not toxic for Ph⁻ cells

Equal amounts of BaF3^{Parental} and BaF3^{p210} cells were maintained in RPMI⁺ supplemented with IL-3, and treated with 150nM DAS, 10 μ M CQ, the combination of 10 μ M CQ, or NDC. The size of each population was monitored by FACS (BaF3^{p210} express GFP-BCR-ABL^{p210}) for the total of 96h. Representative FACS plots gated on the live cells' population.

4 Results (II): Investigation of ATG7 knock-down in combination with TKIs for the elimination of CP CML CD34+ primary cells

In Chapter 3, by performing a series of autophagy monitoring assays, we demonstrated that first, second, and third generation TKIs induce autophagy upon inhibition of BCR-ABL activity. Furthermore, CQ and HCQ enhanced TKI-mediated apoptosis and suppression of the clonogenic ability in a BC CML cell line and CD34+ cells from CP CML patients, suggesting that TKI-induced autophagy has a cytoprotective role.

CQ and HCQ inhibit the maturation of autophagosomes into degradative autolysosomes, and have been used widely for the pharmacological inhibition of autophagy. However, both drugs are lysosomotropic agents rather than exclusive autophagy inhibitors. Thus, based on these data we could not clarify if beneficial results observed upon combination of TKIs and CQ/HCQ were due to the inhibition of autophagy or attributed to effects on non-related pathways/mechanisms. Furthermore, unpublished data from Ravi Amaravadi's lab [348] demonstrate that clinically achievable concentrations of HCQ (1-10 μ M) do not inhibit autophagy sufficiently *in vivo*, highlighting the need for the development of potent inhibitors that specifically target autophagy for clinical use.

In order to shed light on the aforementioned questions, in this chapter we inhibited autophagy in a specific manner, by knocking-down key autophagy gene *ATG7* in CP CML CD34+ cells. Thereafter, cells were treated with TKIs and the significance of an autophagy-inhibited background was evaluated with regards to cell proliferation, apoptosis and clonogenic ability.

The aims of these experiments were to determine:

- if targeted inhibition of autophagy enhances the effects of TKIs in CP CML CD34+ cells
- if *ATG7* knock-down, alone or in the presence of TKI treatment, affects Ph- CD34+ cells
- if *ATG7* can serve as a potential therapeutic target in CML. *ATG7* inhibitors are currently being developed in industry [349].

In order to assess if *ATG7* knock-down has an effect on Ph- CD34+ cells, non-CML cells and CB samples were also included in our experiments.

4.1 Optimisation of ATG7 knock-down techniques in human CD34+ progenitor cells

Human CD34+ cells represent a powerful platform to study CML. More specifically, loss-of-function studies in this cell population can offer an insight into disease mechanisms and reveal therapeutic targets. Nevertheless, primary cells are traditionally difficult to transduce and therefore, the technical part consists a major challenge. Several technologies that vary in complexity, efficiency, reliability and safety, have been developed for the manipulation and modification of HSCs. However, it remains unclear which protocol offers the most efficient and reliable method of gene knock-down in human CML CD34+ cells.

In order to knock-down ATG7 in primary samples, two post-translational approaches were assessed; a) the non-viral nucleofection of siRNA that leads to transient ATG7 knock-down, and b) the lentivirus-based shRNA-mediated stable ATG7 knock-down. These techniques are associated with different advantages and disadvantages and a direct comparison between them was performed so as to evaluate which one is more suitable for the CML system by means of effectiveness and efficiency, taking into account the low numbers of CML CD34+ samples that are available for research studies.

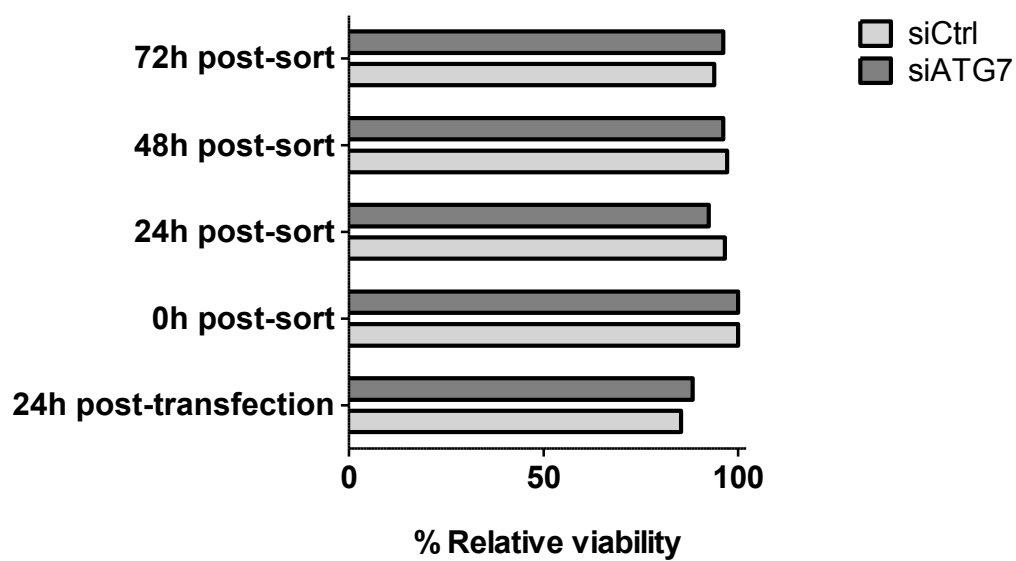
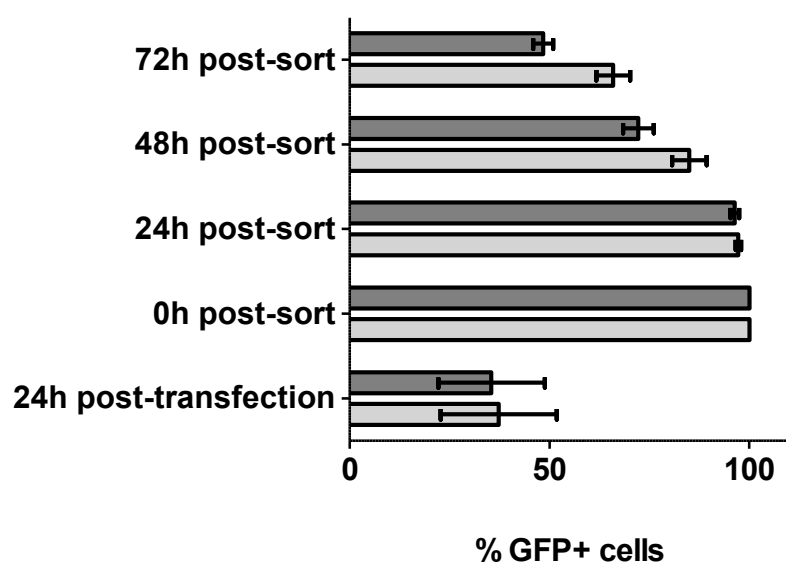
4.1.1 Assessment of the siRNA nucleofection method for the knock-down of ATG7 in cell lines and CD34+ cells

Nucleofection is an electroporation-based method that enables DNA to directly enter the nucleus and therefore, can be performed on non-dividing cells. This method is simple and fast and has been associated with high efficiency.

K562 BC cells and Ph- CD34+ primary cells were transfected with a pool of four ATG7-targeting siRNAs (siATG7) or non-targeting control siRNAs (siCtrl), along with a pmaxGFP® vector (to allow for monitoring of transfection via GFP expression), following the protocol described in §2.2.8.1.4. A pool of siRNAs was preferred over single siRNAs in order to mimic the natural silencing pathway and reduce the off-target effects.

24h following nucleofection, $37.2 \pm 14.4\%$ of the siCtrl-transfected cells and $35.4 \pm 13.3\%$ of the siATG7-transfected cells were expressing GFP and, hence, were successfully transfected. In order to obtain a homogeneous population of transfected cells, siCtrl and siATG7 transfected cells were sorted from non-transfected cells based on expression of the

GFP marker. Monitoring of the sorted siCtrl and siATG7 populations by FACS every 24h following sorting, revealed that cell viability was not affected after DAPI staining (Figure 4-1A); however, GFP expression was depleted in a time-dependent manner with a similar pattern within both siCtrl and siATG7 populations (Figure 4-1B). Furthermore, reduction in GFP expression was associated with lower ATG7 knock-down levels (Figure 4-1C). In an RT-PCR assay, while 24h post-sort siATG7-transfected cells showed significantly reduced ATG7 mRNA levels ($68.1 \pm 2.8\%$ compare to siCtrl; $p=0.0003$), 48h later siCtrl and siATG7 cells showed similar levels of ATG7 mRNA ($p=0.33$ siATG7 versus siCtrl).

A**B**

C

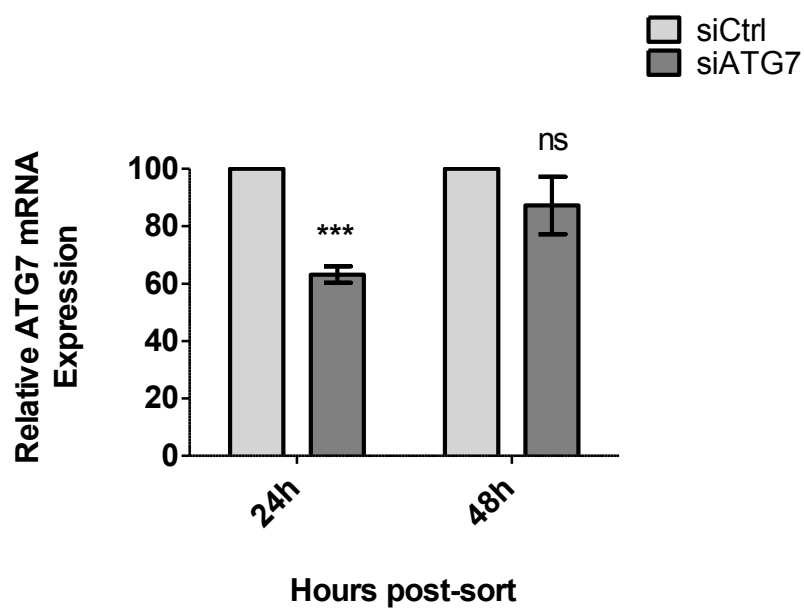


Figure 4-1: Assessment of the siRNA nucleofection method in the viability, transfection efficiency and mRNA knock-down in K562 cells

K562 cells were nucleofected with siCtrl or siATG7, along with a pmaxGFP® vector. Transfected cells were sorted and FACS analysis was performed (A) for the determination of cell viability after DAPI staining (n=1) and (B) for GFP expression monitoring (GFP levels presented as mean±SEM of n=3). (C) ATG7 mRNA levels were measured 24h and 48h post-sort by RT-PCR. Graph represents mean±SEM relative ATG7 mRNA levels compared to the siCtrl (n=3). Statistical analysis was performed by unpaired Student's t-test. (ns; not significant, ***; $p \leq 0.001$)

The siRNA nucleofection method was also tested with regards to ATG7 knock-down in CD34+ cells.

Ph- CD34+ cells were nucleofected with siCtrl and siATG7 along with pmaxGFP®, and cultured overnight in SFM+5GFs. FACS analysis was performed 24h later for the assessment of transfection efficiency by GFP measurement, and cell viability after DAPI staining. The transfected cells were sorted according to GFP expression levels to GFP^{High} expressing cells, and GFP^{Medium} expressing cells for both siCtrl and siATG7 populations.

Figure 4-2A demonstrates that nucleofection severely affected the survival of CD34+ cells; the viability of siRNA-transfected cells was significantly reduced compared to cells of the same samples that had not been nucleofected (Figure 4-2B). Viability was affected in both siCtrl and siATG7 cells, suggesting that this was a method-associated disadvantage and not a knock-down induced effect. ATG7 mRNA levels were suppressed efficiently (>40%) within the GFP^{High} siATG7 CD34+ cells compared to the GFP^{High} siCtrl (Figure 4-2C). Nevertheless, GFP^{Medium} siATG7 CD34+ cells did not show a significant reduction in ATG7 mRNA transcripts (<20%) compared to the GFP^{Medium} siCtrl-transfected cells.

Hence, even if the method was associated with high transfection levels, it was deemed unsuitable:

- (i) for prolonged assays in cell lines, since the overgrowth of untransfected cells would overwhelm and dilute transfected cells,
 - (ii) for experiments with primary samples due to the low number of cells that would be available for experiments after nucleofection and sorting for high GFP-expressing cells.
- Therefore, alternative methods of knock-down were investigated.

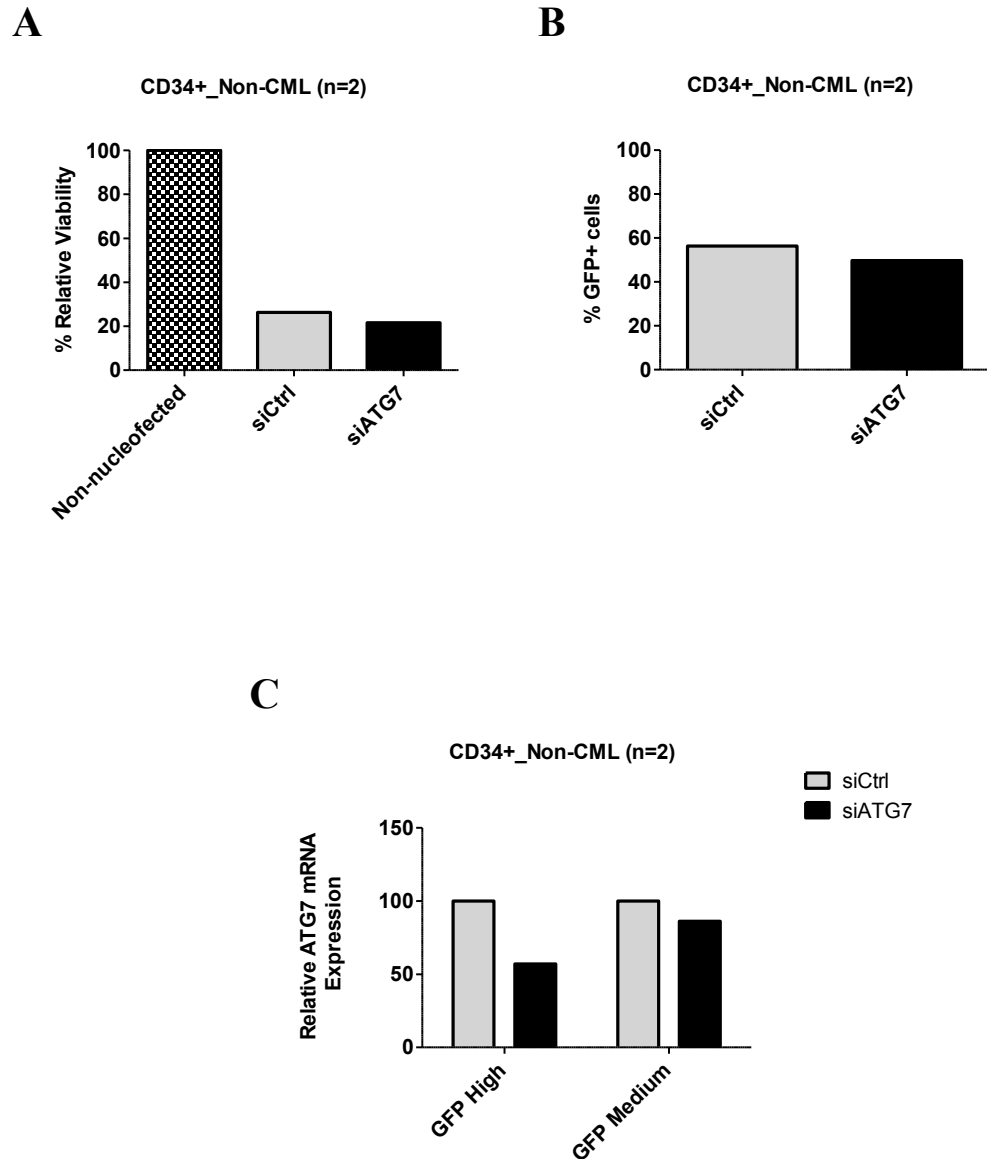


Figure 4-2: Assessment of the siRNA nucleofection method in the viability, transfection and knock-down efficiency in Ph- CD34+ progenitor cells

Ph- CD34+ cells were nucleofected with siCtrl or siATG7, along with a pmaxGFP® vector and cultured overnight in SFM+5GFs. Transfected cells were sorted into GFP^{High}- and GFP^{Medium}-expressing populations. (A) FACS analysis for the determination of cell viability was performed 24h post-nucleofection after DAPI staining. Graph values represent cell viability mean of n=2 relative to non-nucleofected cells. (B) GFP expression was measured by FACS so as to determine transfection efficiency (n=2) (C) ATG7 mRNA levels were assessed 24h post-sort by qRT-PCR within GFP^{High} and GFP^{Medium} sorted cells. Graph values represent mean of n=2 compared to siCtrl.

4.1.2 Optimisation of the lentivirus-mediated shRNA delivery method for the knock-down of ATG7 in CP CML CD34+ primary cells

4.1.2.1 Comparison of concentrated versus unconcentrated lentivirus in the viability and transduction efficiency of CD34+ cells

In order to circumvent the problems of reduced cell viability and knock-down transiency following nucleofection, an HIV-based second generation lentivirus delivery system was used. The sequence-specific silencing of *ATG7* was performed by two shRNAs targeting separate regions of *ATG7* mRNA; shATG7_1 and shATG7_2. A scrambled shRNA (shCtrl) was used as negative control (no homology with any human mRNA). The shRNA hairpins were carried by a pGIPZ-based vector that uses a Pol II CMV promoter to drive expression of shRNA sequences. The vector also encodes a GFP marker, making the direct monitoring of transduced cells possible.

In order to achieve high titer virus, the virus-containing supernatant medium of transfected HEK cells was ultracentrifuged at 625,000 x g for 2h in vacuum at 4°C, as described in §2.2.8.1.3, and resuspended in SFM in 1/100 of the medium volume used for the ultracentrifugation. The protocol followed for virus concentration was successful and virus titer was increased >100fold following ultracentrifugation (Figure 4-3A).

Primary Ph- and Ph+ CD34+ cells were transduced with MOI10 in the presence of Transdux™, every 12h for a total of 36h accompanied by spinoculation, and transduction efficiency was measured 48h after the last round of incubation with virus (to allow for the expression of shRNA and gene silencing). Figure 4-3B demonstrates that cell viability of CD34+ cells was very low 48h after last transduction round with concentrated virus, as measured by FACS after DAPI staining ($p=0.00004$ for siCtrl and $p=0.001$ for shATG7 compared to untransduced cells from the same samples). This could be attributed to the presence of cellular debris that is received at the ultracentrifugation pellet along with the virions. Moreover, transduction efficiency was very low (Figure 4-3C); this could be due to the freeze-thaw procedure that reduces infectivity.

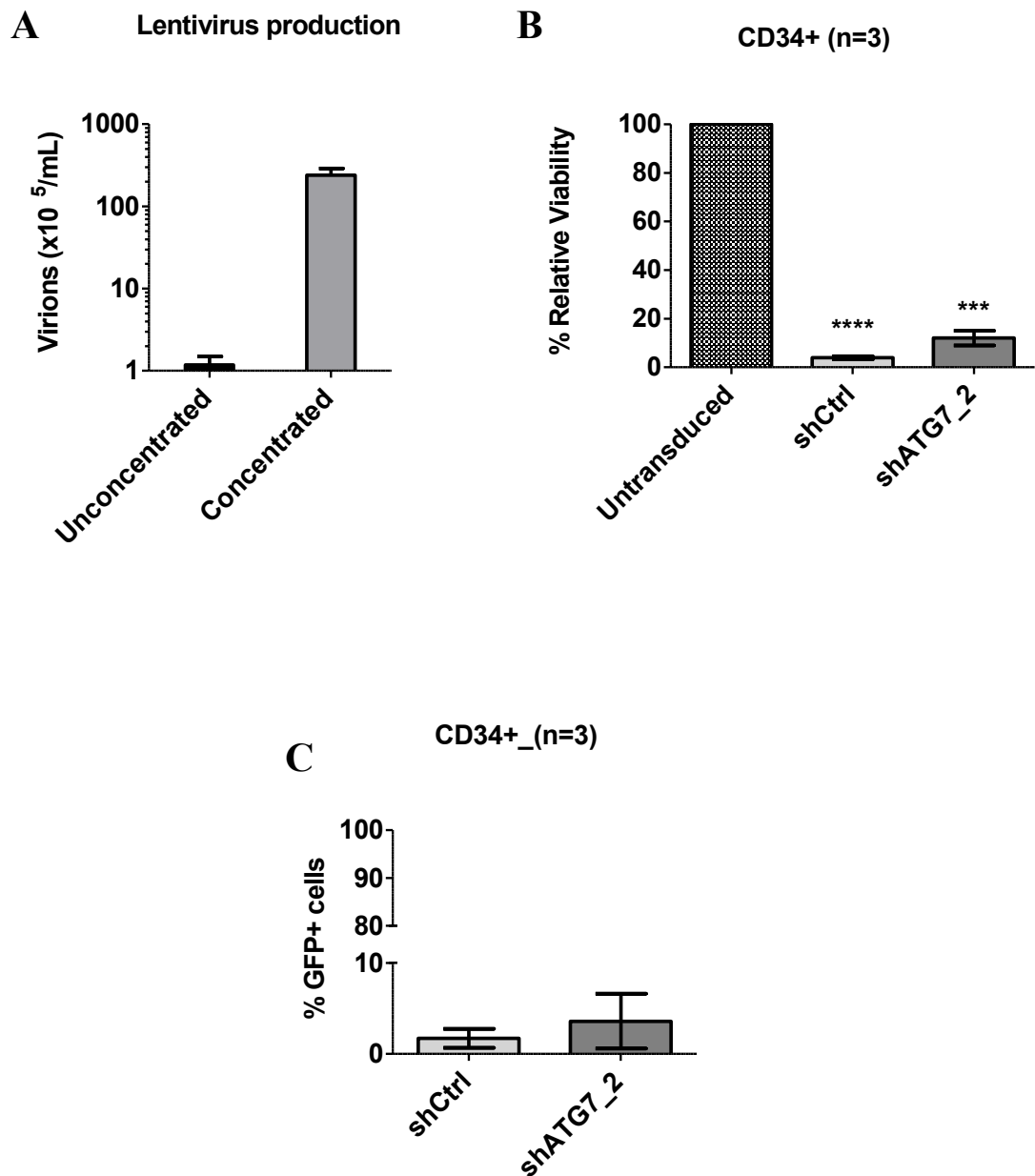


Figure 4-3: Assessment of the use of concentrated HIV-based lentiviral virus in the viability, and transduction efficiency in CD34+ progenitor cells

Ph- and Ph+ CD34+ cells were transduced with 3 rounds of concentrated virus at MOI10 (A). Cell viability was measured 48h after the last transduction round by FACS after DAPI staining. Graph values represent cell viability mean \pm SEM (n=3) relative to untransduced cells. (C) GFP expression was measured by FACS so as to determine transduction efficiency. Graph values represent mean \pm SEM (n=3). (****; $p < 0.0001$, ***; $p \leq 0.001$)

In an attempt to overcome this problem, unconcentrated virus was used for the infection of CD34⁺ cells.

Primary Ph⁻ and Ph⁺ CD34⁺ cells were transduced with freshly produced, filtered, virus-containing medium, as described in §2.2.8.1.2. Transduction was performed in the presence of Transdux™, every 12h for a total of 36h accompanied by spinoculation, and transduction efficiency was measured 48h after the last round of incubation with virus.

Figure 4-4A demonstrates that cell viability of CD34⁺ cells was not severely affected in both mock and ATG7-targeting populations, compared to untransduced cells from the same samples. Furthermore, as illustrated in Figure 4-4B, transduction efficiency associated with this method was relatively high (approximately 30% for both shCtrl and shATG7_2).

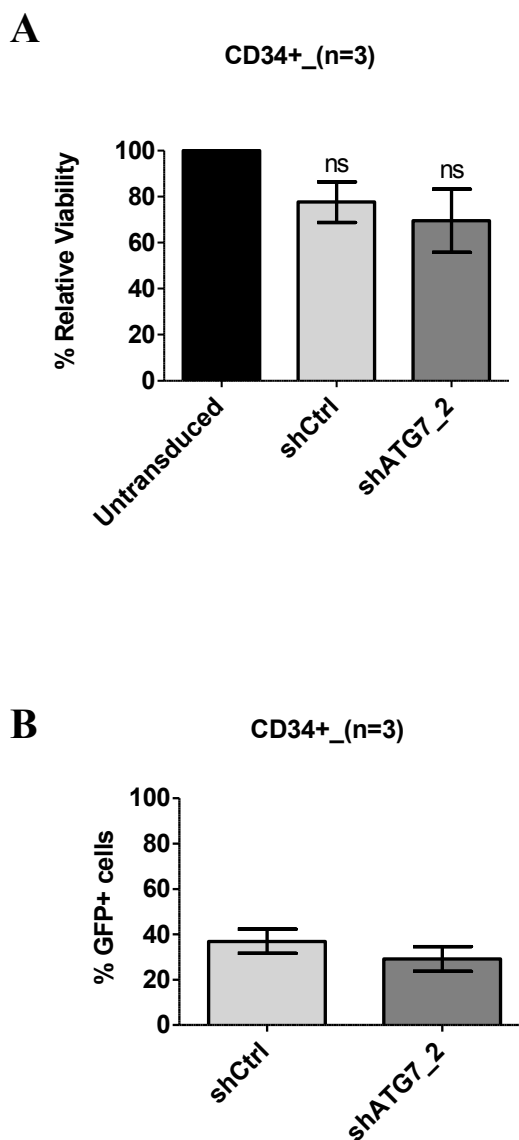


Figure 4-4: Assessment of the use of unconcentrated HIV-based lentiviral virus in the viability, and transduction efficiency in CD34+ cells

Ph- and Ph+ CD34+ cells were transduced with 3 rounds of unconcentrated virus. (A) Cell viability was measured 48h after the last transduction round by FACS after DAPI staining. Graph values represent cell viability mean \pm SEM (n=3) relative to untransduced cells. (B) GFP expression was measured by FACS so as to determine transduction efficiency. Graph values represent mean \pm SEM (n=3). Statistical analysis was performed by paired Student's t-test. (ns; not significant)

4.1.2.2 Assessment of the effect of ATG7 knock-down on basal and TKI-induced autophagy in K562 cells that have been stably transduced with pGIPZ-shATG7-hairpins

Having optimised the lentiviral shRNA-delivery technique, the efficacy of the ATG7-targeting hairpins shATG7_1 and shATG7_2, was tested regarding the knock-down of ATG7. Protein analysis was performed in lysates from sorted K562 cells stably expressing shCtrl, shATG7_1 and shATG7_2 hairpins; GAPDH and actin were measured as loading controls.

Figure 4-5A demonstrates that transduction with either shATG7_1 or shATG7_2 significantly reduced ATG7 protein levels. Densitometry measurements on n=3 western blots revealed that shATG7_1 cells were expressing $59.5 \pm 7.1\%$ ATG7 protein levels ($p=0.01$), while shATG7_2 $64 \pm 4.4\%$ ($p=0.005$) compared to the shCtrl.

Reduction of ATG7 protein had an effect on lipidation of LC3, as illustrated in Figure 4-5B. shATG7_1 and shATG7_2 K562 cells expressed approximately 45% and 35% less LC3-II protein levels compared to the shCtrl, respectively. Hence, knock-down of ATG7 at this level reduced lipidation of LC3.

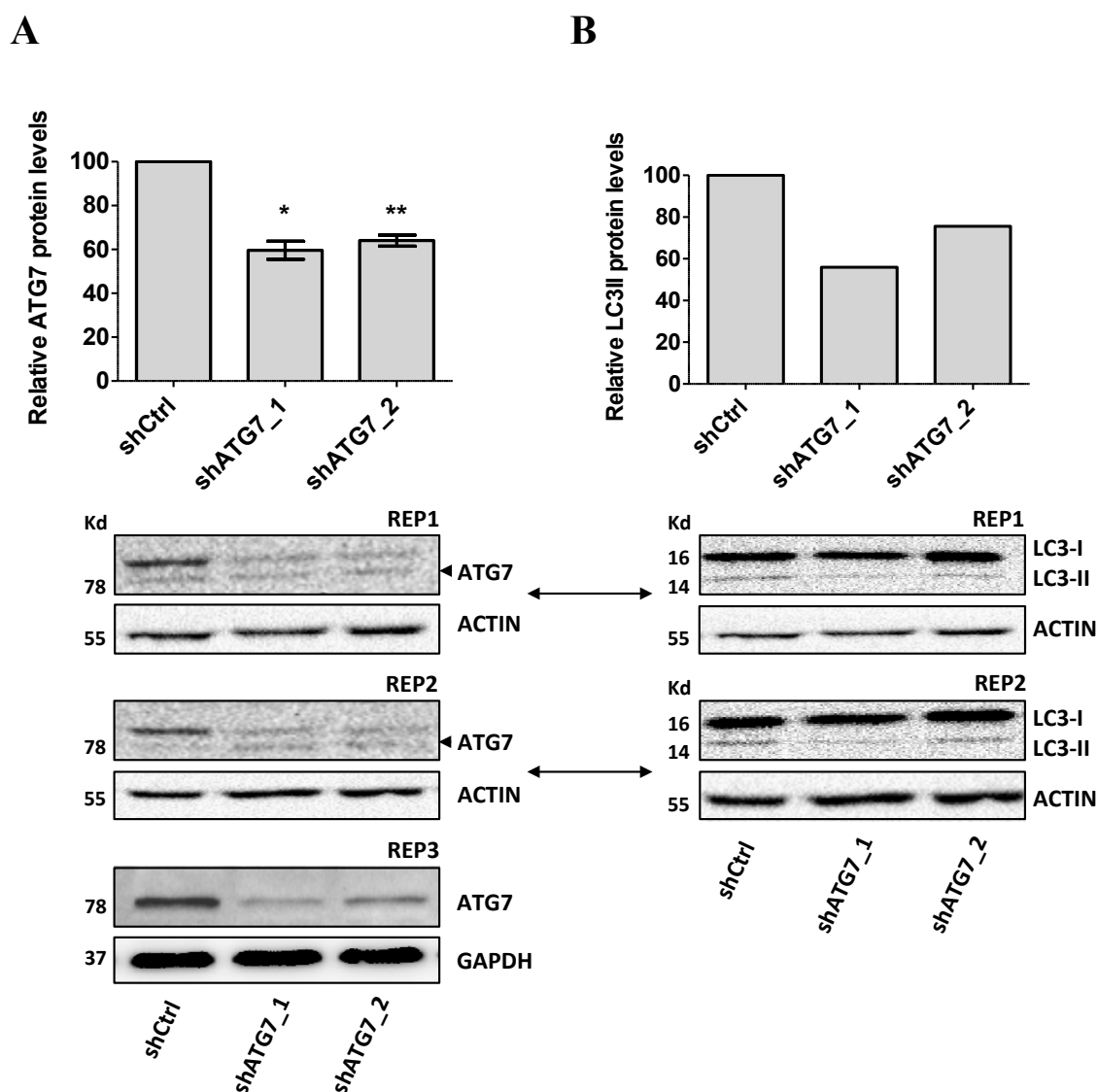


Figure 4-5: Measurement of ATG7 and LC3-II protein levels in K562 cells that stably express ATG7-targeting hairpins carried by pGIPZ vector

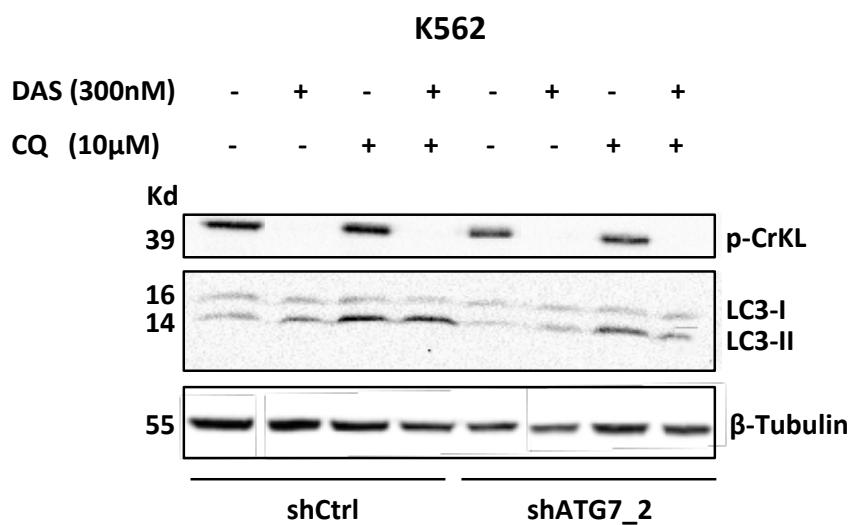
Western blotting was used for the analysis of ATG7 (A) and LC3-II (B) protein levels. Densitometry calculations for western blot data shown were performed by using the Quantity One software (verifying for non-saturation and subtracting background). The graphs represent the relative ATG7 and LC3-II levels (normalised to actin or GAPDH loading levels) compared to the shCtrl. Replicates 1 and 2 refer to the same immunoblots. Graph values represent protein mean \pm SEM with n=3 for (A) and mean for n=2 for (B). Statistical analysis was performed by paired Student's t-test. (*; p \leq 0.05, **; p \leq 0.01). Arrowheads mark non-specific bands.

In order to investigate if the achieved levels of ATG7 knock-down would efficiently suppress autophagy upon TKI treatment, the following experiment was designed.

Sorted K562 cells stably expressing shCtrl or shATG7_2 were treated with 150nM DAS±10µM CQ or NDC. 4h later, cells were lysed and analysed by western blotting. Levels of CrKL phosphorylation were measured as a marker of BCR-ABL activity; β-tubulin was measured as a loading control.

Figure 4-6 demonstrates that treatment of shCtrl with DAS induced autophagy, since LC3-II levels were higher upon exposure to DAS/CQ compared to CQ treatment alone. However, shATG7_2 cells presented similar levels of LC3 lipidation upon DAS/CQ and CQ-alone treatment, suggesting that knock-down of ATG7 successfully inhibited DAS-induced autophagy.

A



B

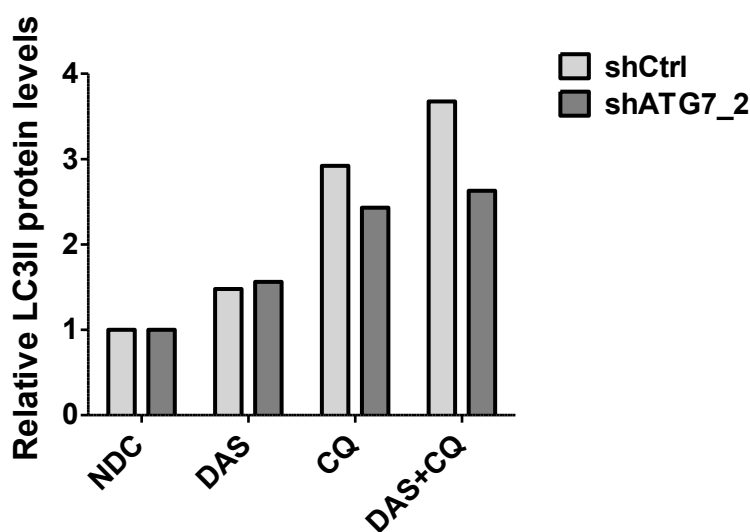


Figure 4-6: Measurement of DAS effect on the autophagic activity of K562 cells in the presence of ATG7 knock-down

K562 shCtrl and shATG7_2 cells were treated for 4h with 150nM DAS \pm 10 μ M CQ or NDC. (A) Cells were lysed and p-CrKL and LC3 protein levels were measured by western blot. B-tubulin was measured as loading control. (B) Densitometry calculations were performed by using the Quantity One software (verifying for non-saturation and subtracting background). The graph represents the relative LC3-II levels (normalised to β -tubulin) compared to NDC.

4.1.2.3 Assessment of the pGIPZ vector that drives shRNA expression under the CMV promoter

K562 cells were transduced according to the protocol described in §2.2.8.1.3 and GFP+ cells were sorted 48h after the last transduction round. Based on previous experiments (Figure 4-2C) where higher GFP expression was associated with higher levels of knock-down, a similar strategy was followed during sorting. The 5-10% highest GFP- expressing K562 cells (GFP^{High}) were sorted in order to achieve a homogeneous population with high levels of knock-down. Sorted cells were maintained afterwards in RPMI⁺ liquid culture and monitored frequently by FACS for GFP expression.

Within 5 days post-sort the GFP expression profile of the GFP^{High}-sorted population (shCtrl, shATG7_1 or shATG7_2) was lower compared to the initial profile before sorting (Figure 4-7). In order to investigate if this was due to promoter silencing, the cells were treated with 5-azacytidine (AZA), a demethylation agent, and GFP expression was monitored every 24h for a total of 72h. Our data demonstrate that loss of GFP expression was reversed upon exposure to AZA, suggesting that the CMV promoter was methylated within K562 cells. Silencing of the CMV promoter would lead to inhibition of shRNA expression and abolishment of ATG7 knock-down. Hence, pGIPZ vector was deemed not suitable for experiments that require long-term and stable knock-down.

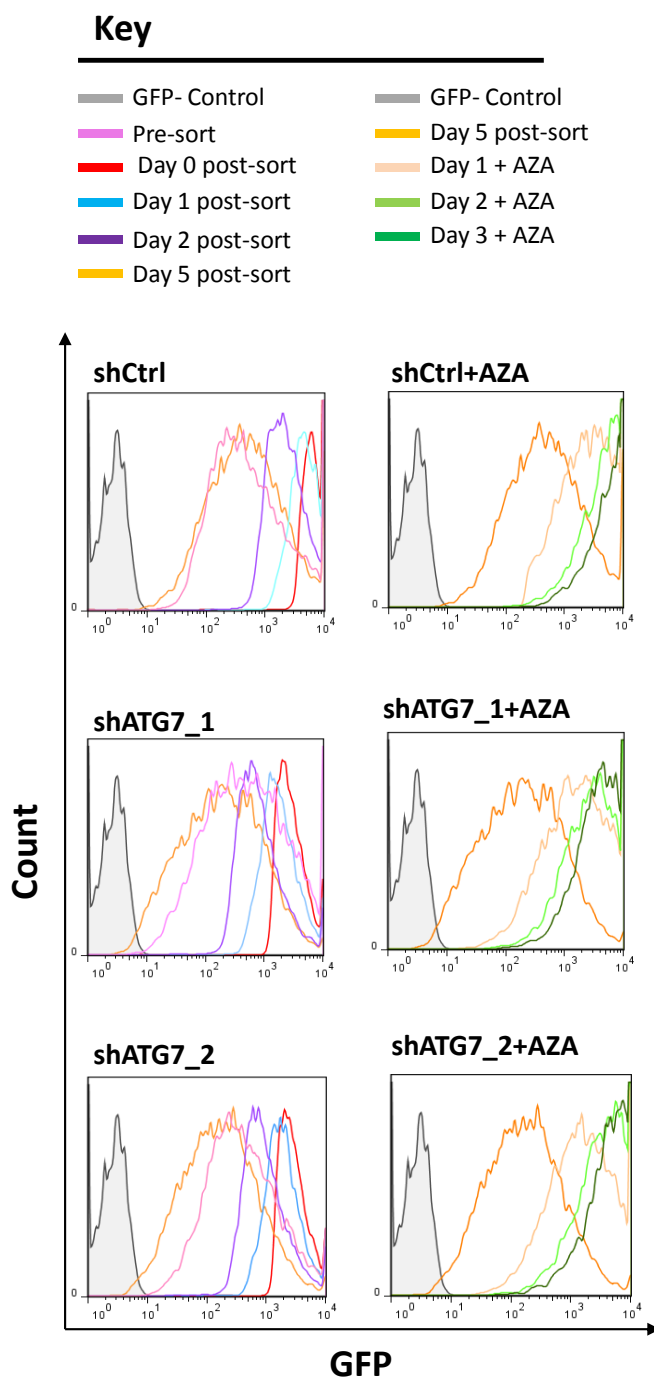


Figure 4-7: The CMV promoter of the pGIPZ vector is methylated in K562 cells

K562 cells transduced with pGIPZ-GFP-shRNA via lentiviral delivery were sorted. GFP expression was monitored by FACS daily over a period of 7 days. The profile of shCtrl, shATG7_1 and shATG7_2 K562 cells revealed reduction in GFP expression in a time-dependent manner. GFP expression was restored upon treatment with 5-azacytidine (AZA), a demethylation agent.

4.1.2.4 Assessment of ATG7 knock-down in CD34+ primitive cells, mediated by an ATG7-targeted hairpin carried by the pLKO.1 vector

In an effort to achieve long-term stable knock-down, the pLKO.1 vector was tested. The shRNA in this vector is under the human U6 promoter that drives RNA Pol III transcription and published data have demonstrated that it is not silenced in human CD34+ cells [350, 351]. The commercially available vector carrying an ATG7-targeting hairpin, encodes as selection marker the resistance gene to puromycin. In order to avoid selecting infected primary CD34+ cells for 6 days in the presence of the antibiotic, it was decided to clone the control and ATG7-targeting hairpins from the pLKO.1-PURO backbone to a pLKO.1-GFP backbone where the puromycin resistance gene was replaced by the one encoding for GFP. At the end of the cloning procedure (described at §2.2.9), two plasmids were generated; the control pLKO-GFP-shCtrl, carrying the shCtrl non-targeting hairpin, and the pLKO.1-GFP-shATG7_E, which carried the shATG7_E hairpin against the ATG7 mRNA. The functionality of the shATG7_E hairpin has been validated by the company and a series of publications, and is well described in the literature [309, 310, 352-354].

In order to test the efficacy of the vector and the shATG7_E hairpin, CD34+ cells from two CP CML patients and one CB sample were incubated with freshly produced, filtered, virus-containing medium, as described in §2.2.8.1.2. Transduction was performed in the presence of Transdux™ every 12h for a total of 36h accompanied by spinoculation. Cells were sorted 48h after the last transduction round based on GFP expression, and knock-down efficiency was measured in whole cell lysates by western blot analysis for ATG7.

Figure 4-8A demonstrates that ATG7 protein levels were significantly reduced ($\geq 60\%$) in shATG7_E CD34+ cells ($p=0.002$) compared to shCtrl. LC3-II levels were also measured in order to assess the effect of 60% ATG7 knock-down on the autophagic activity. As shown in Figure 4-8B, LC3 lipidation was inhibited at approximately 20% in the shATG7_E CD34+ cells compared to the shCtrl.

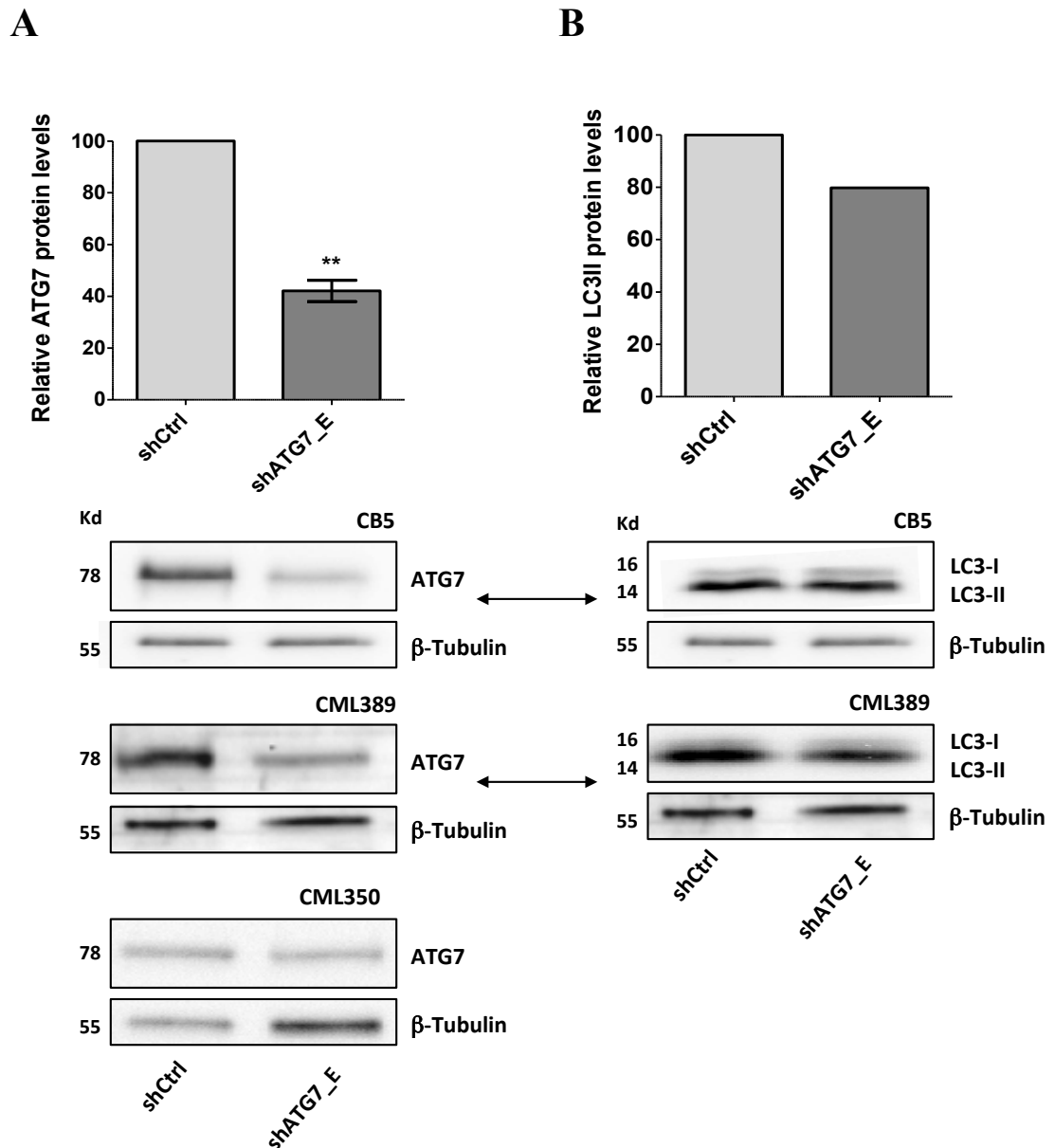


Figure 4-8: Measurement of ATG7 and LC3-II protein levels in CD34+ primitive cells that stably express an ATG7-targeting hairpin carried by the pLKO.1 vector

Western blotting was used for the analysis of ATG7 (A) and LC3-II (B) protein levels in CD34+ cells transduced with shCtrl or shATG7_E pLKO.1 vector via lentiviral delivery. Densitometry calculations for western blot data shown were performed by using the Quantity One software (verifying for non-saturation and subtracting background). The graphs represent the relative ATG7 and LC3-II levels (normalised to β -tubulin loading levels) compared to the shCtrl. Samples CB5 and CML389 refer to the same immunoblot. Graph values represent protein mean \pm SEM with n=3 for (A) and mean for n=2 for (B). Statistical analysis was performed by paired Student's t-test. (**; p \leq 0.01).

4.2 Investigation of ATG7 knock-down in combination with TKIs on CP CML CD34+ cells

Having established stable and efficient knock-down of ATG7 in CP CML CD34+ cells, the efficacy of IM, NIL, DAS and PON was investigated in an autophagy suppressed background. Colleagues' experiments within our laboratory have demonstrated that NIL induces autophagy upon inhibition of BCR-ABL. Hence, this second generation TKI was also included in this series of experiments.

At this point it should also be mentioned that there have been published data supporting that ATG7 and autophagy are necessary for the maintenance of stemness in a mouse model [355]. Therefore, the inclusion of Ph- cells (derived from non-CML donors or CB samples) was necessary in order to investigate how autophagy inhibition, alone or in combination with TKIs, affects the fate of a normal stem cell.

Ph+/Ph- CD34+ cells were transduced with shCtrl or shATG7_E and sorted, as previously described. Since the sorting procedure can be considered as a stress factor, the cells were left to recover in culture overnight and treatment initiation took place the following day (6-7 days post-thaw).

4.2.1 Analysis of CP CML CD34+ cell proliferation following ATG7 knock-down and TKI treatment

shCtrl and shATG7_E transduced cells were treated with 2 μ M NIL, 150nM DAS, 100nM PON or left untreated, and the population size was measured by cell counts 3 and 6 days later. Cell viability was assessed by the trypan blue exclusion method.

As demonstrated in Figure 4-9, cell counts 3 days following treatment initiation revealed that ATG7 knock-down significantly affected the proliferation of shATG7_E CD34+ cells ($p=0.008$ compared to shCtrl). Day 3 or 6 drug treatments, in the presence or absence of ATG7 knock-down, did not inhibit cell proliferation at statistically significant levels. Nevertheless, ATG7 knock-down (i) enhanced the cytotoxicity of NIL, DAS and PON after 3 days of treatment, and (ii) increased the antiproliferative effect of all TKIs after 6 days of treatment. Among the three drugs tested, PON was the most efficient TKI in suppressing the proliferation of CD34+ CML cells, and its effects were further enhanced upon ATG7 knock-down.

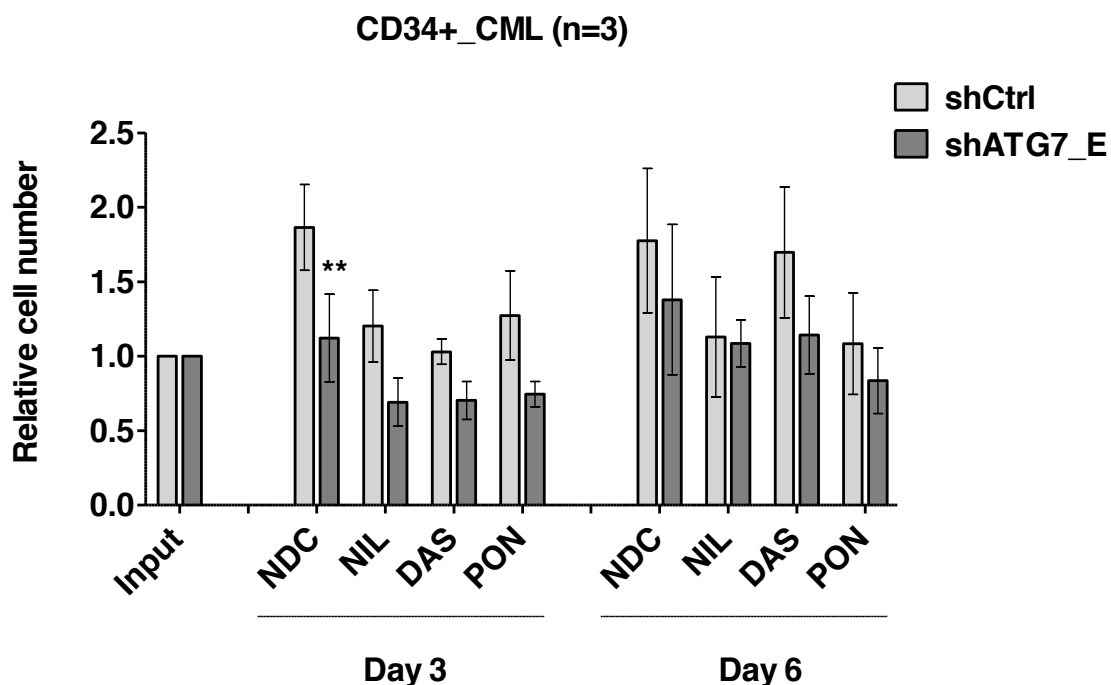


Figure 4-9: Comparison of NIL, DAS and PON treatments in combination with ATG7 knock-down in CP CML CD34+ cells

CP CML CD34+ cells stably expressing an ATG7-targeting (shATG7_E) or a mock hairpin (shCtrl) were treated with 2 μ M NIL, 150nM DAS, 100nM PON or NDC. Cell counts were performed at days 3 and 6 following treatment initiation and viability was determined by using the trypan blue exclusion method. The number of viable cells in each treatment was compared to the input and the relative numbers are presented as mean \pm SEM (n=3). Statistical analysis was performed by using paired t-test. Annotation above a bar refers to statistical significance between the bar and the NDC. (**; p \leq 0.001).

4.2.2 Analysis of CP CML CD34+ cell apoptosis following ATG7 knock-down and TKI treatment

In order to further characterise the effect of ATG7 knock-down in the presence of different TKIs, the apoptosis of CP CML CD34+ cells (n=3) was measured. Transduced shCtrl and shATG7_E cells were cultured post-sort in SFM+PGFs in the presence of 2 μ M NIL, 150nM DAS, 100nM PON or NDC. 6 days following treatment initiation, the cells were analysed by FACS after annexin V/Viaprobe staining for the evaluation of apoptotic cells (early and late).

Figure 4-10 demonstrates that ATG7 knock-down moderately affected the survival of CP CML CD34+ cells; apoptosis levels within the shATG7_E NDC cells were similar to the ones observed in the shCtrl upon TKI treatment.

Nevertheless, apoptosis within the TKI-treated cells was not augmented upon ATG7 knock-down. It should be mentioned that these results refer solely to the induction of apoptosis (early and late) upon TKI treatment of shATG7 knock-down CML CD34+ cells. Hence, these data do not exclude the possibility of induction of non-apoptotic forms of death, such as necrosis.

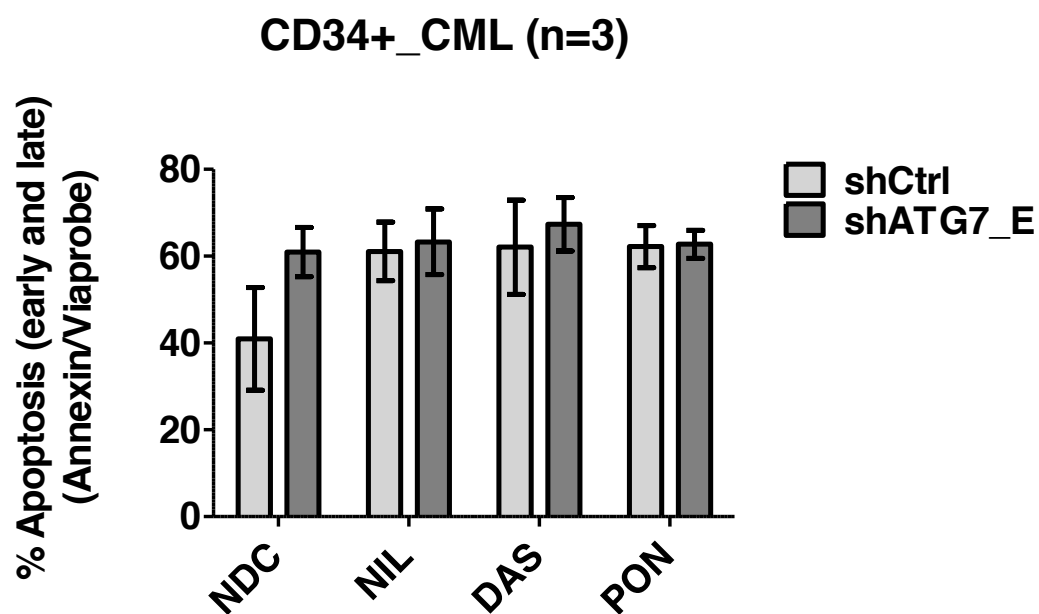


Figure 4-10: Analysis of TKI-induced apoptosis in the presence of ATG7 knock-down in CP CML CD34+ cells

CP CML CD34+ cells were treated for 6 days with 2 μ M NIL, 150nM DAS, 100nM PON or NDC. Apoptosis (early and late) was measured by FACS after annexinV/Viaprobe staining. Graph represents apoptosis relative to NDC and numbers are presented as mean \pm SEM (n=3).

4.2.3 Analysis of CML committed progenitor cell potential and differentiation following ATG7 knock-down and TKI treatment

4.2.3.1 Analysis of CML committed progenitor cell potential following ATG7 knock-down and short exposure TKIs

The CFC assay is a rigorous method used for determining the clonogenic ability and the differentiation capacity of CD34⁺ progenitor cells. In order to investigate how inhibition of autophagy, alone or in combination with TKIs, affects the functionality of CML CD34⁺ cells, shCtrl and shATG7_E-transduced cells were treated *in vitro* for 3 or 6 days in the presence of 2 μ M NIL, 150nM DAS, 100nM PON or NDC. Thereafter, the drugs were washed out and the cells were plated in semi-solid methylcellulose-based medium at low density (2500 cells/1.5mL methylcellulose, in duplicate). The medium was supplemented with GFs, including EPO, SCF, G-CSF, GM-CSF and IL-3, so as to support the proliferation and differentiation of the progenitor cells.

Figure 4-11 demonstrates that in the NDC arm, ATG7 knock-down alone led to >50% reduction in the clonogenic ability of the cells (97 \pm 24.9 colonies) compared to the shCtrl (221.6 \pm 84 colonies), suggesting that basal levels of ATG7 and autophagy play an important role in the clonogenic potential of these cells.

3 day exposure of shCtrl cells to TKIs significantly decreased the number of colonies; 10-fold with DAS (p=0.04), 6-fold with PON (p=0.03), but only 4-fold with NIL (p=0.07). Likewise, TKI-treatment of shATG7_E cells significantly reduced the number of colonies compared to the NDC arm; 5.4-fold with NIL (p=0.01) or PON (p=0.02), and 6.5-fold with DAS (p=0.02). In both shCtrl and shATG7_E arms, DAS was the most potent TKI among the three.

In order to assess if ATG7 knock-down enhanced TKI effect against the clonogenic ability of CD34⁺ cells, comparison was performed between TKI-treated shCtrl and shATG7_E cell. Student's t-test paired analysis revealed that ATG7 knock-down significantly enhanced the effect of NIL (p=0.008) and DAS (p=0.02), but not PON (p=0.21).

Taken together, ATG7 knock-down enhanced the effect of 3 day TKI treatment, reducing the number of progenitor colonies to 8% for NIL (18.6 \pm 8 colonies) and PON (18.3 \pm 5.5 colonies), and 6% for DAS (15.6 \pm 8.7 colonies) compared to the shCtrl NDC arm (221 \pm 84 colonies).

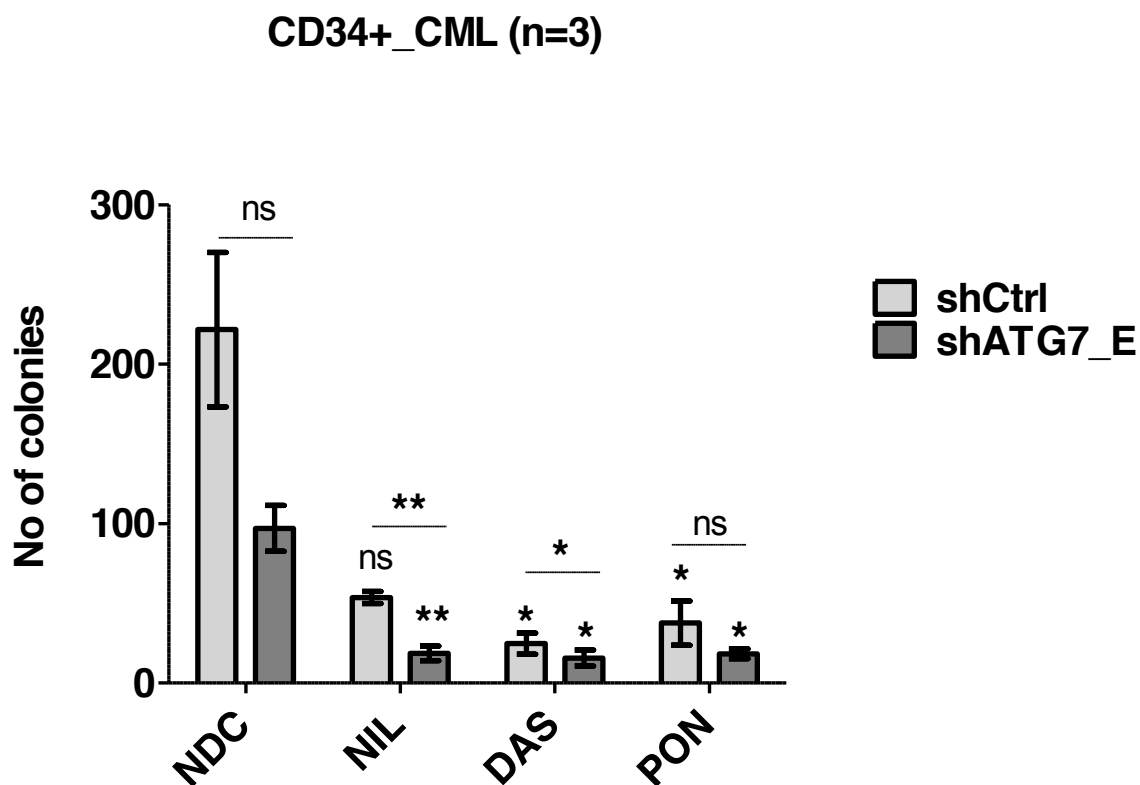


Figure 4-11: ATG7 knock-down-mediated autophagy inhibition enhances 3 day TKI treatment effect against the clonogenic ability of CP CML CD34+ cells

CP CML CD34+ cells were cultured in SFM+PGFs. Cells were treated for 3 days with 2 μ M NIL, 150nM DAS, 100nM PON, or NDC. Drugs were washed out and 2500 cells/arm were transferred to semi-solid medium. Colony counts were performed after 14 days under light microscope. Numbers of colonies are presented as mean \pm SEM (n=3). Statistical analysis was performed by using paired t-test. Annotation above a bar refers to statistical significance between the bar and the NDC. (ns; not significant, *, $p\leq 0.05$, **, $p\leq 0.01$)

CFC assay on cells that had been exposed for 6 days to TKIs, in the presence or absence of ATG7 knock-down, further supported these observations.

Figure 4-12 demonstrates that the effect of all TKIs tested was enhanced in the presence of ATG7 knock-down. In the shCtrl cells, NIL (44 ± 11.7 colonies; $p=0.01$) and DAS (26.3 ± 5.1 colonies; $p=0.01$) suppressed the colony forming ability of the cells upon inhibition of BCR-ABL compared to the NDC (453 ± 93.5 colonies). Treatment with PON followed the same trend (48.5 ± 14.8 , $n=2$).

The ability of shATG7_E cells to form colonies was significantly disrupted in comparison to shCtrl cells within the NDC arm; the colony-forming potential of the cells was reduced approximately 50% (229 ± 31.7 colonies in the shATG7_E arm versus 453 ± 93.5 colonies in the shCtrl arm; $p=0.02$), highlighting the importance of basal ATG7 and autophagy levels for this cellular function.

Likewise, proliferation of the TKI-treated shATG7_E cells was suppressed compared to the NDC (22.6 ± 4 colonies for NIL, $p=0.05$; 9.3 ± 1.5 colonies for DAS, $p=0.006$). Most importantly, it was illustrated that inhibition of autophagy in the shATG7_E arm augmented the clonogenic inhibitory efficacy of all TKIs compared to their shCtrl counterparts (DAS, $p=0.01$; NIL, $p=0.05$). Most importantly, ATG7 knock-down in combination with NIL or DAS, reduced the number of progenitor colonies to 4% and 2% respectively, compared to the shCtrl NDC. This means that the majority of CP CML progenitors (96-98%) was successfully targeted by the TKI/ATG7 knock-down combination. DAS, was again more potent than NIL and PON in suppressing the clonogenicity of CP CML CD34+ cells, in the absence or presence of ATG7 knock-down. Based on these experiments, we report that inhibition of basal autophagy as a single approach significantly affects the functionality of the CML progenitor cells. Furthermore, we demonstrate that autophagy inhibition augments the efficacy of TKIs in reducing the colony forming ability of CD34+ cells from CP CML patients.

Nevertheless, some progenitors managed to survive both ATG7 knock-down and TKI treatment and formed colonies (4% with NIL and 2% with DAS). In order to investigate if prolonged exposure to TKIs would eradicate these cells, the experiment described at §4.2.3.2 was designed.

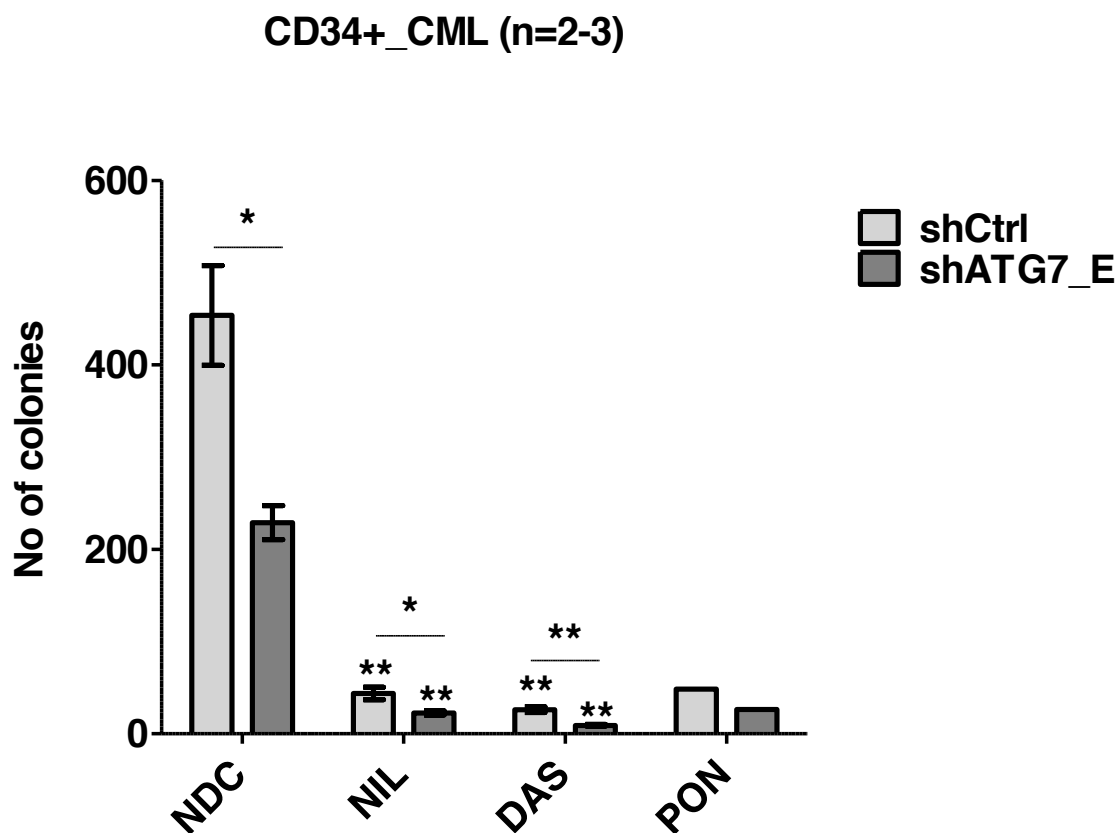


Figure 4-12: ATG7 knock-down-mediated autophagy inhibition enhances 6 day TKI treatment effect against the clonogenic ability of CP CML CD34+ cells

CP CML CD34+ cells were cultured in SFM+PGFs. Cells were treated for 6 days with 2 μ M NIL, 150nM DAS, 100nM PON (n=2), or NDC. Drugs were washed out and 2500 cells/arm were transferred to semi-solid medium. Colony counts were performed after 14 days under light microscope. Numbers of colonies for NIL and DAS are presented as mean \pm SEM (n=3) and for PON mean of n=2. Statistical analysis was performed by using paired t-test. Annotation above a bar refers to statistical significance between the bar and the NDC. (*; p \leq 0.05, **; p \leq 0.01)

CD34⁺CD38⁻ cells from a CP CML CD34⁺ patient sample were isolated following the protocol described at §2.2.2.1. The cells were transduced with shCtrl or shATG7_E virus, isolated by sorting, and their functionality was investigated in a CFC assay. Cells from both arms were plated in semi-solid methylcellulose-based medium at low density (2500 cells/1.5mL methylcellulose, in duplicate).

Figure 4-13A demonstrates that suppression of basal ATG7 levels had a detrimental effect on the clonogenicity of CD34⁺CD38⁻ shATG7_E cells; they completely failed to proliferate and form colonies.

In order to further investigate why CD34⁺CD38⁻ cells are completely ablated upon ATG7 knock-down contrast to CD34⁺CD38⁺ cells, we performed LTC-IC assays on shCtrl and shATG7_E-transduced CP CML CD34⁺ cells. Nevertheless, due to technical problems, the cells failed to give colonies at the end of the assay (in both control and ATG7 knock-down). Future studies should focus on the evaluation of ATG7 knock-down effects on the most primitive population of stem cells, either by LTC-IC or serial replating assays.

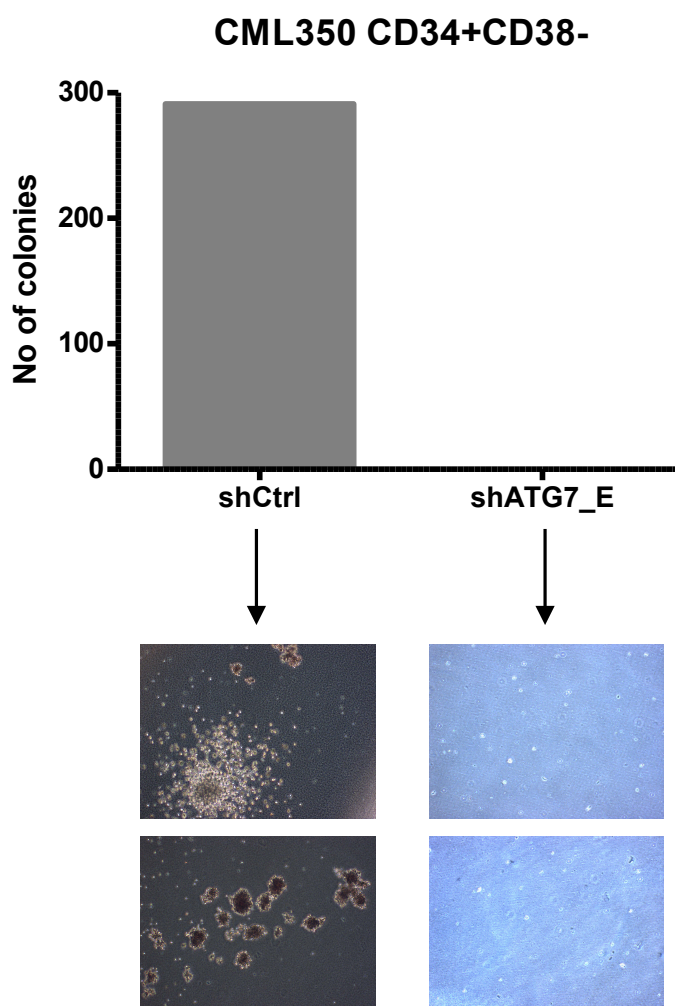


Figure 4-13: Ablation of the clonogenic ability of CD34+CD38- cells from a CP CML patient upon ATG7 knock-down

shCtrl and shATG7_E transduced CP CML CD34+CD38- cells were transferred to semi-solid medium (2500 cells/1.5mL medium). Colony counts were performed after 14 days under light microscope. Photos from representative colonies are included.

4.2.3.2 Analysis of CML committed progenitor cell potential and differentiation following ATG7 knock-down and prolonged exposure to TKIs

In order to evaluate how CML progenitors respond under prolonged exposure to TKIs in the presence of ATG7 knock-down, shCtrl and shATG7_E CP CML CD34+ cells were plated in methycellulose (2500 cells/1.5mL methycellulose, in duplicate) in the presence of 2 μ M NIL, 150nM DAS, 100nM PON or NDC.

Data presented in Figure 4-14 further verify the pivotal role of basal autophagy in the survival of CML progenitors, with shATG7_E cells forming 64% less colonies compared to the shCtrl in the NDC arm (164 \pm 110 colonies for shATG7_E versus 452.7 \pm 122.6 colonies for shCtrl; p=0.002, n=4). It should be highlighted that ATG7 knock-down in the shATG7_E NDC cells gave approximately the same number of colonies compared to the NIL-treated arm of the shCtrl cells (181 \pm 65.8 colonies). Hence, with regards to the colony forming capacity of CP CML CD34+ cells, inhibition of autophagy appeared to have the same effect as TKI-mediated specific targeting of BCR-ABL.

The number of shCtrl colonies was reduced in all TKI-treated arms compared to NDC to 40% with NIL (p=0.04), 16.5% with DAS (p=0.007), and 26.5% with PON (p=0.008). Likewise, the number of shATG7_E colonies was reduced upon TKI treatment; 49% with NIL (p=0.018), 25.6% with DAS (p=0.002) and 30% with PON (p=0.003), compared to the NDC.

Most importantly, the efficacy of TKIs was potentiated in the presence of ATG7 knock-down; NIL (p=0.017), DAS (p=0.009) and PON (p=0.012) reduced the number of colonies to 18%, 9% and 11%, respectively, compared to the shCtrl NDC, suggesting that the TKI/ATG7 knock-down combination eradicated the majority (82-91%) of the CML progenitors.

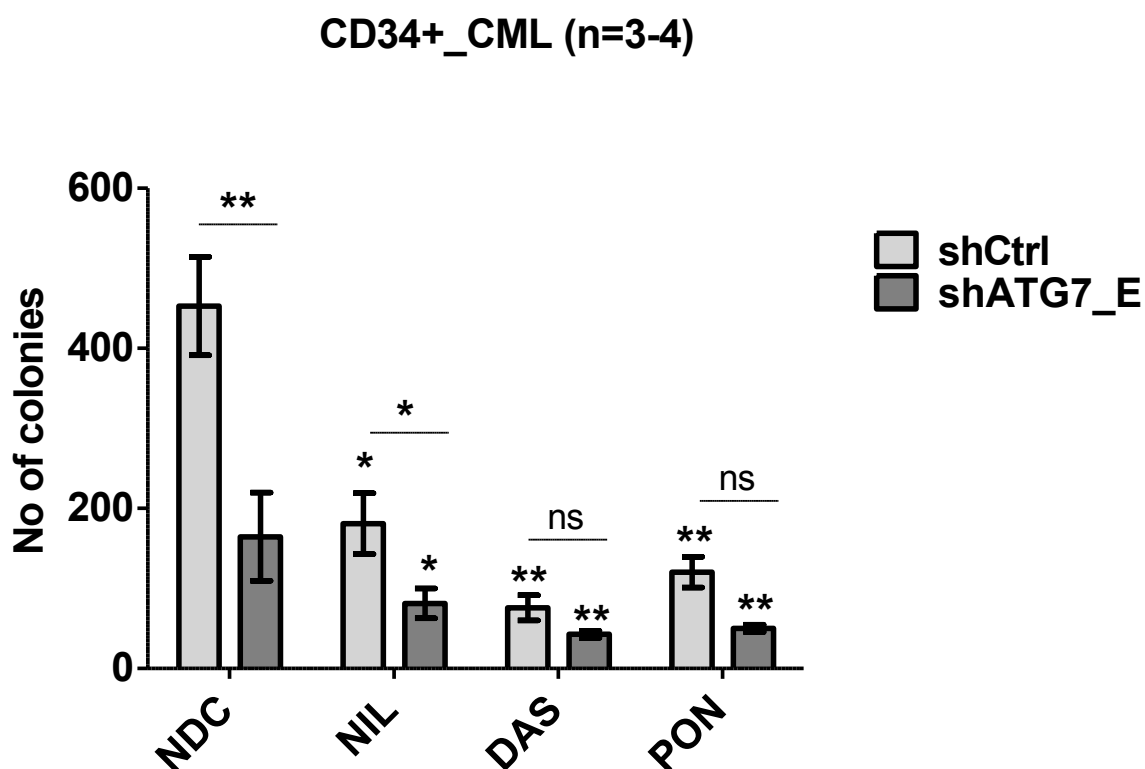


Figure 4-14: ATG7 knock-down-mediated autophagy inhibition enhances prolonged TKI treatment effect against the clonogenic ability of CP CML CD34+ cells

shCtrl and shATG7_E transduced CP CML CD34+ cells were transferred to semi-solid medium containing 2 μ M NIL, 150nM DAS, 100nM PON, or NDC (n=4 for NDC and n=3 for TKI treatments). Colony counts were performed after 14 days under light microscope. Numbers of colonies presented as mean \pm SEM. Statistical analysis was performed by using paired t-test. Annotation above a bar refers to statistical significance between the bar and the NDC. (ns; not significant, *, p \leq 0.05, **, p \leq 0.01)

Furthermore, the potential of the progenitor cells to differentiate into different colonies was assessed morphologically and the cells of origin were classified based on the cellular composition and the size of each colony (Figure 4-15A).

As demonstrated in Figure 4-15B, ATG7 knock-down was associated with suppression of erythroid colony formation; burst forming unit-erythroid (BFU-E) and colony-forming unit erythroid (CFU-E). shATG7_E cells produced significantly lower BFU-E/CFU-E colonies compared to the shCtrl under NDC conditions ($8.8\pm 4\%$ versus $35.8\pm 7.8\%$, $p=0.008$) and DAS treatment ($8.7\pm 5.8\%$ versus $32.9\pm 4\%$, $p=0.05$), while a non-statistically significant decrease was observed under NIL treatment ($8.6\pm 2\%$ versus $29.6\pm 12.5\%$, $p=0.08$) or PON treatment ($18.4\pm 4.9\%$ versus 27.6 ± 11.7 , $p=0.4$). It should be also mentioned that in all cases, the colonies formed in the shATG7_E arm were morphologically similar to the ones in the shCtrl arm by means of size and cell number.

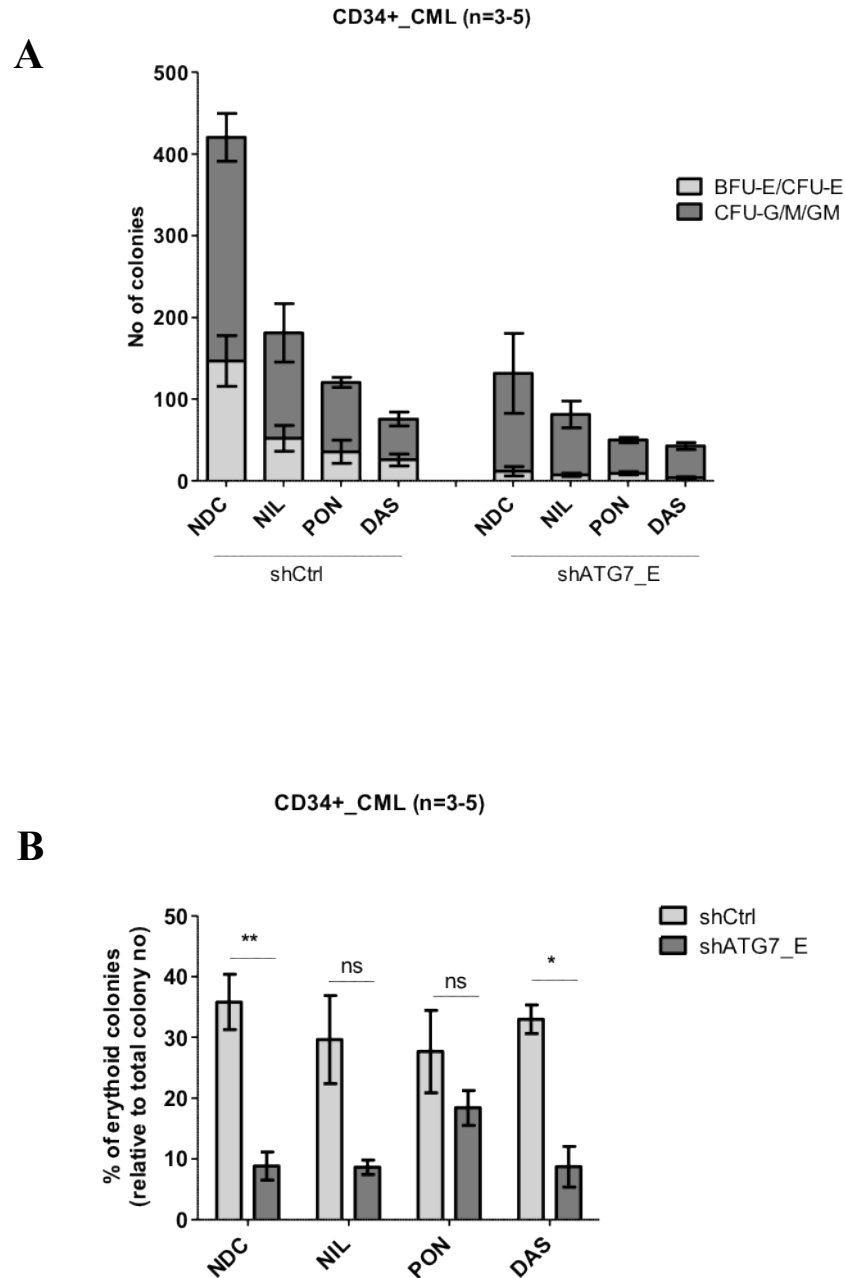


Figure 4-15: ATG7 knock-down-mediated autophagy inhibition is associated with reduced erythroid colony-formation potential in CP CML CD34+ cells

shCtrl and shATG7_E transduced CP CML CD34+ cells were transferred to semi-solid medium containing 2 μ M NIL, 150nM DAS, 100nM PON, or NDC (n=5 for NDC and n=3 for TKI treatments). Colony counts were performed after 14 days and classification was carried out based on morphology under light microscope. Total colony numbers (A) and % relative number of erythroid colonies (compared to total number of colonies) (B) are presented. Graphs present number of colonies as mean \pm SEM. Statistical analysis was performed by using paired t-test. (ns; not significant, *, p \leq 0.05, **, p \leq 0.01)

Cells from 3-5 colonies were pooled from the shCtrl and shATG7_E NDC arms of the CML389 sample so as to investigate if the U6 promoter was still active in these cells, ensuring the transcription of the shRNA hairpins and the GFP protein. The pooled cells were analysed by FACS for the expression of GFP.

As shown in Figure 4-16, almost 90% of the shCtrl cells and 95% of the shATG7_E cells were positive for GFP expression, suggesting that both mock and ATG7-targeting hairpins were expressed.

Taken altogether, these results suggest that ATG7 is playing an important role in the survival of CD34+ CML progenitor cells. Furthermore, autophagy appears to have a cytoprotective role in the CML system upon inhibition of BCR-ABL, since ATG7 knock-down enhanced the effects of TKIs. Finally, ATG7 and/or autophagy appear to take part in the differentiation decisions of CD34+ progenitors, as illustrated by reduced number of erythroid colonies in the shATG7_E cells, in the absence or presence of TKIs.

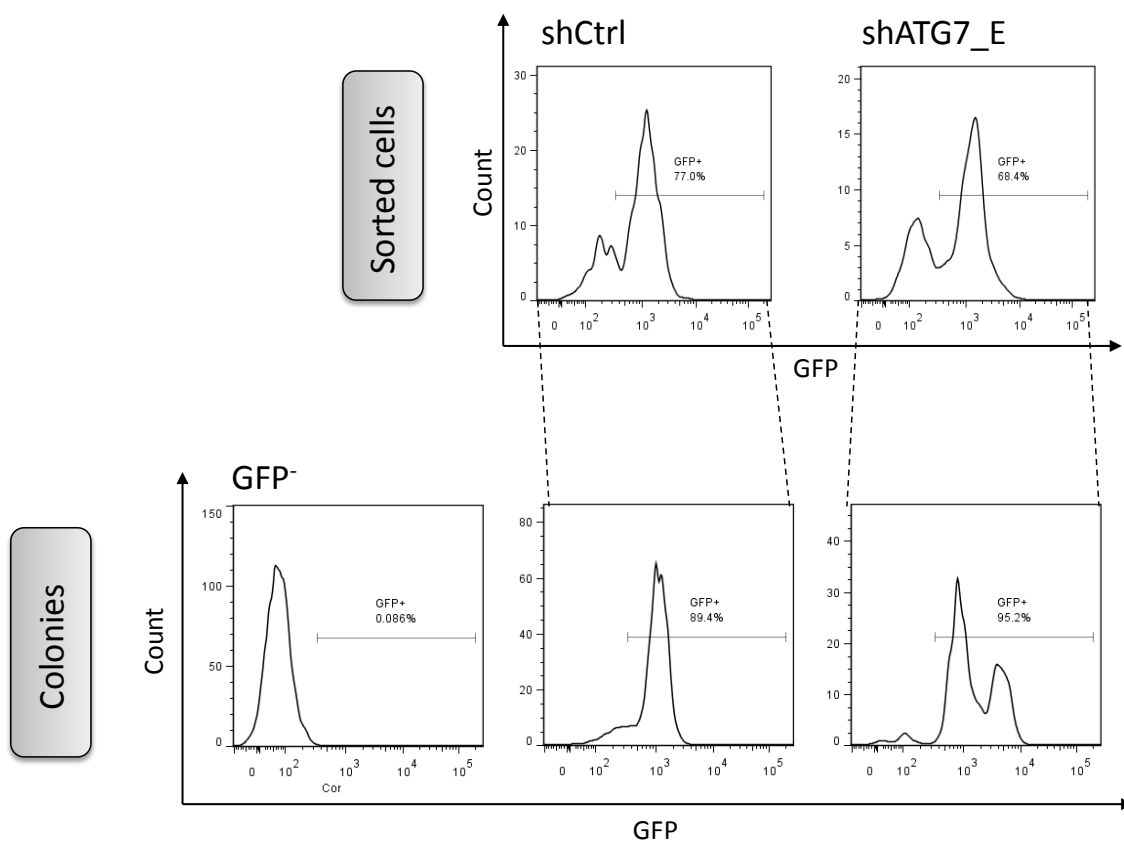


Figure 4-16: Assessment of GFP expression in cells from CML CD34+ progenitor colonies surviving ATG7 knock-down

CD34⁺ cells from a CML patient were lentivirally transduced with a pLKO.1-GFP vector, carrying either a mock (shCtrl) or an ATG7-targeting hairpin (shATG7_E). GFP⁺ cells were sorted in order to obtain homogenous populations of transduced cells (GFP expression profile presented at the top). Following, the committed progenitor cell potential of these populations was tested; shCtrl and shATG7_E cells were transferred to semi-solid medium and colony counts were performed after 14 days under light microscope. GFP expression analysis on pooled cells from 3-5 shCtrl or shATG7_E colonies was performed by FACS. Cells from a colony of the initial CD34⁺ non-infected population were used as GFP⁻ control.

4.3 Investigation of ATG7 knock-down in combination with TKIs on Ph- CD34+ cells

Published studies have underlined the indispensable role of autophagy in the maintenance of stemness [356]. Hence, it was within the aims of this project to evaluate the effect of ATG7 knock-down in a non-BCR-ABL haemopoietic progenitor background and evaluate if targeted autophagy inhibition, in the presence or absence of TKIs, affects normal progenitors.

non-CML CD34+ and CB cells were thawed and cultured overnight in SFM+5GFs and SFM+PGFs, respectively. Thereafter, the cells were transduced with virus carrying a shCtrl or an ATG7-targeting hairpin, as described in §2.2.8.1.2. Transduced cells were sorted based on the expression of GFP, and 24h later TKI treatment was initiated.

4.3.1 Analysis of Ph- CD34+ cell proliferation following ATG7 knock-down and TKI treatment

shCtrl and shATG7_E transduced cells were treated with 2 μ M NIL, 150nM DAS, 100nM PON or NDC, and the population size was measured by cell counts 3 days later. Cell viability was assessed by trypan blue exclusion method.

As demonstrated in Figure 4-17, day 3 cell counts revealed that ATG7 knock-down alone did not suppress the proliferation of the cells ($p=0.21$ shATG7_E versus shCtrl in the NDC arm). Moreover, TKIs, in the presence or absence of ATG7 knock-down, did not inhibit proliferation of the cells.

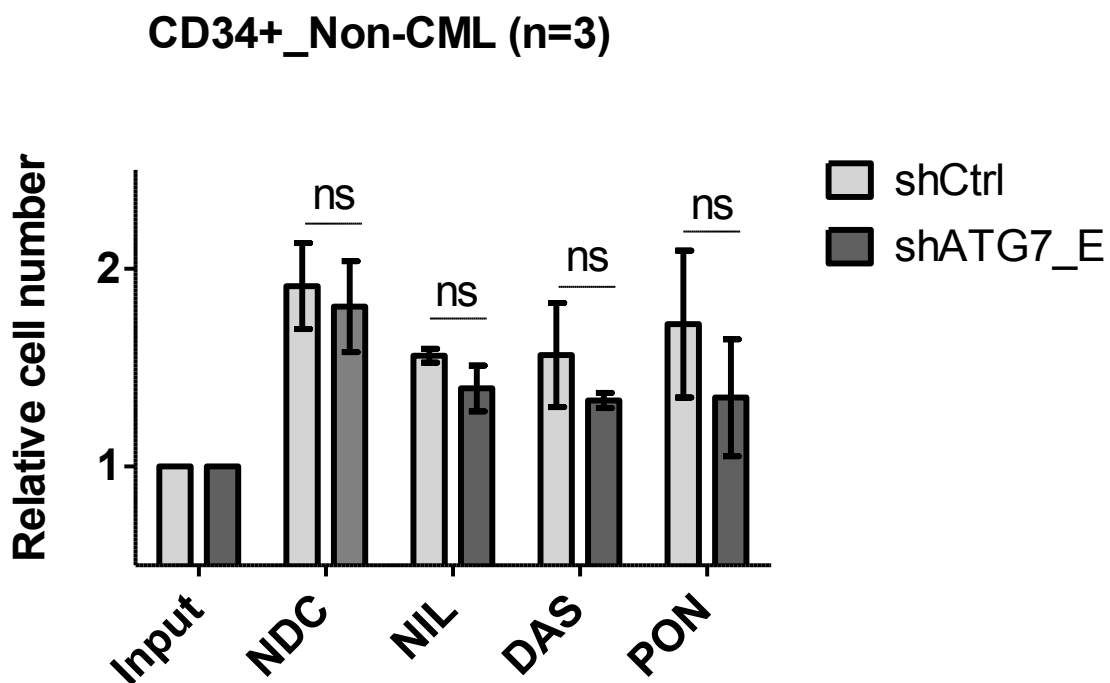


Figure 4-17: Comparison of NIL, DAS and PON treatments in combination with ATG7 knock-down in Ph- CD34+ cells

CD34+ progenitor cells from 2 non-CML donors and a CB sample, stably expressing an ATG7-targeting (shATG7_E) or a mock hairpin (shCtrl) were treated with 2 μ M NIL, 150nM DAS, 100nM PON or NDC. Cell counts were performed 3 days following treatment initiation and viability was determined by using the trypan blue exclusion method. The number of viable cells in each treatment was compared to the input and the relative numbers are presented as mean \pm SEM (n=3). Statistical analysis was performed by using paired t-test. (ns; not significant)

4.3.2 Analysis of Ph- CD34+ cell apoptosis following ATG7 knock-down and TKI treatment

In order to further characterise the effect of ATG7 knock-down in the presence of different TKIs in Ph- CD34+ cells, apoptosis was measured in non-CML and CB CD34+ cells.

Transduced shCtrl and shATG7_E cells were cultured post-sort in SFM+5GFs (for the non-CML samples) or SFM+PGFs (for the CB sample) in the presence of 2 μ M NIL, 150nM DAS, 100nM PON or NDC. 6 days following treatment initiation, the cells were analysed by FACS after annexin V/7-AAD staining for the evaluation of apoptotic cells (early and late).

Figure 4-18 illustrates that the survival of Ph- CD34+ samples was not affected by ATG7 knock-down, as suggested by similar levels of apoptosis between the shCtrl and shATG7_E within the NDC arm. Furthermore, TKIs did not promote apoptosis in the Ph- CD34+ cells, with or without inhibition of ATG7.

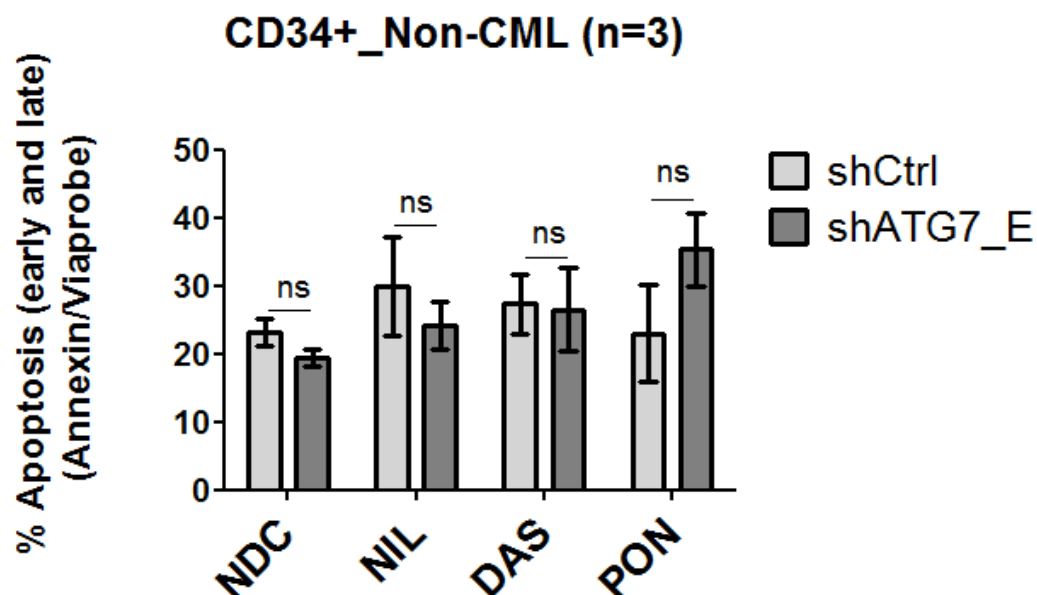


Figure 4-18: Analysis of TKI-induced apoptosis in the presence of ATG7 knock-down in Ph-CD34+ cells

Transduced shCtrl and shATG7_E CD34+ cells from two non-CML donors and a CB sample were treated for 6 days with 2 μ M NIL, 150nM DAS, 100nM PON or NDC. Apoptosis (early and late) was measured by FACS after annexinV/Viaprobe staining. Graph represents apoptosis relative to NDC and numbers are presented as mean \pm SEM (n=3). Statistical analysis was performed by using paired t-test.

4.3.3 Analysis of Ph- committed progenitor cell potential following ATG7 knock-down and exposure to TKIs

In order to investigate how Ph- CD34⁺ cells respond under prolonged exposure to TKIs in the presence of ATG7 knock-down, two non-CML and one CB CD34⁺ samples were transduced with virus carrying either the shCtrl or the shATG7_E hairpin, as described in §2.2.8.1.2. Transduced cells were sorted and plated in methycellulose (2500 cells/1.5mL methycellulose, in duplicate), in the presence of 2µM NIL, 150nM DAS, 100nM PON or NDC.

Data presented in Figure 4-19 demonstrate that knock-down of ATG7 did not affect the clonogenic ability of Ph- CD34⁺ cells ($p=0.93$ in the NDC arm). Furthermore, treatment with NIL, PON or DAS did not suppress the colony forming ability cells alone ($p=0.2$, $p=0.13$, $p=0.44$, respectively) or in combination with ATG7 knockdown ($p=0.1$, $p=0.12$, $p=0.43$, respectively).

Overall, specific inhibition of autophagy via ATG7 knock-down did not affect the functionality of Ph- CD34⁺ stem/progenitor cells, in the absence or presence of TKI treatment.

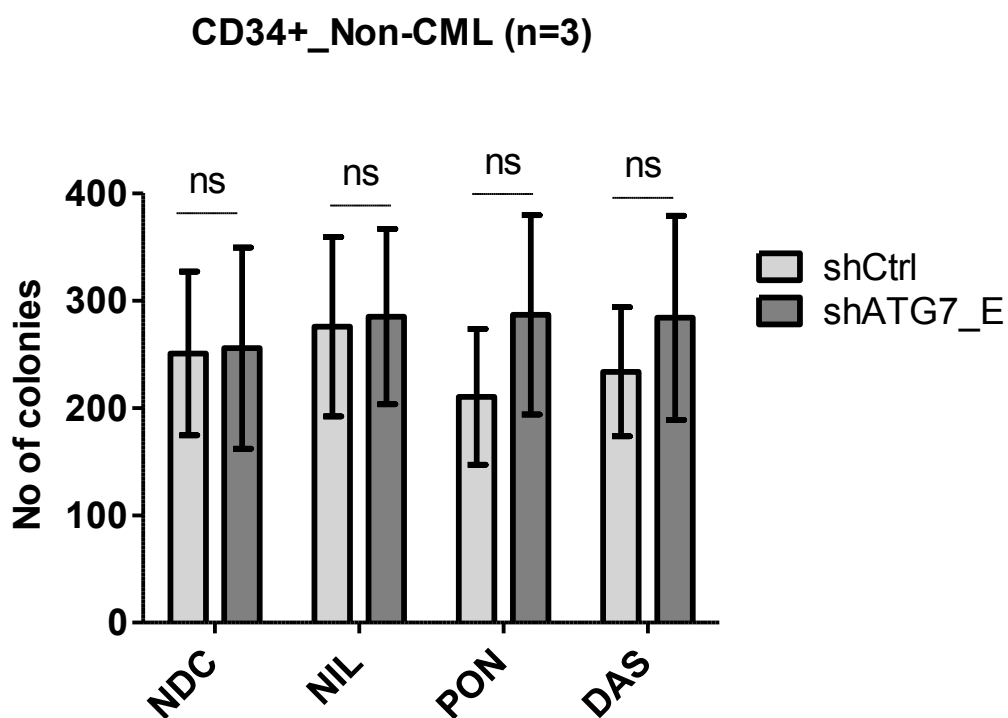


Figure 4-19: ATG7 knock-down-mediated autophagy inhibition alone or in the presence of TKI treatment does not affect the clonogenic ability of Ph- CD34+ cells

shCtrl and shATG7_E transduced Ph- CD34+ cells were transferred to semi-solid medium containing 2 μ M NIL, 150nM DAS, 100nM PON, or NDC. Colony counts were performed after 14 days under light microscope. Numbers of colonies presented as mean \pm SEM. Statistical analysis was performed by using paired t-test. (ns; not significant)

4.3.4 Transcriptional analysis of key autophagy genes in Ph⁺ and Ph⁻ CD34⁺ cells

Data from experiments presented in this chapter pinpoint the importance of autophagy for the survival of cancer cells under steady state conditions. Cancer cells have been reported to have altered nutritional requirements and increased metabolic needs. This could possibly justify partially the addiction of CML stem/progenitor cells to basal autophagy for survival. Interestingly, our results suggest that inhibition of basal ATG7/autophagy levels specifically targets CML and not Ph⁻ CD34⁺ cells.

Single cell amplification (described at §2.2.5.4), followed by Fluidigm® analysis (described at §2.2.5.9), was utilised in order to investigate if there are transcriptional differences in autophagy under steady-state conditions between CML and non-CML CD34⁺ samples (n=3-5). mRNA expression levels were calibrated towards the house-keeping gene GAPDH, and presented as relative fold-change compared to the non-CML samples (control).

Figure 4-20 demonstrates that under normal conditions, CP CML CD34⁺ cells showed lower transcriptional levels of key autophagy genes ATG12, ATG7, BECLIN, GABARAPL and LC3. More specifically, ATG7 expression was approximately 3.5-fold reduced in CP CML CD34⁺ samples compared to Ph⁻ CD34⁺ cells. Such observations have been further characterised by other members in our lab.

These data, suggesting that CML stem/progenitor cells transcribe ATG7 and other autophagy genes at lower levels, could potentially explain why CML cells are more susceptible to ATG7 knock-down compared to non-CML cells. Reduction of ATG7 mRNA levels by 70% within a Ph⁻ CD34⁺ may not affect basal levels of autophagy; nevertheless, such a decrease could have a detrimental effect on a CML cell that by default has lower basal levels of ATG7 and/or autophagy.

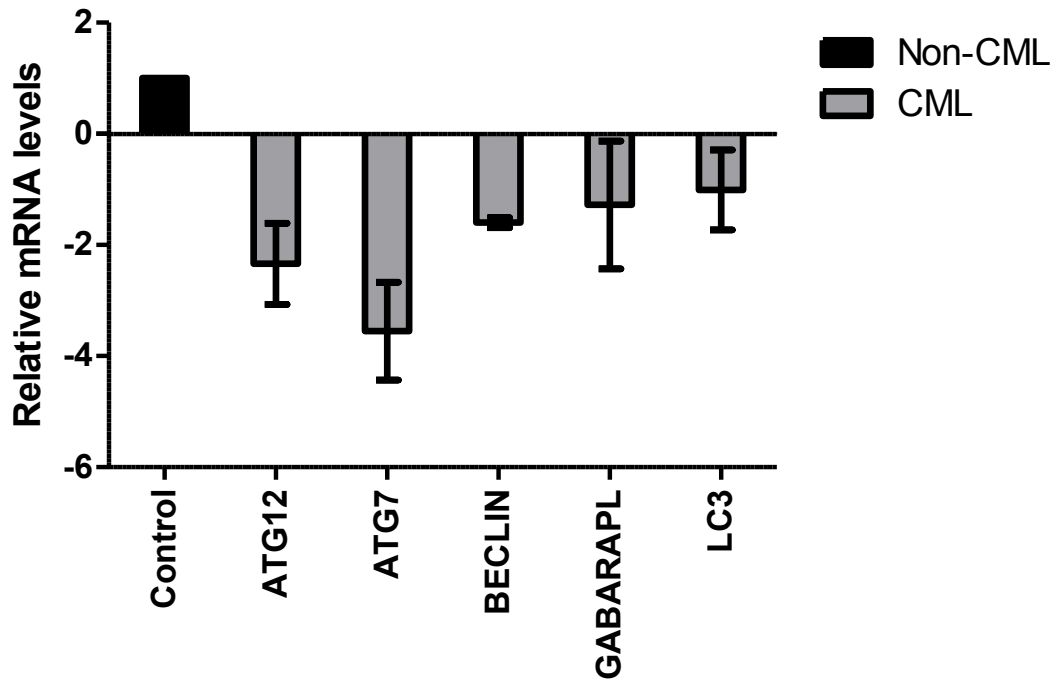


Figure 4-20: Transcriptional analysis of key autophagy genes in Ph⁺ and Ph⁻ CD34⁺ cells
 RNA extracted from CD34⁺ cells of CP CML patients and Ph⁻ donors was analysed by Fluidigm® after PCR amplification (n=3-5). Graph represents mean±SEM relative autophagy genes' mRNA levels in CML samples compared to non-CML samples. GAPDH was used calibrator.

5 Results (III): Investigation of the role of ATG7 and autophagy in the fate decision of leukaemic cells

There is a crosstalk between autophagy and apoptosis, and many scientists view autophagy as a PCD type II. A recent study by Lee and colleagues demonstrated that ATG7 interacts directly with p53 during starvation, inducing p53-dependent apoptosis [287]. ATG5 is another autophagy protein that has been suggested to interplay with apoptosis [288].

Autophagy is also a remodeling mechanism and it has been proposed to take part in mammalian differentiation from the very first stages of development, during the oocyte-to-embryo transition [357]. Recent studies reveal a role for autophagy proteins in the differentiation process of several cell types. For instance, ATG7 has been suggested to be an important component of the adipogenesis process [358], the terminal differentiation of reticulocytes to erythrocytes [359] and the differentiation of macrophages [360]. Additionally, ATG5 has been implicated in the hypoxia-induced osteoclastogenesis [361] and the differentiation of keratinocytes [362].

Autophagy has also been proposed to play a role in the maintenance of the stem cell phenotype; deletion of *Atg7* within the haemopoietic cell compartment in mouse models, lead to stem cell exhaustion, followed by anaemia and lymphopenia [355]. Furthermore, recent studies suggest that autophagy could affect ESCs maintenance and differentiation via regulation of the ATP levels within the cells [356].

In Chapter 4 we demonstrated that autophagy is important for the survival of primary CP CML CD34+ cells and its inhibition enhanced TKI-induced effects. Furthermore, inhibition of ATG7 and autophagy, disrupted partially the erythroid differentiation of the CD34+ progenitors, suggesting that autophagy plays a role in the differentiation of these cells. Therefore, in this chapter, we aimed to investigate the cell fate decisions of immortalised leukaemic cell lines upon ATG7 knock-down, and further characterise the role of autophagy in the survival, proliferation and differentiation of oncogene-transformed cells that carry additional secondary mutations.

5.1 Characterisation of BC CML cells following ATG7 knock-down

The natural history of CML progresses from the CP, which is relatively benign, through AP, to BC. BC is the final and fatal stage of the disease and clinically, presents similar features to acute leukaemia. Progression from CP to BC is associated with genetic instability, disrupted DNA repair, as well as altered proliferation, differentiation, and apoptosis (Figure 5-1).

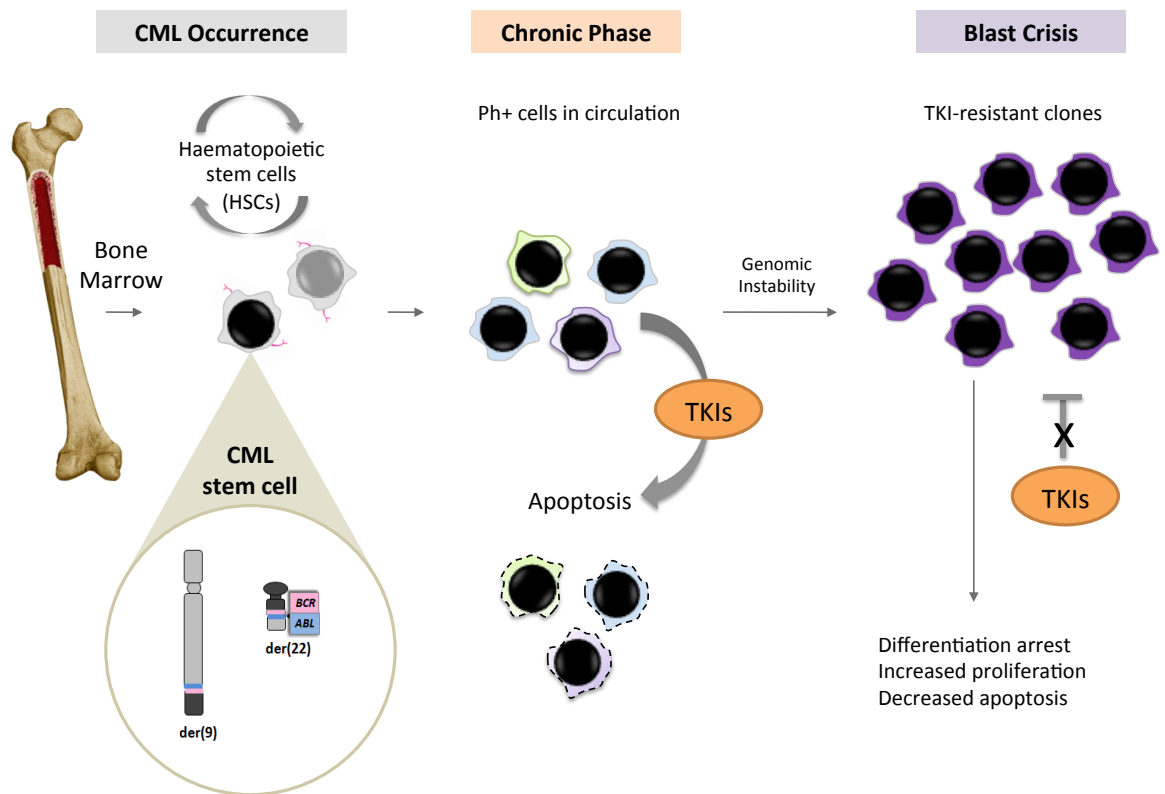


Figure 5-1: CML development and disease progression

Secondary chromosomal abnormalities in BC CML include duplication of the Ph chromosome (38% of the patients), trisomy 8 (38% of the patients), isochromosome 17 (20% of the patients), trisomy 19 (13% of the patients), and other less frequent changes [363]. Furthermore, BC is linked to the development of additional molecular changes; for example, 30% of the myeloid BC cases carry a p53 mutation, while almost half of the lymphoid BC patients have a mutation in p16/ARF.

Unlike CP, where CML progenitor cells present only subtle defects in maturation, BC is characterised by a differentiation arrest. BCR-ABL has been suggested to be the driver of this differentiation blockade via interference with differentiation pathways, including the targeted activation of tissue-specific genes by transcription factors, such as the CEBPa [364], and p53-mediated events.

In order to identify potential roles of autophagy in BC CML cells, the myelomonocytic BC cell line KCL22 and the erythromegakaryocytic BC cell line K562, were used as experimental models.

5.1.1 Assessment of KCL22 viability following ATG7 knock-down

KCL22 myelomonocytic BC cells carry the BCR-ABL1 e13-a2 (b2-a2) isoform, have p53 loss-of-function, and additional cytogenetic which can include [365, 366]:

- a hyperdiploid phenotype with 3.3% polyploidy (- 51(47-51)<2n>X, -X, +1, +6, +8, +8, +14, +22)
- del(1)(p22)
- t(9;22)(q34;q11)
- add(17)(p12-13)
- i(21q)
- der(22)t(9;22)(q34;q11)

KCL22 cells were transduced every 12h with DMEM⁺ virus-containing medium for a total of 36h, as described in §2.2.8.1.2. Transduced cells were sorted 48h after the last transduction round, based on the expression of the GFP marker, and cultured in RPMI⁺.

In order to assess cell viability 4 days post-sort, cells were stained with DAPI and analysed by FACS.

Figure 5-2 demonstrates that the viability of KCL22 cells transduced with the shATG7_E hairpin was severely affected by ATG7 knock-down compared to the shCtrl (p=0.004). Depriving the cells from ATG7 for ~96h had such a severe impact on the cells that 100%

of them died. On the other hand, shCtrl cells' viability was not affected, suggesting that the enhanced cell death in the ATG7 knock-down cells was not attributed to GFP expression or transduction-associated toxicity.

This experiment was repeated for a total of n=5; in all cases, the ATG7 knock-down population died within 4-5 days following sorting, demonstrating the indispensable role of ATG7 and autophagy for the survival of KCL22 cells. Hence, further characterisation was impossible.

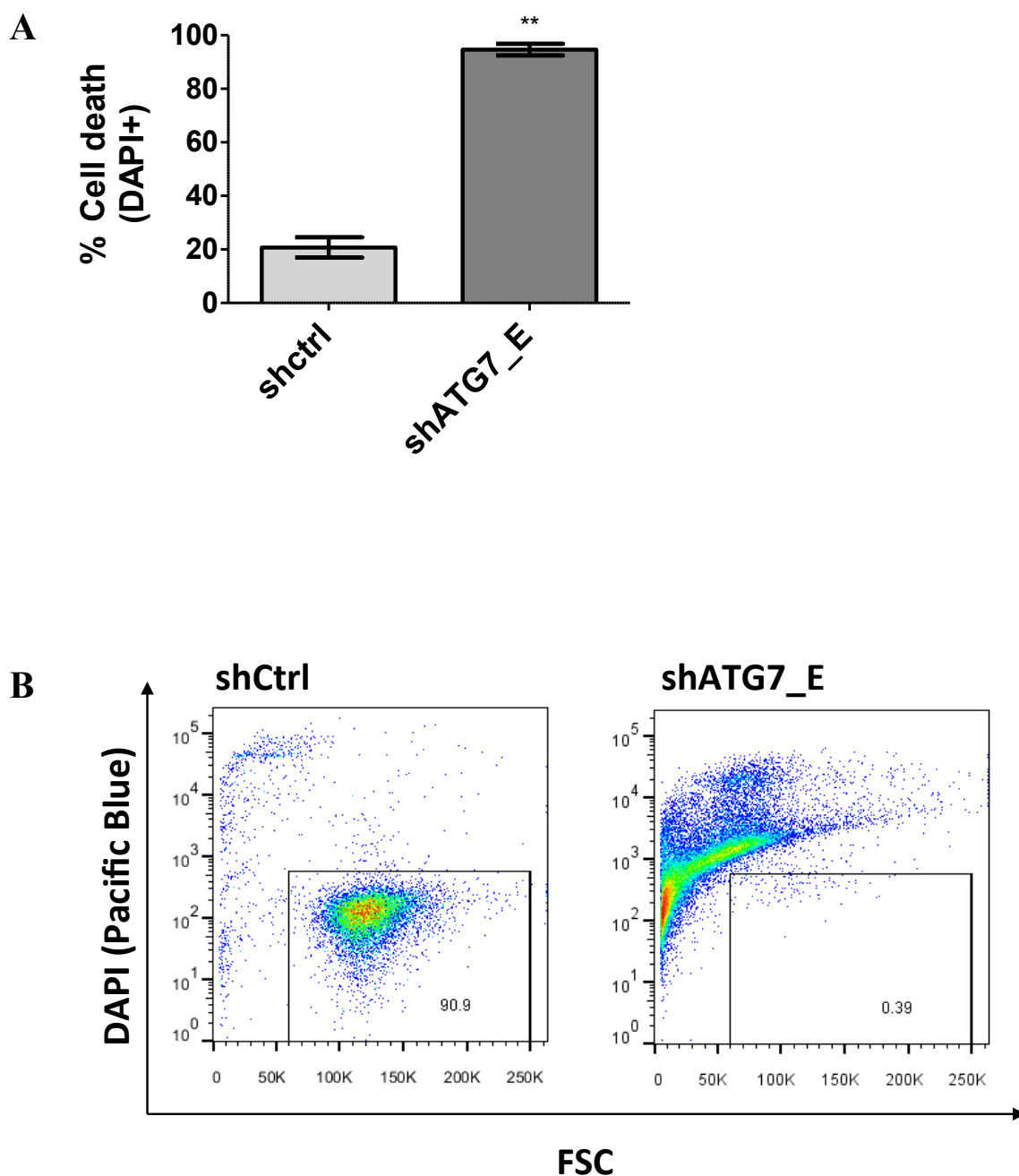


Figure 5-2: Cell death analysis in KCLL22 cells upon ATG7 knock-down

KCLL22 cells were lentivirally transduced with a pLKO.1-GFP vector, carrying either a mock (shCtrl) or an ATG7-targeting hairpin (shATG7_E). GFP⁺ cells were sorted in order to obtain homogenous populations of transduced cells. 96h post-sort, cells were stained with DAPI and cell death was measured by FACS analysis. (A) Graph represents cell death levels as mean \pm SEM (n=3). (B) Representative DAPI/FSC (forward side scatter) plot after FACS analysis of shCtrl and shATG7_E cells; gates depict live cell percentages. Statistical analysis was performed by using paired t-test. (**; p \leq 0.01)

5.1.2 Characterisation of K562 cells following ATG7 knock-down

K562 erythromegakaryocytic BC cells carry the BCR-ABL1 e14-a2 (b3-a2) fusion gene, have a p53 loss-of-function, and additional cytogenetic alterations that may include [367, 368]:

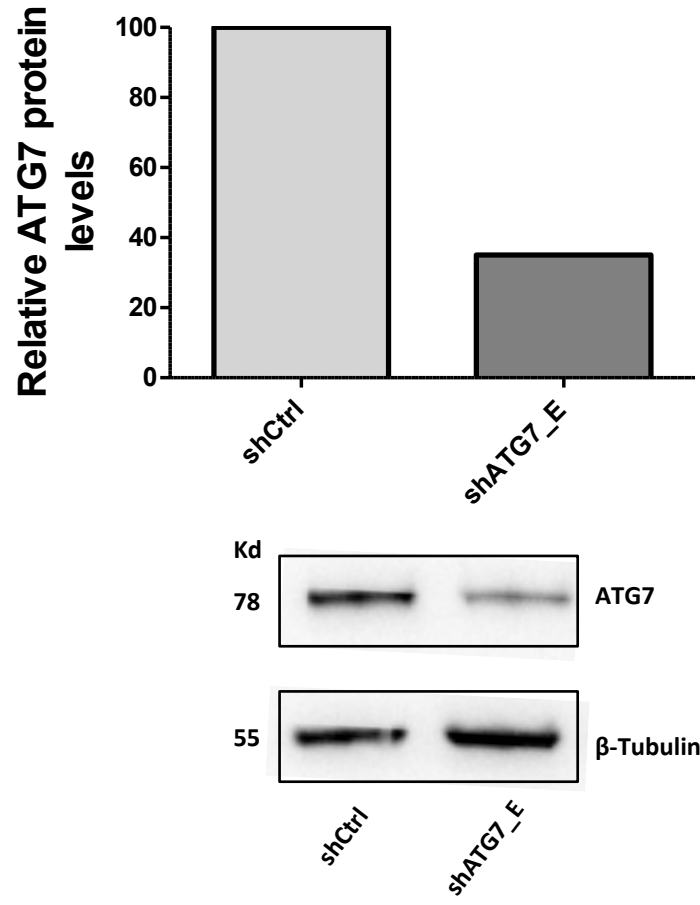
- 61-68<3n>XX
- -X, -3, +7, -13, -18, +3mar
- del(9)(p11/13)
- der(14)t(14;?)(p11;?)
- der(17)t(17;?)(p11/13;?)
- der(?18)t(15;?18)(q21;?q12)
- del(X)(p22)

K562 cells were transduced with shCtrl or shATG7_E, as described in §2.2.8.1.2, and GFP+ cells were sorted 48h after the last transduction round.

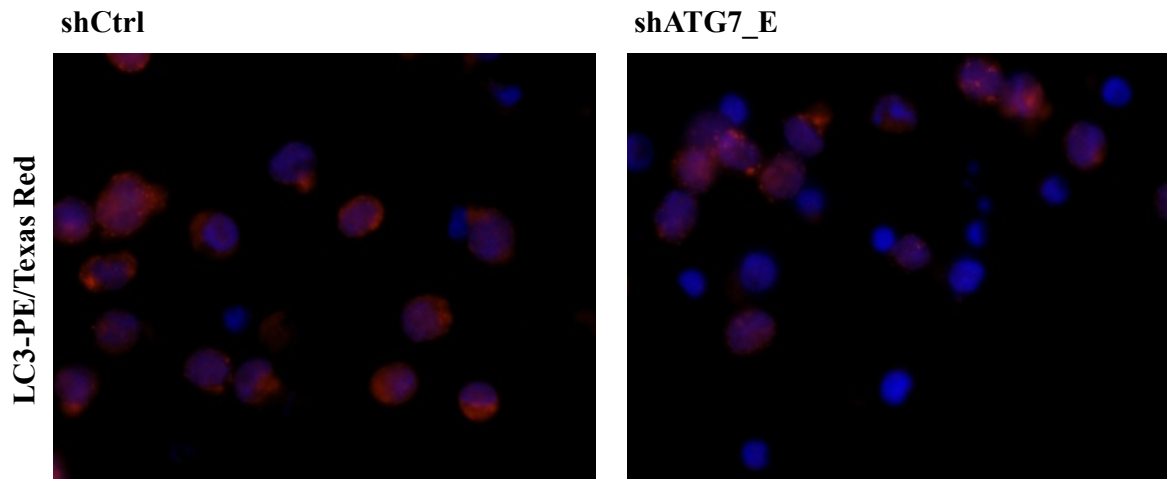
4 days post-sort, lysates from whole cells were prepared for the measurement of ATG7 knock-down. Western blot analysis revealed a $\geq 60\%$ reduction in ATG7 protein levels in the shATG7_E cells (Figure 5-3A).

However, immunofluorescence analysis revealed that the formation of LC3-positive punctae was not completely inhibited, possibly suggesting the presence of residual autophagic activity (Figure 5-3B). Furthermore, accumulation of LC3II was observed 4 weeks following ATG7 knock-down (Figure 5-3C). A potential explanation for this observation could be that the 30-40% of the remaining ATG7 protein is processing partially the lipidation of LC3 but it is not sufficient to allow for the completion of the autophagosome. Hence, incomplete autophagosomes may still form, and since the autophagic process is inhibited, they cannot be degraded and recycled. Hence lipidated LC3II could accumulate within the cells in a time-dependent manner.

A



B



C

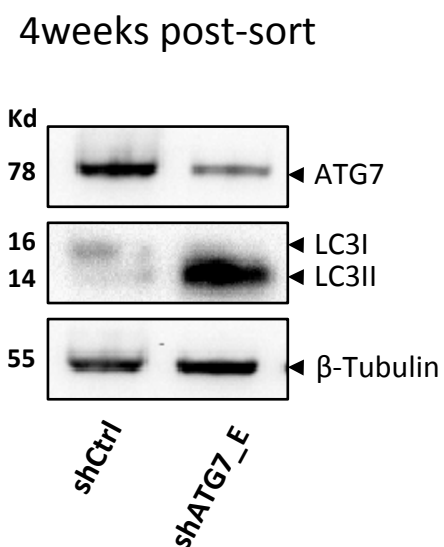


Figure 5-3: ATG7 and LC3 monitoring in K562 cells that stably express an ATG7-targeting hairpin carried by pLKO.1 vector

(A) Western blot was used for the analysis of ATG7 protein levels in shATG7_E-transduced K562 cells. Densitometry calculations for data shown were performed by using the Quantity One software. The graph represents relative ATG7 levels (normalised to β -tubulin) compared to the shCtrl. (B) Immunofluorescence imaging on transduced K562 cells 4 days following sorting. Cells were stained with primary anti-LC3B antibody and secondary PE/Texas Red-fluorochrome conjugated antibody. Captions presented at 200X magnification, DAPI used for nuclei staining. (C) Western blot was used for the analysis of ATG7 and LC3 protein levels in shATG7_E-transduced K562 cells 4 weeks following sorting.

5.1.2.1 Assessment of K562 proliferation and cell viability following ATG7 knock-down

Proliferation of K562 cells transduced with either shCtrl or shATG7_E hairpin was assessed by performing cell counts every 24h following sorting. Cell viability was established by using the trypan blue exclusion method.

Figure 5-4A demonstrates that cells with ATG7 knock-down had a strong anti-proliferative effect on K562 cells and shATG7_E cells presented significantly suppressed proliferation compared to the shCtrl ($p=0.0005$ at 25h, $p=0.03$ at 48h, $p=0.008$ at 72h). Furthermore, it was observed that the number of viable shATG7_E cells was decreased below the number of input cells, suggesting that ATG7 knock-down had a cytotoxic effect.

The anti-proliferative/cytotoxic effect of ATG7 knock-down was further validated by the CellTiter-Glo® luminescence assay that detects metabolically active cells based on quantitation of the ATP present, which is directly proportional to the number of cells present in culture (described at §2.2.1.2.2) (Figure 5-4B).

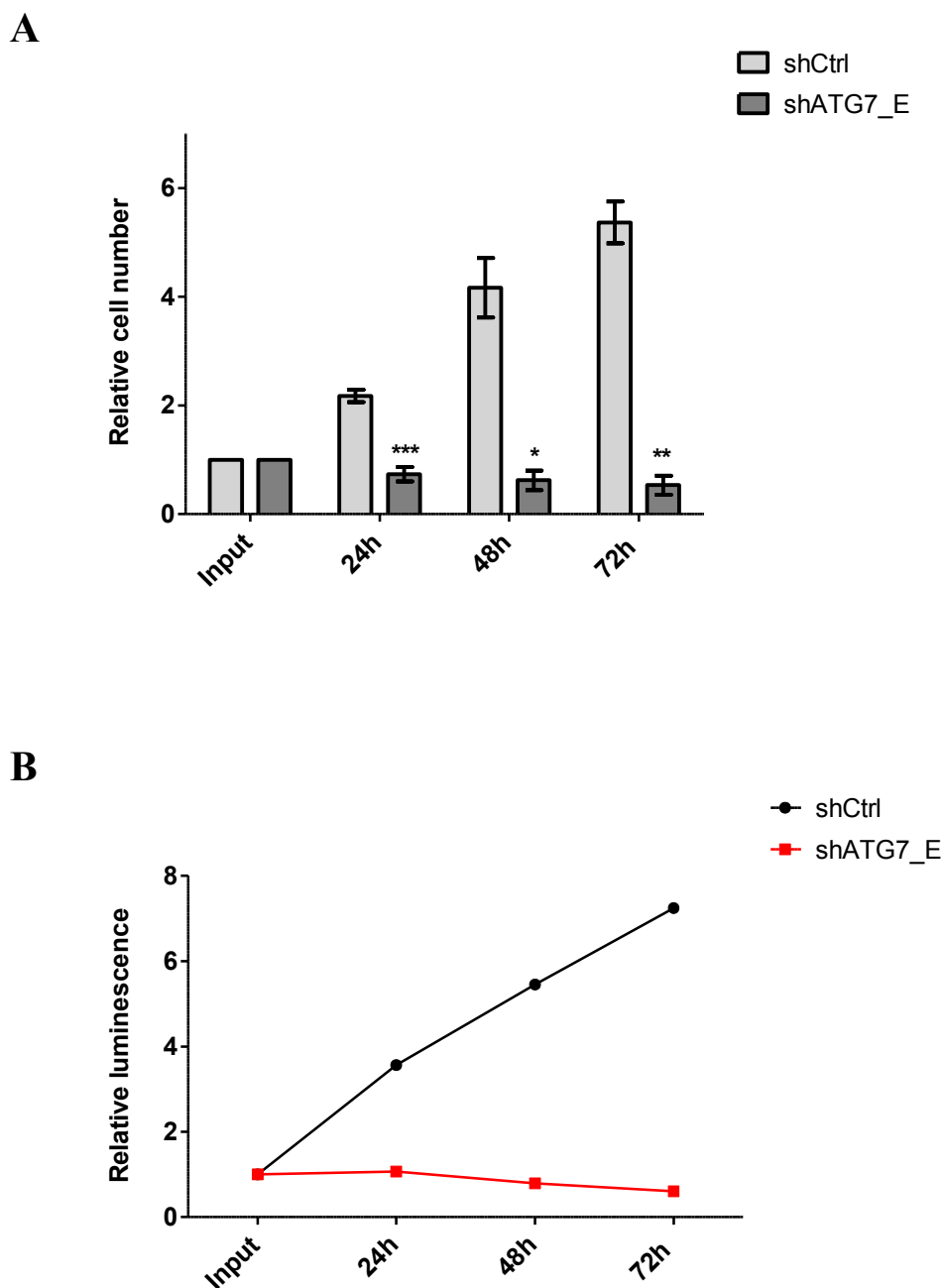


Figure 5-4: Analysis of K562 cell proliferation upon ATG7 knock-down

Cell proliferation was measured in shCtrl and shATG7_E cells by (A) cell counts (n=3) and (B) CellTiter-Glo® luminescence assay (n=2), every 24h post-sort, for a total of 72h. Graph values refer to viable cells (verified by trypan blue) and are presented as mean±SEM (n=3) relative to input. Statistical analysis was performed by using paired t-test. Annotation above a bar refers to statistical significance between the bar and the NDC. (*; p≤0.05, **; p≤0.01, ***; p≤0.001)

6 days post-sort, shCtrl and shATG7_E cells were stained with DAPI and analysed by FACS.

Figure 5-5 reveals that induction of cell death correlated with ATG7 knock-down; while cell death rates in shCtrl cells were low ($6.03 \pm 4.05\%$), shATG7_E cells presented a ≥ 10 -fold increase in death levels ($68.56 \pm 11.47\%$, $p=0.004$ versus shCtrl).

Overall, these data imply that ATG7 autophagy plays a vital role in the cellular integrity and survival of the K562 cells.

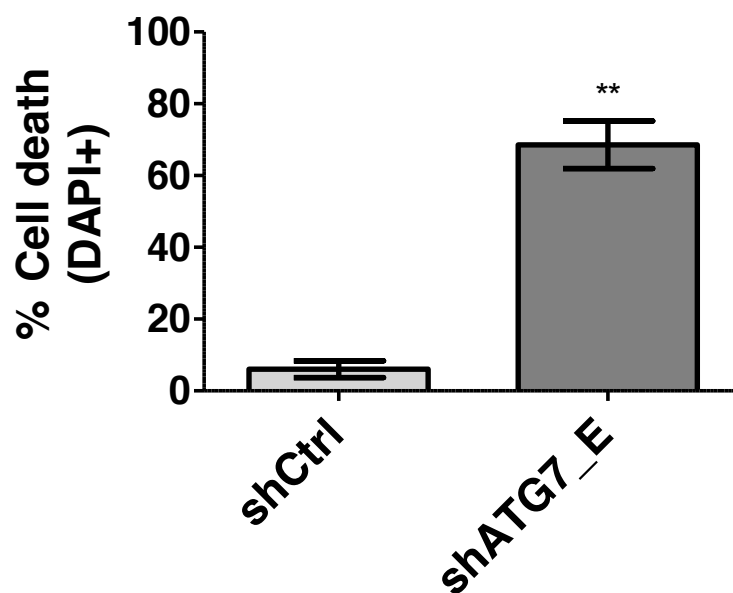


Figure 5-5: Cell death analysis in K562 cells upon ATG7 knock-down

K562 cells were lentivirally transduced with a pLKO.1-GFP vector, carrying either a mock (shCtrl) or an ATG7-targeting hairpin (shATG7_E). GFP+ cells were sorted in order to obtain homogenous populations of transduced cells. 6 days post-sort, cells were stained with DAPI and cell death was measured by FACS analysis. Graph represents cell death levels as mean \pm SEM (n=3). Statistical analysis was performed by using paired t-test. (**; $p \leq 0.01$)

5.1.2.2 Effect of ATG7 knock-down in the erythroid differentiation of K562 cells and their mitochondrial potential

K562 cells are bipotential and, after stimulation with a range of reagents, can be differentiated into cells with erythroid or megakaryocytic properties [369]. For example, treatment with hemin [370, 371], cytosine arabinoside [372], butyric acid [373] or AZA [374], induces erythroid differentiation while treatment with phorbol 12-myristate 13-acetate (PMA) promotes megakaryocytic differentiation.

According to data described in §5.1.2.1, the proliferation of K562 cells upon ATG7 knock-down was severely disrupted during the first 72h following sorting and cell death was significantly increased. In order to explore the fate pathway of the remaining viable population of shATG7_E cells, cell counts were performed every 2 days so as to monitor the proliferation ability. Cell viability was assessed by the trypan blue exclusion method.

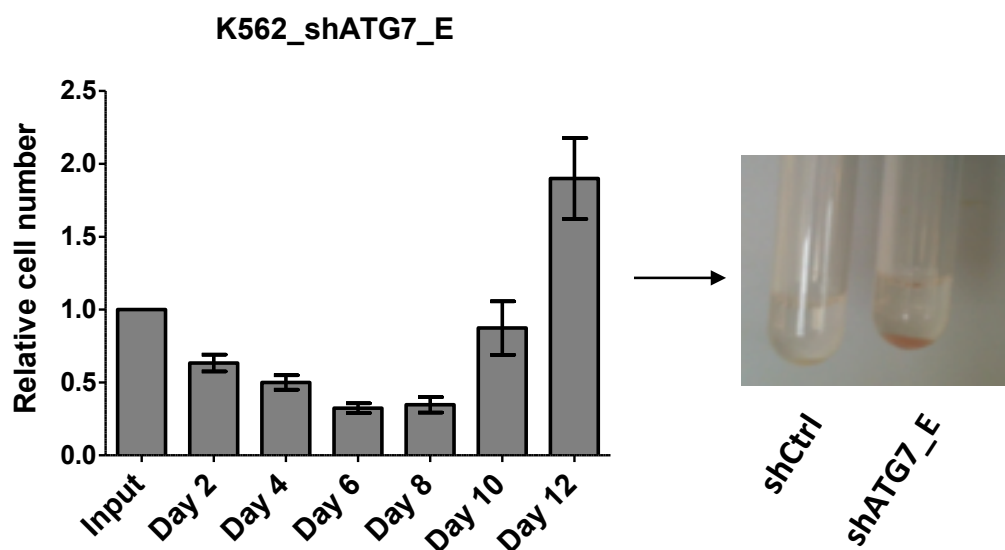
Figure 5-6A demonstrates that shATG7_E cell population failed to efficiently expand up to 10 days post-sort. Nevertheless, proliferation ability was restored afterwards. Interestingly, the ATG7 knock-down surviving population presented increased haemoglobin production compared to the shCtrl cells.

The next question that arose was if increased haemoglobin production was associated with erythroid differentiation. Glycophorin A (GlyA) or CD235a (cluster of differentiation 235a), is the major intrinsic sialoglycoprotein of the human erythrocyte and erythroid precursors membrane. Anti-GlyA antibodies have been used extensively in the characterisation of erythroid cell development and in the diagnosis of erythroid leukaemias. In order to explore if the ATG7 knock-down surviving K562 cells presented erythroid differentiation features, cells were stained with an anti-GlyA antibody (BD, PN 555570) and analysed by FACS.

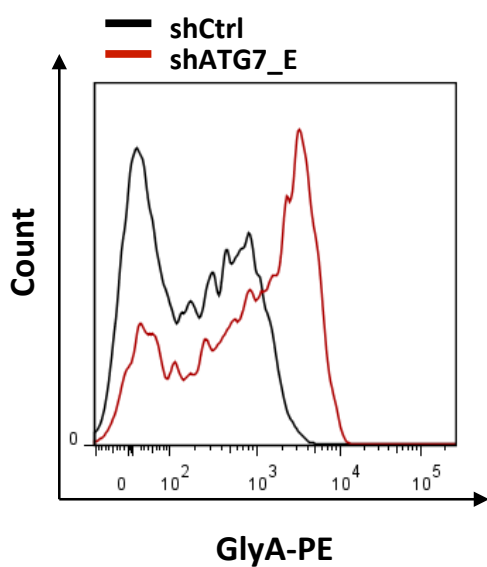
As illustrated in Figure 5-6B, the FACS profile analysis of the shATG7_E cells revealed high levels of GlyA expression compared to the shCtrl. This increase in GlyA expression was not attributed to a corresponding increase in the size of shATG7_E cells (and therefore, cell membrane surface area) (Figure 5-6C).

Taken altogether, these findings suggested that K562 cells that survived prolonged ATG7 knock-down presented with a more differentiated phenotype.

A



B



C

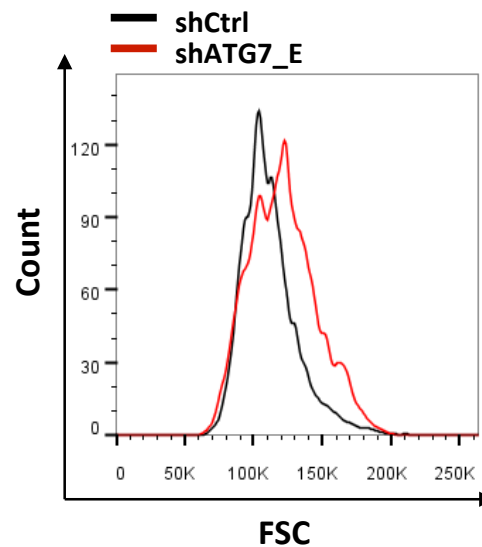


Figure 5-6: Analysis of the erythroid differentiation potential of K562 cells upon ATG7 knock-down

(A) Cell proliferation was measured within the shATG7_E population by cell counts performed every 2 days, for the total of 12 days post-sort. Graph values refer to viable cells (verified by trypan blue) and are presented as mean \pm SEM (n=3) relative to input. FACS analysis profile on the shATG7_E cells 12 days post-sort, regarding (B) GlyA expression and (C) cell size.

In order to examine the morphology of these cells, the "Diff-Quik" staining kit (DADE Behring, PN130832) was used according to the protocol described at §2.2.10.

As depicted in Figure 5-7A, shCtrl and shATG7_E cells 12 days post-sort were not presenting significant morphological differences, despite the fact that shATG7_E cells expressed high levels of GlyA. Nonetheless, this could be attributed to the fact that inhibition of autophagy does not allow for terminal differentiation of reticulocytes. In a study published by Zhang and colleagues in 2009, it was reported that in the absence of ATG7, reticulocyte clearance of mitochondria was suppressed but not completely abolished [375]. Hence, it is likely that shATG7_E cells would not be able to undergo terminal differentiation due to suppressed mitophagy.

In order to investigate this further, shCtrl and shATG7_E K562 cells were stained with MitoTracker® Red CMXRos (Invitrogen, PN M7512). This reduced probe does not fluoresce until it enters live cells, where it is oxidised and sequestered in functional mitochondria and starts emitting red fluorescence. The oxidised dye emits red fluorescence and can be detected by FACS analysis (emission maxima ~599nm).

Figure 5-7B demonstrates that shATG7_E cells presented ~80% more functional mitochondria compared to the shCtrl ($p=0.005$). This is in agreement with other studies where knock-down of autophagy genes results to increased number of mitochondria due to suppression of autophagy [376].

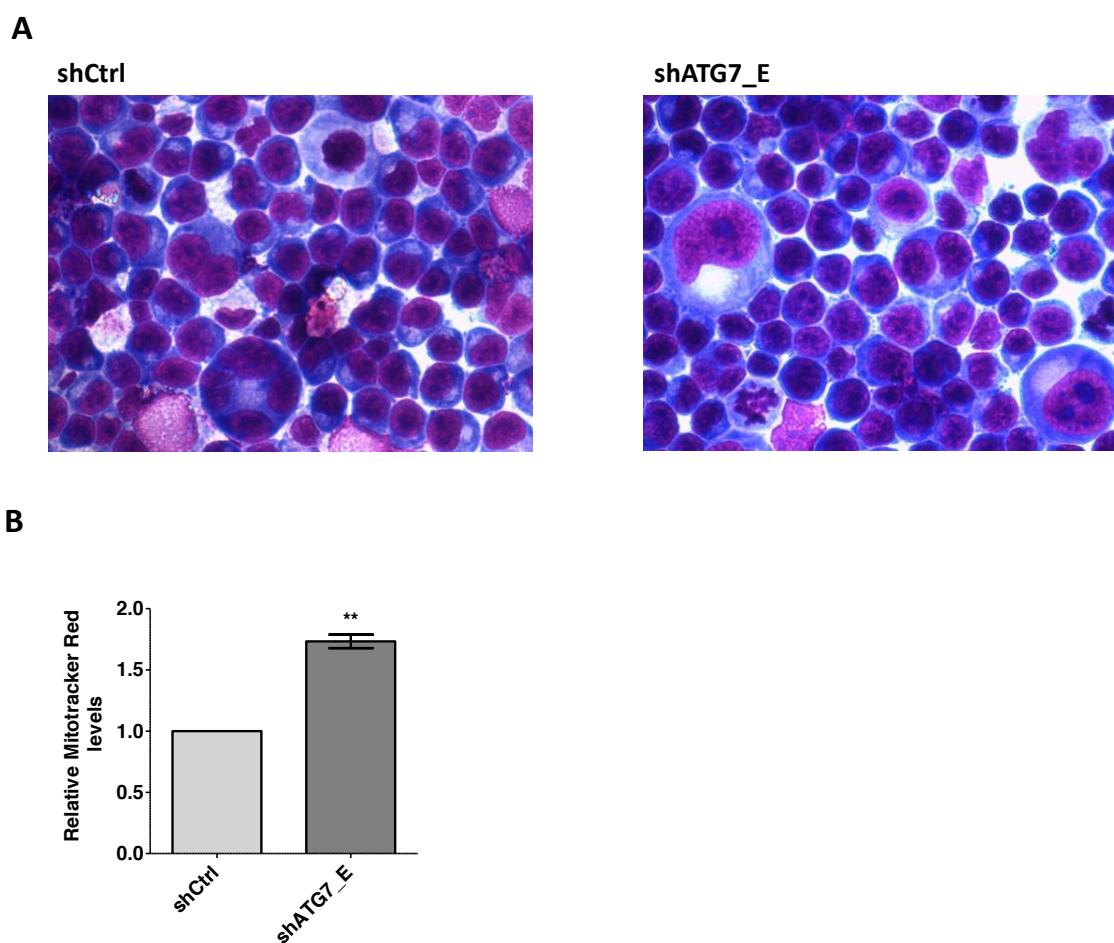


Figure 5-7: Analysis of the morphology and the mitochondrial profile of K562 cells upon ATG7 knock-down

K562 shCtrl and shATG7_E cells were stained 12 days post-sort with the "Diff-Quik" staining kit and examined morphologically under a light microscope. Representative captions of n=3 are presented at 400X magnification. (B) shCtrl and shATG7_E K562 cells were stained with MitoTracker® Red CMXRos and analysed by FACS for the quantification of functional mitochondria. Graph presents MitoTracker® levels relative to shCtrl as mean±SEM (n=3). Statistical analysis was performed by using paired t-test. (**; p≤0.01)

5.1.2.3 Effect of ATG7 knock-down in the megakaryocytic differentiation of K562 cells and the levels of ROS

K562 cells can differentiate either into erythroid cells or megakaryocytes. In order to explore if ATG7 knock-down promotes differentiation only towards the erythroid and not the megakaryocytic line, shATG7_E cells were maintained in culture for a total of 30 days post-sort and monitored frequently for the presence of megakaryocytic features. Progressively, shATG7_E cells proliferated with rates comparable to non-transduced K562 and had increased cell size compared to the shCtrl cells. Moreover, cells within the shATG7_E arm appeared to attach on the plastic surface of the flask used for culture. Cytospin and staining with “Diff-Quik” revealed that a fraction of the cells presented morphologically megakaryocytic features including an apparent increase in cell size, multilobed nuclei, cytoplasmic blebs/pseudopods (Figure 5-8).

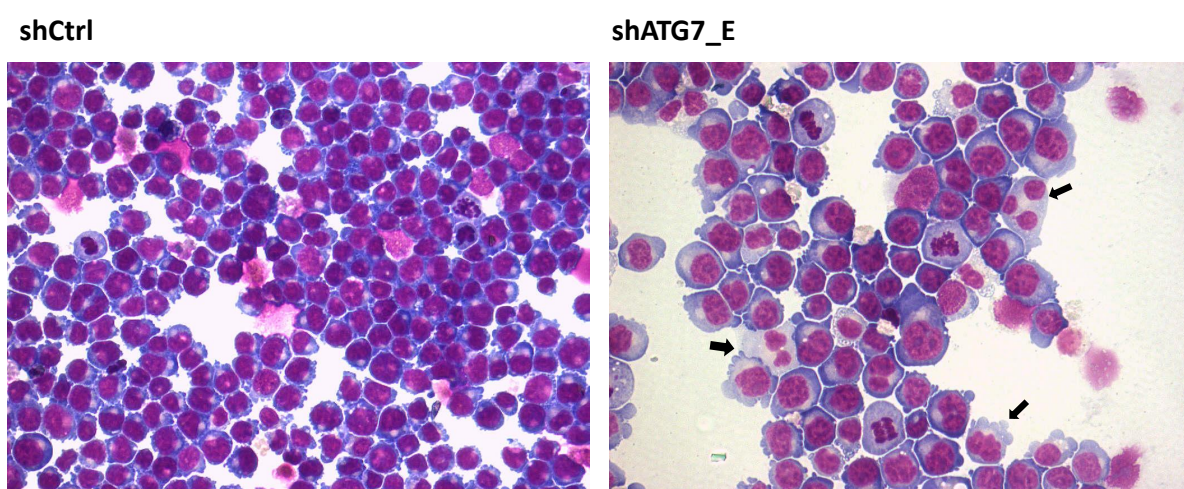


Figure 5-8: Analysis of the morphology K562 cells surviving prolonged ATG7 knock-down

K562 shCtrl and shATG7_E cells were stained 30 days post-sort with the "Diff-Quik" staining kit and examined morphologically under light microscope. Representative captions on n=3 are presented at 200X magnification. Arrows point representative cells with megakaryocytic features.

According to a study performed by Sardina and colleagues (2010), ROS production was required for the PMA-induced megakaryocytic differentiation of K562 cells [377]. During megakaryocytic differentiation ROS was transiently increased and its inhibition by antioxidants hindered differentiation. On the other hand autophagy/mitophagy inhibition has been suggested to lead to increased levels of ROS due to the accumulation of damaged mitochondria and the production of superoxide. Therefore, the next experiment aimed to measure the levels of superoxide produced by mitochondria in the shCtrl and shATG7_E populations that presented megakaryocytic features.

shCtrl and shATG7_E cells were stained with MitoSOX™ Red (Invitrogen, PN M36008), according to the protocol described at §2.2.2.6. This reagent enters live cells and selectively localises to mitochondria where it is oxidised by superoxide but not by other ROS and reactive nitrogen species. As illustrated in Figure 5-9, shATG7_E cells presented almost 2-fold increased superoxide levels compared to the shCtrl ($p=0.01$).

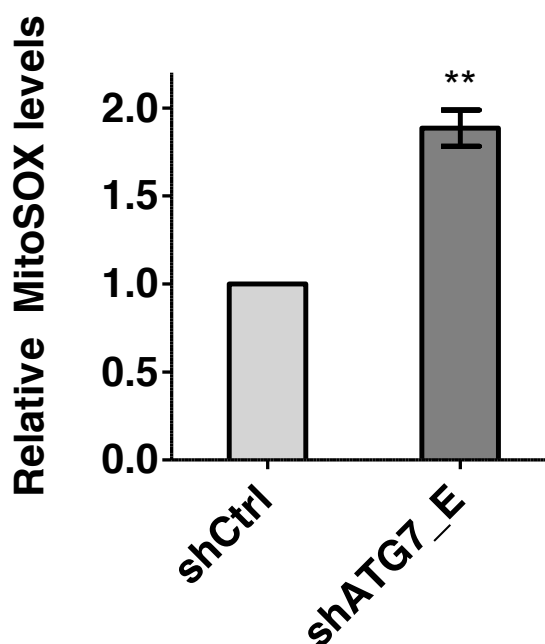


Figure 5-9: Measurement of superoxide levels within K562 cells surviving prolonged ATG7 knock-down

30 days post-sort, shCtrl and shATG7_E K562 cells were stained with MitoSOX[®] Red and analysed by FACS for the quantification of superoxide levels. Graph presents MitoSOX[™] levels relative to shCtrl as mean±SEM (n=3). Statistical analysis was performed by using paired t-test. (**; p≤0.01)

5.1.2.4 Investigation of ATG7 knock-down in erythroid and megakaryocytic differentiation at the single cell level

In experiments described previously, 2 weeks following ATG7 knock-down K562 cells showed erythroid features and another 2 weeks later, a fraction of the population had megakaryocytic phenotype. The experiment described herein was designed in order to investigate:

- i) if ATG7 knock-down “selects” for more differentiated cells within the initial culture or is the driver of the observed differentiation
- ii) if cells with megakaryocyte features were present in the culture 2 weeks following knock-down or developed at a later stage.

K562 cells were transduced with shCtrl or shATG7_E virus, as described in §2.2.8.1.2. Transduced shCtrl and shATG7_E single cells were sorted 48h after the last transduction round into 96-well plates. The ability of each single cell to proliferate and initiate a culture in liquid medium was monitored frequently.

10 days after sorting, shCtrl single cells had proliferated and initiated clones of >50 cells. Nevertheless, the shATG7_E cells did not appear to proliferate by that time. Since shCtrl cells were proliferating fast, each clone was isolated, washed and transferred in a well of a 24-well plate for further examination.

16-20 days following sorting, shATG7_E clones appeared in the knock-down arm. Nevertheless, as demonstrated in Figure 5-10A, the number of single cells that managed to proliferate and form clones in the shATG7_E arm was significantly lower compared to the shCtrl arm ($p=0.002$). Furthermore, in the shATG7_E arm, all clones presented either erythroid or megakaryocytic differentiation features. Erythroid clones consisted of >1000 cells while all megakaryocytic clones contained 10-100 cells (Figure 5-10B). This difference in proliferation kinetics could explain why upon ATG7 knock-down, the cells with erythroid features appear first in the culture and the appearance of cells with megakaryocytic features is more delayed.

Interestingly, none of the shCtrl isolated clones presented features of differentiation. This implies that ATG7 knock-down promoted the differentiation rather than selected for more differentiated cells in the initial culture. If this were the case, then differentiated clones should also be equally represented in the shCtrl arm.

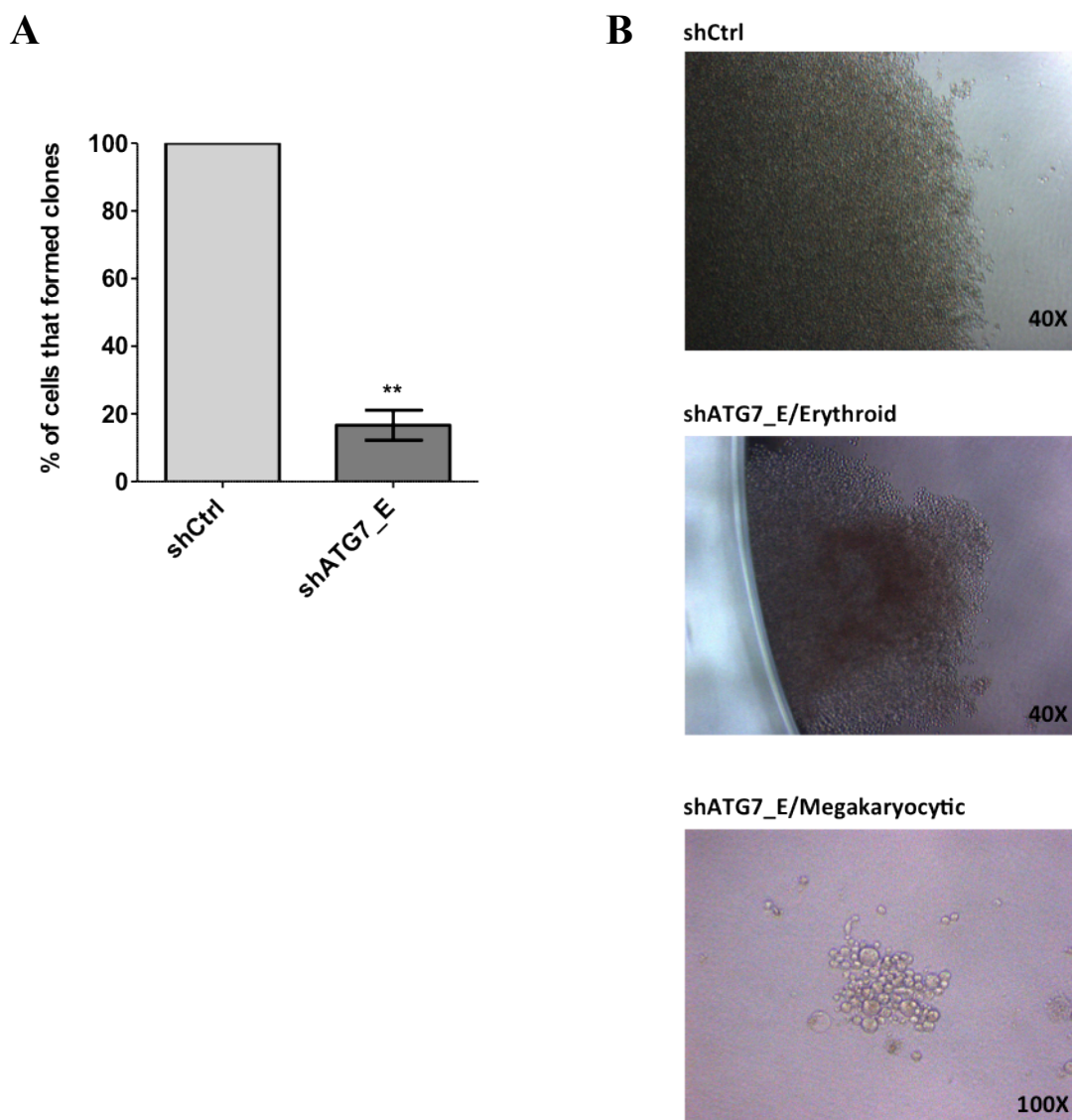


Figure 5-10: Analysis of clone-initiating potential of single-sorted ATG7 knock-down K562 cells

shCtrl and shATG7_E single cells were sorted into a 96-well plate (n=3) and 20 days later, the wells were scored for the presence of cell clones. (A) The graph presents the per cent of sorted single cells that formed clones, relative to the shCtrl as mean \pm SEM (n=3). Statistical analysis was performed by using paired t-test. (**; $p \leq 0.01$). (B) Captions of the shCtrl and shATG7_E clones were examined under light microscope for the estimation of relative cell numbers within each clone.

To summarise, our experiments underline the significance of ATG7 in the cell fate decision of the K562 cell line. It was demonstrated that dependence on ATG7 for K562 cell survival is strong, leading the majority of the population to cell death.

Moreover, cells that evaded cell death upon ATG7 knock-down, presented a more differentiated phenotype. Failure of these cells to terminally differentiate could potentially be attributed to inhibition of autophagy and blockade of this “cell make-over” process. Nevertheless, our data are inconclusive in answering if ATG7 resolves the differentiation block within these blast cells rather than directly promoting differentiation.

5.2 Characterisation of CLL cells following ATG7 knock-down

In order to explore if ATG7 is also playing a role in the cell fate decision of other transformed human leukaemic cells, the recently isolated CLL cell line HG3 was investigated. The HG3 cell line is a lymphoblastoid cell line with B1 cell characteristics. It was established from a CLL clone of a 70-year old man by *in vitro* Epstein-Barr virus infection, and it carries a biallelic chromosome 13q14 deletion, including the loss of *DLEU7* and miR15a/16-1 [378].

HG3 cells were transduced with shCtrl or shATG7_E virus, as described in §2.2.8.1.2. GFP⁺ transduced cells were sorted 48h after the last transduction round and cultured in RPMI⁺. Western blot analysis on lysates from HG3 shCtrl and shATG7_E cells 4 days post-sort, revealed $\geq 50\%$ reduction in ATG7 protein levels in the shATG7_E cells (Figure 5-11).

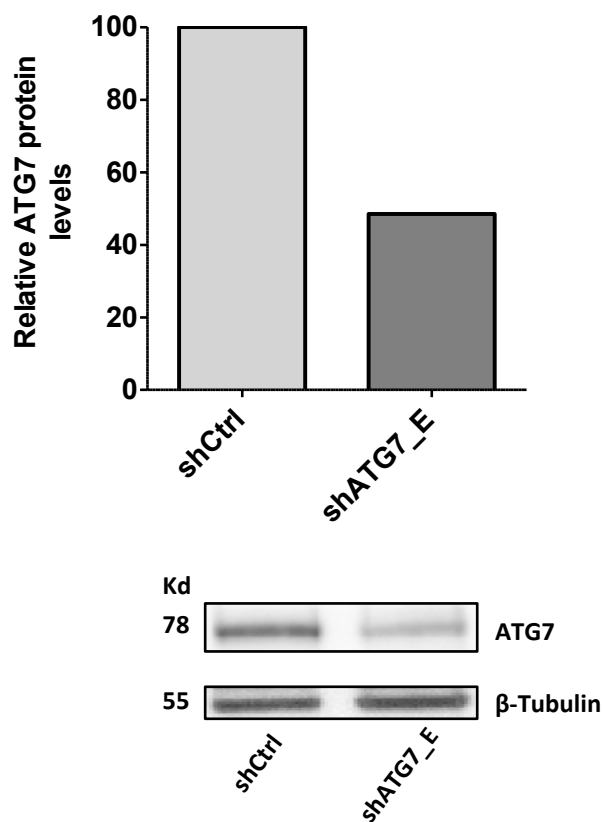


Figure 5-11: Measurement of ATG7 protein levels in HG3 cells that stably express an ATG7-targeting hairpin carried by pLKO.1 vector

Western blot was used for the analysis of ATG7 protein levels in HG3 cells 4 days post-sort. Densitometry calculations for data shown were performed by using the Quantity One software. The graph represents relative ATG7 levels (normalised to β -tubulin) compared to the shCtrl.

5.2.1 Assessment of HG3 proliferation and cell viability following ATG7 knock-down

Proliferation of HG3 cells transduced with either shCtrl or shATG7_E hairpin, was assessed by performing cell counts every 24h after sorting. Cell viability was established by using the trypan blue exclusion method.

Figure 5-12A illustrates that ATG7 knock-down significantly suppressed the proliferation of the HG3 cells compared to the shCtrl ($p=0.018$ at 24h, $p=0.013$ at 48h and $p=0.0008$ at 72h). This was further validated by the CellTiter-Glo® luminescence assay (described at §2.2.1.2.2) that detects metabolically active cells based on quantitation of the ATP present, which is directly proportional to the number of cells present in culture ($n=2$) (Figure 5-12B).

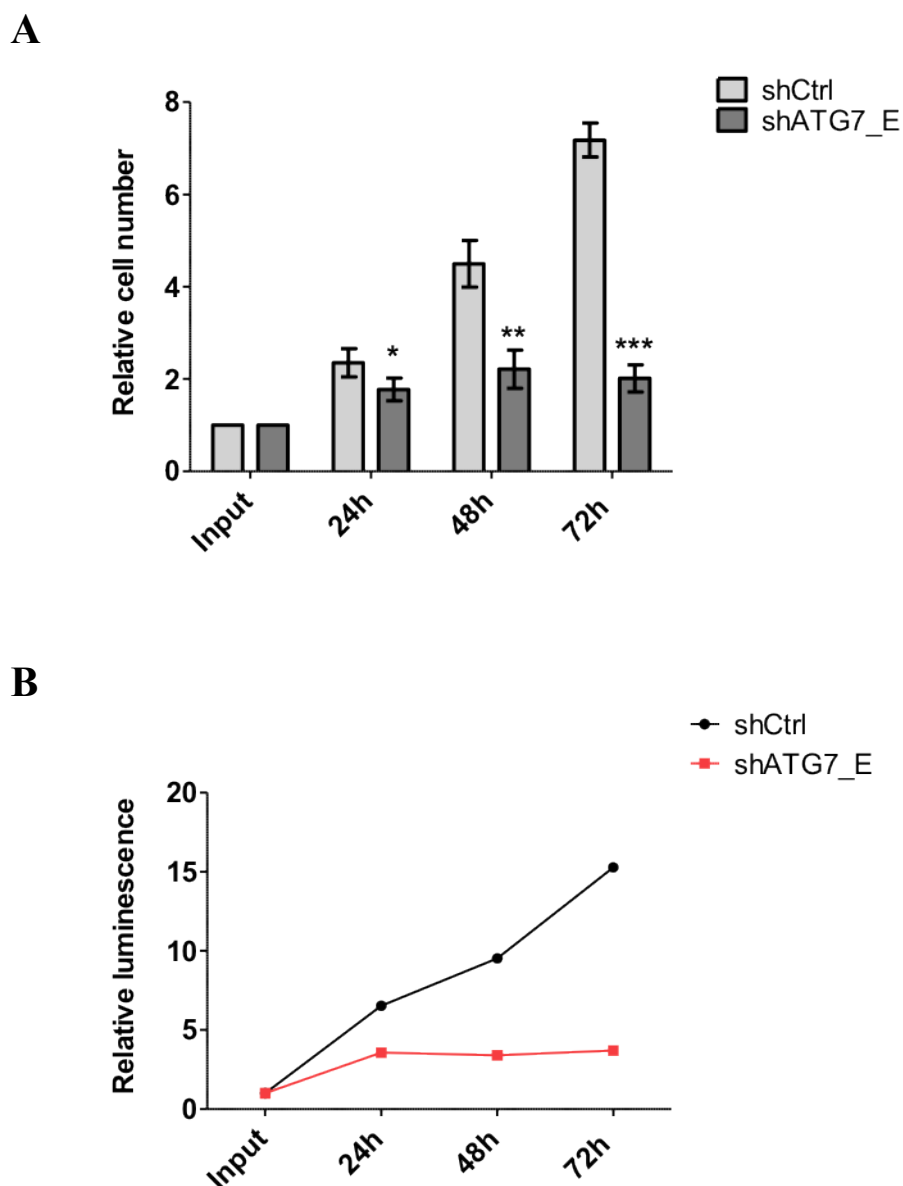


Figure 5-12: Analysis of HG3 cell proliferation upon ATG7 knock-down

Cell proliferation was measured in shCtrl and shATG7_E cells by (A) cell counts (n=3) and (B) CellTiter-Glo® luminescence assay (n=2), every 24h post-sort, for a total of 72h. Graph values refer to viable cells (verified by trypan blue) and are presented as mean±SEM (n=3) relative to input. Statistical analysis was performed by using paired t-test. Annotation above a bar refers to statistical significance between the bar and the relative shCtrl. (*; p≤0.05, **; p≤0.01, ***; p≤0.001)

6 days post-sort, shCtrl and shATG7_E HG3 cells were stained with DAPI and analysed by FACS.

Data presented in Figure 5-13 revealed that induction of cell death correlated with ATG7 knock-down; while cell death rates in shCtrl cells were relatively low ($26.63 \pm 8.79\%$), shATG7_E cells presented a ≥ 2 -fold increase in death levels ($68.50 \pm 4.23\%$, $p=0.01$). These data imply that autophagy plays a role in the survival of the HG3 lymphoblastoid cells.

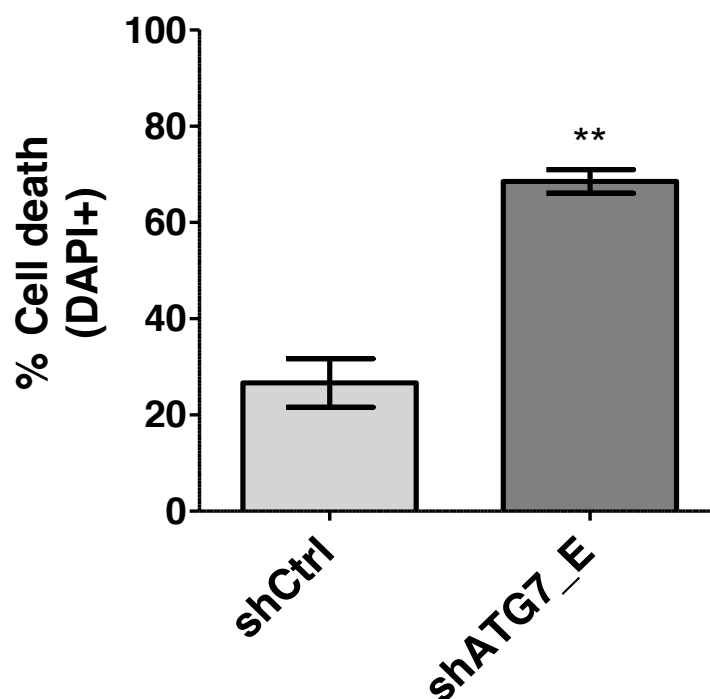


Figure 5-13: Cell death analysis in HG3 cells upon ATG7 knock-down

HG3 cells were lentivirally transduced with a pLKO.1-GFP vector, carrying either a mock (shCtrl) or an ATG7-targeting hairpin (shATG7_E). GFP+ cells were sorted in order to obtain homogenous populations of transduced cells. 6 days post-sort, cells were stained with DAPI and cell death was measured by FACS analysis. Graph presents cell death levels as mean \pm SEM (n=3). Statistical analysis was performed by using paired t-test. (**; $p \leq 0.01$)

5.2.2 Effect of ATG7 knock-down in the differentiation of HG3 cells

HG3 that survived ATG7 knock-down were monitored frequently for the identification of morphological changes. Analysis by FACS revealed that shATG7_E HG3 cells that survived >10 days of ATG7 knock-down had increased cell size (Figure 5-14).

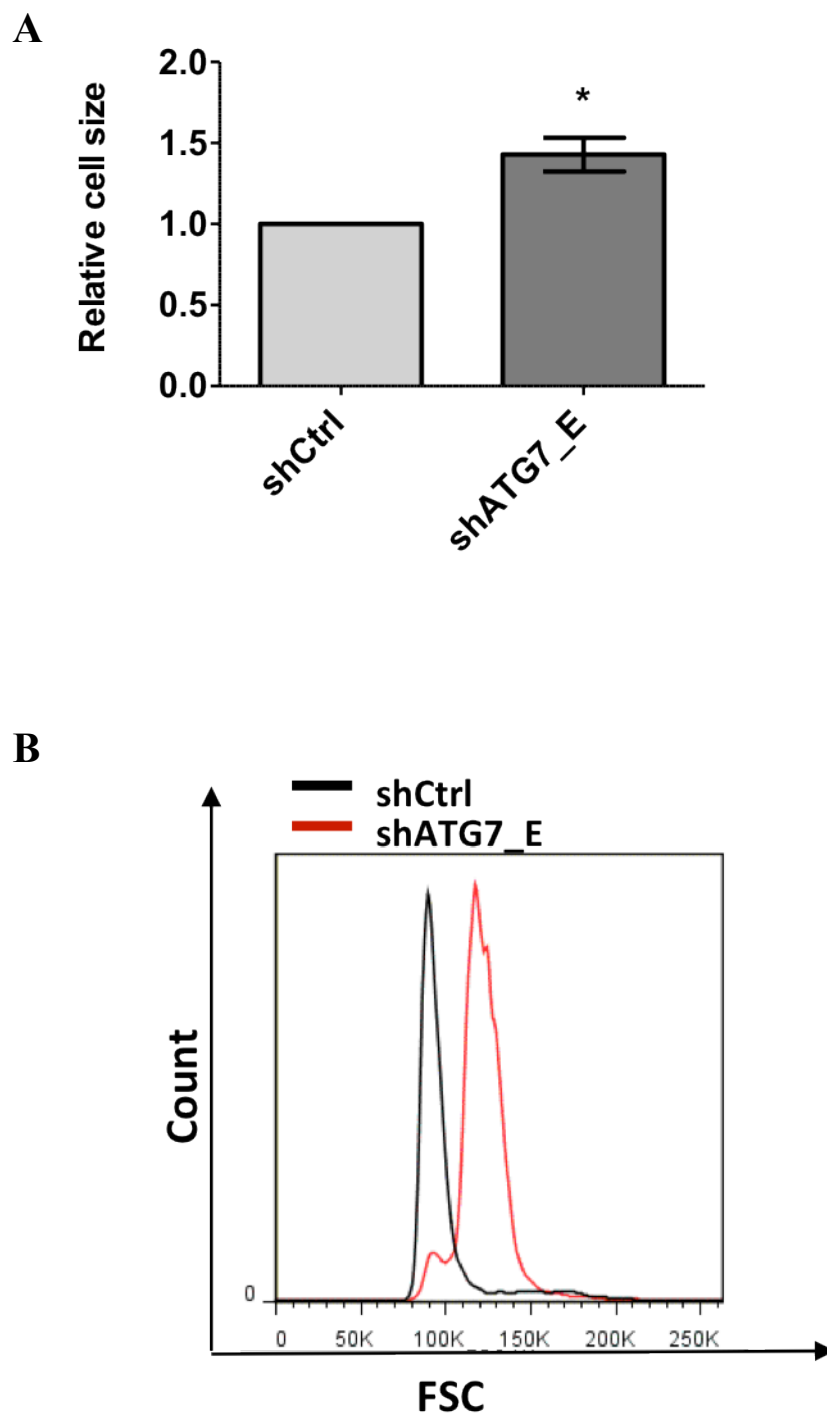


Figure 5-14: Increase in the cell size of HG3 cells upon ATG7 knock-down

The geometrical mean of the FSC (forward side scatter) of shCtrl and shATG7_E cells was measured by FACS analysis 10 days post-sort. (A) The graph represents cell size relative to shCtrl as mean \pm SEM (n=3). (B) A representative FACS plot overlay of the FSC within shCtrl and shATG7_E cells. Statistical analysis was performed by using paired t-test. (*; $p\leq 0.05$)

Interestingly, ATG7 knock-down presented altered features compared to the control in liquid culture. Unlike HG3 WT or shCtrl-transduced cells that grow in clusters, HG3 shATG7_E cells were growing as single cells (Figure 5-15A).

In order to further investigate the morphology of the cells, shCtrl and shATG7_E HG3 cells were adhered onto a slide and stained with the "Diff-Quik" kit. Figure 5-15B demonstrates that shCtrl and shATG7_E cells 15 days post-sort were presenting significant morphological differences. HG3 cells in the absence of ATG7 presented a clear increase in cell size, high proliferation rate (increased number of cells in mitosis in a single field), cytoplasmic blebs/pseudopods and prominent Golgi apparatus.

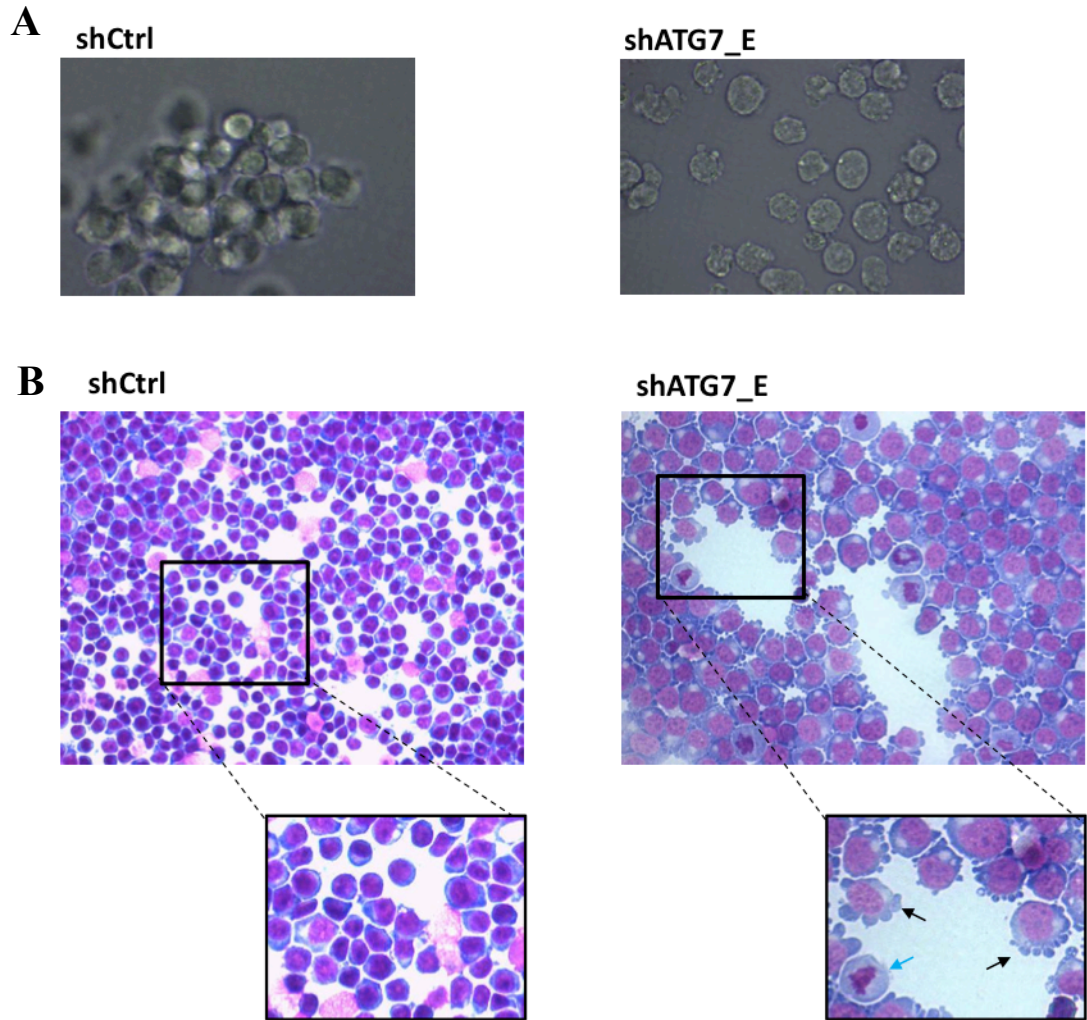


Figure 5-15: Morphological analysis of HG3 cells surviving ATG7 knock-down

(A) HG3 shCtrl and shATG7_E cells 15-20 days post-sort presented different culture features after examination under light microscope. (B) Cell aliquots from these cultures were stained with the "Diff-Quik" staining kit and examined morphologically under light microscope. Black arrows point at representative cells with cytoplasmic blebs/pseudopods and prominent Golgi apparatus. Blue arrow points at a representative cell undergoing mitosis. Representative captions on n=3 are presented at 200X magnification.

Taken altogether, upon ATG7 knock-down the viability of the majority of HG3 cells was severely affected and approximately 70% of the population died within 6 days following sorting. However, the remaining shATG7_E cells that survived presented significantly altered phenotype regarding morphology and cell-cell adhesion habits in culture.

5.3 Effect of Atg7 knock-down in mouse c-kit enriched MLL-ENL transformed cells

Previous experiments have demonstrated that ATG7 plays an important role in cell fate decisions of human CML and CLL cells. In order to further investigate how ATG7 knock-down affects the cell fate of AML mouse cells, c-kit enriched mouse bone marrow cells transformed with the oncogene MLL-ENL were used.

Mouse c-kit enriched MLL-ENL transformed cells were infected with a lentiviral system based on a pLKO.1 vector that encoded for the puromycin resistance gene and carried either an Atg7-targeting hairpin (shAtg7) or a mock hairpin (shCtrl). Following three rounds of transduction, cells were washed and cultured in IMDM supplemented with 10 ng/ml of mIL3. Selection of transduced cells was initiated 48h after the last transduction round, by adding PURO (1µg/mL) in the culture. After 3 days of antibiotic selection, PURO was washed out, and the cells were examined under the light microscope.

Figure 5-16A demonstrates that by the end of the selection process, Atg7 knock-down cells presented increased numbers of dead cells (viewed as condensed cellular debris). The shAtg7 population was maintained in culture for another 3 days, so as to allow for expansion of the live cells, and analysed by FACS after DAPI staining.

Analysis 3 days post-selection termination revealed that all shAtg7 cells were dead, unlike the shCtrl cells that presented high viability (approx. 70%). Assuming equal efficacy of transduction between the shCtrl and shAtg7 virions, the complete eradication of the shAtg7 cells was attributed to knock-down of Atg7.

Overall, these data are in agreement with previously observed effects on human leukaemic cell lines. Viability of the mouse c-kit enriched MLL-ENL cells was completely ablated upon deprivation of the cells from the Atg7 protein and no cells survived in order to experiment further.

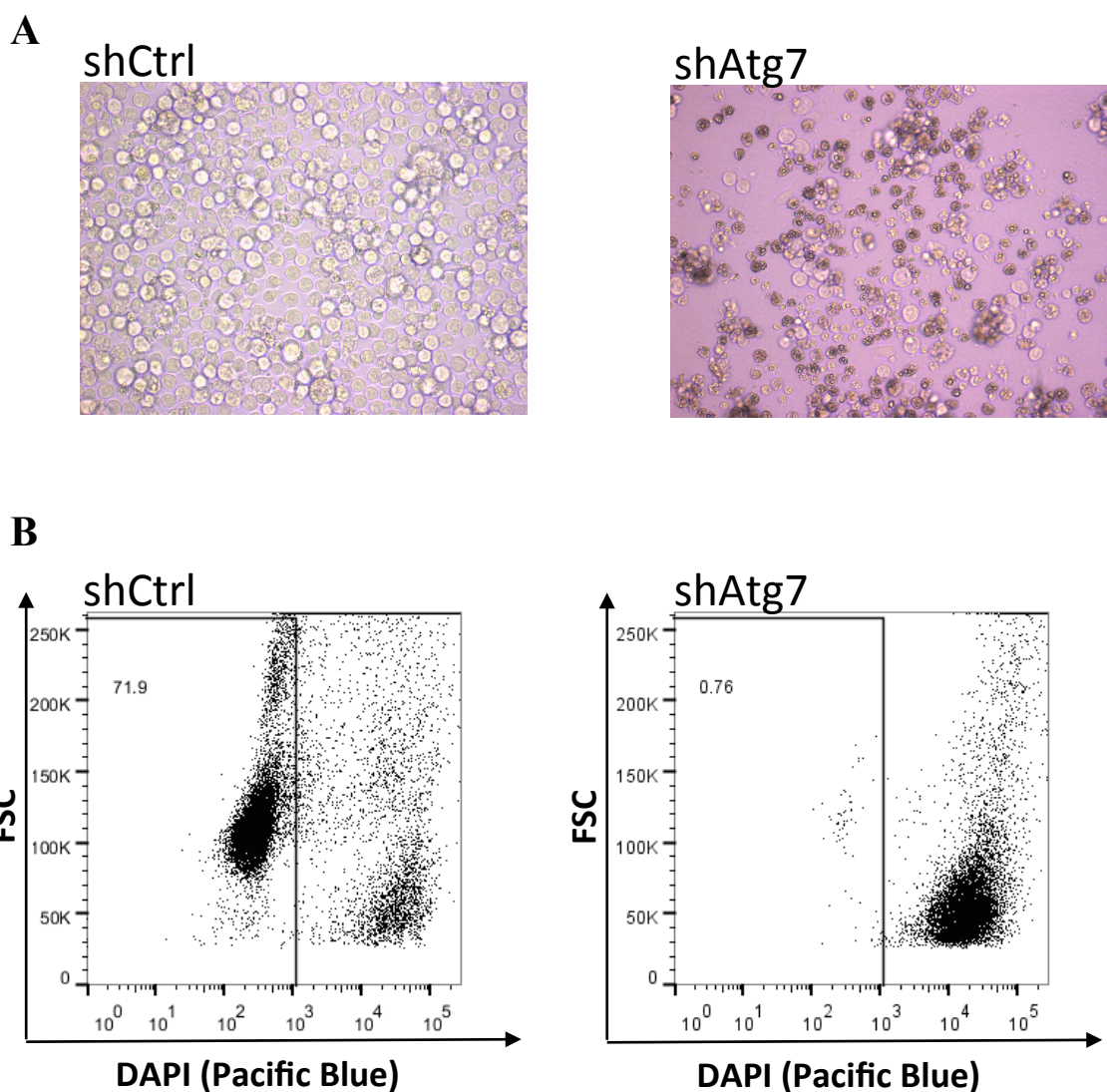


Figure 5-16: Cell death analysis in mouse c-kit enriched MLL-ENL transformed cells upon Atg7 knock-down

Mouse c-kit enriched MLL-ENL transformed cells were lentivirally infected with a pLKO.1-PURO vector, carrying either a mock (shCtrl) or an Atg7-targeting hairpin (shAtg7). Infected cells were selected in PURO for 3 days at the end of the selection the cells were examined under a light microscope (captions at 200X) (A). 3 days post-selection, cells were stained with DAPI and cell death was measured by FACS analysis. FSC/DAPI plots are representative of n=2 and gate percentages refer to live cells.

6 Discussion

The development of IM in the 1990s opened a new era in cancer cell targeted therapy; this 2-phenylaminopyrimidine was the product of rational drug design, identified by high-throughput screening and modified in order to inhibit the activity of the constitutively active BCR-ABL tyrosine kinase, the product of the chimeric *BCR-ABL* oncogene located on the Ph [379]. The 6-year follow-up data from the phase III IRIS study highlighted the clinical superiority of IM versus the combination of IFN α with cytarabine, which was used at that time as standard treatment [161]. Standard dose IM was associated with an EFS of 83% and 93% estimated rate of freedom from progression to AP and BC, while the EOS was 88% (95% when only CML-related deaths were taken into account). The estimated cumulative rate of complete CyR for IM-treated patients was approximately 82%. Since then, IM has served as the frontline therapy for patients with newly diagnosed CP CML.

However, it was observed that almost a quarter of the newly diagnosed CP patients on IM did not achieve complete CyR within the first 18 months of treatment. Interestingly, it has been reported that CML patients achieving complete CyR within the first two years of treatment have a favourable long-term outcome and a life expectancy comparable to the general population [380]. Another limitation of IM treatment was the restricted number of patients that achieve CMR and have undetectable BCR-ABL mRNA levels [166]. Furthermore, IM was not effective in advanced disease stages and any response to treatment was only transient [381]. Ultimately, the development of resistance was shown to be the Achilles' heel of IM.

So far, a plethora of mechanisms have been reported to lead to IM resistance, either BCR-ABL-dependent (such as kinase domain mutations or BCR-ABL overexpression) or BCR-ABL-independent (such as secondary mutations, drug delivery defects, and compliance issues). In an effort to override resistance, IM dose escalation (up to 800mg/day) was investigated in CML patients previously treated with 400mg/day that had relapsed or developed resistance [212, 213]. Unfortunately, even if responses were moderately improved, IM dose escalation was not sufficient to eliminate the issue of resistance. In order to tackle IM resistance, 2nd generation TKIs, DAS and NIL, were designed.

DAS, a potent TKI that targets ABL kinases and SFKs, had *in vitro* high affinity for BCR-ABL mutants refractory to IM. Likewise, NIL was demonstrated to be more potent than IM, targeting BCR-ABL conformations inaccessible to IM. Most importantly, both of these TKIs were superior to IM in the clinic; the DASISION clinical trial demonstrated *in vivo* that DAS is more efficacious over IM, while the ENESTnd trial illustrated that NIL was

associated with better responses compared to standard dose IM. However, both DAS and NIL were ineffective in targeting the gatekeeper T315I mutation [216, 222].

Nevertheless, the major problem of all the above mentioned TKIs, and the reason why they fail to cure CML patients, is disease persistence. Two independent studies, the STIM [171] and the Australian group [172], demonstrated that discontinuation of IM in CMR patients led rapidly to relapse due to MRD. *In vitro* CML CD34+ can survive very high IM concentrations, indicating that LSCs are inherently refractory [173]. Additionally, this IM-resistant fraction of LSCs that can replenish disease was not targeted by either DAS [221] or NIL [226]. At this point it should be highlighted that development of TKI resistance and molecular persistence is not always attributed to inaccessibility of BCR-ABL. For instance, the presence of BCR-ABL mutants does not always explain clinical resistance to IM [382], and CML patient cells resistant *in vitro* to TKIs may carry native, unmutated BCR-ABL [221].

In 2011, Corbin and colleagues provided evidence suggesting that CML LT-HSCs and ST-HSCs are not eradicated by IM treatment despite complete inhibition of BCR-ABL activity [234]. A few months later, a published study by our lab further validated these observations [235]. CML patient-derived CD34+ cells were lentivirally transduced in order to knock-down BCR-ABL. A fraction of these LSCs managed to escape cell death despite inhibition of BCR-ABL activity, even after DAS treatment and withdrawal of GFs. This observation was of great interest; it implied that the LSCs can override almost complete removal of internal (BCR-ABL) and external (GFs in culture medium) survival stimuli, and activate alternative pathways for evading cell death. Interestingly, this cell population was enriched for primitive leukemic cells that had LTC-IC potential.

Taken together, these studies underlined that the leukaemia-initiating/repopulating TKI-refractory fraction of LSCs does not depend on BCR-ABL for survival. Hence, it became clear that no TKI treatment would be effective in eradicating these cells, offering a curative option to CML patients. Based on such observations, scientists within the field of CML treatment research are trying to identify the BCR-ABL-independent alternative pathways that the LSC fraction is relying on for survival upon suppression of BCR-ABL signaling. Towards this direction, currently on-going clinical trials are evaluating the efficacy of single agents for the elimination of MRD in CML; examples include zileuton, panobinostat and BMS-833923, which are targeting fatty acid metabolism, histone acetylation and WNT signaling, respectively.

On the other hand, high levels of BCR-ABL oncoprotein within CML CD34+ cells have been associated with disease progression and development of resistance [383]. This may

not be associated with *BCR-ABL* amplification since primitive CML HSCs have been reported to transcribe *BCR-ABL* at high levels despite the presence of a single gene copy [384]. It should also be highlighted that TKIs induce in general good responses during CP and, even if they do not eradicate the most primitive population of LSCs, they have a significant effect on more differentiated CML cells. Therefore, even if the above mentioned clinical trials reveal that non-*BCR-ABL* targeting single agents have a significant effect on the survival of LSCs, it is unlikely that they will be preferred as a first-line treatment option over TKIs.

An approach in developing a therapeutic strategy that (i) would have a stronger efficacy against refractory LSCs than TKIs alone, and (ii) could be used as first-line treatment, would be to combine TKIs with agents that target secondary pathways that are vital for the survival of LSCs. The success of such an approach would rely on the identification of appropriate targets within the primitive CML stem cells.

6.1 Autophagy in cancer

Autophagy occurs at basal levels in the majority of mammalian cells, functioning as a quality control mechanism, maintaining homeostasis via the degradation of cytoplasmic contents, including damaged organelles and misfolded proteins. Nonetheless, under starvation or other stressful conditions, autophagy is induced as a survival mechanism in the cells in order to (i) sustain metabolism by breaking-down intracellular components and supplying the cells with building blocks to be used in energy replenishing pathways, and (ii) to remove damaged organelles and proteins generated under such stressful conditions.

Autophagy has a paradoxical role in cancer, functioning as a tumour suppressor or promoter depending on the context. Mice genetically modified so as to have defective autophagy in their whole body or specific tissues have been reported to be susceptible to pathogen infection [385], muscle damage [386], neurodegeneration [387] and chronic inflammation, that can eventually lead to development of cancer [388]. In humans, defects in autophagy genes have been associated with the development of various pathologic conditions, including cancer. For example, haploinsufficiency in *BECLIN* [389] has been associated with tumorigenesis, and frameshift mutations in *ATG2B*, *ATG5*, *ATG9B* and *ATG12* have been identified in gastric and colorectal cancers [390]. Nevertheless, it is not always clear if the defective phenotype is attributed to gene-specific autophagy-independent functions or dysfunctional autophagy. *UVRAG* monoallelic mutations have been reported in almost a third of colon cancers; however, these mutations do not appear to have an effect on autophagy [391]. At this point it should be mentioned that *UVRAG* has also been reported to have extra-autophagic roles, taking part in membrane trafficking and regulation of endocytosis along with *BECLIN* [392]. Hence, caution must be taken when interpreting loss-of-function studies on autophagy genes and the role of autophagy in cancer, because these observations may be due to other functions of these genes.

Nonetheless, defects in proteins that interplay with autophagy have also been linked to development of cancer and other diseases. For example, increased p62 levels have been associated with cancer development [393], and loss-of-function mutations in the PTEN-induced putative kinase 1 (*PINK1*) or the E3 ligase parkin (*PARK2*) have been identified in Parkinson's disease [394]. Interestingly, deletion of *Park2* in mice has been reported to cause hepatocellular carcinoma that phenocopies loss of *Beclin* [296].

On the other hand, an increasing number of studies has highlighted that autophagy supports cancer cell survival. During the first steps in the process of tumour establishment, cancer cells have to overcome stress-inducing factors, such as hypoxia and limited nutrients, due to insufficient blood supply [395]. In 2006, Degenhardt and colleagues demonstrated that autophagy is induced in hypoxic tumour regions and is required for tumour cell survival, and inhibition of inflammation and metabolic crisis-induced necrosis [396]. Apoptosis-defective cancer cells seem to rely on autophagy for evading necrosis [397].

Cancer cells have been reported to have high basal autophagy levels even under optimal conditions, suggesting that they may be autophagy-addicted [307, 311]. It has been reported that activation of oncogenic signals induces autophagy; for instance, activation of RAS at levels sufficient to induce tumourigenesis, leads to increased levels of basal autophagy. RAS-driven cancers require autophagy in order to induce/maintain transformation, and autophagy deficiency abolishes tumourigenesis [309, 310]. Mitochondria play a key role in cancer cells by supplying ATP and building blocks for other pathways (such as citrate for fatty acid synthesis). High levels of autophagy may be required in order to sustain increased mitochondrial metabolism within cancer cells.

It has been suggested that pharmacological inhibition of autophagy facilitates the apoptotic effect of anticancer therapies such as irradiation, alkylating agents, and various targeted anticancer agents [398, 399]. Based on similar observations, where autophagy appears to support the survival of established cancer cells, recent clinical trials have investigated the effect of chemotherapeutic agents in combination with CQ/HCQ-mediated autophagy inhibition in a wide range of cancer types including breast, colorectal, lung, pancreatic, prostate cancer, as well as glioblastoma [318].

Nevertheless, excessive autophagy can also lead to cell death, and there are studies suggesting that autophagy is required in order to allow for cell death in apoptosis-deficient cells [400, 401]. For example, RAPA-induced autophagy has been demonstrated to enhance radiation-mediated cell death in PTEN-defective prostate cancer cells [402].

Taken together, the role of autophagy and autophagy genes in the development of cancer still remains unclear. Autophagy appears to play different roles in different tissues, cancer types, and disease stages. Therefore, caution should be taken when deciding upon the modulation of the autophagic activity for the improvement of cancer treatment.

6.2 Is autophagy a survival factor for CML?

In 2007, Ertmer and colleagues first reported that IM induces autophagy in a dose-dependent manner, regardless of cell type or species [403]. A couple of months later, Carew and colleagues suggested that the HDAC inhibitor SAHA, among its other biological effects, induces autophagy in CML TKI-resistant cells [320]. Pharmacological inhibition of the SAHA-induced autophagy enhanced the anticancer efficacy of the drug, implying that autophagy may play a cytoprotective role in CML. In agreement with this observation, Mishima and colleagues reported that IM induces cytoprotective autophagy in CML cell lines [322].

However, in 2009, as part of a collaborative effort, our lab published the most rigorous evidence demonstrating induction of protective autophagy upon TKI treatment of CML cells [323]. Bellodi and colleagues aimed to investigate if TKI-mediated inhibition of BCR-ABL signaling, apart from inducing apoptosis, potentially has an effect on autophagy. As described in Chapter 1, the BCR-ABL oncoprotein is mimicking GF signaling, allowing the cells to survive and proliferate in the absence of extracellular GFs. By that time, a series of reports had already demonstrated that GF removal could lead to cellular autophagy in order to support survival [404-406]. On the basis of these observations, the authors hypothesised that a sudden withdrawal of the BCR-ABL GF mimicking signals could potentially induce cytoprotective autophagy.

First of all, the authors demonstrated that treatment with 2 μ M IM induced LC3 lipidation and accumulation of LC3-positive punctae in K562 cells. Likewise, 1 μ M IM induced autophagy in 32D cells transformed with native BCR-ABL^{p210} (murine IL-3-independent myeloid cell line). The observed IM-mediated autophagic increase was attributed to suppression of survival signals upon BCR-ABL inhibition since addition of IL-3 to the culture disrupted IM-induced autophagy. Most importantly, IM-induced autophagy was observed only upon BCR-ABL inhibition; IM treatment did not induce autophagy in 32D cells transformed with the BCR-ABL^{T3151} mutant, a conformation refractory to IM. These results appeared to be in contrast with the very first observations from Ertmer and colleagues, suggesting that IM induces autophagy even in BCR-ABL negative cells [403]. However, we should highlight that in the publication from Ertmer and colleagues (i) IM was used at doses up to 20 μ M, a concentration 10- to 20-fold higher compared to the ones in the Bellodi paper, and (ii) the authors reported that inhibition of ABL, but not PDGFR or KIT, induced autophagy.

Thereafter, Bellodi and colleagues performed a series of experiments in order to answer the question: is IM-induced autophagy protecting from cell death? CQ-mediated autophagy inhibition enhanced the effects of IM in IM-sensitive but not IM-insensitive 32D cells, indicating that BCR-ABL inhibition induces autophagy as a survival mechanism. To further validate if autophagy protects CML cells from TKI-induced death, the key autophagy genes ATG7 and ATG5 were targeted by RNAi in K562 cells. Specific autophagy inhibition augmented IM treatment, further supporting that TKI-induced autophagy prevents drug-mediated cell death.

Subsequently, the authors investigated *in vitro* the role of autophagy in TKI-treated CD34+ cells from CML patients. Interestingly, CQ-mediated autophagy inhibition in combination with IM, DAS or NIL, suppressed the colony forming potential of CML CD34+ cells, including cells from patients carrying partially IM-resistant BCR-ABL mutants. Most significantly, pharmacological inhibition of autophagy enhanced the effect of IM and DAS in the most primitive fraction of CML HSCs, illustrated by reduction of colonies in LTC-IC assays. Overall, this publication demonstrated for the first time that cytoprotective autophagy is induced in CML cell lines and primary samples upon TKI-induced BCR-ABL inhibition.

Based on the data Bellodi and colleagues provided, CHOICES, a phase II Medical Research Council funded trial was initiated on March 2010 (and is currently ongoing). Despite the fact that in *in vitro* experiments described in the paper CQ was used for the pharmacological inhibition of autophagy, it was not the preferred autophagy inhibitor for the clinical trial because this drug has been associated with retinal toxicity [407]. Therefore, CQ was replaced in the clinic by HCQ, an agent with significantly lower toxicity, used extensively for the treatment of autoimmune diseases and malaria [408].

The aim of the CHOICES trial is to evaluate the responses of IM versus IM/HCQ for CML patients. Primary objectives of the trial include (i) providing preliminary evidence that the IM/HCQ combination is more effective than IM alone in terms of BCR-ABL levels in CML patients who are in major CyR with residual BCR-ABL+ cells after at least 12 months of IM treatment, and (ii) to determine the safety and tolerability of HCQ when given in combination with IM to patients.

In 2011, Altman and colleagues provided *in vivo* data further supporting the hypothesis behind the CHOICES clinical trial. The authors demonstrated that autophagy not only protects from TKI-induced cell death in established CML, but also plays an indispensable role in disease initiation. Transplantation of BCR-ABL-expressing HSCs where Atg3 was

conditionally knocked-out (KO) failed to induce leukaemia after transplantation to lethally irradiated mice.

This study was launched a few months following the publication of Bellodi and colleagues. The primary objective was to investigate whether or not the enhancement of TKI treatment in the presence of CQ or HCQ is principally through inhibition of autophagy. Both CQ and HCQ are not exclusive autophagy inhibitors and affect lysosome-associated cellular processes, including immunosuppression. Therefore, it cannot be excluded that their beneficial properties are attributed to off target effects on non-autophagic mechanisms. In order to override problems of non-specificity and give direct answers regarding the role of autophagy in the survival of CML cells, autophagy was specifically targeted by knocking-down the key autophagy gene *ATG7*.

As described earlier, in the study published by Bellodi and colleagues [323], IM induced autophagy in cells carrying BCR-ABL^{p210} but not in BCR-ABL^{T3151}; this suggests that induction of autophagy upon TKI treatment is due to inhibition of BCR-ABL. Nevertheless, induction of cytoprotective autophagy has been reported in CML cells following treatment with anti-CML agents that do not inhibit BCR-ABL; these include the histone deacetylase inhibitor SAHA [320], the dual mTORC1/2 inhibitor OSI-027 [326], the AKT inhibitor perifosine [329], as well as IFN α [409]. Hence, CQ/HCQ-mediated autophagy inhibition could prove beneficial for CML patient treatment based on non-TKI agents.

The maximum dose of HCQ currently used in most of the anticancer clinical trials, including CHOICES, is 800mg. Nonetheless, unpublished data from our collaborator Ravi Amaravadi suggest that administration of 800mg HCQ/day may not significantly inhibit autophagy in all patients, raising questions about the achievable levels of autophagy inhibition *in vivo* mediated by non-specific autophagy inhibitors. Consequently, ATG7 knock-down studies would also elucidate if ATG7 is a promising target for clinical use, especially since specific ATG7 inhibitors are in development [349]. Therefore, this study is original and important for the investigation of this novel approach in CML treatment, as well as for the role of autophagy in the survival of cancer cells.

The first part of this project included the investigation of the effects of TKIs on autophagy upon inhibition of BCR-ABL. Our data from the BC CML cell lines and CP CML CD34+ cells verify previously published observations, suggesting that IM and DAS induce autophagy [323, 410].

PON is a novel multitargeted TKI that in our experiments had high specificity against BaF3 cells carrying either BCR-ABL^{p210} or BCR-ABL^{T3151}, while not affecting parental

Ph- BaF3 cells. This is in agreement with previously published studies reporting that *in vitro* PON is effective against all tested BCR-ABL mutants that are refractory to IM, including the ones carrying the gatekeeper T315I mutation [227, 411, 412].

In the clinic PON has successfully progressed from a phase I [413], to the phase II PACE trial [229], and in July 2012 ARIAD announced the launch of the phase III EPIC trial for the investigational treatment of newly diagnosed CP CML adult patients with PON [230]. In December 2012, based on the auspicious results of the PACE trial, PON received FDA approval for clinical use in resistant or intolerant CML patients.

Recently, Cortes and colleagues [228] provided data supporting the *in vivo* efficacy of PON in heavily pretreated CML patients that had previously failed two or three first and second generation TKIs. Overall, PON has been reported to be potent against all BCR-ABL mutants and could potentially be the most effective TKI available in the clinic. Despite its effectiveness against all BCR-ABL mutants, PON treatment alone is unlikely to cure CML since the most refractory fraction of CML stem cells has been reported to survive and proliferate independent of BCR-ABL signaling [234, 235]. There have been no published papers so far monitoring the autophagy flow upon PON treatment of CML cells; this study is the first one to demonstrate that PON-mediated BCR-ABL inhibition induces autophagy in CML cells.

At the time this project was initiated, there were no published reports regarding the molecular mechanism by which TKI treatment induces autophagy. However, in 2011, Sheng and colleagues deciphered a part of this complex mechanism [324]. They suggested that under steady state conditions BCR-ABL is suppressing autophagy via activation of the ATF5 transcription factor and mTOR. However, treatment with IM inhibits BCR-ABL signaling and therefore, suppresses the ATF5/mTOR pathway, leading to induction of autophagy (Figure 6-1). This mechanism is in agreement with data presented in this report, demonstrating induction of autophagy upon IM-, DAS- and PON-mediated BCR-ABL inhibition, and possibly explains why in the hereby-described experiments Ph⁺ CD34⁺ cells had lower levels of autophagy gene transcription under steady state conditions compared to Ph⁻ CD34⁺ cells. Furthermore, it should be mentioned that other members in our lab have demonstrated that TKIs lead to upregulation of the transcription of autophagy genes in CP CML CD34⁺ cells compared to NDC (unpublished data).

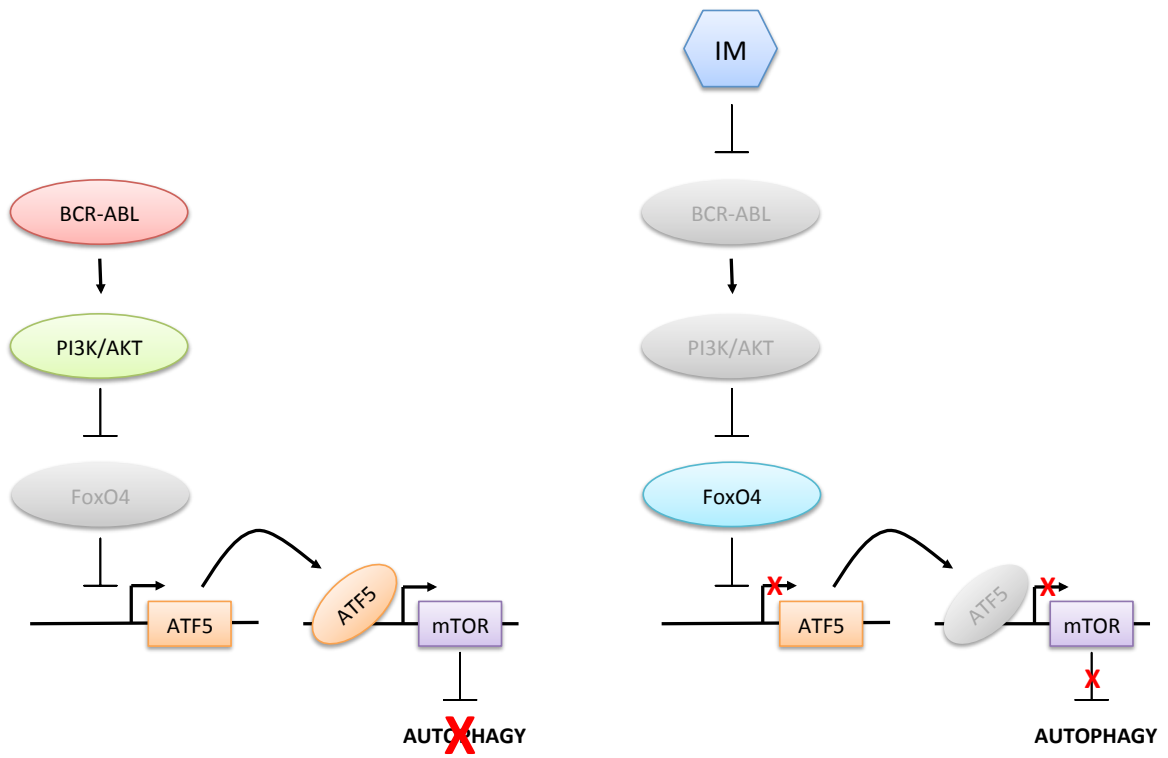


Figure 6-1: The BCR-ABL/PI3K/AKT/FOXO4/ATF5/mTOR-mediated autophagy-inhibition pathway

Fading of a protein indicates loss of function. (Modified from [324])

Our data from the BC CML cell lines and CP CML CD34+ cells suggest that autophagy plays a cytoprotective role in CML and its suppression via CQ/HCQ enhances TKI treatment (Figure 6-2). These observations are in agreement with reports previously published by our [323] and other labs [322, 325, 328].

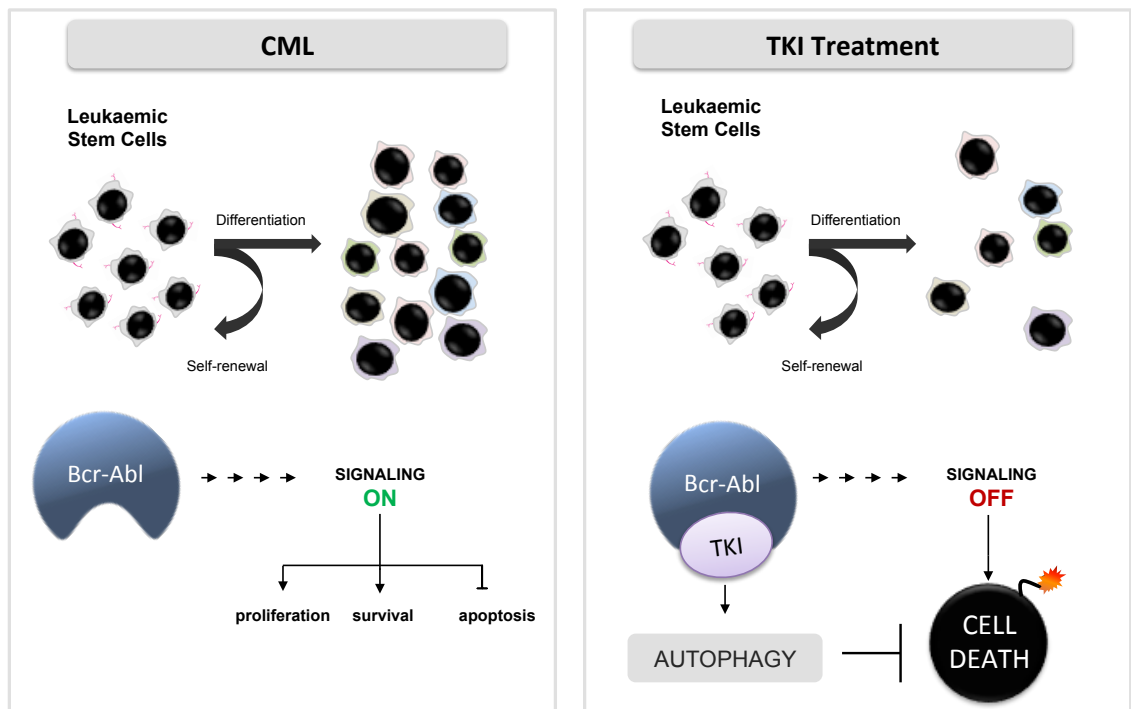


Figure 6-2: Induction of cytoprotective autophagy upon TKI-treatment of CML cells

On the other hand, a number of studies support that autophagy induction mediated by non-TKI investigational agents is enhancing CML cell death. Reagents such as acadesine [414], the plant phytoalexin resveratrol [331] and lapatinib (dual TKI of EGFRs and HER2) [415] have been suggested to increase the apoptosis of CML cells via induction of autophagy. Nevertheless, it has not been clarified yet if the chemotherapeutic effect of these agents is the critical mechanism of action of these reagents and further investigation has to be carried out before supporting the up-regulation of autophagy for the treatment of CML. Recently, Goussetis and colleagues [416] suggested that autophagy induction mediated by arsenic trioxide enhances the drug's effects via degradation of BCR-ABL in the cells of CML patients. It would be interesting, therefore, to investigate the levels of BCR-ABL protein in autophagy-ablated CML cells; blockade of the autophagy recycling mechanism could lead to accumulation of BCR-ABL and hence, lead to toxic death of the cells. Autophagic targeting of specific proteins has been implicated with cancer cell survival; Sandilands and colleagues [417] reported that upon disruption of FAK signalling, c-Cbl mediates the autophagic targeting of Src to a Src/LC3 complex. Inhibition of autophagy restores Src at peripheral adhesions, and ultimately leads to cancer cell death.

A growing number of published studies are highlighting the significance of the PI3K/AKT/mTOR pathway in the survival of TKI-refractory CML cells. Hence, an alternative approach for the treatment of leukaemic cells includes inhibition of the PI3K/AKT/mTOR pathway by using drugs such as RAPA and BEZ. Nevertheless, since these drugs inhibit mTOR, they ultimately induce autophagy. This was also demonstrated by our experiments, where treatment with RAPA or BEZ IC₅₀ values was associated with accumulation of LC3-positive punctae in the CD34⁺ cells of CP CML patient.

A recent study by Bray and colleagues [353] suggests that activation of autophagy upon mTOR inhibition enables the survival of cancer cells by suppressing RIP kinase-dependent necrosis and promoting cellular integrity by ROS reduction, since mTOR inhibition abolishes NRF2 antioxidant defense. In order to investigate if inhibition of autophagy could potentiate the effects of these drugs, apoptosis was measured in KCL22^{T3151} cells treated with PON, BEZ or RAPA ± CQ. PON, which can target the BCR-ABL^{T3151} mutants, significantly enhanced apoptosis and CQ further augmented its effect. Interestingly, CQ-mediated autophagy inhibition enhanced the apoptotic effect of both RAPA and BEZ (used in proliferation IC₅₀ concentrations), with BEZ/CQ having the most auspicious effects among all the treatment arms. These observations highlight the promising role of these drugs in the treatment of CML. Further experiments should be

carried out to identify RAPA and BEZ concentrations that completely inhibit mTOR activity, and investigate the effect of these concentrations in the proliferation, survival and clonogenic ability of CML cells carrying the T315I mutation.

One of the greatest challenges when designing knock-down experiments within stem and progenitor cells, is the technical part. First of all these cells are hard to transfect and secondly, the number of cells available for experiments is limited. Different gene silencing techniques are linked to different advantages and disadvantages, efficacy, reliability and safety, which can be altered depending on the type of cell. Therefore, a major factor in the success of our experiments relied on choosing the best fitting gene silencing method for CD34⁺ cells, and optimising it for the scope of our experiments. The hairpins we used (mock and targeting) were carried by a pLKO.1 vector under the expression of a U6 promoter, establishing long-term knock-down. Western blot analysis on shATG7_E-transduced cells 24-48h post-sort revealed a 60-70% reduction in ATG7 levels and 25% reduction in LC3 lipidation. A study by Komatsu and colleagues has reported that ATG7 is a long-lived protein with a half-life of approximately a week [418]. Hence, it is possible that if we had performed the analysis at a later point we could have detected even lower levels of ATG7 protein and LC3 lipidation.

In this study we first demonstrate the dependence of CML stem/progenitor cells on basal levels of ATG7 for their proliferation and survival; ATG7 knock-down alone significantly inhibited the proliferation of CP CML CD34⁺ cells and induced apoptosis at comparable levels to TKI treatment. The committed progenitor cell potential of CD34⁺ cells from CP CML patients was also reduced consistently at levels $\geq 50\%$ compared to the control, suggesting that basal ATG7 and autophagy levels are required for the clonogenicity of the cells.

These observations pinpoint the importance of autophagy for the survival of cancer cells under steady state conditions. Cancer cells have been reported to have altered nutritional requirements and increased metabolic needs [419]. This could possibly justify partially the addiction of CML stem/progenitor cells to basal autophagy for survival. Interestingly, our data suggest that CML cells express lower basal levels of ATG7 compared to non-CML CD34⁺ cells. This could partially explain why similar levels of ATG7 knock-down have a significant impact on CML cells and not Ph- CD34⁺ cells.

The differentiation potential of shATG7_E-transduced CML CD34⁺ cells was also altered, compared to the control. ATG7 knock-down-mediated autophagy inhibition was associated with an approximate 75% decrease in the erythroid colony-formation potential of the cells. Autophagy has been reported to be essential for the maturation of erythroid cells through

the promotion of mitochondrial clearance [420] and recently, ATG7 was demonstrated to be essential for the maturation and maintenance of the cellular integrity of erythroid cells [375, 421]. In our experiments, it remains unclear if ATG7 knock-down (i) drove differentiation of CML CD34⁺ stem/progenitor cells, or (ii) preferentially eradicated or suppressed the maturation of cells committed to erythroid lineage. Future studies will shed more light on these questions.

In any case, our observations on the proliferation, survival and differentiation of CML CD34⁺ cells upon ATG7 knock-down have to be further validated by knock-down studies of other indispensable ATG genes since our data cannot exclude a potential dependence on autophagy-independent roles of ATG7.

Autophagy and ATG7 have been suggested to be vital for the maintenance of embryonic and adult HSCs; loss of autophagy within this fraction of cells has been demonstrated to lead to severe anaemia, lymphopenia, haemopoietic malignancies and exhaustion of the stem cell population. In 2011 Liu and colleagues reported that FIP200 is vital for the function and maintenance of foetal murine HSCs in a cell-autonomous manner [422]. HSCs with ablated FIP200 presented high levels of proliferation, increased mitochondrial mass and ROS levels, and failed to reconstitute haemopoiesis in lethally irradiated mice. Subsequently, Mortensen and colleagues reported that adult Atg7-deficient HSCs fail to engraft lethally irradiated recipients, further underlining the significance of autophagy in HSC maintenance [355]. Recently, similar observations were made upon KO of Atg5 [423]. Thus, a range of experiments was designed in our study in order to investigate if the therapeutic approach of combined TKI/autophagy inhibition could affect Ph- haemopoietic stem/progenitor cells.

Our data are in contrast to the above mentioned published studies. Our observations suggested that ATG7 knock-down, alone or in combination with TKIs, did not significantly affect the proliferation, survival, and clonogenic ability of Ph- CD34⁺ cells. However, it should be underlined that there is a major difference between KO and knocking-down a gene. KO of any key autophagy genes leads to complete ablation of the targeted protein and almost 100% inhibition of LC3 lipidation. In our experiments we used a knock-down approach that resulted in 70% reduction of ATG7 at protein level and 25% reduction of LC3 lipidation. This could explain why in our system the normal HSCs were not affected by ATG7 knock-down. However, our data cannot exclude a possible loss of the stemness within the primitive cells, followed by extended proliferation. In order to address this question robustly, we performed LTC-IC assays on shCtrl and shATG7_E-transduced Ph⁺ and Ph- CD34⁺ cells. Nevertheless, due to technical problems, the cells

failed to give colonies at the end of the assay (in both control and ATG7 knock-down). Future studies should focus on the evaluation of ATG7 knock-down effects on the most primitive population of Ph⁻ and Ph⁺ HSCs, either by LTC-IC or serial replating assays.

Apoptosis is a programmed cell process, associated with a range of biochemical and cellular changes. Unlike apoptosis, necrosis is a less regulated and controlled procedure, and its patterns change according to the factor that triggered the mechanism. In 2006, Degenhardt and colleagues [396] demonstrated that inhibition of autophagy in apoptosis-defective cells could restore cell death by inducing necrosis, *in vitro* and *in vivo*. Hence, it was suggested that the cytoprotective role of autophagy in cancer cells might be attributed to the ablation of necrotic cell death. Furthermore, in 2008 Wu and colleagues [424] provided evidence supporting that pharmacological inhibition of autophagy can enhance zVAD-induced necrosis. Finally, a recent study by Bray and colleagues [353] suggested that increase in autophagic flow upon mTOR inhibition supports cell survival and autophagy inhibition allows for necroptosis. Altogether, these studies suggest that in the presence of defective apoptosis, cancer cells rely on autophagy for their survival; inhibition of autophagy leads to a “metabolic catastrophe”, where the cells cannot overcome stress and die by necrosis [425]. This could explain why in our experiments ATG7 knock-down did not enhance TKI-induced apoptosis in CML CD34⁺ cells. Specific targeting of autophagy in a BCR-ABL-inhibited background could lead to a disproportional increase of necrotic versus apoptotic cell death. Hence, for future experiments, it would be recommended to also monitor necrosis, in addition to apoptosis.

Data from this study demonstrate that ATG7 knock-down significantly augments TKI treatment regarding the suppression of colony forming ability of CML CD34⁺ cells. The combination of TKI/ATG7 knock-down reduced by 92-98% the potential of CP CML CD34⁺ cells to form colonies, compared to NDC shCtrl cells. These observations suggest that within CML CD34⁺ cells TKI-mediated autophagy induction is important for evading cell death upon inhibition of BCR-ABL signaling.

In order to evaluate the effect of specific autophagy inhibition in the presence of prolonged TKI exposure, CML CD34⁺ stem/progenitor cells were cultured for 2 weeks in semi-solid medium containing NIL, DAS or PON. Interestingly, the number of colonies within the prolonged TKI treatment arms was higher compared to that followed by 6-day TKI treatment. This could be attributed to deactivation of the TKIs' activity in the semi-solid medium before the completion of the assay (14 days). Even so, the effects of all TKIs tested were augmented in the presence of ATG7 knock-down, suppressing by 82-91% the clonogenic potential of these cells compared to NDC shCtrl cells.

Overall, our experiments demonstrate the significance of basal autophagy for the survival, proliferation and differentiation potential of the CML stem/progenitor cells under steady state conditions. Furthermore, we illustrate that ATG7 knock-down and inhibition of autophagy in the presence of TKIs, potentiate treatment and enhance TKI effects. Nevertheless, TKIs failed to completely eradicate the colony forming potential of the progenitor cells alone or in combination with ATG7 knock-down. FACS analysis of such colonies revealed that the cells expressed GFP, suggesting that the shRNA hairpins were expressed. Therefore, supplementary investigation should be carried out for the characterisation of the cells that evade both autophagy and BCR-ABL inhibition. A possible explanation could be that within these cells autophagy was not sufficiently inhibited due to lower levels of ATG7 knock-down.

Autophagy has been suggested to be vital for the maintenance and differentiation of stem cells [356, 426]. A recent study by Oliver and colleagues [427] proposed that stem cells have high levels of autophagy while differentiated cells have very low levels of basal autophagy. Preliminary studies from our lab are in agreement with these data; from our observations, CD34⁻ cells have lower levels of autophagy compared to CD34⁺ cells. It should be mentioned that within CD34⁺ cells of a CML patient we observed that even if ATG7 knock-down did not induce apoptosis, the percentage of CD34⁺ cells within the double negative annexin/DAPI compartment was decreased compared to the control (data not shown). Further investigation is required in order to elucidate if this reduction in CD34⁺ cells upon ATG7 knock-down is attributed to cell cycle arrest, differentiation or cell death. A potential explanation could be that ATG7 knock-down and inhibition of autophagy lead to eradication of primitive cells because they gravely depend on this mechanism for their survival. On the other hand, autophagy inhibition would not equally affect more differentiated cells under stress free conditions, since these cells do not exclusively rely on autophagy for their survival. In order to answer these questions, stem cell assays, such as LTC-IC, should be performed in order to evaluate the effect of ATG7 knock-down in the presence of TKIs and investigate if this therapeutic approach can eliminate the persistent CML stem cells.

Autophagy has been suggested to interplay with many cellular processes, including cell death (apoptosis and necrosis), differentiation [357-362] and stem cell maintenance [355, 422, 426] (Figure 6-2).

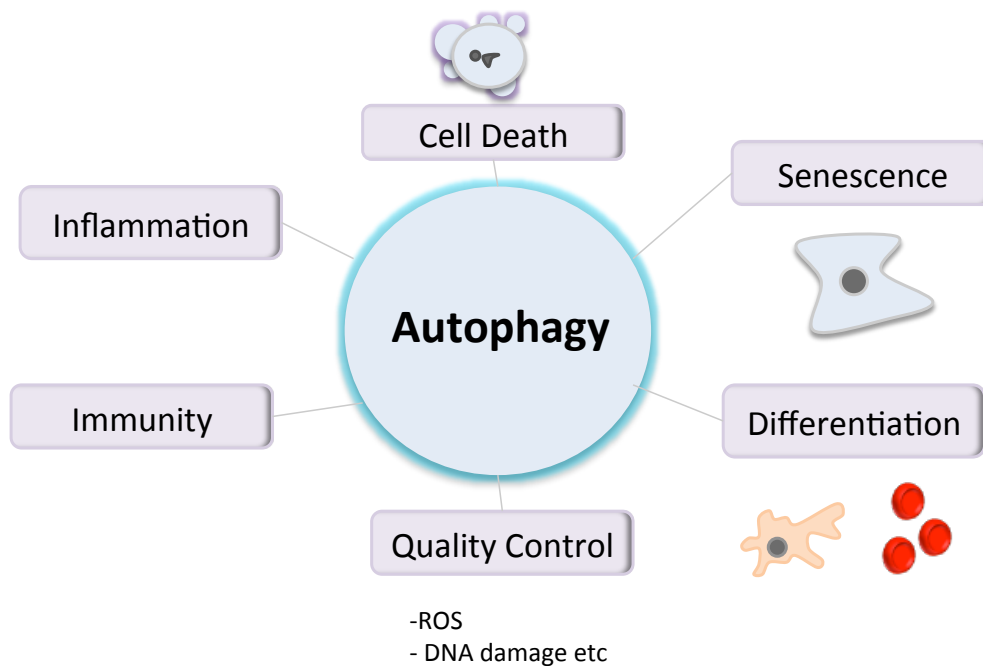


Figure 6-3: Autophagy takes part in many cellular processes

Previous experiments demonstrated the importance of ATG7 and autophagy for the survival and differentiation of CP CML cells. Hence, in this section we aimed to explore the cell fate decisions of BC leukaemic cells upon ATG7 knock-down.

As a model of BC CML study, the human myelomonocytic cell line KCL22 was employed. Surprisingly, ATG7 proved to be indispensable for the survival of these cells and the complete population of shATG7_E transduced cells was rapidly eradicated upon ATG7 knock-down. Similarly, the total population of murine c-kit enriched MLL-ENL-transformed cells died upon inhibition of Atg7. Further investigation should be carried out regarding the mechanisms of cell death induction upon ATG7 knock-down.

Subsequently, ATG7 was knocked-down in K562 cells, a BC CML erythromegakaryocytic cell line. K562 cells transduced with shATG7_E presented $\geq 60\%$ reduced ATG7 protein levels compared to the control and their ability to proliferate was severely impaired. Furthermore, cell survival was significantly affected, with $\sim 70\%$ of the ATG7 knock-

down cells staining positive for DAPI. Interestingly, K562 cells that survived ATG7 knock-down 12 days post-sort were producing higher levels of haemoglobin and GlyA compared to the control, suggesting that the cells were more differentiated and committed to the erythroid lineage. However, as mentioned earlier, autophagy and ATG7 have been reported to be essential for the erythroid differentiation. Morphologic examination of K562 shATG7_E-transduced cells after staining with “Diff Quik” revealed that the cells did not present erythroid cell features. Failure of K562 cells to terminally differentiate upon ATG7 knock-down could be attributed to suppressed mitophagy and inability to clear the mitochondria (a vital step for reticulocyte maturation), since these cells presented accumulation of mitochondria. Remarkably, a fraction of K562 cells that survived prolonged ATG7 knock-down (4 weeks), presented morphologically megakaryocytic features, had altered adhesion properties, and produced elevated levels of ROS. Sardina and colleagues [377] suggested that increased ROS levels are necessary for the megakaryocytic differentiation of K562. Hence, a possible hypothesis is that upon ATG7 knock-down, mitophagy is inhibited and a subsequent increase in ROS levels could favour the megakaryocytic differentiation of the cells.

These experiments could not answer if ATG7 knock-down is the driver of the observed erythroid/megakaryocytic differentiation of the K562 cells, or if it is “selecting” for more differentiated cells within the initial culture. Hence, the survival and differentiation potential upon ATG7 knock-down was investigated at the single-cell level, by sorting shATG7_E and shCtrl K562 cells into single wells. The results suggested that less than 20% of K562 cells managed to survive and proliferate upon ATG7 knock-down, compared to the control. Interestingly, all the clones generated within the ATG7 knock-down arm presented either erythroid or megakaryocytic features. Erythroid clones consisted of significantly higher cell numbers compared to the megakaryocytic clones, and this difference in proliferation kinetics could possibly explain why upon ATG7 knock-down K562 cells with erythroid features precede the appearance of cells with megakaryocytic features. On the other hand, none of the clones produced by shCtrl cells presented features of differentiation. This is in support with the notion that ATG7 knock-down promotes the differentiation observed in K562 cells; however, more experiments have to be carried out in order to clarify this. Both hypotheses are very interesting to study; if autophagy interplays with differentiation, the underlying mechanism of the crosstalk has not been investigated. On the other hand, if these ATG7 "survivors" pre-existed and they manage to outgrow, it is important to investigate why these cells can survive and proliferate with accelerated rates in the absence of ATG7 and/or autophagy.

Stem cells have been reported to differentiate upon increased levels of ROS and DNA damage [428]. In our experiments ATG7 knock-down was linked to increased levels of ROS. Hence, it would be interesting to perform assays evaluating the cellular integrity by means of mitochondrial potential, levels of ROS and DNA damage on K562 ATG7 knock-down cells. Finally, future studies should elucidate if ATG7 knock-down is directly implicated in the differentiation process or ATG7/autophagy suppression is abolishing the differentiation block these BC cells present and consequently, allows for their differentiation.

In order to investigate the role of ATG7 and autophagy in other transformed leukaemic cells, ATG7 was knocked down in HG3 cells, a human CLL cell line. Reduction of ATG7 protein to $\geq 50\%$ levels was associated with significantly suppressed proliferation and increased cell death, underlining the significance of ATG7 and autophagy for the survival of these cells. Interestingly, HG3 cells surviving for 15 days ATG7 knock-down presented a very different phenotype compared to the control; HG3 shATG7_E cells had increased cell size, prominent Golgi apparatus and presented cytoplasmic blebbing (pseudopods). Moreover, HG3 shATG7_E cells had altered cell-to-cell adhesion features and were growing in culture as single cells, unlike the shCtrl cell that were growing in clusters. This observation, in combination with the fact that K562 shATG7_E cells were partially attaching to the substrate, reflects that ATG7 knock-down may be associated with changes in the cytoskeleton.

Taken altogether, ATG7 and autophagy appear to affect the cell fate decisions of transformed human leukaemic cells. Survival of these cells relies significantly on ATG7 and its inhibition, as a single event, was consistently associated with a dramatic increase in cell death. The dependence of transformed cells lines on ATG7/autophagy appeared to be greater compared to CML CD34+ stem/progenitor cells, but this may reflect differences in metabolic needs due to higher proliferation rates.

Future studies should focus on knock-down of other ATGs within leukaemic cells and clarify if the observed differentiation upon ATG7 knock-down is attributed to inhibition of autophagy or other non-autophagy related roles of ATG7. A possible explanation could be that the observed molecular, biochemical and morphological changes in BC cells upon ATG7 knock-down reflect inhibition of differentiation arrest rather than induction of differentiation *per se*. Additionally, the role of ATG7 knock-down should be investigated within non-transformed cells in order to identify if this protein is affecting the differentiation of normal cells.

6.3 Summary and future directions

The findings from the present study demonstrate that all three generation TKIs (IM, DAS and PON) induce cytoprotective autophagy upon inhibition of BCR-ABL and pharmacological inhibition of autophagy via CQ or HCQ potentiates the effects of TKIs.

Most importantly, this study first demonstrates that specific targeting of basal autophagy in CP CML CD34⁺ cells via ATG7 knock-down significantly impairs their survival, proliferation and differentiation. ATG7 knock-down reduced the total number of CP CML CD34⁺ colonies (50%) as well the relative number of erythroid colonies (75%) compared to the control. Interestingly, ATG7 knock-down enhanced TKI-induced effects, eradicating 98% of the clonogenic ability of CP CML stem and progenitors compared to the control. Future studies should focus on the most primitive fraction of the CML stem cells and evaluate the effects of autophagy inhibition, alone or in combination with TKIs. However, knocking-down ATG7 or any other indispensable autophagy gene *in vitro* has two main drawbacks: (i) technically achievable knock-down levels do not completely abolish autophagy and residual autophagy levels may be sufficient for cell survival, and (ii) the cells are investigated under optimum, controlled conditions that differ considerably from the hypoxic niche of HSCs *in vivo*. It would be interesting to investigate in *in vivo* mouse models if Atg7 knock-out HSCs (i) will repopulate the haemopoiesis of NOD/SCID mice, (ii) will lead to development of CML upon expression/transduction with Bcr-Abl, and if yes, if the disease will progress with faster or slower rates.

Nevertheless, our results reveal a contradictory role for ATG7 in the differentiation of CML cells; ATG7 knock-down suppressed the erythroid differentiation of CP CML cells, while within BC cells it promoted differentiation. This possibly reflects the different roles of ATG7 and/or autophagy within different stages of the disease or the technical cell differences between primary samples and immortalised cell lines (such as BCR-ABL copy number, presence of secondary mutation etc). More specifically, it has to be clarified if the observed erythroid differentiation of K562 cells upon ATG7 knock-down is attributed to a “true” induction of differentiation or release of blocks that inhibit differentiation in BC cells.

ATG7 knock-down surviving cells had high levels of superoxide and increased numbers of functional mitochondria, potentially due to inhibition of mitophagy. It would be interesting to further characterise the mitochondrial profile of these cells, as well as monitor cellular integrity by means of DNA damage. Such changes have been associated in other studies with initiation of differentiation and, could be the case here. For example, it should be explored if NAC-mediated ROS reduction can abolish differentiation upon ATG7 knock-

down. Another suggestion would be to transduce the cells with inducible ATG7-hairpin and explore if the ATG7 knock-down-induced differentiation is reversible upon recovery of ATG7 levels. Most importantly, it should be further investigated if the observed effects on cell differentiation upon ATG7 knock-down are attributed to reduced autophagy levels or ATG7 autophagy-independent roles. Hence, these experiments should be validated by knock-down other ATG genes, such as ATG5 or BECLIN.

In conclusion, the data we provide in this study suggest that basal autophagy is indispensable for the survival of CP CML cell and inhibition of TKI-induced autophagy can augment therapy. Therefore, the development of specific autophagy inhibitors is critical since, in combination with TKIs, they could potentially lead to eradication of CML stem cells and cure of the disease. Further studies are required for the unravelling of the mechanism by which autophagy inhibition sensitises CML cells to TKIs.

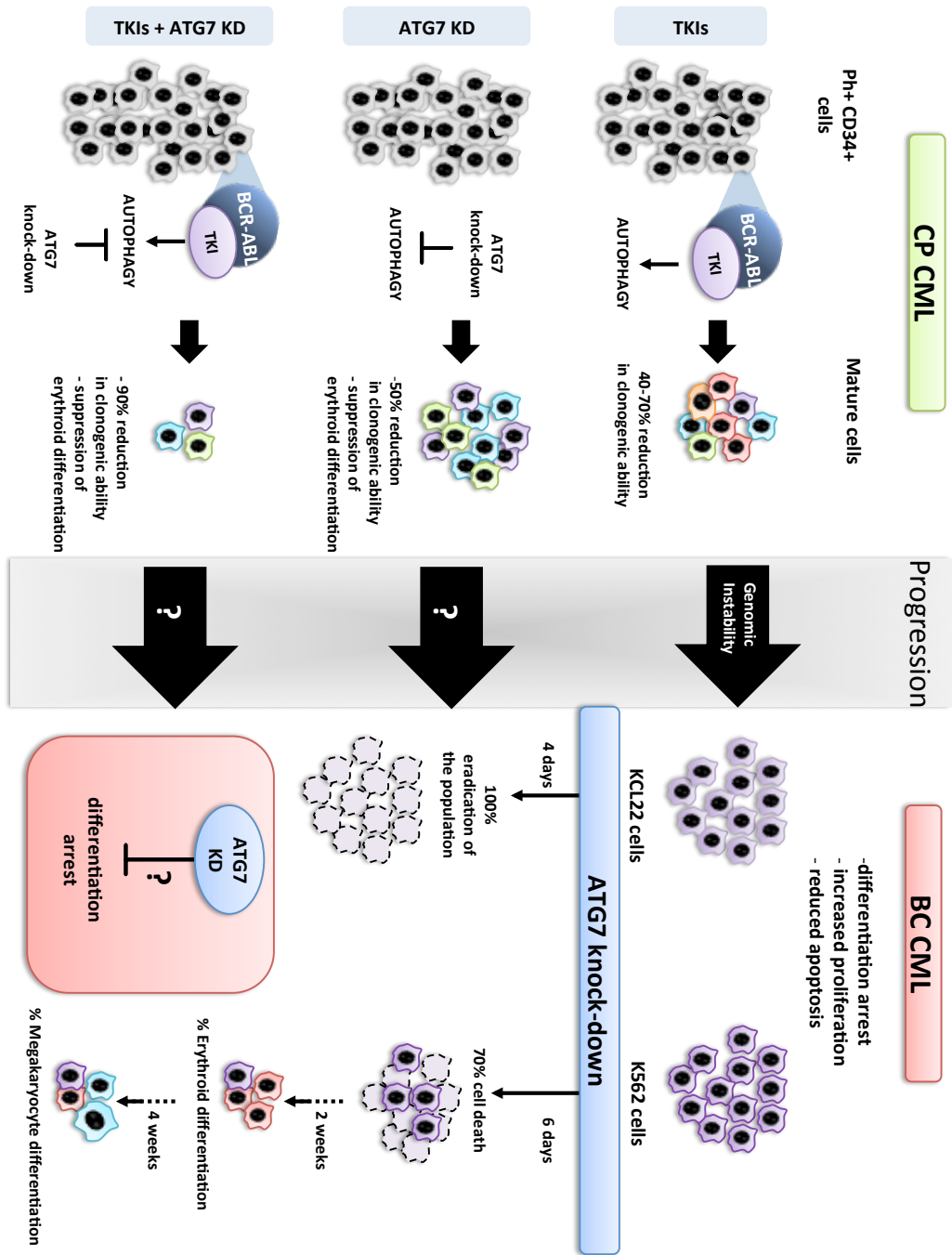
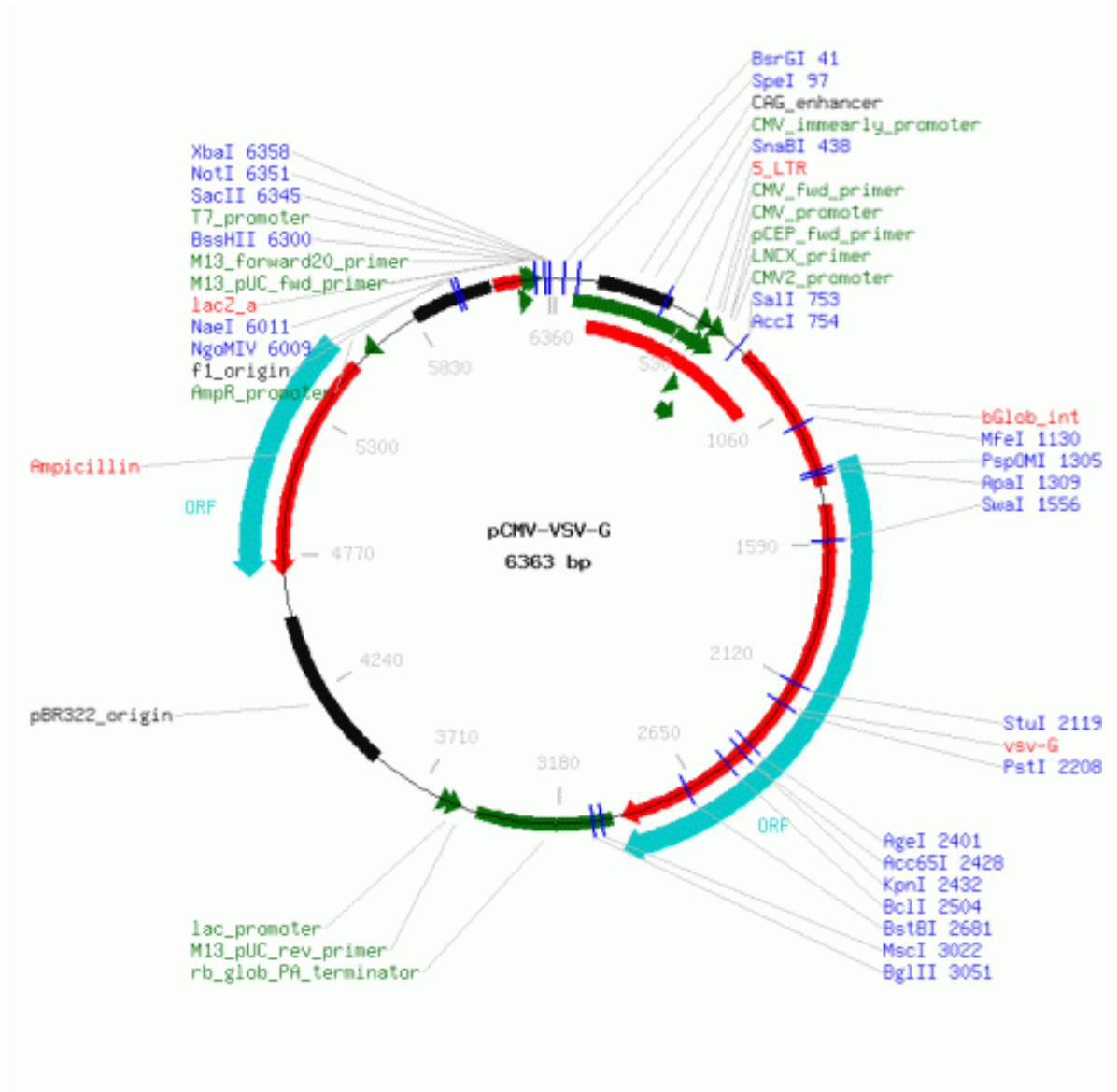
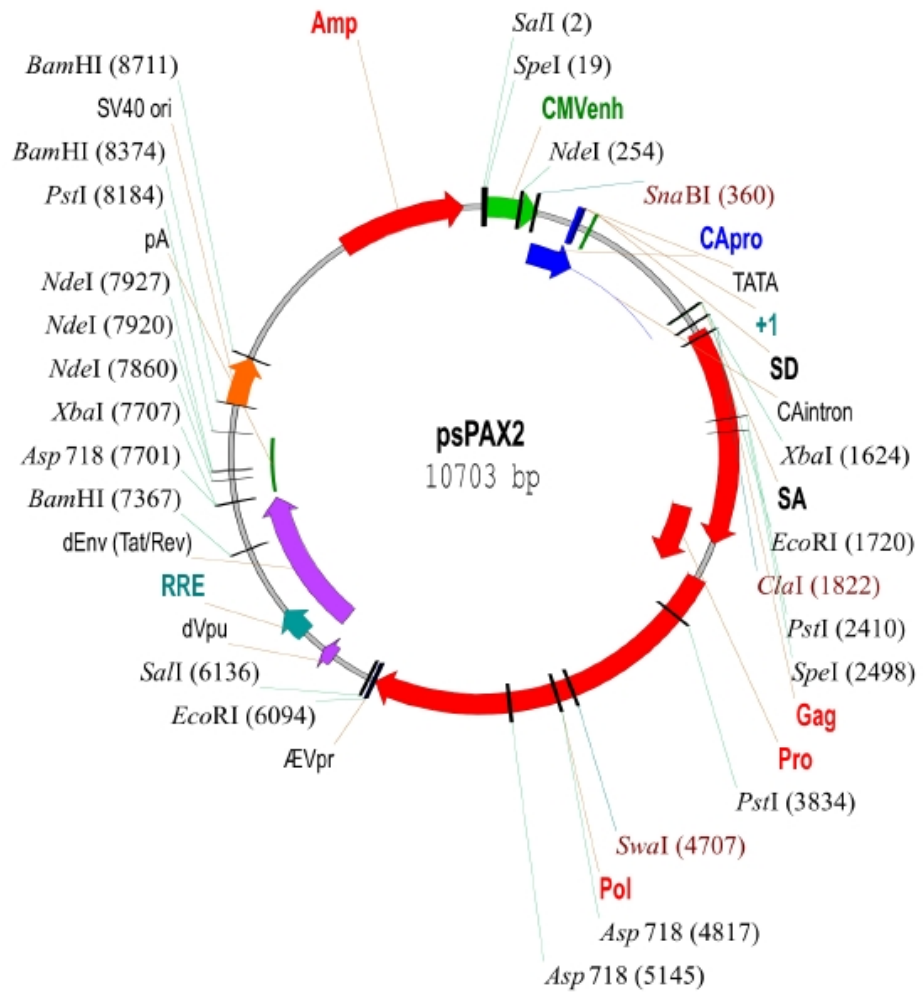
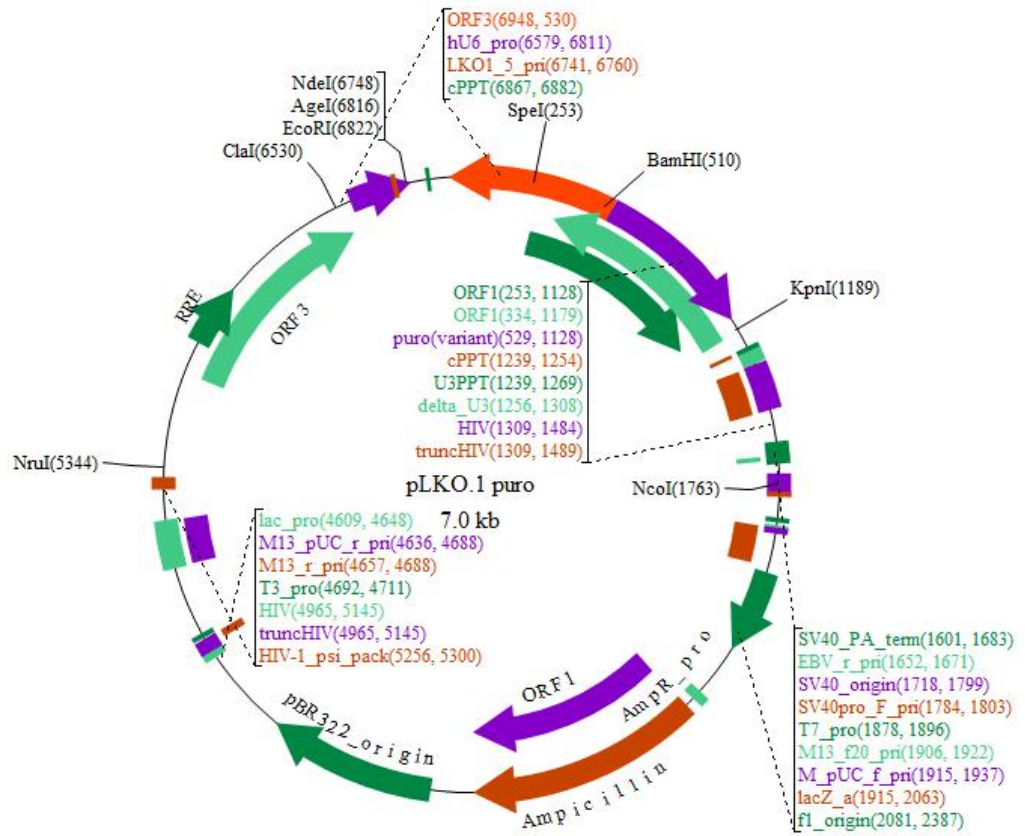


Figure 6-4: Overview of the observed effects upon ATG7 knock-down in CP and BC CML cells

Appendix







List of References

1. Passegue, E., et al., *Global analysis of proliferation and cell cycle gene expression in the regulation of hematopoietic stem and progenitor cell fates*. *J Exp Med*, 2005. 202(11): p. 1599-611.
2. Spangrude, G.J., S. Heimfeld, and I.L. Weissman, *Purification and characterization of mouse hematopoietic stem cells*. *Science*, 1988. 241(4861): p. 58-62.
3. Morrison, S.J. and I.L. Weissman, *The long-term repopulating subset of hematopoietic stem cells is deterministic and isolatable by phenotype*. *Immunity*, 1994. 1(8): p. 661-73.
4. Baum, C.M., et al., *Isolation of a candidate human hematopoietic stem-cell population*. *Proc Natl Acad Sci U S A*, 1992. 89(7): p. 2804-8.
5. Osawa, M., et al., *Long-term lymphohematopoietic reconstitution by a single CD34-low/negative hematopoietic stem cell*. *Science*, 1996. 273(5272): p. 242-5.
6. Muller, A.M., et al., *Development of hematopoietic stem cell activity in the mouse embryo*. *Immunity*, 1994. 1(4): p. 291-301.
7. Morrison, S.J., N. Uchida, and I.L. Weissman, *The biology of hematopoietic stem cells*. *Annu Rev Cell Dev Biol*, 1995. 11: p. 35-71.
8. Orkin, S.H., *Diversification of haematopoietic stem cells to specific lineages*. *Nat Rev Genet*, 2000. 1(1): p. 57-64.
9. Marley, S.B. and M.Y. Gordon, *Chronic myeloid leukaemia: stem cell derived but progenitor cell driven*. *Clin Sci (Lond)*, 2005. 109(1): p. 13-25.
10. Schofield, R., *The relationship between the spleen colony-forming cell and the haemopoietic stem cell*. *Blood Cells*, 1978. 4(1-2): p. 7-25.
11. Sutherland, H.J., et al., *Characterization and partial purification of human marrow cells capable of initiating long-term hematopoiesis in vitro*. *Blood*, 1989. 74(5): p. 1563-70.
12. Sutherland, H.J., et al., *Functional characterization of individual human hematopoietic stem cells cultured at limiting dilution on supportive marrow stromal layers*. *Proc Natl Acad Sci U S A*, 1990. 87(9): p. 3584-8.
13. Wang, J.C., M. Doedens, and J.E. Dick, *Primitive human hematopoietic cells are enriched in cord blood compared with adult bone marrow or mobilized peripheral blood as measured by the quantitative in vivo SCID-repopulating cell assay*. *Blood*, 1997. 89(11): p. 3919-24.
14. Morrison, S.J., et al., *Identification of a lineage of multipotent hematopoietic progenitors*. *Development*, 1997. 124(10): p. 1929-39.
15. Suda, T., J. Suda, and M. Ogawa, *Proliferative kinetics and differentiation of murine blast cell colonies in culture: evidence for variable G0 periods and constant doubling rates of early pluripotent hemopoietic progenitors*. *J Cell Physiol*, 1983. 117(3): p. 308-18.
16. Leary, A.G., et al., *Survival of hemopoietic progenitors in the G0 period of the cell cycle does not require early hemopoietic regulators*. *Proc Natl Acad Sci U S A*, 1989. 86(12): p. 4535-8.
17. Leary, A.G., et al., *Growth factor requirements for survival in G0 and entry into the cell cycle of primitive human hemopoietic progenitors*. *Proc Natl Acad Sci U S A*, 1992. 89(9): p. 4013-7.
18. Vickers, M., et al., *Modelling haemopoietic stem cell division by analysis of mutant red cells*. *Br J Haematol*, 2000. 110(1): p. 54-62.

19. Terstappen, L.W., et al., *Sequential generations of hematopoietic colonies derived from single nonlineage-committed CD34+CD38- progenitor cells*. *Blood*, 1991. 77(6): p. 1218-27.
20. DiGiusto, D., et al., *Human fetal bone marrow early progenitors for T, B, and myeloid cells are found exclusively in the population expressing high levels of CD34*. *Blood*, 1994. 84(2): p. 421-32.
21. Link, H., et al., *Transplantation of allogeneic CD34+ blood cells*. *Blood*, 1996. 87(11): p. 4903-9.
22. Krause, D.S., et al., *CD34: structure, biology, and clinical utility*. *Blood*, 1996. 87(1): p. 1-13.
23. Kung, P., et al., *Monoclonal antibodies defining distinctive human T cell surface antigens*. *Science*, 1979. 206(4416): p. 347-9.
24. Hogan, C.J., E.J. Shpall, and G. Keller, *Differential long-term and multilineage engraftment potential from subfractions of human CD34+ cord blood cells transplanted into NOD/SCID mice*. *Proc Natl Acad Sci U S A*, 2002. 99(1): p. 413-8.
25. Trumpp, A., M. Essers, and A. Wilson, *Awakening dormant haematopoietic stem cells*. *Nat Rev Immunol*, 2010. 10(3): p. 201-9.
26. Sipkins, D.A., et al., *In vivo imaging of specialized bone marrow endothelial microdomains for tumour engraftment*. *Nature*, 2005. 435(7044): p. 969-73.
27. Calvi, L.M., et al., *Osteoblastic cells regulate the haematopoietic stem cell niche*. *Nature*, 2003. 425(6960): p. 841-6.
28. Zhang, J., et al., *Identification of the haematopoietic stem cell niche and control of the niche size*. *Nature*, 2003. 425(6960): p. 836-41.
29. Yoshihara, H., et al., *Thrombopoietin/MPL signaling regulates hematopoietic stem cell quiescence and interaction with the osteoblastic niche*. *Cell Stem Cell*, 2007. 1(6): p. 685-97.
30. Kiel, M.J. and S.J. Morrison, *Maintaining hematopoietic stem cells in the vascular niche*. *Immunity*, 2006. 25(6): p. 862-4.
31. Lo Celso, C., et al., *Live-animal tracking of individual haematopoietic stem/progenitor cells in their niche*. *Nature*, 2009. 457(7225): p. 92-6.
32. Bonnet, D. and J.E. Dick, *Human acute myeloid leukemia is organized as a hierarchy that originates from a primitive hematopoietic cell*. *Nat Med*, 1997. 3(7): p. 730-7.
33. Visvader, J.E. and G.J. Lindeman, *Cancer stem cells in solid tumours: accumulating evidence and unresolved questions*. *Nat Rev Cancer*, 2008. 8(10): p. 755-68.
34. Reya, T., et al., *Stem cells, cancer, and cancer stem cells*. *Nature*, 2001. 414(6859): p. 105-11.
35. Ito, M., et al., *NOD/SCID/gamma(c)(null) mouse: an excellent recipient mouse model for engraftment of human cells*. *Blood*, 2002. 100(9): p. 3175-82.
36. Passegue, E., et al., *Normal and leukemic hematopoiesis: are leukemias a stem cell disorder or a reacquisition of stem cell characteristics?* *Proc Natl Acad Sci U S A*, 2003. 100 Suppl 1: p. 11842-9.
37. Turhan, A.G., et al., *Highly purified primitive hematopoietic stem cells are PML-RARA negative and generate nonclonal progenitors in acute promyelocytic leukemia*. *Blood*, 1995. 85(8): p. 2154-61.
38. Cozzio, A., et al., *Similar MLL-associated leukemias arising from self-renewing stem cells and short-lived myeloid progenitors*. *Genes Dev*, 2003. 17(24): p. 3029-35.
39. Jamieson, C.H., et al., *Granulocyte-macrophage progenitors as candidate leukemic stem cells in blast-crisis CML*. *N Engl J Med*, 2004. 351(7): p. 657-67.

40. Deshpande, A.J., et al., *Acute myeloid leukemia is propagated by a leukemic stem cell with lymphoid characteristics in a mouse model of CALM/AF10-positive leukemia*. *Cancer Cell*, 2006. 10(5): p. 363-74.
41. Kirstetter, P., et al., *Modeling of C/EBPalpha mutant acute myeloid leukemia reveals a common expression signature of committed myeloid leukemia-initiating cells*. *Cancer Cell*, 2008. 13(4): p. 299-310.
42. Huntly, B.J., et al., *MOZ-TIF2, but not BCR-ABL, confers properties of leukemic stem cells to committed murine hematopoietic progenitors*. *Cancer Cell*, 2004. 6(6): p. 587-96.
43. Domingo-Domenech, J., et al., *Suppression of Acquired Docetaxel Resistance in Prostate Cancer through Depletion of Notch- and Hedgehog-Dependent Tumor-Initiating Cells*. *Cancer Cell*, 2012. 22(3): p. 373-88.
44. Nowell, P.C. and D.A. Hungerford, *Chromosome studies on normal and leukemic human leukocytes*. *J Natl Cancer Inst*, 1960. 25: p. 85-109.
45. Rowley, J.D., *Letter: A new consistent chromosomal abnormality in chronic myelogenous leukaemia identified by quinacrine fluorescence and Giemsa staining*. *Nature*, 1973. 243(5405): p. 290-3.
46. Daley, G.Q., R.A. Van Etten, and D. Baltimore, *Induction of chronic myelogenous leukemia in mice by the P210bcr/abl gene of the Philadelphia chromosome*. *Science*, 1990. 247(4944): p. 824-30.
47. Elefanty, A.G., I.K. Hariharan, and S. Cory, *bcr-abl, the hallmark of chronic myeloid leukaemia in man, induces multiple haemopoietic neoplasms in mice*. *EMBO J*, 1990. 9(4): p. 1069-78.
48. Heisterkamp, N., et al., *Acute leukaemia in bcr/abl transgenic mice*. *Nature*, 1990. 344(6263): p. 251-3.
49. Kelliher, M.A., et al., *Induction of a chronic myelogenous leukemia-like syndrome in mice with v-abl and BCR/ABL*. *Proc Natl Acad Sci U S A*, 1990. 87(17): p. 6649-53.
50. Fialkow, P.J., S.M. Gartler, and A. Yoshida, *Clonal origin of chronic myelocytic leukemia in man*. *Proc Natl Acad Sci U S A*, 1967. 58(4): p. 1468-71.
51. Fialkow, P.J., et al., *Chronic myelocytic leukemia. Origin of some lymphocytes from leukemic stem cells*. *J Clin Invest*, 1978. 62(4): p. 815-23.
52. Martin, P.J., et al., *Involvement of the B-lymphoid system in chronic myelogenous leukaemia*. *Nature*, 1980. 287(5777): p. 49-50.
53. Faderl, S., et al., *The biology of chronic myeloid leukemia*. *N Engl J Med*, 1999. 341(3): p. 164-72.
54. Kantarjian, H.M., et al., *Characteristics of accelerated disease in chronic myelogenous leukemia*. *Cancer*, 1988. 61(7): p. 1441-6.
55. Kantarjian, H.M., et al., *Chronic myelogenous leukemia: a concise update*. *Blood*, 1993. 82(3): p. 691-703.
56. Wong, S. and O.N. Witte, *Modeling Philadelphia chromosome positive leukemias*. *Oncogene*, 2001. 20(40): p. 5644-59.
57. Smith, D.L., J. Burthem, and A.D. Whetton, *Molecular pathogenesis of chronic myeloid leukaemia*. *Expert Rev Mol Med*, 2003. 5(27): p. 1-27.
58. Perrotti, D., et al., *Chronic myeloid leukemia: mechanisms of blastic transformation*. *J Clin Invest*, 2010. 120(7): p. 2254-64.
59. Voncken, J.W., et al., *Increased neutrophil respiratory burst in bcr-null mutants*. *Cell*, 1995. 80(5): p. 719-28.
60. Reuther, G.W., et al., *Association of the protein kinases c-Bcr and Bcr-Abl with proteins of the 14-3-3 family*. *Science*, 1994. 266(5182): p. 129-33.
61. McWhirter, J.R., D.L. Galasso, and J.Y. Wang, *A coiled-coil oligomerization domain of Bcr is essential for the transforming function of Bcr-Abl oncoproteins*. *Mol Cell Biol*, 1993. 13(12): p. 7587-95.

62. Boguski, M.S. and F. McCormick, *Proteins regulating Ras and its relatives*. Nature, 1993. 366(6456): p. 643-54.
63. Diekmann, D., et al., *Bcr encodes a GTPase-activating protein for p21rac*. Nature, 1991. 351(6325): p. 400-2.
64. Van Etten, R.A., P. Jackson, and D. Baltimore, *The mouse type IV c-abl gene product is a nuclear protein, and activation of transforming ability is associated with cytoplasmic localization*. Cell, 1989. 58(4): p. 669-78.
65. Wetzler, M., et al., *Subcellular localization of Bcr, Abl, and Bcr-Abl proteins in normal and leukemic cells and correlation of expression with myeloid differentiation*. J Clin Invest, 1993. 92(4): p. 1925-39.
66. Ren, R., Z.S. Ye, and D. Baltimore, *Abl protein-tyrosine kinase selects the Crk adapter as a substrate using SH3-binding sites*. Genes Dev, 1994. 8(7): p. 783-95.
67. Kipreos, E.T. and J.Y. Wang, *Cell cycle-regulated binding of c-Abl tyrosine kinase to DNA*. Science, 1992. 256(5055): p. 382-5.
68. McWhirter, J.R. and J.Y. Wang, *An actin-binding function contributes to transformation by the Bcr-Abl oncoprotein of Philadelphia chromosome-positive human leukemias*. EMBO J, 1993. 12(4): p. 1533-46.
69. Van Etten, R.A., et al., *The COOH terminus of the c-Abl tyrosine kinase contains distinct F- and G-actin binding domains with bundling activity*. J Cell Biol, 1994. 124(3): p. 325-40.
70. Kharbanda, S., et al., *The stress response to ionizing radiation involves c-Abl-dependent phosphorylation of SHPTP1*. Proc Natl Acad Sci U S A, 1996. 93(14): p. 6898-901.
71. Raitano, A.B., Y.E. Whang, and C.L. Sawyers, *Signal transduction by wild-type and leukemogenic Abl proteins*. Biochim Biophys Acta, 1997. 1333(3): p. F201-16.
72. Pendergast, A.M., et al., *Evidence for regulation of the human ABL tyrosine kinase by a cellular inhibitor*. Proc Natl Acad Sci U S A, 1991. 88(13): p. 5927-31.
73. Kharbanda, S., et al., *Activation of the c-Abl tyrosine kinase in the stress response to DNA-damaging agents*. Nature, 1995. 376(6543): p. 785-8.
74. Liu, Z.G., et al., *Three distinct signalling responses by murine fibroblasts to genotoxic stress*. Nature, 1996. 384(6606): p. 273-6.
75. Welch, P.J. and J.Y. Wang, *A C-terminal protein-binding domain in the retinoblastoma protein regulates nuclear c-Abl tyrosine kinase in the cell cycle*. Cell, 1993. 75(4): p. 779-90.
76. Lewis, J.M., et al., *Integrin regulation of c-Abl tyrosine kinase activity and cytoplasmic-nuclear transport*. Proc Natl Acad Sci U S A, 1996. 93(26): p. 15174-9.
77. Copland, M., H.G. Jorgensen, and T.L. Holyoake, *Evolving molecular therapy for chronic myeloid leukaemia--are we on target?* Hematology, 2005. 10(5): p. 349-59.
78. Deininger, M.W., et al., *The prognosis for patients with chronic myeloid leukemia who have clonal cytogenetic abnormalities in philadelphia chromosome-negative cells*. Cancer, 2007. 110(7): p. 1509-19.
79. Bedi, A., et al., *BCR-ABL-mediated inhibition of apoptosis with delay of G2/M transition after DNA damage: a mechanism of resistance to multiple anticancer agents*. Blood, 1995. 86(3): p. 1148-58.
80. Pendergast, A.M., et al., *BCR-ABL-induced oncogenesis is mediated by direct interaction with the SH2 domain of the GRB-2 adaptor protein*. Cell, 1993. 75(1): p. 175-85.

81. Million, R.P. and R.A. Van Etten, *The Grb2 binding site is required for the induction of chronic myeloid leukemia-like disease in mice by the Bcr/Abl tyrosine kinase*. *Blood*, 2000. 96(2): p. 664-70.
82. Puil, L., et al., *Bcr-Abl oncoproteins bind directly to activators of the Ras signalling pathway*. *EMBO J*, 1994. 13(4): p. 764-73.
83. Chang, E.H., et al., *Human genome contains four genes homologous to transforming genes of Harvey and Kirsten murine sarcoma viruses*. *Proc Natl Acad Sci U S A*, 1982. 79(16): p. 4848-52.
84. Sattler, M., et al., *Critical role for Gab2 in transformation by BCR/ABL*. *Cancer Cell*, 2002. 1(5): p. 479-92.
85. Wohrle, F.U., et al., *Gab2 signaling in chronic myeloid leukemia cells confers resistance to multiple Bcr-Abl inhibitors*. *Leukemia*, 2013. 27(1): p. 118-29.
86. Kapeller, R. and L.C. Cantley, *Phosphatidylinositol 3-kinase*. *Bioessays*, 1994. 16(8): p. 565-76.
87. Divecha, N. and R.F. Irvine, *Phospholipid signaling*. *Cell*, 1995. 80(2): p. 269-78.
88. Alessi, D.R., et al., *Mechanism of activation of protein kinase B by insulin and IGF-1*. *EMBO J*, 1996. 15(23): p. 6541-51.
89. Alessi, D.R., et al., *Characterization of a 3-phosphoinositide-dependent protein kinase which phosphorylates and activates protein kinase Balpha*. *Curr Biol*, 1997. 7(4): p. 261-9.
90. Koo, E.H. and S.L. Squazzo, *Evidence that production and release of amyloid beta-protein involves the endocytic pathway*. *J Biol Chem*, 1994. 269(26): p. 17386-9.
91. Bhaskar, P.T. and N. Hay, *The two TORCs and Akt*. *Dev Cell*, 2007. 12(4): p. 487-502.
92. Wullschleger, S., R. Loewith, and M.N. Hall, *TOR signaling in growth and metabolism*. *Cell*, 2006. 124(3): p. 471-84.
93. Kim, D.H., et al., *mTOR interacts with raptor to form a nutrient-sensitive complex that signals to the cell growth machinery*. *Cell*, 2002. 110(2): p. 163-75.
94. Kim, D.H., et al., *GbetaL, a positive regulator of the rapamycin-sensitive pathway required for the nutrient-sensitive interaction between raptor and mTOR*. *Mol Cell*, 2003. 11(4): p. 895-904.
95. Pullen, N., et al., *Phosphorylation and activation of p70s6k by PDK1*. *Science*, 1998. 279(5351): p. 707-10.
96. Peterson, R.T. and S.L. Schreiber, *Translation control: connecting mitogens and the ribosome*. *Curr Biol*, 1998. 8(7): p. R248-50.
97. Chiang, G.G. and R.T. Abraham, *Phosphorylation of mammalian target of rapamycin (mTOR) at Ser-2448 is mediated by p70S6 kinase*. *J Biol Chem*, 2005. 280(27): p. 25485-90.
98. Pause, A., et al., *Insulin-dependent stimulation of protein synthesis by phosphorylation of a regulator of 5'-cap function*. *Nature*, 1994. 371(6500): p. 762-7.
99. Guertin, D.A. and D.M. Sabatini, *Defining the role of mTOR in cancer*. *Cancer Cell*, 2007. 12(1): p. 9-22.
100. Frias, M.A., et al., *mSin1 is necessary for Akt/PKB phosphorylation, and its isoforms define three distinct mTORC2s*. *Curr Biol*, 2006. 16(18): p. 1865-70.
101. Sarbassov, D.D., et al., *Rictor, a novel binding partner of mTOR, defines a rapamycin-insensitive and raptor-independent pathway that regulates the cytoskeleton*. *Curr Biol*, 2004. 14(14): p. 1296-302.
102. Sarbassov, D.D., et al., *Phosphorylation and regulation of Akt/PKB by the rictor-mTOR complex*. *Science*, 2005. 307(5712): p. 1098-101.

103. Sarbassov, D.D., et al., *Prolonged rapamycin treatment inhibits mTORC2 assembly and Akt/PKB*. Mol Cell, 2006. 22(2): p. 159-68.
104. Maira, S.M., et al., *Identification and characterization of NVP-BEZ235, a new orally available dual phosphatidylinositol 3-kinase/mammalian target of rapamycin inhibitor with potent in vivo antitumor activity*. Mol Cancer Ther, 2008. 7(7): p. 1851-63.
105. Fan, Q.W., et al., *A dual PI3 kinase/mTOR inhibitor reveals emergent efficacy in glioma*. Cancer Cell, 2006. 9(5): p. 341-9.
106. Ghaffari, S., et al., *Cytokines and BCR-ABL mediate suppression of TRAIL-induced apoptosis through inhibition of forkhead FOXO3a transcription factor*. Proc Natl Acad Sci U S A, 2003. 100(11): p. 6523-8.
107. Salomoni, P., et al., *Versatility of BCR/ABL-expressing leukemic cells in circumventing proapoptotic BAD effects*. Blood, 2000. 96(2): p. 676-84.
108. Mayo, L.D. and D.B. Donner, *A phosphatidylinositol 3-kinase/Akt pathway promotes translocation of Mdm2 from the cytoplasm to the nucleus*. Proc Natl Acad Sci U S A, 2001. 98(20): p. 11598-603.
109. Goetz, A.W., et al., *Requirement for Mdm2 in the survival effects of Bcr-Abl and interleukin 3 in hematopoietic cells*. Cancer Res, 2001. 61(20): p. 7635-41.
110. Trotta, R., et al., *BCR/ABL activates mdm2 mRNA translation via the La antigen*. Cancer Cell, 2003. 3(2): p. 145-60.
111. ten Hoeve, J., et al., *Tyrosine phosphorylation of CRKL in Philadelphia+ leukemia*. Blood, 1994. 84(6): p. 1731-6.
112. Reichman, C.T., et al., *The product of the cellular crk gene consists primarily of SH2 and SH3 regions*. Cell Growth Differ, 1992. 3(7): p. 451-60.
113. Oda, T., et al., *Crkl is the major tyrosine-phosphorylated protein in neutrophils from patients with chronic myelogenous leukemia*. J Biol Chem, 1994. 269(37): p. 22925-8.
114. de Jong, R., et al., *Tyrosine 207 in CRKL is the BCR/ABL phosphorylation site*. Oncogene, 1997. 14(5): p. 507-13.
115. de Jong, R., et al., *Crkl is complexed with tyrosine-phosphorylated Cbl in Philadelphia+ leukemia*. J Biol Chem, 1995. 270(37): p. 21468-71.
116. Sattler, M., et al., *Steel factor induces tyrosine phosphorylation of CRKL and binding of CRKL to a complex containing c-kit, phosphatidylinositol 3-kinase, and p120(CBL)*. J Biol Chem, 1997. 272(15): p. 10248-53.
117. Salgia, R., et al., *CRKL links p210BCR/ABL with paxillin in chronic myelogenous leukemia cells*. J Biol Chem, 1995. 270(49): p. 29145-50.
118. Grumbach, I.M., et al., *Engagement of the CrkL adaptor in interferon alpha signalling in BCR-ABL-expressing cells*. Br J Haematol, 2001. 112(2): p. 327-36.
119. Druker, B.J., et al., *Efficacy and safety of a specific inhibitor of the BCR-ABL tyrosine kinase in chronic myeloid leukemia*. N Engl J Med, 2001. 344(14): p. 1031-7.
120. Hamilton, A., et al., *BCR-ABL activity and its response to drugs can be determined in CD34+ CML stem cells by CrkL phosphorylation status using flow cytometry*. Leukemia, 2006. 20(6): p. 1035-9.
121. Hebenstreit, D., J. Horejs-Hoeck, and A. Duschl, *JAK/STAT-dependent gene regulation by cytokines*. Drug News Perspect, 2005. 18(4): p. 243-9.
122. Ilaria, R.L., Jr. and R.A. Van Etten, *P210 and P190(BCR/ABL) induce the tyrosine phosphorylation and DNA binding activity of multiple specific STAT family members*. J Biol Chem, 1996. 271(49): p. 31704-10.
123. Chai, S.K., G.L. Nichols, and P. Rothman, *Constitutive activation of JAKs and STATs in BCR-Abl-expressing cell lines and peripheral blood cells derived from leukemic patients*. J Immunol, 1997. 159(10): p. 4720-8.

124. Ye, D., et al., *STAT5 signaling is required for the efficient induction and maintenance of CML in mice*. *Blood*, 2006. 107(12): p. 4917-25.
125. Hoelbl, A., et al., *Stat5 is indispensable for the maintenance of bcr/abl-positive leukaemia*. *EMBO Mol Med*, 2010. 2(3): p. 98-110.
126. Gesbert, F. and J.D. Griffin, *Bcr/Abl activates transcription of the Bcl-X gene through STAT5*. *Blood*, 2000. 96(6): p. 2269-76.
127. Huang, M., et al., *Inhibition of Bcr-Abl kinase activity by PD180970 blocks constitutive activation of Stat5 and growth of CML cells*. *Oncogene*, 2002. 21(57): p. 8804-16.
128. Warsch, W., et al., *High STAT5 levels mediate imatinib resistance and indicate disease progression in chronic myeloid leukemia*. *Blood*, 2011. 117(12): p. 3409-20.
129. Klejman, A., et al., *The Src family kinase Hck couples BCR/ABL to STAT5 activation in myeloid leukemia cells*. *EMBO J*, 2002. 21(21): p. 5766-74.
130. Steelman, L.S., et al., *JAK/STAT, Raf/MEK/ERK, PI3K/Akt and BCR-ABL in cell cycle progression and leukemogenesis*. *Leukemia*, 2004. 18(2): p. 189-218.
131. Roberts, A.W., *G-CSF: a key regulator of neutrophil production, but that's not all!* *Growth Factors*, 2005. 23(1): p. 33-41.
132. Holyoake, T.L., et al., *Primitive quiescent leukemic cells from patients with chronic myeloid leukemia spontaneously initiate factor-independent growth in vitro in association with up-regulation of expression of interleukin-3*. *Blood*, 2001. 97(3): p. 720-8.
133. Holyoake, T.L., et al., *Elucidating critical mechanisms of deregulated stem cell turnover in the chronic phase of chronic myeloid leukemia*. *Leukemia*, 2002. 16(4): p. 549-58.
134. Jiang, X., et al., *Autocrine production and action of IL-3 and granulocyte colony-stimulating factor in chronic myeloid leukemia*. *Proc Natl Acad Sci U S A*, 1999. 96(22): p. 12804-9.
135. Chang, J.M., et al., *Nonneoplastic hematopoietic myeloproliferative syndrome induced by dysregulated multi-CSF (IL-3) expression*. *Blood*, 1989. 73(6): p. 1487-97.
136. Wong, P.M., et al., *Retrovirus-mediated transfer and expression of the interleukin-3 gene in mouse hematopoietic cells result in a myeloproliferative disorder*. *Mol Cell Biol*, 1989. 9(2): p. 798-808.
137. Just, U., et al., *Targeted in vivo infection with a retroviral vector carrying the interleukin-3 (multi-CSF) gene leads to immortalization and leukemic transformation of primitive hematopoietic progenitor cells*. *Growth Factors*, 1993. 9(1): p. 41-55.
138. Arai, F., et al., *Tie2/angiopoietin-1 signaling regulates hematopoietic stem cell quiescence in the bone marrow niche*. *Cell*, 2004. 118(2): p. 149-61.
139. Teixeira, J., et al., *Role of beta 1 and beta 2 integrins in the adhesion of human CD34hi stem cells to bone marrow stroma*. *J Clin Invest*, 1992. 90(2): p. 358-67.
140. Hurley, R.W., J.B. McCarthy, and C.M. Verfaillie, *Direct adhesion to bone marrow stroma via fibronectin receptors inhibits hematopoietic progenitor proliferation*. *J Clin Invest*, 1995. 96(1): p. 511-9.
141. Gordon, M.Y., et al., *Altered adhesive interactions with marrow stroma of haematopoietic progenitor cells in chronic myeloid leukaemia*. *Nature*, 1987. 328(6128): p. 342-4.
142. Verfaillie, C.M., et al., *Integrin-mediated regulation of hematopoiesis: do BCR/ABL-induced defects in integrin function underlie the abnormal circulation and proliferation of CML progenitors?* *Acta Haematol*, 1997. 97(1-2): p. 40-52.

143. Geay, J.F., et al., *p210BCR-ABL inhibits SDF-1 chemotactic response via alteration of CXCR4 signaling and down-regulation of CXCR4 expression*. *Cancer Res*, 2005. 65(7): p. 2676-83.
144. Jin, L., et al., *CXCR4 up-regulation by imatinib induces chronic myelogenous leukemia (CML) cell migration to bone marrow stroma and promotes survival of quiescent CML cells*. *Mol Cancer Ther*, 2008. 7(1): p. 48-58.
145. Geary, C.G., *The story of chronic myeloid leukaemia*. *Br J Haematol*, 2000. 110(1): p. 2-11.
146. Waxman, S. and K.C. Anderson, *History of the development of arsenic derivatives in cancer therapy*. *Oncologist*, 2001. 6 Suppl 2: p. 3-10.
147. Galton, D.A., *Myleran in chronic myeloid leukaemia; results of treatment*. *Lancet*, 1953. 264(6753): p. 208-13.
148. Thomas, E.D., et al., *Marrow transplantation for acute nonlymphoblastic leukemia in first remission*. *N Engl J Med*, 1979. 301(11): p. 597-9.
149. Goldman, J.M., et al., *Bone marrow transplantation for patients with chronic myeloid leukemia*. *N Engl J Med*, 1986. 314(4): p. 202-7.
150. Goldman, J., *Hematopoietic stem cell transplantation*. *Curr Opin Hematol*, 1998. 5(6): p. 417-8.
151. Gratwohl, A., et al., *Risk assessment for patients with chronic myeloid leukaemia before allogeneic blood or marrow transplantation*. *Chronic Leukemia Working Party of the European Group for Blood and Marrow Transplantation*. *Lancet*, 1998. 352(9134): p. 1087-92.
152. Faderl, S., et al., *Chronic myelogenous leukemia: biology and therapy*. *Ann Intern Med*, 1999. 131(3): p. 207-19.
153. Sawyers, C.L., *Chronic myeloid leukemia*. *N Engl J Med*, 1999. 340(17): p. 1330-40.
154. Talpaz, M., et al., *Leukocyte interferon-induced myeloid cyto reduction in chronic myelogenous leukemia*. *Blood*, 1983. 62(3): p. 689-92.
155. Bhatia, R., et al., *Interferon-alpha restores normal adhesion of chronic myelogenous leukemia hematopoietic progenitors to bone marrow stroma by correcting impaired beta 1 integrin receptor function*. *J Clin Invest*, 1994. 94(1): p. 384-91.
156. Druker, B.J., et al., *Effects of a selective inhibitor of the Abl tyrosine kinase on the growth of Bcr-Abl positive cells*. *Nat Med*, 1996. 2(5): p. 561-6.
157. Buchdunger, E., et al., *Inhibition of the Abl protein-tyrosine kinase in vitro and in vivo by a 2-phenylaminopyrimidine derivative*. *Cancer Res*, 1996. 56(1): p. 100-4.
158. Deininger, M.W., et al., *The tyrosine kinase inhibitor CGP57148B selectively inhibits the growth of BCR-ABL-positive cells*. *Blood*, 1997. 90(9): p. 3691-8.
159. Kantarjian, H., et al., *Hematologic and cytogenetic responses to imatinib mesylate in chronic myelogenous leukemia*. *N Engl J Med*, 2002. 346(9): p. 645-52.
160. Daley, G.Q. and D. Baltimore, *Transformation of an interleukin 3-dependent hematopoietic cell line by the chronic myelogenous leukemia-specific P210bcr/abl protein*. *Proc Natl Acad Sci U S A*, 1988. 85(23): p. 9312-6.
161. O'Brien, S.G., et al., *Imatinib compared with interferon and low-dose cytarabine for newly diagnosed chronic-phase chronic myeloid leukemia*. *N Engl J Med*, 2003. 348(11): p. 994-1004.
162. Hochhaus, A., et al., *Six-year follow-up of patients receiving imatinib for the first-line treatment of chronic myeloid leukemia*. *Leukemia*, 2009. 23(6): p. 1054-61.

163. Li, S., et al., *The P190, P210, and P230 forms of the BCR/ABL oncogene induce a similar chronic myeloid leukemia-like syndrome in mice but have different lymphoid leukemogenic activity.* J Exp Med, 1999. 189(9): p. 1399-412.
164. Pane, F., et al., *Neutrophilic-chronic myeloid leukemia: a distinct disease with a specific molecular marker (BCR/ABL with C3/A2 junction).* Blood, 1996. 88(7): p. 2410-4.
165. O'Brien, S.G. and M.W. Deininger, *Imatinib in patients with newly diagnosed chronic-phase chronic myeloid leukemia.* Semin Hematol, 2003. 40(2 Suppl 2): p. 26-30.
166. Druker, B.J., et al., *Five-year follow-up of patients receiving imatinib for chronic myeloid leukemia.* N Engl J Med, 2006. 355(23): p. 2408-17.
167. Branford, S., et al., *Imatinib produces significantly superior molecular responses compared to interferon alfa plus cytarabine in patients with newly diagnosed chronic myeloid leukemia in chronic phase.* Leukemia, 2003. 17(12): p. 2401-9.
168. Hughes, T.P., et al., *Frequency of major molecular responses to imatinib or interferon alfa plus cytarabine in newly diagnosed chronic myeloid leukemia.* N Engl J Med, 2003. 349(15): p. 1423-32.
169. Tokarski, J.S., et al., *The structure of Dasatinib (BMS-354825) bound to activated ABL kinase domain elucidates its inhibitory activity against imatinib-resistant ABL mutants.* Cancer Res, 2006. 66(11): p. 5790-7.
170. Alvarado, Y., et al., *Significance of suboptimal response to imatinib, as defined by the European LeukemiaNet, in the long-term outcome of patients with early chronic myeloid leukemia in chronic phase.* Cancer, 2009. 115(16): p. 3709-18.
171. Mahon, F.X., et al., *Discontinuation of imatinib in patients with chronic myeloid leukaemia who have maintained complete molecular remission for at least 2 years: the prospective, multicentre Stop Imatinib (STIM) trial.* Lancet Oncol, 2010. 11(11): p. 1029-35.
172. Ross, D.M., et al., *Patients with chronic myeloid leukemia who maintain a complete molecular response after stopping imatinib treatment have evidence of persistent leukemia by DNA PCR.* Leukemia, 2010. 24(10): p. 1719-24.
173. Graham, S.M., et al., *Primitive, quiescent, Philadelphia-positive stem cells from patients with chronic myeloid leukemia are insensitive to STI571 in vitro.* Blood, 2002. 99(1): p. 319-25.
174. Michor, F., et al., *Dynamics of chronic myeloid leukaemia.* Nature, 2005. 435(7046): p. 1267-70.
175. Holtz, M.S., et al., *Imatinib mesylate (STI571) inhibits growth of primitive malignant progenitors in chronic myelogenous leukemia through reversal of abnormally increased proliferation.* Blood, 2002. 99(10): p. 3792-800.
176. le Coutre, P., et al., *Induction of resistance to the Abelson inhibitor STI571 in human leukemic cells through gene amplification.* Blood, 2000. 95(5): p. 1758-66.
177. Mahon, F.X., et al., *Selection and characterization of BCR-ABL positive cell lines with differential sensitivity to the tyrosine kinase inhibitor STI571: diverse mechanisms of resistance.* Blood, 2000. 96(3): p. 1070-9.
178. Weisberg, E. and J.D. Griffin, *Mechanism of resistance to the ABL tyrosine kinase inhibitor STI571 in BCR/ABL-transformed hematopoietic cell lines.* Blood, 2000. 95(11): p. 3498-505.
179. Quintas-Cardama, A., H.M. Kantarjian, and J.E. Cortes, *Mechanisms of primary and secondary resistance to imatinib in chronic myeloid leukemia.* Cancer Control, 2009. 16(2): p. 122-31.
180. Stoklosa, T., et al., *BCR/ABL inhibits mismatch repair to protect from apoptosis and induce point mutations.* Cancer Res, 2008. 68(8): p. 2576-80.

181. Gorre, M.E., et al., *Clinical resistance to STI-571 cancer therapy caused by BCR-ABL gene mutation or amplification*. *Science*, 2001. 293(5531): p. 876-80.
182. von Bubnoff, N., et al., *A cell-based screen for resistance of Bcr-Abl-positive leukemia identifies the mutation pattern for PD166326, an alternative Abl kinase inhibitor*. *Blood*, 2005. 105(4): p. 1652-9.
183. Corbin, A.S., et al., *Several Bcr-Abl kinase domain mutants associated with imatinib mesylate resistance remain sensitive to imatinib*. *Blood*, 2003. 101(11): p. 4611-4.
184. Nicolini, F.E., et al., *Mutation status and clinical outcome of 89 imatinib mesylate-resistant chronic myelogenous leukemia patients: a retrospective analysis from the French intergroup of CML (Fi(phi)-LMC GROUP)*. *Leukemia*, 2006. 20(6): p. 1061-6.
185. Soverini, S., et al., *Contribution of ABL kinase domain mutations to imatinib resistance in different subsets of Philadelphia-positive patients: by the GIMEMA Working Party on Chronic Myeloid Leukemia*. *Clin Cancer Res*, 2006. 12(24): p. 7374-9.
186. O'Hare, T., C.A. Eide, and M.W. Deininger, *Bcr-Abl kinase domain mutations, drug resistance, and the road to a cure for chronic myeloid leukemia*. *Blood*, 2007. 110(7): p. 2242-9.
187. Karvela, M., G.V. Helgason, and T.L. Holyoake, *Mechanisms and novel approaches in overriding tyrosine kinase inhibitor resistance in chronic myeloid leukemia*. *Expert Rev Anticancer Ther*, 2012. 12(3): p. 381-92.
188. Hochhaus, A., *Cytogenetic and molecular mechanisms of resistance to imatinib*. *Semin Hematol*, 2003. 40(2 Suppl 2): p. 69-79.
189. Tang, C., et al., *Tyrosine kinase inhibitor resistance in chronic myeloid leukemia cell lines: investigating resistance pathways*. *Leuk Lymphoma*, 2011. 52(11): p. 2139-47.
190. Hochhaus, A., et al., *Molecular and chromosomal mechanisms of resistance to imatinib (STI571) therapy*. *Leukemia*, 2002. 16(11): p. 2190-6.
191. Brusa, G., et al., *P210 Bcr-abl tyrosine kinase interaction with histone deacetylase 1 modifies histone H4 acetylation and chromatin structure of chronic myeloid leukaemia haematopoietic progenitors*. *Br J Haematol*, 2006. 132(3): p. 359-69.
192. Lee, S.M., et al., *Bcr-Abl-independent imatinib-resistant K562 cells show aberrant protein acetylation and increased sensitivity to histone deacetylase inhibitors*. *J Pharmacol Exp Ther*, 2007. 322(3): p. 1084-92.
193. Carette, J.E., et al., *Generation of iPSCs from cultured human malignant cells*. *Blood*, 2010. 115(20): p. 4039-42.
194. Fioretos, T., et al., *Isochromosome 17q in blast crisis of chronic myeloid leukemia and in other hematologic malignancies is the result of clustered breakpoints in 17p11 and is not associated with coding TP53 mutations*. *Blood*, 1999. 94(1): p. 225-32.
195. Schutte, J., et al., *Analysis of the p53 gene in patients with isochromosome 17q and Ph1-positive or -negative myeloid leukemia*. *Leuk Res*, 1993. 17(6): p. 533-9.
196. Donato, N.J., et al., *Imatinib mesylate resistance through BCR-ABL independence in chronic myelogenous leukemia*. *Cancer Res*, 2004. 64(2): p. 672-7.
197. Donato, N.J., et al., *BCR-ABL independence and LYN kinase overexpression in chronic myelogenous leukemia cells selected for resistance to STI571*. *Blood*, 2003. 101(2): p. 690-8.
198. Wang, Y., et al., *Adaptive secretion of granulocyte-macrophage colony-stimulating factor (GM-CSF) mediates imatinib and nilotinib resistance in*

- BCR/ABL+ progenitors via JAK-2/STAT-5 pathway activation.* *Blood*, 2007. 109(5): p. 2147-55.
199. Nishioka, C., et al., *Long-term exposure of leukemia cells to multi-targeted tyrosine kinase inhibitor induces activations of AKT, ERK and STAT5 signaling via epigenetic silencing of the PTEN gene.* *Leukemia*, 2010. 24(9): p. 1631-40.
 200. de Lavallade, H., et al., *A gene expression signature of primary resistance to imatinib in chronic myeloid leukemia.* *Leuk Res*, 2010. 34(2): p. 254-7.
 201. Mahon, F.X., et al., *MDR1 gene overexpression confers resistance to imatinib mesylate in leukemia cell line models.* *Blood*, 2003. 101(6): p. 2368-73.
 202. Hatziieremia, S., et al., *Inhibition of MDR1 does not sensitize primitive chronic myeloid leukemia CD34+ cells to imatinib.* *Exp Hematol*, 2009. 37(6): p. 692-700.
 203. Gambacorti-Passerini, C., et al., *Role of alpha1 acid glycoprotein in the in vivo resistance of human BCR-ABL(+) leukemic cells to the abl inhibitor STI571.* *J Natl Cancer Inst*, 2000. 92(20): p. 1641-50.
 204. Gambacorti-Passerini, C., et al., *Alpha1 acid glycoprotein binds to imatinib (STI571) and substantially alters its pharmacokinetics in chronic myeloid leukemia patients.* *Clin Cancer Res*, 2003. 9(2): p. 625-32.
 205. Jorgensen, H.G., et al., *Alpha1-acid glycoprotein expressed in the plasma of chronic myeloid leukemia patients does not mediate significant in vitro resistance to STI571.* *Blood*, 2002. 99(2): p. 713-5.
 206. Thomas, J., et al., *Active transport of imatinib into and out of cells: implications for drug resistance.* *Blood*, 2004. 104(12): p. 3739-45.
 207. Wang, L., et al., *Expression of the uptake drug transporter hOCT1 is an important clinical determinant of the response to imatinib in chronic myeloid leukemia.* *Clin Pharmacol Ther*, 2008. 83(2): p. 258-64.
 208. Giannoudis, A., et al., *The hOCT1 SNPs M420del and M408V alter imatinib uptake and M420del modifies clinical outcome in imatinib-treated chronic myeloid leukaemia.* *Blood*, 2012.
 209. Green, H., et al., *CYP3A activity influences imatinib response in patients with chronic myeloid leukemia: a pilot study on in vivo CYP3A activity.* *Eur J Clin Pharmacol*, 2010. 66(4): p. 383-6.
 210. Noens, L., et al., *Prevalence, determinants, and outcomes of nonadherence to imatinib therapy in patients with chronic myeloid leukemia: the ADAGIO study.* *Blood*, 2009. 113(22): p. 5401-11.
 211. Marin, D., et al., *Adherence is the critical factor for achieving molecular responses in patients with chronic myeloid leukemia who achieve complete cytogenetic responses on imatinib.* *J Clin Oncol*, 2010. 28(14): p. 2381-8.
 212. Kantarjian, H.M., et al., *Dose escalation of imatinib mesylate can overcome resistance to standard-dose therapy in patients with chronic myelogenous leukemia.* *Blood*, 2003. 101(2): p. 473-5.
 213. Jabbour, E., et al., *Imatinib mesylate dose escalation is associated with durable responses in patients with chronic myeloid leukemia after cytogenetic failure on standard-dose imatinib therapy.* *Blood*, 2009. 113(10): p. 2154-60.
 214. Lombardo, L.J., et al., *Discovery of N-(2-chloro-6-methyl- phenyl)-2-(6-(4-(2-hydroxyethyl)- piperazin-1-yl)-2-methylpyrimidin-4- ylamino)thiazole-5-carboxamide (BMS-354825), a dual Src/Abl kinase inhibitor with potent antitumor activity in preclinical assays.* *J Med Chem*, 2004. 47(27): p. 6658-61.
 215. O'Hare, T., et al., *In vitro activity of Bcr-Abl inhibitors AMN107 and BMS-354825 against clinically relevant imatinib-resistant Abl kinase domain mutants.* *Cancer Res*, 2005. 65(11): p. 4500-5.
 216. Shah, N.P., et al., *Overriding imatinib resistance with a novel ABL kinase inhibitor.* *Science*, 2004. 305(5682): p. 399-401.

217. Hochhaus, A., et al., *Dasatinib induces durable cytogenetic responses in patients with chronic myelogenous leukemia in chronic phase with resistance or intolerance to imatinib*. *Leukemia*, 2008. 22(6): p. 1200-6.
218. Kantarjian, H., et al., *Dasatinib versus imatinib in newly diagnosed chronic-phase chronic myeloid leukemia*. *N Engl J Med*, 2010. 362(24): p. 2260-70.
219. Cortes, J., et al., *Efficacy and safety of dasatinib in imatinib-resistant or -intolerant patients with chronic myeloid leukemia in blast phase*. *Leukemia*, 2008. 22(12): p. 2176-83.
220. Apperley, J.F., et al., *Dasatinib in the treatment of chronic myeloid leukemia in accelerated phase after imatinib failure: the START a trial*. *J Clin Oncol*, 2009. 27(21): p. 3472-9.
221. Copland, M., et al., *Dasatinib (BMS-354825) targets an earlier progenitor population than imatinib in primary CML but does not eliminate the quiescent fraction*. *Blood*, 2006. 107(11): p. 4532-9.
222. O'Hare, T., et al., *AMN107: tightening the grip of imatinib*. *Cancer Cell*, 2005. 7(2): p. 117-9.
223. Golemovic, M., et al., *AMN107, a novel aminopyrimidine inhibitor of Bcr-Abl, has in vitro activity against imatinib-resistant chronic myeloid leukemia*. *Clin Cancer Res*, 2005. 11(13): p. 4941-7.
224. Weisberg, E., et al., *Characterization of AMN107, a selective inhibitor of native and mutant Bcr-Abl*. *Cancer Cell*, 2005. 7(2): p. 129-41.
225. Kantarjian, H.M., et al., *Nilotinib versus imatinib for the treatment of patients with newly diagnosed chronic phase, Philadelphia chromosome-positive, chronic myeloid leukaemia: 24-month minimum follow-up of the phase 3 randomised ENESTnd trial*. *Lancet Oncol*, 2011. 12(9): p. 841-51.
226. Jorgensen, H.G., et al., *Nilotinib exerts equipotent antiproliferative effects to imatinib and does not induce apoptosis in CD34+ CML cells*. *Blood*, 2007. 109(9): p. 4016-9.
227. O'Hare, T., et al., *AP24534, a pan-BCR-ABL inhibitor for chronic myeloid leukemia, potently inhibits the T315I mutant and overcomes mutation-based resistance*. *Cancer Cell*, 2009. 16(5): p. 401-12.
228. Cortes, J.E., et al., *Ponatinib in refractory Philadelphia chromosome-positive leukemias*. *N Engl J Med*, 2012. 367(22): p. 2075-88.
229. Jorge E. Cortes, D.-W.K., Javier Pinilla-Ibarz, Ronald Paquette, Philipp D. le Coutre, Charles Chuah, Franck E. Nicolini, Jane Apperley, Hanna Jean Khoury, Moshe Talpaz, John F DiPersio, Daniel J DeAngelo, Delphine Rea, Elisabetta Abruzzese, Martin C Müller, Michele Baccarani, Carlo Gambacorti-Passerini, Christopher D. Turner, Frank G. Haluska, Hagop Kantarjian; University of Texas M. D. Anderson Cancer Center, Houston, TX; The Catholic University of Korea, Seoul, South Korea; H. Lee Moffitt Cancer Center & Research Institute, Tampa, FL; Ronald Reagan UCLA Medical Center, Los Angeles, CA; Charité University of Medicine Berlin, Berlin, Germany; Singapore General Hospital, Singapore, Singapore; Centre Hospitalier Lyon Sud, Pierre Bénite, France; Hammersmith Hospital, Imperial College London, London, United Kingdom; Emory Winship Cancer Institute, Atlanta, GA; Comprehensive Cancer Center, University of Michigan, Ann Arbor, MI, *J Clin Oncol* 30, 2012: p. suppl; abstr 6503)
230. *ARIAD Pharmaceuticals commences ponatinib Phase 3 trial in newly diagnosed CML*. July 28, 2012 [cited 2012 18 September].
231. Zhang, J., et al., *Targeting Bcr-Abl by combining allosteric with ATP-binding-site inhibitors*. *Nature*, 2010. 463(7280): p. 501-6.

232. Chan, W.W., et al., *Conformational control inhibition of the BCR-ABL1 tyrosine kinase, including the gatekeeper T315I mutant, by the switch-control inhibitor DCC-2036*. *Cancer Cell*, 2011. 19(4): p. 556-68.
233. Smahel, M., *Antigens in chronic myeloid leukemia: implications for vaccine development*. *Cancer Immunol Immunother*, 2011. 60(12): p. 1655-68.
234. Corbin, A.S., et al., *Human chronic myeloid leukemia stem cells are insensitive to imatinib despite inhibition of BCR-ABL activity*. *J Clin Invest*, 2011. 121(1): p. 396-409.
235. Hamilton, A., et al., *Chronic myeloid leukemia stem cells are not dependent on Bcr-Abl kinase activity for their survival*. *Blood*, 2012. 119(6): p. 1501-10.
236. Zhang, B., et al., *Effective targeting of quiescent chronic myelogenous leukemia stem cells by histone deacetylase inhibitors in combination with imatinib mesylate*. *Cancer Cell*, 2010. 17(5): p. 427-42.
237. Preudhomme, C., et al., *Imatinib plus peginterferon alfa-2a in chronic myeloid leukemia*. *N Engl J Med*, 2010. 363(26): p. 2511-21.
238. Chen, Y., et al., *Loss of the Alox5 gene impairs leukemia stem cells and prevents chronic myeloid leukemia*. *Nat Genet*, 2009. 41(7): p. 783-92.
239. Zhao, C., et al., *Hedgehog signalling is essential for maintenance of cancer stem cells in myeloid leukaemia*. *Nature*, 2009. 458(7239): p. 776-9.
240. Kundu, M. and C.B. Thompson, *Autophagy: basic principles and relevance to disease*. *Annu Rev Pathol*, 2008. 3: p. 427-55.
241. Rosenfeldt, M.T. and K.M. Ryan, *The multiple roles of autophagy in cancer*. *Carcinogenesis*, 2011. 32(7): p. 955-63.
242. Huang, J. and D.J. Klionsky, *Autophagy and human disease*. *Cell Cycle*, 2007. 6(15): p. 1837-49.
243. Nakatogawa, H., et al., *Dynamics and diversity in autophagy mechanisms: lessons from yeast*. *Nat Rev Mol Cell Biol*, 2009. 10(7): p. 458-67.
244. Rubinsztein, D.C., et al., *Potential therapeutic applications of autophagy*. *Nat Rev Drug Discov*, 2007. 6(4): p. 304-12.
245. He, C. and D.J. Klionsky, *Regulation mechanisms and signaling pathways of autophagy*. *Annu Rev Genet*, 2009. 43: p. 67-93.
246. Helgason, G.V., M. Karvela, and T.L. Holyoake, *Kill one bird with two stones: potential efficacy of BCR-ABL and autophagy inhibition in CML*. *Blood*, 2011. 118(8): p. 2035-43.
247. Kim, J., et al., *AMPK and mTOR regulate autophagy through direct phosphorylation of Ulk1*. *Nat Cell Biol*, 2011. 13(2): p. 132-41.
248. Hara, T., et al., *FIP200, a ULK-interacting protein, is required for autophagosome formation in mammalian cells*. *J Cell Biol*, 2008. 181(3): p. 497-510.
249. Jung, C.H., et al., *ULK-Atg13-FIP200 complexes mediate mTOR signaling to the autophagy machinery*. *Mol Biol Cell*, 2009. 20(7): p. 1992-2003.
250. Hosokawa, N., et al., *Nutrient-dependent mTORC1 association with the ULK1-Atg13-FIP200 complex required for autophagy*. *Mol Biol Cell*, 2009. 20(7): p. 1981-91.
251. Vanhaesebroeck, B., et al., *Synthesis and function of 3-phosphorylated inositol lipids*. *Annu Rev Biochem*, 2001. 70: p. 535-602.
252. Lindmo, K. and H. Stenmark, *Regulation of membrane traffic by phosphoinositide 3-kinases*. *J Cell Sci*, 2006. 119(Pt 4): p. 605-14.
253. Kihara, A., et al., *Beclin-phosphatidylinositol 3-kinase complex functions at the trans-Golgi network*. *EMBO Rep*, 2001. 2(4): p. 330-5.
254. Liang, X.H., et al., *Induction of autophagy and inhibition of tumorigenesis by beclin 1*. *Nature*, 1999. 402(6762): p. 672-6.

255. Sun, Q., et al., *Identification of Barkor as a mammalian autophagy-specific factor for Beclin 1 and class III phosphatidylinositol 3-kinase*. Proc Natl Acad Sci U S A, 2008. 105(49): p. 19211-6.
256. Itakura, E., et al., *Beclin 1 forms two distinct phosphatidylinositol 3-kinase complexes with mammalian Atg14 and UVRAG*. Mol Biol Cell, 2008. 19(12): p. 5360-72.
257. Itakura, E. and N. Mizushima, *Characterization of autophagosome formation site by a hierarchical analysis of mammalian Atg proteins*. Autophagy, 2010. 6(6): p. 764-76.
258. Matsunaga, K., et al., *Autophagy requires endoplasmic reticulum targeting of the PI3-kinase complex via Atg14L*. J Cell Biol, 2010. 190(4): p. 511-21.
259. Maiuri, M.C., et al., *Functional and physical interaction between Bcl-X(L) and a BH3-like domain in Beclin-1*. EMBO J, 2007. 26(10): p. 2527-39.
260. Pattingre, S., et al., *Bcl-2 antiapoptotic proteins inhibit Beclin 1-dependent autophagy*. Cell, 2005. 122(6): p. 927-39.
261. Liang, C., et al., *Autophagic and tumour suppressor activity of a novel Beclin1-binding protein UVRAG*. Nat Cell Biol, 2006. 8(7): p. 688-99.
262. Di Bartolomeo, S., et al., *The dynamic interaction of AMBRA1 with the dynein motor complex regulates mammalian autophagy*. J Cell Biol, 2010. 191(1): p. 155-68.
263. Tooze, S.A. and T. Yoshimori, *The origin of the autophagosomal membrane*. Nat Cell Biol, 2010. 12(9): p. 831-5.
264. Mizushima, N., et al., *Mouse Apg16L, a novel WD-repeat protein, targets to the autophagic isolation membrane with the Apg12-Apg5 conjugate*. J Cell Sci, 2003. 116(Pt 9): p. 1679-88.
265. He, H., et al., *Post-translational modifications of three members of the human MAP1LC3 family and detection of a novel type of modification for MAP1LC3B*. J Biol Chem, 2003. 278(31): p. 29278-87.
266. Xin, Y., et al., *Cloning, expression patterns, and chromosome localization of three human and two mouse homologues of GABA(A) receptor-associated protein*. Genomics, 2001. 74(3): p. 408-13.
267. Kirisako, T., et al., *The reversible modification regulates the membrane-binding state of Apg8/Aut7 essential for autophagy and the cytoplasm to vacuole targeting pathway*. J Cell Biol, 2000. 151(2): p. 263-76.
268. Kabeya, Y., et al., *LC3, a mammalian homologue of yeast Apg8p, is localized in autophagosomal membranes after processing*. EMBO J, 2000. 19(21): p. 5720-8.
269. Fujita, N., et al., *The Atg16L complex specifies the site of LC3 lipidation for membrane biogenesis in autophagy*. Mol Biol Cell, 2008. 19(5): p. 2092-100.
270. Hanada, T., et al., *The Atg12-Atg5 conjugate has a novel E3-like activity for protein lipidation in autophagy*. J Biol Chem, 2007. 282(52): p. 37298-302.
271. Pankiv, S., et al., *p62/SQSTM1 binds directly to Atg8/LC3 to facilitate degradation of ubiquitinated protein aggregates by autophagy*. J Biol Chem, 2007. 282(33): p. 24131-45.
272. Wang, Q.J., et al., *Induction of autophagy in axonal dystrophy and degeneration*. J Neurosci, 2006. 26(31): p. 8057-68.
273. Nakai, A., et al., *The role of autophagy in cardiomyocytes in the basal state and in response to hemodynamic stress*. Nat Med, 2007. 13(5): p. 619-24.
274. Kirkin, V., et al., *A role for NBR1 in autophagosomal degradation of ubiquitinated substrates*. Mol Cell, 2009. 33(4): p. 505-16.
275. Geng, J. and D.J. Klionsky, *The Atg8 and Atg12 ubiquitin-like conjugation systems in macroautophagy. 'Protein modifications: beyond the usual suspects' review series*. EMBO Rep, 2008. 9(9): p. 859-64.

276. Jager, S., et al., *Role for Rab7 in maturation of late autophagic vacuoles*. J Cell Sci, 2004. 117(Pt 20): p. 4837-48.
277. Tanaka, Y., et al., *Accumulation of autophagic vacuoles and cardiomyopathy in LAMP-2-deficient mice*. Nature, 2000. 406(6798): p. 902-6.
278. Liang, C., et al., *Beclin1-binding UVRAG targets the class C Vps complex to coordinate autophagosome maturation and endocytic trafficking*. Nat Cell Biol, 2008. 10(7): p. 776-87.
279. Tanida, I., et al., *Lysosomal turnover, but not a cellular level, of endogenous LC3 is a marker for autophagy*. Autophagy, 2005. 1(2): p. 84-91.
280. Bursch, W., et al., *Programmed cell death (PCD). Apoptosis, autophagic PCD, or others?* Ann N Y Acad Sci, 2000. 926: p. 1-12.
281. Hotchkiss, R.S., et al., *Cell death*. N Engl J Med, 2009. 361(16): p. 1570-83.
282. Hollstein, M., et al., *p53 mutations in human cancers*. Science, 1991. 253(5015): p. 49-53.
283. Sigal, A. and V. Rotter, *Oncogenic mutations of the p53 tumor suppressor: the demons of the guardian of the genome*. Cancer Res, 2000. 60(24): p. 6788-93.
284. Crighton, D., et al., *DRAM, a p53-induced modulator of autophagy, is critical for apoptosis*. Cell, 2006. 126(1): p. 121-34.
285. Crighton, D., S. Wilkinson, and K.M. Ryan, *DRAM links autophagy to p53 and programmed cell death*. Autophagy, 2007. 3(1): p. 72-4.
286. Tasdemir, E., et al., *A dual role of p53 in the control of autophagy*. Autophagy, 2008. 4(6): p. 810-4.
287. Lee, I.H., et al., *Atg7 modulates p53 activity to regulate cell cycle and survival during metabolic stress*. Science, 2012. 336(6078): p. 225-8.
288. Yousefi, S., et al., *Calpain-mediated cleavage of Atg5 switches autophagy to apoptosis*. Nat Cell Biol, 2006. 8(10): p. 1124-32.
289. Qu, X., et al., *Promotion of tumorigenesis by heterozygous disruption of the beclin 1 autophagy gene*. J Clin Invest, 2003. 112(12): p. 1809-20.
290. Yue, Z., et al., *Beclin 1, an autophagy gene essential for early embryonic development, is a haploinsufficient tumor suppressor*. Proc Natl Acad Sci U S A, 2003. 100(25): p. 15077-82.
291. Mizushima, N. and M. Komatsu, *Autophagy: renovation of cells and tissues*. Cell, 2011. 147(4): p. 728-41.
292. Levine, B., N. Mizushima, and H.W. Virgin, *Autophagy in immunity and inflammation*. Nature, 2011. 469(7330): p. 323-35.
293. Kirkin, V., et al., *A role for ubiquitin in selective autophagy*. Mol Cell, 2009. 34(3): p. 259-69.
294. Wang, G., Z.Q. Yang, and K. Zhang, *Endoplasmic reticulum stress response in cancer: molecular mechanism and therapeutic potential*. Am J Transl Res, 2010. 2(1): p. 65-74.
295. Jin, S.M., et al., *Mitochondrial membrane potential regulates PINK1 import and proteolytic destabilization by PARL*. J Cell Biol, 2010. 191(5): p. 933-42.
296. Fujiwara, M., et al., *Parkin as a tumor suppressor gene for hepatocellular carcinoma*. Oncogene, 2008. 27(46): p. 6002-11.
297. Mathew, R., et al., *Autophagy suppresses tumorigenesis through elimination of p62*. Cell, 2009. 137(6): p. 1062-75.
298. Komatsu, M., et al., *The selective autophagy substrate p62 activates the stress responsive transcription factor Nrf2 through inactivation of Keap1*. Nat Cell Biol, 2010. 12(3): p. 213-23.
299. Lau, A., et al., *A noncanonical mechanism of Nrf2 activation by autophagy deficiency: direct interaction between Keap1 and p62*. Mol Cell Biol, 2010. 30(13): p. 3275-85.

300. Komatsu, M., et al., *Homeostatic levels of p62 control cytoplasmic inclusion body formation in autophagy-deficient mice*. *Cell*, 2007. 131(6): p. 1149-63.
301. Takamura, A., et al., *Autophagy-deficient mice develop multiple liver tumors*. *Genes Dev*, 2011. 25(8): p. 795-800.
302. Lau, A., et al., *Dual roles of Nrf2 in cancer*. *Pharmacol Res*, 2008. 58(5-6): p. 262-70.
303. Colotta, F., et al., *Cancer-related inflammation, the seventh hallmark of cancer: links to genetic instability*. *Carcinogenesis*, 2009. 30(7): p. 1073-81.
304. Cadwell, K., et al., *A key role for autophagy and the autophagy gene Atg16l1 in mouse and human intestinal Paneth cells*. *Nature*, 2008. 456(7219): p. 259-63.
305. Mareninova, O.A., et al., *Impaired autophagic flux mediates acinar cell vacuole formation and trypsinogen activation in rodent models of acute pancreatitis*. *J Clin Invest*, 2009. 119(11): p. 3340-55.
306. Funderburk, S.F., Q.J. Wang, and Z. Yue, *The Beclin 1-VPS34 complex--at the crossroads of autophagy and beyond*. *Trends Cell Biol*, 2010. 20(6): p. 355-62.
307. White, E., *Deconvoluting the context-dependent role for autophagy in cancer*. *Nat Rev Cancer*, 2012. 12(6): p. 401-10.
308. Cuervo, A.M., *Autophagy: in sickness and in health*. *Trends Cell Biol*, 2004. 14(2): p. 70-7.
309. Guo, J.Y., et al., *Activated Ras requires autophagy to maintain oxidative metabolism and tumorigenesis*. *Genes Dev*, 2011. 25(5): p. 460-70.
310. Lock, R., et al., *Autophagy facilitates glycolysis during Ras-mediated oncogenic transformation*. *Mol Biol Cell*, 2011. 22(2): p. 165-78.
311. Yang, S., et al., *Pancreatic cancers require autophagy for tumor growth*. *Genes Dev*, 2011. 25(7): p. 717-29.
312. Solomon, V.R. and H. Lee, *Chloroquine and its analogs: a new promise of an old drug for effective and safe cancer therapies*. *Eur J Pharmacol*, 2009. 625(1-3): p. 220-33.
313. Levy, G.D., et al., *Incidence of hydroxychloroquine retinopathy in 1,207 patients in a large multicenter outpatient practice*. *Arthritis Rheum*, 1997. 40(8): p. 1482-6.
314. Blommaart, E.F., et al., *The phosphatidylinositol 3-kinase inhibitors wortmannin and LY294002 inhibit autophagy in isolated rat hepatocytes*. *Eur J Biochem*, 1997. 243(1-2): p. 240-6.
315. Caro, L.H., et al., *3-Methyladenine, an inhibitor of autophagy, has multiple effects on metabolism*. *Eur J Biochem*, 1988. 175(2): p. 325-9.
316. Kochl, R., et al., *Microtubules facilitate autophagosome formation and fusion of autophagosomes with endosomes*. *Traffic*, 2006. 7(2): p. 129-45.
317. Klionsky, D.J., et al., *Guidelines for the use and interpretation of assays for monitoring autophagy in higher eukaryotes*. *Autophagy*, 2008. 4(2): p. 151-75.
318. Townsend, K.N., et al., *Autophagy inhibition in cancer therapy: metabolic considerations for antitumor immunity*. *Immunol Rev*, 2012. 249(1): p. 176-94.
319. Yan, C.H., et al., *Contributions of autophagic and apoptotic mechanisms to CrTX-induced death of K562 cells*. *Toxicol*, 2006. 47(5): p. 521-30.
320. Carew, J.S., et al., *Targeting autophagy augments the anticancer activity of the histone deacetylase inhibitor SAHA to overcome Bcr-Abl-mediated drug resistance*. *Blood*, 2007. 110(1): p. 313-22.
321. Kamitsuji, Y., et al., *The Bcr-Abl kinase inhibitor INNO-406 induces autophagy and different modes of cell death execution in Bcr-Abl-positive leukemias*. *Cell Death Differ*, 2008. 15(11): p. 1712-22.
322. Mishima, Y., et al., *Autophagy and autophagic cell death are next targets for elimination of the resistance to tyrosine kinase inhibitors*. *Cancer Sci*, 2008. 99(11): p. 2200-8.

323. Bellodi, C., et al., *Targeting autophagy potentiates tyrosine kinase inhibitor-induced cell death in Philadelphia chromosome-positive cells, including primary CML stem cells*. J Clin Invest, 2009. 119(5): p. 1109-23.
324. Sheng, Z., et al., *BCR-ABL suppresses autophagy through ATF5-mediated regulation of mTOR transcription*. Blood, 2011. 118(10): p. 2840-8.
325. Crowley, L.C., et al., *Autophagy induction by Bcr-Abl-expressing cells facilitates their recovery from a targeted or nontargeted treatment*. Am J Hematol, 2011. 86(1): p. 38-47.
326. Carayol, N., et al., *Critical roles for mTORC2- and rapamycin-insensitive mTORC1-complexes in growth and survival of BCR-ABL-expressing leukemic cells*. Proc Natl Acad Sci U S A, 2010. 107(28): p. 12469-74.
327. Carella, A.M., et al., *Clarithromycin potentiates tyrosine kinase inhibitor treatment in patients with resistant chronic myeloid leukemia*. Leuk Lymphoma, 2012. 53(7): p. 1409-11.
328. Yu, Y., et al., *Targeting microRNA-30a-mediated autophagy enhances imatinib activity against human chronic myeloid leukemia cells*. Leukemia, 2012. 26(8): p. 1752-60.
329. Tong, Y., et al., *Perifosine induces protective autophagy and upregulation of ATG5 in human chronic myelogenous leukemia cells in vitro*. Acta Pharmacol Sin, 2012. 33(4): p. 542-50.
330. Altman, B.J., et al., *Autophagy is essential to suppress cell stress and to allow BCR-Abl-mediated leukemogenesis*. Oncogene, 2011. 30(16): p. 1855-67.
331. Puissant, A., et al., *Resveratrol promotes autophagic cell death in chronic myelogenous leukemia cells via JNK-mediated p62/SQSTM1 expression and AMPK activation*. Cancer Res, 2010. 70(3): p. 1042-52.
332. Goussetis, D.J., E. Gounaris, and L.C. Platanias, *BCR-ABL1-induced leukemogenesis and autophagic targeting by arsenic trioxide*. Autophagy, 2012. 9(1).
333. Goussetis, D.J., et al., *Autophagic degradation of the BCR-ABL oncoprotein and generation of antileukemic responses by arsenic trioxide*. Blood, 2012.
334. Livak, K.J. and T.D. Schmittgen, *Analysis of relative gene expression data using real-time quantitative PCR and the 2(-Delta Delta C(T)) Method*. Methods, 2001. 25(4): p. 402-8.
335. Deguchi, T., et al., *Comparison of the intrusion effects on the maxillary incisors between implant anchorage and J-hook headgear*. Am J Orthod Dentofacial Orthop, 2008. 133(5): p. 654-60.
336. Shah, N.P., et al., *Transient potent BCR-ABL inhibition is sufficient to commit chronic myeloid leukemia cells irreversibly to apoptosis*. Cancer Cell, 2008. 14(6): p. 485-93.
337. Mauro, M.J. and B.J. Druker, *STI571: targeting BCR-ABL as therapy for CML*. Oncologist, 2001. 6(3): p. 233-8.
338. Deguchi, Y., et al., *Comparison of imatinib, dasatinib, nilotinib and INNO-406 in imatinib-resistant cell lines*. Leuk Res, 2008. 32(6): p. 980-3.
339. Klionsky, D.J., et al., *Guidelines for the use and interpretation of assays for monitoring autophagy*. Autophagy, 2012. 8(4): p. 445-544.
340. Eskelinen, E.L., et al., *Seeing is believing: the impact of electron microscopy on autophagy research*. Autophagy, 2011. 7(9): p. 935-56.
341. Rubinsztein, D.C., et al., *In search of an "autophagometer"*. Autophagy, 2009. 5(5): p. 585-9.
342. Kimura, S., et al., *Monitoring autophagy in mammalian cultured cells through the dynamics of LC3*. Methods Enzymol, 2009. 452: p. 1-12.

343. Kimura, S., T. Noda, and T. Yoshimori, *Dissection of the autophagosome maturation process by a novel reporter protein, tandem fluorescent-tagged LC3*. *Autophagy*, 2007. 3(5): p. 452-60.
344. Mizushima, N., T. Yoshimori, and B. Levine, *Methods in mammalian autophagy research*. *Cell*, 2010. 140(3): p. 313-26.
345. Mleczak, A., et al., *Regulation of autophagosome formation by Rho kinase*. *Cell Signal*, 2013. 25(1): p. 1-11.
346. Shah, N.P., et al., *Sequential ABL kinase inhibitor therapy selects for compound drug-resistant BCR-ABL mutations with altered oncogenic potency*. *J Clin Invest*, 2007. 117(9): p. 2562-9.
347. Schuster, K., et al., *Selective targeting of the mTORC1/2 protein kinase complexes leads to antileukemic effects in vitro and in vivo*. *Blood Cancer J*, 2011. 1(9): p. e34.
348. Amaravadi, R. *Autophagy Inhibition in Cancer Therapy: Progress and Unanswered*

Questions in AAAS Annual Meeting, Autophagy: An Emerging Therapeutic Target in Human

Disease. 2012.

349. Zhang, W.H., KB. Spelman, J. LeRoy, P., et al, *Identification of small molecule inhibitors of ATG7*, in *Keystone Symposia 2011*,
350. Wilber, A., et al., *Therapeutic levels of fetal hemoglobin in erythroid progeny of beta-thalassemic CD34+ cells after lentiviral vector-mediated gene transfer*. *Blood*, 2011. 117(10): p. 2817-26.
351. Modi, H., et al., *Inhibition of Grb2 expression demonstrates an important role in BCR-ABL-mediated MAPK activation and transformation of primary human hematopoietic cells*. *Leukemia*, 2011. 25(2): p. 305-12.
352. Yang, D., et al., *Therapeutic potential of a synthetic lethal interaction between the MYC proto-oncogene and inhibition of aurora-B kinase*. *Proc Natl Acad Sci U S A*, 2010. 107(31): p. 13836-41.
353. Bray, K., et al., *Autophagy suppresses RIP kinase-dependent necrosis enabling survival to mTOR inhibition*. *PLoS One*, 2012. 7(7): p. e41831.
354. Wilson, E.N., et al., *A switch between cytoprotective and cytotoxic autophagy in the radiosensitization of breast tumor cells by chloroquine and vitamin D*. *Horm Cancer*, 2011. 2(5): p. 272-85.
355. Mortensen, M., et al., *The autophagy protein Atg7 is essential for hematopoietic stem cell maintenance*. *J Exp Med*, 2011. 208(3): p. 455-67.
356. Vessoni, A.T., A.R. Muotri, and O.K. Okamoto, *Autophagy in stem cell maintenance and differentiation*. *Stem Cells Dev*, 2012. 21(4): p. 513-20.
357. Tsukamoto, S., A. Kuma, and N. Mizushima, *The role of autophagy during the oocyte-to-embryo transition*. *Autophagy*, 2008. 4(8): p. 1076-8.
358. Singh, R., et al., *Autophagy regulates adipose mass and differentiation in mice*. *J Clin Invest*, 2009. 119(11): p. 3329-39.
359. Takano-Ohmuro, H., et al., *Autophagy in embryonic erythroid cells: its role in maturation*. *Eur J Cell Biol*, 2000. 79(10): p. 759-64.
360. Jacquet, A., et al., *Autophagy is required for CSF-1-induced macrophagic differentiation and acquisition of phagocytic functions*. *Blood*, 2012. 119(19): p. 4527-31.

361. Zhao, Y., et al., *Autophagy regulates hypoxia-induced osteoclastogenesis through the HIF-1alpha/BNIP3 signaling pathway*. J Cell Physiol, 2012. 227(2): p. 639-48.
362. Aymard, E., et al., *Autophagy in human keratinocytes: an early step of the differentiation?* Exp Dermatol, 2011. 20(3): p. 263-8.
363. Calabretta, B. and D. Perrotti, *The biology of CML blast crisis*. Blood, 2004. 103(11): p. 4010-22.
364. Perrotti, D., et al., *BCR-ABL suppresses C/EBPalpha expression through inhibitory action of hnRNP E2*. Nat Genet, 2002. 30(1): p. 48-58.
365. Kubonishi, I. and I. Miyoshi, *Establishment of a Ph1 chromosome-positive cell line from chronic myelogenous leukemia in blast crisis*. Int J Cell Cloning, 1983. 1(2): p. 105-17.
366. Rosenhahn, J., et al., *Cytogenetic characterisation and proteomic profiling of the Imatinib-resistant cell line KCL22-R*. Int J Oncol, 2007. 31(1): p. 121-8.
367. Law, J.C., et al., *Mutational inactivation of the p53 gene in the human erythroid leukemic K562 cell line*. Leuk Res, 1993. 17(12): p. 1045-50.
368. Naumann, S., et al., *Complete karyotype characterization of the K562 cell line by combined application of G-banding, multiplex-fluorescence in situ hybridization, fluorescence in situ hybridization, and comparative genomic hybridization*. Leuk Res, 2001. 25(4): p. 313-22.
369. Lockhart, D.J., et al., *Expression monitoring by hybridization to high-density oligonucleotide arrays*. Nat Biotechnol, 1996. 14(13): p. 1675-80.
370. Rutherford, T.R., J.B. Clegg, and D.J. Weatherall, *K562 human leukaemic cells synthesise embryonic haemoglobin in response to haemin*. Nature, 1979. 280(5718): p. 164-5.
371. Gambari, R., et al., *Predominant expression of zeta and epsilon globin genes in human leukemia K-562(S6) variant cell line*. Experientia, 1983. 39(4): p. 415-6.
372. Bianchi Scarra, G.L., et al., *Terminal erythroid differentiation in the K-562 cell line by 1-beta-D-arabinofuranosylcytosine: accompaniment by c-myc messenger RNA decrease*. Cancer Res, 1986. 46(12 Pt 1): p. 6327-32.
373. Cioe, L., et al., *Differential expression of the globin genes in human leukemia K562(S) cells induced to differentiate by hemin or butyric acid*. Cancer Res, 1981. 41(1): p. 237-43.
374. Gambari, R., et al., *Human leukemia K-562 cells: induction of erythroid differentiation by 5-azacytidine*. Cell Differ, 1984. 14(2): p. 87-97.
375. Zhang, J., et al., *Mitochondrial clearance is regulated by Atg7-dependent and -independent mechanisms during reticulocyte maturation*. Blood, 2009. 114(1): p. 157-64.
376. Tal, M.C., et al., *Absence of autophagy results in reactive oxygen species-dependent amplification of RLR signaling*. Proc Natl Acad Sci U S A, 2009. 106(8): p. 2770-5.
377. Sardina, J.L., et al., *p22phox-dependent NADPH oxidase activity is required for megakaryocytic differentiation*. Cell Death Differ, 2010. 17(12): p. 1842-54.
378. Rosen, A., et al., *Lymphoblastoid cell line with B1 cell characteristics established from a chronic lymphocytic leukemia clone by in vitro EBV infection*. Oncoimmunology, 2012. 1(1): p. 18-27.
379. Druker, B.J. and N.B. Lydon, *Lessons learned from the development of an abl tyrosine kinase inhibitor for chronic myelogenous leukemia*. J Clin Invest, 2000. 105(1): p. 3-7.
380. Gambacorti-Passerini, C., et al., *Multicenter independent assessment of outcomes in chronic myeloid leukemia patients treated with imatinib*. J Natl Cancer Inst, 2011. 103(7): p. 553-61.

381. Druker, B.J., et al., *Activity of a specific inhibitor of the BCR-ABL tyrosine kinase in the blast crisis of chronic myeloid leukemia and acute lymphoblastic leukemia with the Philadelphia chromosome.* N Engl J Med, 2001. 344(14): p. 1038-42.
382. Khorashad, J.S., et al., *The presence of a BCR-ABL mutant allele in CML does not always explain clinical resistance to imatinib.* Leukemia, 2006. 20(4): p. 658-63.
383. Barnes, D.J., et al., *Bcr-Abl expression levels determine the rate of development of resistance to imatinib mesylate in chronic myeloid leukemia.* Cancer Res, 2005. 65(19): p. 8912-9.
384. Jiang, X., et al., *Chronic myeloid leukemia stem cells possess multiple unique features of resistance to BCR-ABL targeted therapies.* Leukemia, 2007. 21(5): p. 926-35.
385. Yuk, J.M., T. Yoshimori, and E.K. Jo, *Autophagy and bacterial infectious diseases.* Exp Mol Med, 2012. 44(2): p. 99-108.
386. Masiero, E., et al., *Autophagy is required to maintain muscle mass.* Cell Metab, 2009. 10(6): p. 507-15.
387. Jaeger, P.A. and T. Wyss-Coray, *All-you-can-eat: autophagy in neurodegeneration and neuroprotection.* Mol Neurodegener, 2009. 4: p. 16.
388. White, E., et al., *Role of autophagy in suppression of inflammation and cancer.* Curr Opin Cell Biol, 2010. 22(2): p. 212-7.
389. Liang, X.H., et al., *Protection against fatal Sindbis virus encephalitis by beclin, a novel Bcl-2-interacting protein.* J Virol, 1998. 72(11): p. 8586-96.
390. Kang, M.R., et al., *Frameshift mutations of autophagy-related genes ATG2B, ATG5, ATG9B and ATG12 in gastric and colorectal cancers with microsatellite instability.* J Pathol, 2009. 217(5): p. 702-6.
391. Knaevelsrud, H., et al., *UVRAG mutations associated with microsatellite unstable colon cancer do not affect autophagy.* Autophagy, 2010. 6(7): p. 863-70.
392. Liang, C., et al., *Beyond autophagy: the role of UVRAG in membrane trafficking.* Autophagy, 2008. 4(6): p. 817-20.
393. Moscat, J. and M.T. Diaz-Meco, *p62 at the crossroads of autophagy, apoptosis, and cancer.* Cell, 2009. 137(6): p. 1001-4.
394. Cheung, Z.H. and N.Y. Ip, *The emerging role of autophagy in Parkinson's disease.* Mol Brain, 2009. 2: p. 29.
395. Harris, A.L., *Hypoxia--a key regulatory factor in tumour growth.* Nat Rev Cancer, 2002. 2(1): p. 38-47.
396. Degenhardt, K., et al., *Autophagy promotes tumor cell survival and restricts necrosis, inflammation, and tumorigenesis.* Cancer Cell, 2006. 10(1): p. 51-64.
397. Mathew, R., V. Karantza-Wadsworth, and E. White, *Role of autophagy in cancer.* Nat Rev Cancer, 2007. 7(12): p. 961-7.
398. Amaravadi, R.K., et al., *Autophagy inhibition enhances therapy-induced apoptosis in a Myc-induced model of lymphoma.* J Clin Invest, 2007. 117(2): p. 326-36.
399. Sasaki, K., et al., *Chloroquine potentiates the anti-cancer effect of 5-fluorouracil on colon cancer cells.* BMC Cancer, 2010. 10: p. 370.
400. Mujumdar, N. and A.K. Saluja, *Autophagy in pancreatic cancer: an emerging mechanism of cell death.* Autophagy, 2010. 6(7): p. 997-8.
401. Shimizu, S., et al., *Role of Bcl-2 family proteins in a non-apoptotic programmed cell death dependent on autophagy genes.* Nat Cell Biol, 2004. 6(12): p. 1221-8.
402. Cao, C., et al., *Inhibition of mammalian target of rapamycin or apoptotic pathway induces autophagy and radiosensitizes PTEN null prostate cancer cells.* Cancer Res, 2006. 66(20): p. 10040-7.

403. Ertmer, A., et al., *The anticancer drug imatinib induces cellular autophagy*. *Leukemia*, 2007. 21(5): p. 936-42.
404. Lum, J.J., et al., *Growth factor regulation of autophagy and cell survival in the absence of apoptosis*. *Cell*, 2005. 120(2): p. 237-48.
405. Codogno, P. and A.J. Meijer, *Autophagy and signaling: their role in cell survival and cell death*. *Cell Death Differ*, 2005. 12 Suppl 2: p. 1509-18.
406. Lum, J.J., R.J. DeBerardinis, and C.B. Thompson, *Autophagy in metazoans: cell survival in the land of plenty*. *Nat Rev Mol Cell Biol*, 2005. 6(6): p. 439-48.
407. Finbloom, D.S., et al., *Comparison of hydroxychloroquine and chloroquine use and the development of retinal toxicity*. *J Rheumatol*, 1985. 12(4): p. 692-4.
408. Munster, T., et al., *Hydroxychloroquine concentration-response relationships in patients with rheumatoid arthritis*. *Arthritis Rheum*, 2002. 46(6): p. 1460-9.
409. Zhu, S., et al., *Inhibiting autophagy potentiates the anticancer activity of IFN1 α in chronic myeloid leukemia cells*. *Autophagy*, 2012. 9(3).
410. Schafranek, L., et al., *Clarithromycin enhances dasatinib-induced cell death in chronic myeloid leukemia cells, by inhibition of late stage autophagy*. *Leuk Lymphoma*, 2012.
411. Huang, W.S., et al., *Discovery of 3-[2-(imidazo[1,2-b]pyridazin-3-yl)ethynyl]-4-methyl-N-{4-[(4-methylpiperazin-1-yl)methyl]-3-(trifluoromethyl)phenyl}benzamide (AP24534), a potent, orally active pan-inhibitor of breakpoint cluster region-abelson (BCR-ABL) kinase including the T315I gatekeeper mutant*. *J Med Chem*, 2010. 53(12): p. 4701-19.
412. Cassuto, O., et al., *All tyrosine kinase inhibitor-resistant chronic myelogenous cells are highly sensitive to Ponatinib*. *Oncotarget*, 2012.
413. Eiring, A.M., et al., *Advances in the treatment of chronic myeloid leukemia*. *BMC Med*, 2011. 9: p. 99.
414. Robert, G., et al., *Acadesine kills chronic myelogenous leukemia (CML) cells through PKC-dependent induction of autophagic cell death*. *PLoS One*, 2009. 4(11): p. e7889.
415. Huang, H.L., et al., *Lapatinib induces autophagy, apoptosis and megakaryocytic differentiation in chronic myelogenous leukemia K562 cells*. *PLoS One*, 2011. 6(12): p. e29014.
416. Goussetis, D.J., et al., *Autophagic degradation of the BCR-ABL oncoprotein and generation of antileukemic responses by arsenic trioxide*. *Blood*, 2012. 120(17): p. 3555-62.
417. Sandilands, E., et al., *Autophagic targeting of Src promotes cancer cell survival following reduced FAK signalling*. *Nat Cell Biol*, 2012. 14(1): p. 51-60.
418. Komatsu, M., et al., *Impairment of starvation-induced and constitutive autophagy in Atg7-deficient mice*. *J Cell Biol*, 2005. 169(3): p. 425-34.
419. Cairns, R.A., I.S. Harris, and T.W. Mak, *Regulation of cancer cell metabolism*. *Nat Rev Cancer*, 2011. 11(2): p. 85-95.
420. Chen, M., H. Sandoval, and J. Wang, *Selective mitochondrial autophagy during erythroid maturation*. *Autophagy*, 2008. 4(7): p. 926-8.
421. Mortensen, M., et al., *Loss of autophagy in erythroid cells leads to defective removal of mitochondria and severe anemia in vivo*. *Proc Natl Acad Sci U S A*, 2010. 107(2): p. 832-7.
422. Liu, F. and J.L. Guan, *FIP200, an essential component of mammalian autophagy is indispensable for fetal hematopoiesis*. *Autophagy*, 2011. 7(2): p. 229-30.
423. Kelli P.A. MacDonald, L.L., Therese Vu, Claudia Bruedigam, Geoffrey R. Hill and Steven W. Lane. *Autophagy is a constitutively active process in long-term hematopoietic stem cells and is essential for their survival and function*. in

Keystone Symposia, Autophagy, Inflammation and Immunity. 2013. Montreal, Canada.

424. Wu, Y.T., et al., *Autophagy plays a protective role during zVAD-induced necrotic cell death*. *Autophagy*, 2008. 4(4): p. 457-66.
425. Jin, S., et al., *Metabolic catastrophe as a means to cancer cell death*. *J Cell Sci*, 2007. 120(Pt 3): p. 379-83.
426. Salemi, S., et al., *Autophagy is required for self-renewal and differentiation of adult human stem cells*. *Cell Res*, 2012. 22(2): p. 432-5.
427. Oliver, L., et al., *Basal autophagy decreased during the differentiation of human adult mesenchymal stem cells*. *Stem Cells Dev*, 2012. 21(15): p. 2779-88.
428. Wang, J., et al., *A differentiation checkpoint limits hematopoietic stem cell self-renewal in response to DNA damage*. *Cell*, 2012. 148(5): p. 1001-14.